



VNIVERSITAT  
D VALÈNCIA

Instituto Interuniversitario de Investigación de Reconocimiento  
Molecular y Desarrollo Tecnológico (IDM)

Programa de Doctorado en Química

**Design, synthesis and evaluation of chromo  
and fluorogenic chemosensors to detect liquid  
ecstasy**

PhD Thesis

Submitted by

**Silvia Rodríguez Nuévalos**

PhD Supervisors

**Ana María Costero Nieto and Margarita Parra Álvarez**

Valencia, October 2022





Margarita Parra Álvarez , PhD in Chemistry and Professor at the Universitat de València, and Ana María Costero Nieto, PhD in Chemistry and Professor at the Universitat de València.

CERTIFY

That the work **“Design, synthesis and evaluation of chromo and fluorogenic chemosensors to detect liquid ecstasy”** has been developed by Silvia Rodríguez Nuévalos under their supervision in the Instituto Interuniversitario de Investigación de Reconocimiento Molecular y Desarrollo Tecnológico (IDM) of the Universitat de València, as a Thesis Project in order to obtain the degree of PhD in Chemistry at the Univeristat de València.

Valencia, October 2022

Margarita Parra Álvarez

Ana María Costero Nieto





## **Acknowledgements**

Recorrido este camino, cuando echo la vista atrás, no puedo evitar sonreír con nostalgia. La semilla de la ilusión por la investigación se plantó durante el desarrollo del trabajo de final de grado en el grupo de la profesora Ana María Costero y, a partir de ese momento, supe que esa semilla había venido para quedarse.

En primer lugar, me gustaría hacer una mención especial a mis directoras de tesis, Ana Costero y Margarita Parra. Gracias por todo, por aceptarme como vuestra estudiante, por enseñarme, por guiarme y, sobre todo, por ser pilares y ayudarme tanto en el ámbito académico como en el personal. Por supuesto, quiero agradecer también al resto de profesores del grupo MODeLiC: Pablo Gaviña, Salvador Gil, Jose Sáez y Pau Arroyo. Gracias a los seis por vuestras puertas siempre abiertas, por buscar siempre lo mejor de mí, de mi trabajo y brindarme un segundo hogar.

En segundo lugar, me gustaría agradecer a todos mis compañeros de laboratorio. Estefanía, Carlos, Elena, Dani, Tania y Samuel gracias por los buenos momentos y por enseñarme a trabajar en el laboratorio. Alejandro y Borja, gracias por haber hecho tan divertidos los primeros años de esta aventura y vuestro apoyo en los momentos difíciles. Jordi y Mariana, gracias por estos últimos años, por compartir tanto conmigo y estar ahí cuando ha sido necesario. A Álex, por tu alegría, por tus consejos y tu saber “quitarle hierro al asunto”. Por supuesto, gracias a todos los técnicos y personal de administración con los que he tenido la oportunidad de trabajar, pero sobre todo Amparo y Esther, gracias por cuidarme tanto y ayudarme en todo lo posible.

Gracias Paola por aceptarme en tu grupo durante mi estancia y ayudarme con todo lo que estuvo en tu mano. Elena y Alberto, gracias por enseñarme tantas cosas de vuestra química y aceptarme como una más. Y, en especial, gracias Andrea por todo tu apoyo y tu tiempo.

## *Acknowledgements*

También me gustaría agradecer al Ministerio de Universidades por la financiación de este proyecto, así como al personal del SCSIE por su ayuda durante estos años.

No me olvido de mi pequeña familia de químicos, a todos vosotros, gracias por todos esos magníficos momentos, por hacer de mi tiempo en la universidad tan bonito e inolvidable que me dan ganas de estudiar cualquier cosa, pero con vosotros.

Gracias de nuevo al grupo MODeLiC y a la gente de ScienceFlow, Empar, Yolanda y Carolina, porque juntos hemos creado un gran proyecto llamado NoSUM. Ha sido muy gratificante trabajar en un ámbito tan distinto al que estoy acostumbrada y que hayamos conseguido algo tan espectacular como es NoSUM.

Gracias a mis amigos de fuera de la universidad, especialmente a María y Lorena, por escuchar mis penas y alegrías, por hacer tan divertidos los momentos que estamos juntos y por pasar también juntos los que no lo son tanto.

Finalmente, quiero darle las gracias a mi familia. A mis abuelos, por enseñarme tantas lecciones que no se aprenden en los libros. A ti Sandra, por apoyarme tanto y tantas veces, por compartir mochilas y seguir caminando juntas. Y, en especial, a mi madre. Gracias por ser quien eres y por hacer que cada día quiera ser mejor persona, porque sin ti, nada de esto habría sido posible.

Muchas gracias a todos por quererme, por cuidarme, por creer en mí cuando yo no lo hice y darme las fuerzas para seguir.

*A mi familia,  
por todo su apoyo incondicional*



*“En la vida, no hay nada que  
temer, sólo hay que comprender”*

*(Marie Curie)*

*“Lo esencial es invisible a los ojos”*

*(Antoine de Saint-Exupéry, El principito)*



## **Abstract**

The present PhD thesis entitled “Design, synthesis and evaluation of chromo and fluorogenic chemosensors to detect liquid ecstasy” is based on the supramolecular host-guest interactions to develop new chromo-fluorogenic probes to detect liquid ecstasy, a drug of abuse with a great social concern currently, in drinks or beverages.

For this purpose, the first part of this research work has been divided into four chapters, where in each one is described the synthesis, characterization and evaluation of different sets of organic molecules as chromo and/or fluorogenic chemosensors of liquid ecstasy. Every set of molecules was designed considering the complementarity between the functional groups present in the analyte and in the probes.

The paradigm of detection of every probe is based on acid-base reactions, aggregation or redox reaction. The synthesized sensors have proved not only considerably notable limits of detection, but also selective sensing in complex matrixes such as drinks, allowing their use in real samples. Additionally, it has been proved the suitability of one of the sensors to detect another family of drugs of abuse, synthetic cathinones.

The last part of the thesis, included as an annex, describes the scientific social project called NoSUM. In this project, the main objectives have been to contact with university students to allow them to know about the troublesome situation with liquid ecstasy, develop a personal use kit to immediately detect this drug in drinks or beverages and test it in a real environment by these students and receive the feedback to improve it.

## **Resumen**

La presente tesis titulada “Design, synthesis and evaluation of chromo and fluorogenic chemosensors to detect liquid ecstasy” se basa en las interacciones supramoleculares hospedador-huésped para desarrollar nuevas sondas cromo-fluorogénicas para detectar éxtasis líquido usada en bebidas o combinados y que actualmente supone un problema social.

Para ello, la primera parte de este trabajo de investigación ha sido dividido en cuatro capítulos, en cada uno de los cuales se describe la síntesis, caracterización y evaluación quimiosensores cromo y/o fluorogénicos de éxtasis líquido. Cada uno de estos conjuntos se diseñó considerando la complementariedad ente los grupos funcionales presentes en el analito y en las sondas.

El paradigma de detección de cada prueba está basado en reacciones ácido-base, agregación o una reacción redox. Los sensores sintetizados han demostrado no solamente bajos límites de detección, sino también la detección selectiva en matrices complejas como las bebidas y esto ha permitido su uso en muestras reales. Además, se ha demostrado que uno de los sensores es adecuado para detectar otra familia de drogas de abuso, las catinonas sintéticas.

La última parte de la tesis, incluida como anexo, describe el proyecto científico-social llamado NoSUM. En este proyecto, los objetivos principales han sido contactar con estudiantado universitario para informarle sobre la problemática situación con el éxtasis líquido, desarrollar un kit de uso personal que permita detectar inmediatamente esta droga en la bebida y testarlo en un ambiente real por el estudiantado y recibir retroalimentación con el fin de mejorarlo para su comercialización.



## Scientific Contributions

The work carried out in this thesis and other collaborations have resulted in the following scientific publications and patents:

- ❖ Silvia Rodríguez-Nuévalos, Ana M. Costero, Pau Arroyo, José A. Sáez, Margarita Parra, Félix Sancenón, Ramón Martínez-Máñez. Protection against chemical submission: naked-eye detection of  $\gamma$ -hydroxybutyric acid (GHB) in soft drinks and alcoholic beverages. *Chem. Commun.*, **2020**, 56, 12600-126003.
  
- ❖ Silvia Rodríguez-Nuévalos, Margarita Parra, Salvador Gil, Pablo Gaviña, Pau Arroyo, Jose A. Sáez, Ana M. Costero. Heteroditopic chemosensor to detect  $\gamma$ -hydroxybutyric acid (GHB) in soft drinks and alcoholic beverages *Analyst*, **2021**, 146, 5601-5609.
  
- ❖ Silvia Rodríguez-Nuévalos, Ana M. Costero, Salvador Gil, Margarita Parra, Pablo Gaviña. Bifunctionalized Gold Nanoparticles for the Colorimetric Detection of the Drug  $\gamma$ -Hydroxybutyric Acid (GHB) in Beverages *Chemosensors*, **2021**, 9(7), 160-169.
  
- ❖ Silvia Rodríguez-Nuévalos, Ana M. Costero, Margarita Parra, Salvador Gil, Pau Arroyo, Jose A. Sáez, Pablo Gaviña, Paola Ceroni, Andrea Fermi. Colorimetric and fluorescent hydrazone-BODIPY probes for the detection of  $\gamma$ -hydroxybutyric acid (GHB) and cathinones. *Dyes and Pigments*, **2022**, 207, 110757-110765.
  
- ❖ Lorente, Alejandro; Costero, Ana; Jaque, Pablo; Gil, Salvador; Sáez, José; Rodríguez-Nuévalos, Silvia; Rodríguez Lavado, Julio; Ochoa, Andrés. Unconventional OFF-ON response of a mono(calix[4]arene)-substituted BODIPY sensor for  $Hg^{2+}$  through dimerization reversion *ACS Omega*. Submitted.

❖ Patent: Nuevos compuestos derivados de benzoxazol, procedimiento de obtención y su uso en la detección de GHB en bebidas. Nº de solicitud: P202030840. Silvia Rodríguez Nuévalos, Ana M. Costero Nieto; Margarita Parra Álvarez; Salvador Gil Grau; Pablo Gaviña Costero; Jordi Hernández Contreras. 6<sup>th</sup> August 2020. Universitat de València, España.

❖ Patent: Nuevos compuestos de base tiourea, procedimiento de obtención y su uso en la detección de GHB en bebidas. Nº de solicitud: P202030841. Silvia Rodríguez Nuévalos, Ana M. Costero Nieto; Margarita Parra Álvarez; Salvador Gil Grau; Pablo Gaviña Costero; Jordi Hernández Contreras. 6<sup>th</sup> August 2020. Universitat de València, España.

.

## **Abbreviations**

AMPH: Amphetamine

AVI: Agencia Valenciana de Innovación

AuNP: Gold nanoparticle

BC: Before Christ

BD: 1,4-butanediol

BODIPY: 4,4-difluoro-4-bora-3a,4a-diaza-s-indacene

*ca.: circa*

CI: Configuration Interaction

<sup>13</sup>C NMR: Carbon Nuclear Magnetic Resonance

CNS: Central Nervous System

CS: Chemical Submission

DCNP: Diethylcyanophosphonate

DFP: Diisopropylfluorophosphate

DNA: Deoxyribonucleic Acid

DFSA: Drug-Facilitated Sexual Assaults

DLS: Dynamic Light Scattering

*e.g.: exempli gratia*

em: emission

EMCDDA: European Monitoring Centre for Drugs and Drug Addiction

equiv. (eq.): equivalent

ESI: Electrospray Ionization

ESIPT: Excited-State Intramolecular Proton Transfer

*et al.: et alii*

exc: excitation

<sup>19</sup>F NMR: Fluorine Nuclear Magnetic Resonance

GABA: *gamma*-aminobutyric acid

GBL: *gamma*-butyrolactone

GHB: *gamma*-hydroxybutyrate

HBO: 2-(2'-Hydroxyphenyl)benzoxazole

<sup>1</sup>H NMR: Proton Nuclear Magnetic Resonance

HOMO: Highest Occupied Molecular Orbital

HRMS: High Resolution Mass Spectroscopy

ICT: Intramolecular Charge Transference

i.e.: *id est*

INE: Instituto Nacional de Estadística

ISO: International Organization for Standardization

IUPAC: International Union of Pure and Applied Chemistry

LC-MS/MS: Liquid Chromatography with tandem Mass Spectrometry

LUMO: Lowest Unoccupied Molecular Orbital

LoD: Limit of Detection

MDMC: 3,4-methylenedioxy-N-methylcathinone

MDMA: Methylenedioxy-methylamphetamine

MDPV: Methylenedioxypropylone

3,4-MDPHP: 3',4'-methylenedioxy- $\alpha$ -pyrrolidinohexiophenone

MIP: Molecular Imprinted Polymer

4-MMC: 4-methylmethcathinone or mephedrone

MPHP: 4'-methyl- $\alpha$ -pyrrolidinohexiophenone

NAD<sup>+</sup>/ NADH: Nicotinamide Adenine Dinucleotide  
NCDAS: National Centre of Drug abuse Statistics  
NM: Nanomaterial  
NP: Nanoparticle  
NPS: New Psychoactive Substances  
PCDA: 10,12-Pentacosadiynoic acid  
PCM: Polarizable continuum model  
PES: Potential Energy Hypersurface  
PPi: Pyrophosphate Ion  
RNA: Ribonucleic Acid  
RR-QHO: Rigid-Rotor Quasiharmonic Oscillator  
SC: Synthetic Cathinone  
S<sub>E</sub>Ar: Electrophilic Aromatic Substitution  
SMD: Solvation Model Based on Density  
S<sub>N</sub>2: Bimolecular Nucleophilic Substitution  
S<sub>N</sub>Ar: Nucleophilic Aromatic Substitution  
SPR: Surface Plasmon Resonance  
SSA: Succinic semialdehyde  
TBAOH: Tetrabutyl ammonium hydroxyl  
TD-DFT: Time-Dependent Density Functional Theory  
TEM: Transmission Electron Microscopy  
TPE: Tetraphenylethylene  
TS: Transition State  
UNODC: United Nations Office on Drugs and Crime

UV-Vis: Ultraviolet-Visible

# Table of content

<b>Chapter 1. General introduction</b> .....	<b>3</b>
1.1. Current concern related to drugs abuse .....	5
1.1.1. Drugs misuse and Drug Facilitated Sexual Assaults .....	5
1.1.2. <i>Gamma</i> -hydroxybutyrate.....	8
1.1.3. Synthetic Cathinones .....	11
1.2. Supramolecular Chemistry .....	13
1.2.1. General concepts .....	13
1.2.2. Chemosensor Design .....	15
1.2.3. Optical chemosensors .....	16
1.2.4. Receptor and Signalling Units .....	17
1.3. GHB and Synthetic Cathinones detection .....	20
1.3.1. GHB detection .....	20
1.3.2. Synthetic Cathinones detection .....	22
<b>Chapter 2: GHB detection through the use of ditopic ligands</b> .....	<b>25</b>
2.1 Introduction.....	27
2.2. Ditopic ligand design .....	28
2.3. Objectives .....	30
2.4. Heteroditopic chemosensor to detect $\gamma$ -hydroxybutyric acid (GHB) in soft drinks and alcoholic beverages .....	31
<b>Chapter 3: Colorimetric and fluorimetric GHB detection with benzoxazole derivatives</b> .....	<b>93</b>
3.1 Introduction.....	95
3.2. Chemosensor design .....	97
3.3. Objectives .....	99

3.4. Protection against chemical submission: Naked-eye detection of $\gamma$ -hydroxybutyric acid (GHB) in soft drinks and alcoholic beverages .....	101
<b>Chapter 4: Colorimetric detection of GHB using gold nanoparticles .....</b>	<b>143</b>
4.1 Introduction.....	145
4.1.1. Nanomaterials .....	145
4.1.2. Gold Nanoparticles.....	146
4.2. Ligands design .....	149
4.3. Objectives .....	150
4.4. Bifunctionalized gold nanoparticles for the colorimetric detection of the drug $\gamma$ -hydroxybutyric acid (GHB) in beverages .....	151
<b>Chapter 5: GHB and synthetic cathinones detection using BODIPY derivatives .....</b>	<b>179</b>
5.1 Introduction.....	181
5.1.1. BODIPY core .....	181
5.1.2. Synthesis and postfunctionalization .....	182
5.2. Chemosensors design .....	185
5.3. Objectives .....	186
5.4. Colorimetric and fluorescent hydrazone-BODIPY probes for the detection of $\gamma$ -hydroxybutyric acid (GHB) and cathinone.....	187
<b>Chapter 6: Conclusions .....</b>	<b>241</b>
<b>References .....</b>	<b>247</b>
<b>Annex I: NoSUM .....</b>	<b>265</b>



# **Chapter 1: General introduction**



## 1.1. Current concern related to drugs abuse

### 1.1.1. Drugs misuse and Drug Facilitated Sexual Assaults

Historically, drugs have been part of human being culture and society since the ancient times. Related to religious ceremonies, medical or recreational use, drugs exhibited an important role within these widely spread events.<sup>1,2</sup> For instance, in religious rituals, which used to take place in Central Asia, *Amanita muscaria*, the wellknown white-spotted red mushroom, has been vastly used for at least 4000 years. Another early drug-use example would be the consume of opium, with medical purposes, described in Homer's *Odyssey*, dates from the 9<sup>th</sup> century BC. In terms of recreational encounters, some licit drugs such as caffeine, nicotine and alcohol have been embedded in our culture and they have been consumed for a considerably long period of time. For instance, tea has been consumed since the 3<sup>rd</sup> century BC.<sup>2</sup>

In spite of the fact that human beings have been consuming drugs for such social rites, the current consumption situation is considerably alarming. According to UNDOC (United Nations Office on Drugs and Crime), in 2013 almost 25 million people, aged between 15 and 64 years old, consumed some illicit drugs.<sup>3</sup> More recent statistical studies, from NCDAS (National Centre of Drug Abuse Statistics), show that 31.9 million Americans were users of some illegal drugs.<sup>4</sup> In Europe, the situation is not reassuring, either. As can be seen in Figure 1.1, statistics from EMCDDA (European Monitoring Centre for Drugs and Drug Addition) show that consume of common illicit drugs such as cannabis or cocaine is very popular among the population, ranging from 4.3 to 25.2 million people.<sup>5</sup>

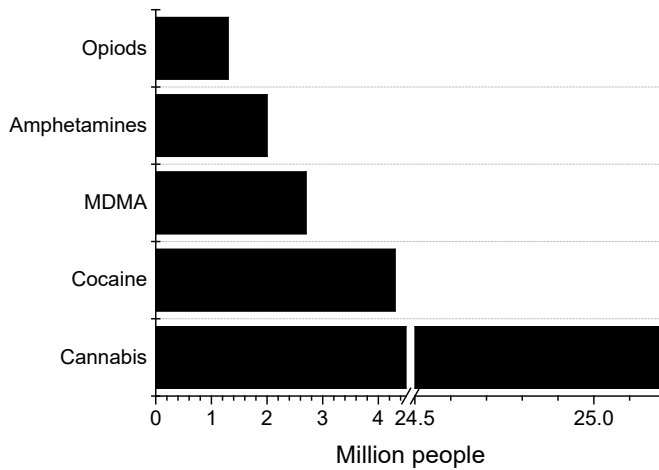


Figure 1.1. Some common drugs consumption in Europe (extracted from EMCDDA)<sup>5</sup>

Even though personal consumption of drugs is a truly worrying issue of our society, more recent dangerous situations, in which are involved drugs, are gaining concerned: chemical submission (CS). CS term, first time used in 1982, refers to ‘the substance administration to a person without his/her knowledge to cause him/her a change in the alertness, state of consciousness and judgment’.<sup>1,6</sup> In every single case, the main aim is the same: to achieve the victim’s vulnerability to take advantage of their situation and carry out a criminal act. Among all those illegal acts, DFSA (Drug-Facilitated Sexual Assaults) is the most common one. Not only drugs are used in these types of abuse, but also to change children’s behaviour, in order to make them more docile, to carry out a robbery or even to induce someone to commit a crime.<sup>7</sup> DFSA is defined as an unwanted sexual act carried out when a person (male or female) is incapacitated or unconscious due to the effect of ethanol and/or a drug and therefore unable to resist or consent to such acts.<sup>8,9</sup> It has been widely described in the literature two main forms of DFSA: proactive and opportunistic. Proactive DFSA is referred to those sexual assaults in

which the assailant administers an incapacitating substance to the victim without this one realizes it. By contrast, opportunistic DFSA is that assault in which someone is intoxicated on their own decision and the assailant takes advantage of their vulnerability.<sup>9,10</sup>

The number of DFSA, commonly called 'date rape' by mass media, has increased over the past few years. However, it is impossible to uncover exactly what is the true prevalence of DFSA cases. Several studies suggest that between 10-20% of sexual assaults are reported to the law enforcements agencies.<sup>8-11</sup> Among the reasons behind this fact, those related to victims can be highlighted: self-blame, guilt, shame, embarrassment, fear or, even, denial.<sup>10</sup> On the other hand, there are also several factors that can complicate the investigations, such as lack of experience among law enforcement agencies and/or medical personnel or the extensive variety of drugs that might be used.<sup>8</sup> Several surveys have been carried out in some European countries uncovering that up to 20% of women have suffered some form of sexual assault during their adulthood life.<sup>9</sup> Although, it is true that most vulnerable victims are young women (under 20), also men can suffer these aggressions.<sup>1,10</sup>

The most common way to force someone to ingest a drug without their consent is through spiking drinks, usually by some victim's acquaintance.<sup>1</sup> The most popular drugs used in sexual assaults, also known as 'date rape drugs', are Central Nervous System (CNS) depressants such as ethanol, benzodiazepines (Rohypnol, i.e. Flunitrazepam), *gamma*-hydroxybutyrate (GHB) and ketamine (see Chart 1.1).<sup>9-11</sup> CNS depressants are medicines that can slow brain activity, making them appropriate to treat some mental states such as anxiety, panic, acute stress and sleep disorders. The vast majority of them acts increasing the activity of *gamma*-aminobutyric acid (GABA), a neurotransmitter able to inhibit brain activity.<sup>12</sup> These compounds cause alteration of the victim's behaviour, from drowsiness to loss of inhibition and consciousness<sup>9</sup> and, also, exhibit

the appropriate organoleptic properties (lack of colour, taste and odour) to make them unnoticeable in the spiked drink.<sup>13</sup>

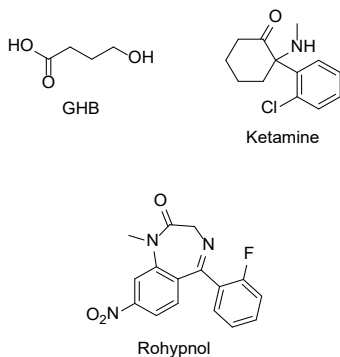
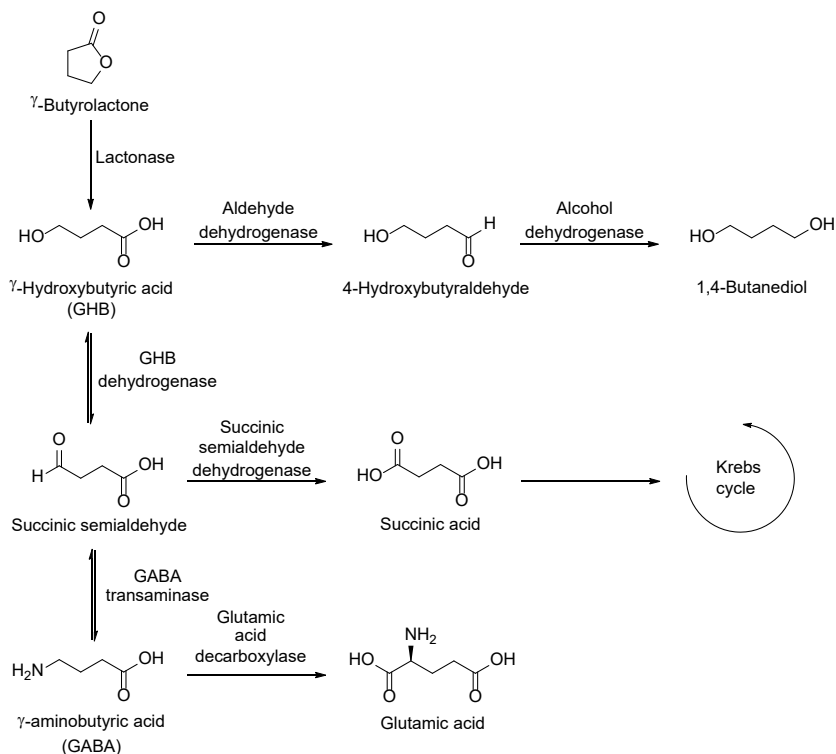


Chart 1.1. Chemical structure of the most common drugs used in DFSA

### 1.1.2. Gamma-hydroxybutyrate

As far as this work is concerned, the main attention will be focused on one of these date rape drugs: GHB. This compound is a very particularly problematic drug not only for its ready availability, but also by its organoleptic properties.<sup>14</sup> It is a white powder, which provides colourless, odourless and slight salty dissolutions making the victim completely unaware of its intake. GHB was synthesised in 1961 by Henri Laborit, a French surgeon, who was looking for a more effective drug in terms of anaesthetics. Because of its sedative effects, it has been used in the treatment of sleep disturbance, such as narcolepsy and cataplexy, as well as a possible antidote to alcohol withdrawal symptoms.<sup>15-20</sup>

*Gamma*-hydroxybutyrate is an endogenous short-chain fatty acid found in human body. Although it is true that the highest concentration of this substance is found in brain (mainly basal ganglia and hypothalamus), it can be found in liver, kidneys, bones and brown fat, as well.<sup>15-17</sup> As can be seen in Scheme 1.1, this compound is, at the same time, a precursor and a metabolite of the neurotransmitter GABA and, also, can act as a neuromodulator of dopamine, serotonin and opioid system.<sup>15,16,18,20</sup>

Scheme 1.1. Different metabolic pathways of gamma-hydroxybutyrate<sup>18</sup>

GHB recreational use emerged in the early 90s. Some of its slang or street names are 'Liquid Ecstasy', 'G', 'Liquid X' or 'Fantasy'. In order to keep under control its misuse, GHB became a controlled substance in USA (United States of America) in 2000 (schedule I) and in EU (European Union) in 2001 (schedule III or IV).<sup>14,15,18</sup> However, one of the issues to avoid the misuse or abuse of this drug is related to its prodrugs: GBL (*gamma*-butyrolactone) and BD (1,4-butanediol). *In vivo*, these prodrugs are quickly metabolised to GHB (see Scheme 1.1), being this latter the one that exerts the pharmacological effects. Nevertheless, to classify them as controlled substances is not an easy task because they are common solvents used in industry.<sup>14,15,17,18</sup>

*Gamma*-hydroxybutyrate is considered as a CNS depressant due to its interaction and binding to GABA receptors. It can cross fairly quickly

the blood-barrier brain as well as being absorbed from the gastrointestinal tract. Depending on the dose, the maximum peak plasma concentration is reached between 25 and 45 min after the intake, for doses ranging from 12.5 mg/kg to 50 mg/kg. The onset of the effects is around 15 min after ingesting it. GHB is metabolised with a half-life time of 20-42 min and notable little quantities are excreted with no changes in urine (1-5%). Moreover, for therapeutics doses (12.5-50 mg/kg), it is utterly eliminated from blood in a short time frame (2-8 h) and its recovery from urine is only possible within 8-12 h, (see Figure 1.2).<sup>14,15,18,21</sup> This truly short window makes, on one hand, extremely important the appropriate sample collections in DFSA suspicion cases in order to avoid the loss of crucial proves and, on the other hand, another key point would be anticipating these assaults directly. In this sense, it is essential the development of real-time and naked-eye detection methods of GHB in drinks.

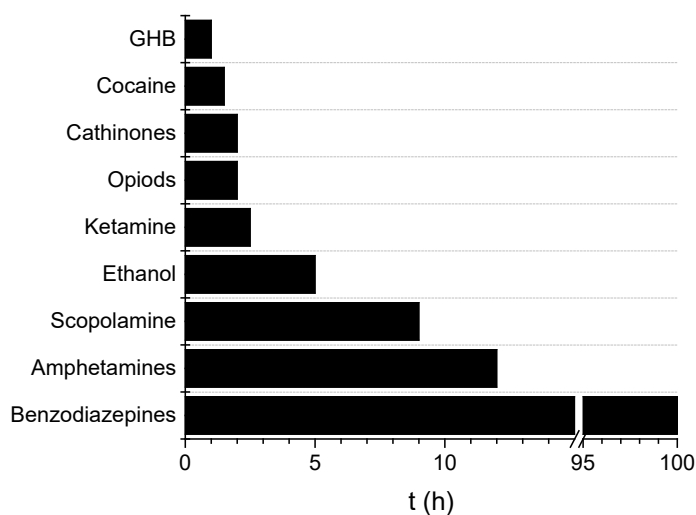


Figure 1.2. Half-life times observed for several drugs in blood<sup>10</sup>



### 1.1.3. Synthetic Cathinones

Another social huge concern related to drugs is the currently emerging New Psychoactive Substances (NPS). This varied group of recreational psychotropic substances appeared around 15 years ago, being commonly marketed as “research chemical”, “legal highs” or “designer drugs” across the world. NPS are sold as lawful, inexpensive and non-detectable substitutes for controlled drugs of abuse. Some of the most relevant classes of NPS are synthetic cathinones (SCs), synthetic cannabimimetics or phenethylamines. UNODC employs the term ‘New Psychoactive Substances’ to refer those “*substances of abuse, either in a pure form or a preparation, which are not controlled by the 1961 Single Convention on Narcotic Drugs or the 1971 Convention on Psychotropic Substances, but which may pose a public health threat*”. Since several of these NPS were first synthesised some decades ago, the term “novel” not necessarily implies “recently synthesised or discovered”. Besides, over the past years, several hundred compounds have been documented as NPS by the early warning system of the European Union (see Figure 1.3).<sup>22–24</sup>

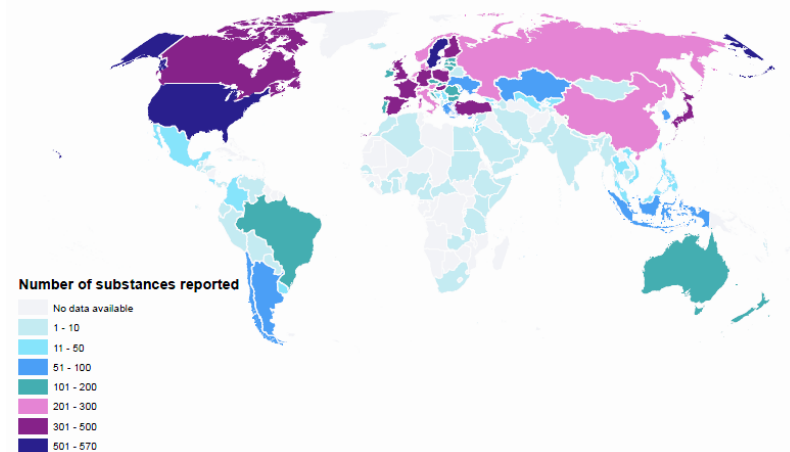


Figure 1.3. Global emergence of new psychoactive substances up to December 2021 (extracted from UNODC)<sup>22</sup>

In particular, SCs have gained more and more attention in the last few years. SCs are sold commonly as ‘bath salts’ or ‘jewellery clearer’ and they are among the most prevalent consumed and developed NPS, grouping more than 620 different types of compounds. Cathinone, a beta-keto derivative of amphetamines (AMPHs), is found naturally in khat plant (*Catha edulis*), especially in its leaves. The leaves of this plant are chewed, mostly in several African countries and the Middle East, for its ability to produce euphoria and stimulation. These drugs usually mimic psychostimulant effects of AMPHs, MDMA (Methylenedioxy-methylamphetamine) or cocaine and they act augmenting the synaptic levels of some monoamine-type neurotransmitters: noradrenaline, dopamine and serotonin, by interfering with their transporters.<sup>24–26</sup> According to the literature, there are three SCs particularly troublesome, 3Ms: mephedrone, methylone and MDPV (Methylenedioxypropylvalerone). Not only it is concerning the large number of police seizures of these drugs, but also the great toxicity they exhibit.<sup>27</sup> In Chart 1.2, it can be observed the structure similarities and differences between amphetamines and cathinones.

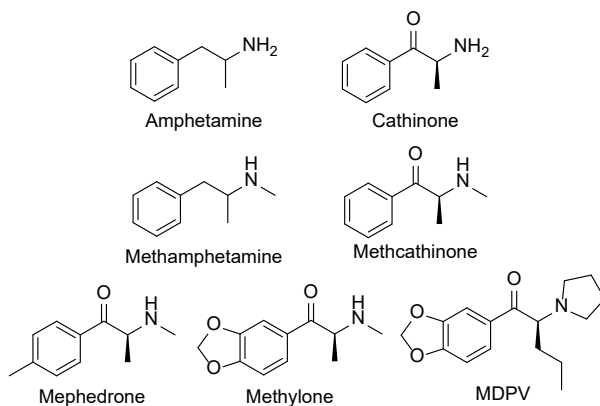


Chart 1.2. Chemical structure of amphetamine, cathinone and some common SCs<sup>25</sup>

Owing to the fact that SCs are appearing in market much quicker than law enforcement agencies are able to control them and address

their manufacturing and sale, the development of real-time detection systems has become crucial to give some tools to the police to make them capable of recognising these substances and act as soon as possible.

## 1.2. Supramolecular Chemistry

### 1.2.1. General concepts

The term and the concept of supramolecular chemistry were introduced in 1978 by Jean-Marie Lehn defined as *“Just as there is a field of molecular chemistry based on the covalent bond, there is a field of supramolecular chemistry, the chemistry of molecular assemblies and of the intermolecular bond”*. However, it has been reformulated as *“the chemistry beyond the molecule”*, which implies that a more complex organization and, as a result, a higher complexity in structures can be found thanks to the association of two or more chemical species kept together by intermolecular forces.<sup>28</sup>

Historically, supramolecular chemistry used to be divided in two main branches: host-guest recognition, i.e. discrete entities caused by the association of few components (for instance, a receptor and its ligand), and self-assembly, polymolecular entities originated from the spontaneous association of a large number of components. These species have risen to systems such as molecular machines, molecular knots, films or micelles.<sup>28,29</sup> However, over the years, the application of supramolecular chemistry in other scientific areas has been expanded; some of them are medicine, biomimetics, data storage and processing. This field focuses on the study of non-covalent interactions such as hydrogen bonding, van der Waals forces, dipole-dipole, hydrophobic, electrostatic and  $\pi$ - $\pi$  stacking interactions.<sup>28-30</sup> Even, recently, reversible covalent bonds have been accepted in the lexicon of supramolecular chemistry. In Figure 1.4, it can be seen, in

basic terms, the difference among molecular and supramolecular chemistry.

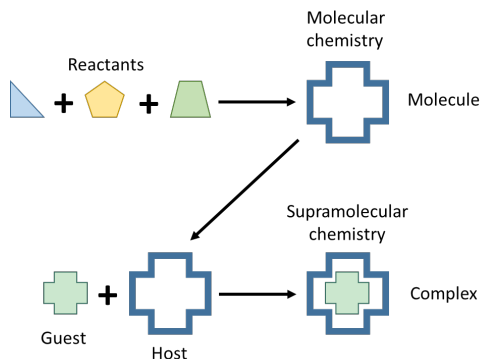


Figure 1.4. Schematic way to highlight the differences between molecular and supramolecular chemistry

As it has just been mentioned, one of the traditional branches of supramolecular chemistry is the formation of host-guest complexes thanks to the molecular recognition, which is taking place between the receptor (host) and the ligand (guest). Some of the most common host molecules used have been cyclodextrins, calixarenes, and coronands (see Chart 1.3).<sup>28–30</sup> This approach is considerably crucial in sensing field, as it is the basis of the detection of relevant substances.

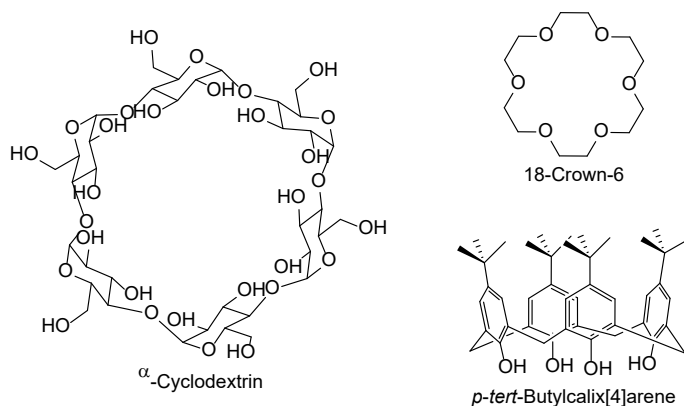


Chart 1.3. Some examples of common host units used in sensing field

### 1.2.2. Chemosensor Design

A chemosensor or probe is a device, which allows the user to notice the presence of an analyte of interest. Two processes are involved in this event: molecular recognition and signal transduction. As it has been mentioned before, molecular recognition takes place when the receptor interacts with the analyte, provoking some physical or chemical change. Thus, for the purpose of binding a guest to a particular molecular receptor, the latter has to be carefully designed. For this reason, in the design moment, it has to be taken into consideration three main factors: complementarity, preorganization and convergence, since they will influence the molecular recognition process. Whilst the signal transduction consists of the transformation of the sensing event, (the variation of a chemical or physical property of the chemosensor), into an analytically suitable signal. Two very relevant features that a sensor has to exhibit are the specific interaction with the target analyte in the presence of other substances that may interfere, this is known as selectivity, and the least quantity of analyte that it is capable of distinguishing statistically from a blank (complete absence of analyte), known as sensitivity.<sup>29,31,32</sup>

Usually, a chemosensor comprised three main parts known as receptor, spacer and signalling subunit (see Figure 1.5).

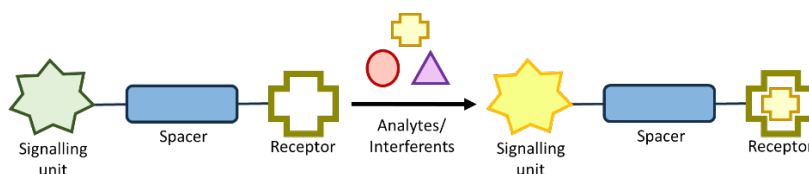


Figure 1.5. Schematic presentation of a chemosensor<sup>32</sup>

The receptor subunit is designed to provide a fast and reversible binding to the analyte. The spacer consists of a bridge between the other two subunits and, even, can exhibit an active function since its properties upon the molecular recognition may change, acting as a

transducer; however, this part is not compulsory to be present. Finally, the signalling unit is in charge of reporting the binding event through a measurable signal, such as a change in the absorbance or redox potential.<sup>29,32</sup>

### 1.2.3. Optical chemosensors

The molecular recognition in optical chemosensors should induce a change in the electromagnetic properties of the system. This event can be based on different optical principles such as absorbance, fluorescence, phosphorescence, reflectance, emitted light scattering or refractive index. As the apparatus involved in spectroscopic techniques are usually inexpensive, affordable and no high qualified personnel is required to use them, optical sensors have become more and more appealing over the years. In fact, their scope is so great that a large amount of wearable chemosensors has been developed for several purposes such as healthcare or human motion monitoring.<sup>33</sup>

Depending on the transduction mechanism, chemosensors can be classified in three main categories (see Figure 1.6).<sup>34,35</sup>

- Biding site-signalling subunit approach  
This category has been the most extensively used and it consists of the covalent linkage of the two subunits in such a way that the optical properties of the signalling one are modified after the recognition event.
- Displacement approach  
In this case, it is also involved the presence of two subunits, binding and signalling, but unlike the previous approach, here they are forming a supramolecular assembly. The addition of an analyte to these types of sensors triggers a displacement reaction, where the signalling subunit is released when the recognition takes place.

- Chemodosimeter approach

This last perspective involves irreversible interactions between the sensor and the analyte, contrary to the previous alternatives. Usually, this approach implies higher selectivity and sensitivity and promotes remarkable changes in the sensor optical properties.

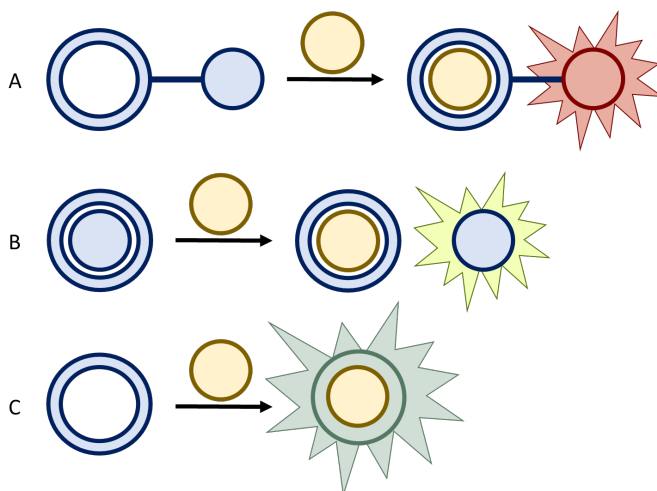


Figure 1.6. Cartoon representation of the three categories of chemosensors (A) binding-signalling subunit (B) displacement (C) chemodosimeter approach

#### 1.2.4. Receptor and Signalling Units

There are a large number of substances in which human beings are interested in detecting and, roughly speaking, they can be organised in three categories: cations, anions and neutral molecules. Due to the simplicity in their geometry and their key role in body, cations were the first ones in being successfully recognised. To do so, several macrocycles, acting as receptor units, were designed and synthesised in order to accommodate in their cavities those cations. Some examples of these structures are crown ethers, podands, lariat ethers and cryptands (see Chart 1.4), where the coordination with the cation is the basis of the detection process.<sup>28,36</sup>

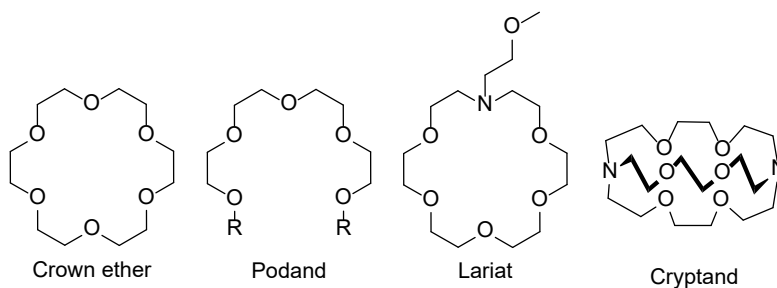


Chart 1.4. Some of the most common receptor units used to detect cations

Next milestone to achieve was anion detection. It took some time to do so due to the more complex geometry of anions. Several receptor units were designed with this purpose, and they were mostly based on the incorporation of appropriate functional groups to establish hydrogen bonds.<sup>28,29,36</sup> Numerous receptor units have been created over the years. Among them, groups such as thioureas, ureas, amides, guanidine and derivatives from pyrrole are the most common ones (see Chart 1.5), but also there are quite a few examples of metal complexes.<sup>28</sup>

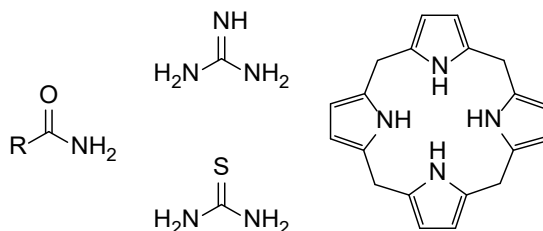


Chart 1.5. Some examples of receptor units to recognise anions

The last breakthrough to get involved with was the detection of neutral molecules. For this reason, different compounds with cavities that exhibited different properties, such as size and polarity, were synthesised. Some of these compounds are cyclodextrines, molecular tweezers, cucurbiturils and cyclophanes (see Chart 1.6).<sup>28,29</sup>



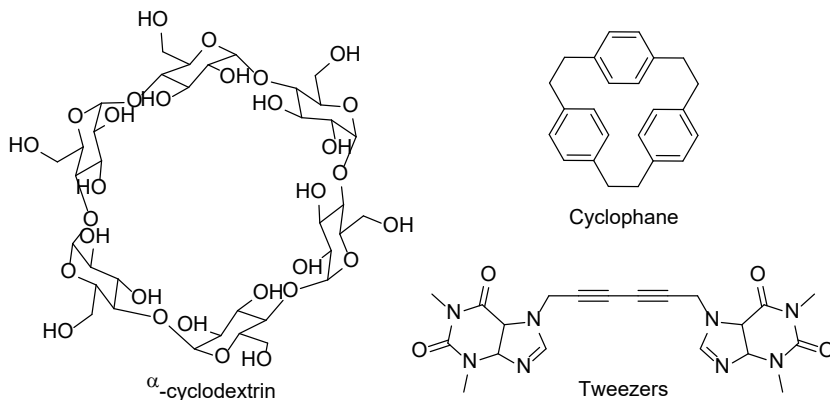


Chart 1.6. Structures of some common host units for neutral analytes

Signalling units are predominantly well-known dyes, such as derivatives from xantene (fluoresceine and rhodamine), pyrene, coumarin and BODIPY (4,4-difluoro-4-bora-3a,4a-diaza-s-indacene). These dyes present noticeable characteristics: well-known synthesis, tunable photophysical properties, usability in biologic systems or ability to show excimer or exciplex complexes. The structures of these examples are shown in Chart 1.7.

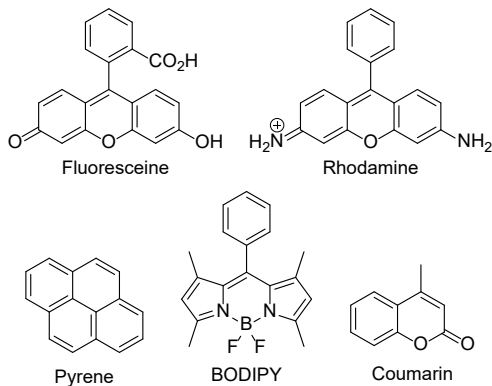


Chart 1.7. Chemical structures of some dye typically used as signalling units

### 1.3. GHB and Synthetic Cathinones detection

#### 1.3.1. GHB detection

Over the last few years, the number of reports regarding abuse drugs has increased gradually. For this reason, several chemosensors have been designed to detect both GHB and SCs.

On one hand, related to a chemosensor approach, Chang *et al.* developed a probe with a BODIPY core, compound A, to detect GHB (see Chart 1.8). The molecular recognition was based on the establishment of hydrogen bond interaction between the carboxylate present in GHB and the phenol moiety that contains the BODIPY derivative. The limit of detection (LoD) found for this sensor was 5 mg/mL.<sup>37</sup> Moreover, the same authors also reported another BODIPY chemosensor, compound B, to detect GBL (see Chart 1.8). In this case, the probe forms aggregates in aqueous media, quenching its fluorescence. Upon the addition of GBL, a disassembly took place and the fluorescence was restored. In this case, the LoD was 10 mg/mL.<sup>38</sup>

Sheng Lin *et al.* reported an iridium complex (compound C) that upon the addition of GHB exhibited a quenching of the initial fluorescence, being the LoD 0.15 mg/mL (see Chart 1.8).<sup>39</sup>

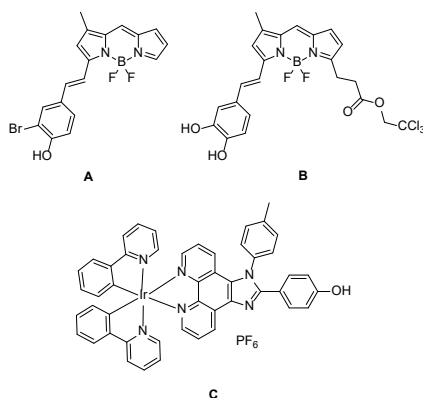
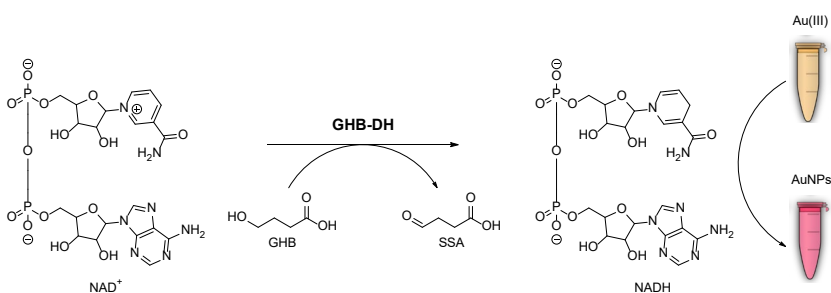


Chart 1.8. Chemosensors reported in literature to detect GHB

Following a different approach, García *et al.* developed a colorimetric sensor array. It included seven common dyes, which show a strong emission in the visible region upon the illumination with UV light. The recognition was based on the interaction of the cationic dyes, encapsulated in a cucurbituril derivative, with GHB.<sup>40</sup>

Another more recent sensor is related to an enzymatic process. Xing *et al.* developed a three-component system, which relied on the oxidation of GHB to succinic semialdehyde (SSA) through the action of GHB dehydrogenase and the concomitant reduction of  $\text{NAD}^+$  to NADH. This redox process promotes the reduction of a gold (III) complex to gold nanoparticles (AuNPs). All this process is depicted in Scheme 1.2.<sup>41</sup>



Scheme 1.2. Detection paradigm of GHB through the formation of AuNPs coupled to the oxidation of GHB to SSA<sup>41</sup>

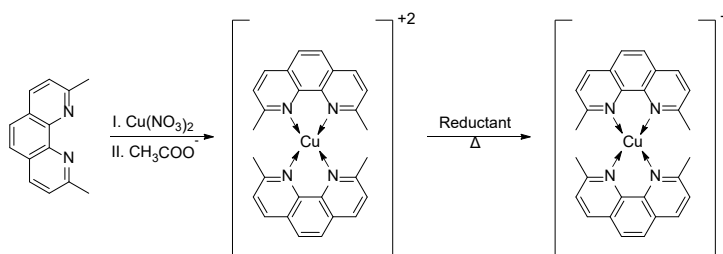
Finally, two new sensors employed on a solid support have been reported.<sup>42,43</sup> The first one is based on a polymeric matrix which contains a mixture of 10,12-Pentacosadiynoic acid (PCDA) and gabazine as sensing material. Due to the  $\pi$  conjugation system distortion of PCDA in the presence of GHB, a change of colour from blue to red was observed, allowing the authors (H. Kim *et al.*) to calculate a LoD of 9.6  $\mu\text{g/mL}$ .<sup>42</sup> The second sensor relied on a coordination displacement mechanism. Y. Kim *et al.* reported a BODIPY core probe which was coordinating a  $\text{Fe(III)}$  cation thanks to a carboxylate group as a binding unit and using cellulose acetate membrane filter as solid support. Upon the addition of GHB, this

Fe(III) was displaced and the initial optical properties of the probe were restored, recovering its initial absorbance and fluorescence. The LoDs calculated, provided by the authors in solution, were 0.25  $\mu\text{g/mL}$  (absorption) and 0.01  $\mu\text{g/mL}$  (fluorescence).<sup>43</sup>

### 1.3.2. Synthetic Cathinones detection

Some colorimetric tests have been developing to detect SCs in seized materials. Even though these tests have shown quite good sensitivity, that is not the case of selectivity. False-positive results can be obtained due to adulteration, diluents or contaminants.<sup>44–46</sup> Consequently, most of the detection methods are based on classical techniques such as LC-MS/MS (Liquid Chromatography with tandem Mass Spectrometry)<sup>47,48</sup> or LC-Q/TOF (Liquid Chromatography-Quadrupole/Time of Flight) mass spectrometry.<sup>49</sup> Nevertheless, these techniques are expensive, sample-destructive and the presence of well-trained personnel to use them is required.

Despite this, some colorimetric or fluorogenic probes have been recently reported in the literature.<sup>50–54</sup> The two first ones consist of the reduction of a Cu(II)-neocuprine complex by cathinones. Al-Obaid *et al.* reported the detection of cathinone without any type of functionalization,<sup>50</sup> meanwhile Philp *et al.* reported the detection of 4-MMC (mephedrone) and a large quantity of SCs. The redox reaction proposed for these last authors is summarised in Scheme 1.3.<sup>51</sup>



Scheme 1.3. Reaction equation for the formation of the Cu(I):neocuprine<sub>2</sub> complex<sup>51</sup>

Yen *et al.* reported bovine serum albumin-stabilized gold nanoclusters<sup>52</sup> and carbon dots functionalized papers<sup>53</sup> as photoluminescent probes, whose LoD were 0.14 mM. These systems were based on a fluorescence quenching due to the ability of cathinones to act as a reducing agent. Another example found in the literature was reported by Huang *et al.*<sup>54</sup> The authors synthesized a MIP (Molecular Imprinted Polymer), which comprised in its structure an TPE (tetraphenylethylene) derivative. Thanks to the AIE (Aggregation-Induced Emission) phenomenon, the probe showed an enhancement of its fluorescence in the presence of cathinones.

In the light of everything that has been said above, the development of reliable, real-time, inexpensive and user-friendly chemosensors is vital due to the current concerns regarding the increasing number of criminal acts related to drugs, from their illegal synthesis, distribution and consumption to their use in chemical submission to take advantage of victim's vulnerability. This will allow our society to confront these criminal acts from several different strands: personal, health care services and law enforcement agencies.



## **Chapter 2: GHB detection through the use of ditopic ligands**





## 2.1. Introduction

Molecular recognition, as it has been mentioned in previous chapter, is based on the complementarity between both host or receptor subunit and the analyte of interest. In order to gain selectivity, specially in complex matrices such as human fluids, and create a more efficient chemosensor, the development of ligands with more than one interaction point has been broadly explored. The principal purpose in creating ditopic ligands is to provide the molecule with a dual host system, improving not only complexation selectivity, but also sensing.<sup>55,56</sup> Among them, our interest is focused on molecular sensors that present two remote binding sites. Several examples of ditopic probes have been described in the literature to detect metal cations such as Cd(II),<sup>57</sup> Cu(I),<sup>58</sup> Al(III),<sup>59</sup> or K(I)<sup>60,61</sup> because of their industrial interest or toxic effects on human health.

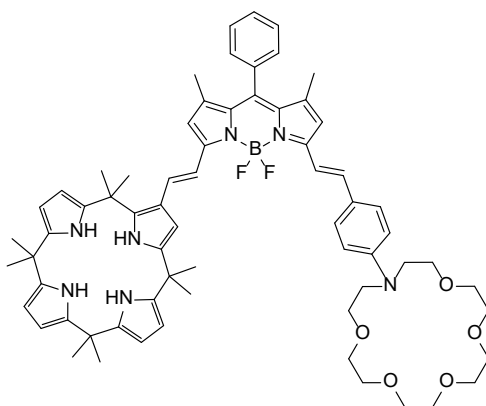


Chart 2.1. Example of a ditopic ligand used in sensing filed<sup>60,61</sup>

One of these examples is depicted in Chart 2.1. The authors reported a heteroditopic chemosensor based on a BODIPY core with two host units: a calix[4]pyrrole and a 16-azacrown-6 cycles. Initially, this probe was tested as a logic gate, in which K(I) and fluoride were the chemical inputs when interacted with the azacrown and the calixpyrrole, respectively.<sup>60</sup> Additionally, this heteroditopic chemosensor proved to be able to detect not only ion pairs, but also

zwitterionic species with the appropriate length, such as the GABA neurotransmitter.<sup>61</sup>

Normally, most of the compounds used as receptor units contain some heteroatoms such as nitrogen, oxygen, phosphorus and/or sulphur, grouped in different cores like phenanthrolines,  $\beta$ -diketone, phosphole and thiophene moieties, among many others, thanks to their coordinating properties.<sup>55</sup> Some of these coordinating moieties are shown in Chart 2.2.

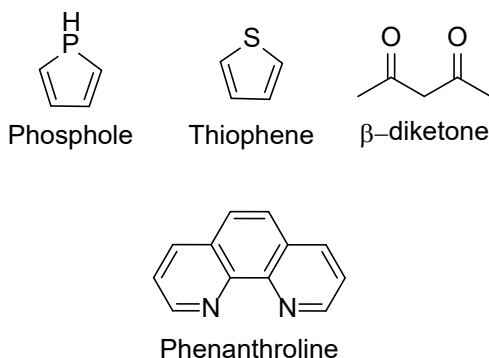


Chart 2.2. Some examples of binding units used in ditopic ligands

## 2.2. Ditopic ligands design

A little family of heteroditopic chemosensors was designed, which comprised a thiourea moiety and a trifluoroacetyl group as host units. The selection of these functional groups was based on their well-established capabilities as recognition moieties. On one hand, as it was mentioned in the previous chapter, thioureas have been widely employed to interact with carboxylates, showing several coordination modes with them: the formation of hydrogen bonds, an acid-base reactions or, even, taking place both at the same time during the recognition event (see Chart 2.3).<sup>62-64</sup> On the other hand, trifluoroacetyl group has been widely used as fluorinating agent to increase the reactivity of some functional groups due to its remarkable electrophilicity.<sup>65,66</sup> This fact makes it considerably appropriate to recognise nucleophiles such as hydroxyl and amine

## Chapter 2: GHB detection through the use of ditopic ligands

groups through the formation of hemiacetals or hemiaminals, respectively.<sup>67,68</sup>

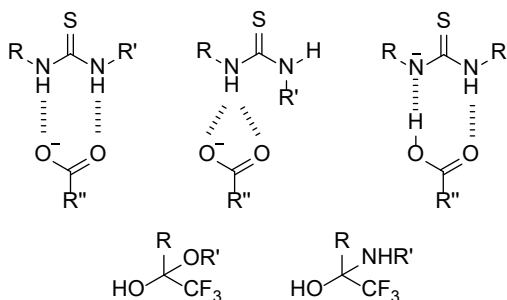


Chart 2.3. Different coordination modes of thioureas with carboxylates and reaction of trifluoroacetyl group with alcohols and amines

Considering what it has been explained so far, ligands **2.1** and **2.2** were designed and synthesized. Since we were interested in exploring how the rigidity properties of the linker affected GHB recognition, the use of an aliphatic chain or a cyclohexane moiety as bridge was decided (see Chart 2.4).

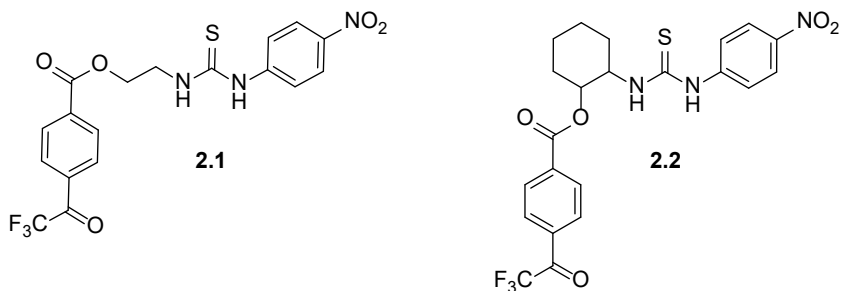
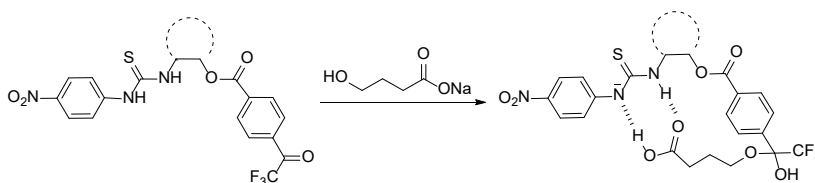


Chart 2.4. Ditopic probes initially designed to detect GHB

### 2.3. Objectives

Since the target molecule, GHB, presents two functional groups in its structure and it will be found in a competitive media, such as drinks, the main goal in this chapter is to increase the selectivity of the probes by including in their structures two binding units, providing each of them the appropriate complementarity to detect GHB. To do so, this objective was divided into three specific ones:

- Synthesis of the two heteroditopic chemosensors (compounds **2.1** and **2.2**).
- Analyzing the recognition event using UV-Visible and  $^1\text{H}$  NMR spectroscopies.
- Study the potential interferents present in drinks and determine GHB in different beverages.



Scheme 2.1. Proposal of the GHB detection mechanism

## 2.4. Heteroditopic chemosensor to detect $\gamma$ -hydroxybutyric acid (GHB) in soft drinks and alcoholic beverages

Silvia Rodríguez-Nuévalos<sup>a,b</sup>, , Margarita Parra<sup>a,b,c</sup>, Salvador Gil<sup>a,b,c</sup>, Pablo Gaviña<sup>a,b,c</sup>, Pau Arroyo<sup>a,b</sup>, Jose A. Sáez<sup>a,b</sup>, , Ana M. Costero<sup>a,b,c\*</sup>

<sup>a</sup>Instituto Interuniversitario de Investigación de Reconocimiento Molecular y Desarrollo Tecnológico (IDM). Universitat Politècnica de València, Universitat de València, Doctor Moliner 50, Burjassot, 46100, Valencia, Spain.

<sup>b</sup>Departamento de Química Orgánica, Universitat de València, Doctor Moliner 50, Burjassot, 46100, Valencia, Spain.

<sup>c</sup>CIBER de Bioingeniería, Biomateriales y Nanomedicina (CIBER-BBN) (Spain)

\* Correspondence: ana.costero@uv.es

**Received:** 18th June 2021

**Accepted:** 5th August 2021

*Analyst*, **2021**, 146, 5601-5609



## **Abstract**

Drug-Facilitated Sexual Assault (DFSA) is a problem of considerable dimensions on a global scale. Among the different compounds used in DFSA assaults, 4-hydroxybutyric acid (GHB) is one of the most elusive due to its physical and biological characteristics. Therefore, the development of real-time detection methods to detect GHB not only in drinks but also in urine is very important for personal and social security. Here, we report two new heteroditopic chemosensors capable of recognizing and detecting GHB in soft drinks, alcoholic beverages and synthetic urine. The compounds have two moieties: a trifluoroacetyl group and a thiourea, which are able to interact respectively with the hydroxyl and the carboxylic groups present in the GHB structure. In addition, the distance between these two groups has been optimized to allow a double interaction which guarantees the recognition even in very competitive media such as beverages or urine samples.

## **Introduction**

Consumption and abuse of drugs is a general problem that concerns our entire society and, as a consequence, the authorities and certain state agencies are developing concrete plans to detect and stop the illegal trafficking of these substances. However, the development of procedures to increase the safety of potential victims of assaults by chemical submission has received less attention. Specifically, the practice of sexual crimes associated with drug use, called Drug-Facilitated Sexual Assault (DFSA), is a problem of considerable dimensions on a global scale. According to a report published by the National Center for Injury Prevention and Control Division of Violence Prevention, approximately 11 million women in the United States between 2010 and 2012 have been raped while they were drunk or drugged.<sup>1</sup> There have been identified different compounds used in DFSA assaults but among them, 4-hydroxybutyric acid (GHB) is one of the most elusive. GHB is an odorless, colourless and slightly salty liquid, which is almost undetectable in drinks and is, therefore, widely used to carry out this type of aggression. It is one of those preferred by the aggressors, due to the short time it needs to take

effect and how quickly it disappears from the victim's body.<sup>2</sup> More specifically, GHB is metabolized with an elimination half-life of 20–42 min and remarkable low quantities are excreted without further change in urine (1-5%). In therapeutic doses (12.5–50 mg/kg), GHB is completely eliminated from blood within 2–8 h and it is possible to recover it from urine in a period of 8–12 h.<sup>3</sup> Therefore, the development of real-time detection methods to detect GHB in drinks is very important for personal safety and, in consequence, beneficial for the society.

Following the chemosensor approach, not many methods have been reported to detect GHB. Thus, Chang *et al.* reported the use of compound A (Chart 1) as a chemosensor to detect GHB. The interaction with the analyte was based on a hydrogen bond interaction between the phenol group in the sensor and the carboxylate unit in GHB.<sup>4</sup>

Additionally, the same authors also reported the use of compound B to detect the corresponding lactone (GBL) and the interaction was related to the formation of a hydrogen bond.<sup>5</sup> On the other hand, Sheng Lin and Dik-Lung Ma prepared complex C (Chart 1) which was able to detect GHB (Chart 1).<sup>6</sup> The complex showed a luminescence quenching in presence of the analyte that was observed using UV light. Recently, our research group has published the synthesis of two naphthoxazol derivatives (D and E) able to detect GHB in alcoholic beverages<sup>7</sup> through an acid-base reaction that induced colour changes in one case and fluorescence enhancement in the other. Even though all these probes have given rise to interesting detection results, they present limited selectivity due to the recognition mechanism (hydrogen bond formation or acid-base reaction). In fact, both interactions are too unspecific and they could give rise to false positive responses in some cases.

Following a different approach, Bravo *et al.*<sup>8</sup> described the use of  $\gamma$ -hydroxybutyrate dehydrogenase (GHB-DH) to detect GHB. Enzymatic oxidation of GHB by NAD<sup>+</sup> is coupled with the reduction of a dye that shows a change of colour. Ethanol is an interferent that can be avoided by drying the sample to be studied.



## Chapter 2: GHB detection through the use of ditopic ligands

On the other hand, classical analytical methods based on more expensive techniques such as GC/MS, GC/FTIR and GC/FIR (Finite Impulse Response filter) have also been developed.<sup>3</sup>

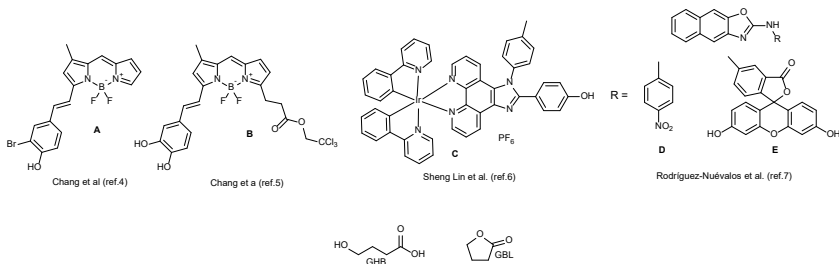


**Chart 1.** Compounds used in the literature to recognize GHB.

Taking into account these precedents and given our expertise in the design, synthesis and evaluation of chemosensors and probes for other different biologically active species,<sup>9-11</sup> we decided to explore the use of ditopic probes. The presence in the probe of two functional groups separated by a suitable spacer and able to interact with both, the hydroxyl and the carboxylic groups present in the GHB, will increase selectivity (Chart 2). This double interaction would avoid the limitations stated above for the previously reported probes and permit to carry out the recognition in a highly competitive media such as beverages or urine (a comparative table with the previously reported probes has been included in the supporting information).

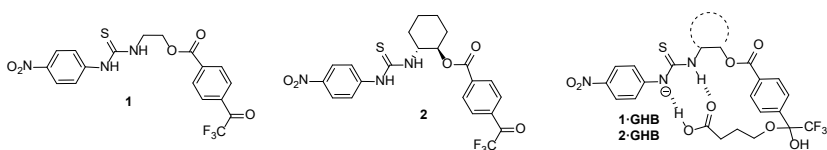


**Chart 2.** Chemosensors **1** and **2** designed to recognize GHB and proposed mode of interaction.

## Experimental

### Material and methods

The reagents employed in the synthesis were acquired in Sigma Aldrich and used without further purification. Synthetic urine was supplied by Vimarlabs.  $^1\text{H}$  NMR,  $^{13}\text{C}$  NMR and  $^{19}\text{F}$  NMR spectra were registered with Bruker Advance 300 MHz, 400 MHz or 500 MHz spectrophotometers, all of them referenced to solvent peak, DMSO- $d_6$  or THF- $d_3$ . UV-Vis spectra were registered with a Shimadzu UV-2600 spectrophotometer, using a cuvette with 1 cm of path length. Mass spectrometry spectra were carried out with a TripleTOFTM 5600 LC/MS/MS System, with 2 gas sources (both to 35 psi), 450 °C and ion gas voltage of 5500 V. Origin 2020 was the program to plot titrations and calculate complexation constants.

### Synthesis of the chemosensors

#### Synthesis of compound 4a

Ethanolamine (**3a**) (500  $\mu\text{L}$ , 8.31 mmol) in 10 mL of MeOH and 1400  $\mu\text{L}$  of  $\text{NEt}_3$  (9.97 mmol) were stirred and  $\text{Boc}_2\text{O}$  (2300  $\mu\text{L}$ , 9.97 mmol) was added dropwise. The mixture was stirred overnight. Next, MeOH was removed under vacuum and the resulting colourless oil was dissolved in 30 mL of AcOEt. The organic phase was washed with deionized water (2 x 15 mL) and brine (15 mL), dried over  $\text{MgSO}_4$ , filtered and the solvent was removed to vacuum to yield compound **4a** as a white powder (676 mg, 50% yield).  $^1\text{H}$  NMR (300 MHz, DMSO)  $\delta$  6.67 (t,  $J = 5.9$  Hz, 1H), 4.56 (t,  $J = 5.6$  Hz, 1H), 3.34 (q,  $J = 6.6, 5.6$  Hz, 2H), 2.97 (q,  $J = 6.6, 5.9$  Hz, 2H), 1.37 (s, 9H).

#### Synthesis of compound 5a

4-(Trifluoroacetyl)benzoic acid (807 mg, 3.70 mmol), DMAP (452 mg, 3.70 mmol) and EDC (660  $\mu\text{L}$ , 3.70 mmol) were dissolved in 10 mL of dry THF under argon atmosphere. After 45 min of stirring, 500 mg of **4a**, dissolved in 10 mL of dry THF were added. The mixture was kept stirring for 2 days. After that, THF was removed under vacuum. The yellow oil was dissolved in 30 mL of AcOEt. The organic phase was washed with 15 mL of 1% aqueous HCl,  $\text{NaHCO}_3$  (sat) (2 x 15 mL) and

NaCl (sat) (15 mL), dried over anhydrous  $\text{MgSO}_4$  and filtered. After the solvent evaporation, 1 g of compound **5a** was obtained as a white powder (90% yield).  $^1\text{H}$  NMR (300 MHz,  $\text{DMSO-}d_6$ )  $\delta$  8.01 (d,  $J$  = 8.3 Hz, 2H), 7.76 (s, 2H, OH), 7.73 (d,  $J$  = 8.3 Hz, 2H), 7.07 (t,  $J$  = 5.9 Hz, 1H), 4.24 (t,  $J$  = 5.3 Hz, 2H), 3.35 – 3.27 (m, 2H), 1.36 (s, 9H).  $^{19}\text{F}$  NMR (282 MHz, DMSO)  $\delta$  -70.90, -82.78.

#### Synthesis of compound 6a

**5a** (1 g, 2.77 mmol) and 1 mL of TFA (13.06 mmol) were stirred in 4.5 mL of dry DCM for 15 min under argon atmosphere. Then, solvent was removed and compound **6a** was obtained as a colourless oil (616 mg, 60% yield).  $^1\text{H}$  NMR (300 MHz,  $\text{DMSO-}d_6$ )  $\delta$  8.31 (d,  $J$  = 8.5 Hz, 1.35H), 8.17 (d,  $J$  = 8.5, 1.3H), 8.11 (d,  $J$  = 8.5 Hz, 0.7H), 7.75 (d,  $J$  = 8.5 Hz, 0.7H), 4.57 – 4.34 (m, 2H), 3.26 (p,  $J$  = 5.7 Hz, 2H).  $^{19}\text{F}$  NMR (282 MHz, DMSO)  $\delta$  -70.91, -74.87, -82.77.

#### Synthesis of compound 1

**6a** (566 mg, 2.17 mmol) and 4-nitrophenyl isothiocyanate (323 mg, 1.81 mmol) were dissolved in 20 mL of pyridine under argon atmosphere and stirred for 2 days. Next, solvent was removed to vacuum and the yellow oil was dissolved in 30 mL AcOEt, washed with aqueous HCl 1 M (15 mL),  $\text{NaHCO}_3$  (sat) (2 x 15 mL) and NaCl (sat) (15 mL). The organic phase was dried over  $\text{MgSO}_4$ , filtered and the solvent removed to vacuum. The yellow powder was purified by chromatographic column using as eluent hexane: AcOEt (from 7:3 to 6:4). 400 mg of compound **1** were isolated as a yellow powder (50% yield).  $^1\text{H}$  NMR (500 MHz,  $\text{DMSO-}d_6$ )  $\delta$  10.76 (s, 0,2H), 10.24 (s, 0,8H), 8.50 (s, 1H), 8.23 (d,  $J$  = 9.2 Hz, 0,35H), 8.16 (d,  $J$  = 9.2 Hz, 1.65H), 8.06 (d,  $J$  = 8.5 Hz, 2H), 7.84 (d,  $J$  = 8.9 Hz, 0,35H), 7.80 (d,  $J$  = 9.2 Hz, 1.65H), 7.76 (d,  $J$  = 8.7 Hz, 4H), 4.48 (t,  $J$  = 5.3 Hz, 2H), 3.96 – 3.89 (m, 2H).  $^{19}\text{F}$  NMR (282 MHz, DMSO)  $\delta$  -70.87, -82.73.  $^{13}\text{C}$  NMR (126 MHz, DMSO)  $\delta$  180.6, 165.4, 146.2, 143.6, 142.0, 130.3, 128.9, 127.8, 124.5, 122.1, 120.7, 115.5, 92.4, 63.1, 42.9. HRMS (ESI):  $m/z$  calculated for  $\text{C}_{18}\text{H}_{17}\text{F}_3\text{N}_3\text{O}_6\text{S}$  ( $\text{M}+1 + \text{H}_2\text{O}$ ): 460.0790; found: 460.0778 [ $\text{M}+1+\text{H}_2\text{O}$ ] $^+$ .

Synthesis Compound 4b

**3b** (500 mg, 3.30 mmol) and Na<sub>2</sub>CO<sub>3</sub> (842 mg, 7.91 mmol) were stirred in 50 mL of MeOH for 30 min and, then Boc<sub>2</sub>O (910 μL, 3.96 mmol) was added dropwise. Stirring was kept overnight at room temperature. Next, MeOH was removed to vacuum and 30 mL approximately of deionized water was added. The aqueous phase was extracted with AcOEt (3 x 20 mL), dried over anhydrous MgSO<sub>4</sub>, filtered and the solvent was removed to vacuum. Compound **4b** was obtained as a white powder (635 mg, 89 % yield). <sup>1</sup>H NMR (300 MHz, DMSO-*d*<sub>6</sub>) δ 6.48 (d, J = 7.8 Hz, 1H), 4.46 (d, J = 5.1 Hz, 1H), 3.16 (dq, J = 9.4, 4.5 Hz, 1H), 3.14 – 2.95 (m, 1H), 1.87 – 1.70 (m, 2H), 1.63 – 1.49 (m, 2H), 1.37 (s, 9H), 1.24 – 0.93 (m, 4H).

Synthesis Compound 5b

365 mg of 4-(trifluoroacetyl)benzoic acid (1.67 mmol), DMAP (202 mg, 1.67 mmol) and EDC (300 μL, 1.67 mmol) were mixed in 10 mL of dry THF under argon atmosphere for 30 min. Then, 300 mg of **4b** (1.39 mmol) dissolved in 10 mL of dry THF were added dropwise. Stirring was kept for 2 days. Next, THF was removed to vacuum and the yellow oil was dissolved in 20 mL of AcOEt. The organic phase was washed with aqueous HCl 1% (2 x 10 mL), NaHCO<sub>3</sub> (sat) (2 x 10 mL) and NaCl (sat) (10 mL); then, it was dried over anhydrous MgSO<sub>4</sub>, filtered and AcOEt was removed to vacuum. 524 mg of compound **5b** were isolated (91% yield). <sup>1</sup>H NMR (300 MHz, DMSO-*d*<sub>6</sub>) δ 7.97 (d, J = 8.5 Hz, 1H), 7.74 (s, 1H), 7.73 (s, 1H), 7.69 (d, J = 8.5 Hz, 1H), 6.84 (d, J = 9.3 Hz, 1H), 4.64 (td, J = 10.1, 4.2 Hz, 1H), 3.71 – 3.50 (m, 1H), 2.14 – 2.02 (m, 1H), 1.85 – 1.62 (m, 3H), 1.48 – 0.92 (m, 13H). <sup>19</sup>F NMR (282 MHz, DMSO) δ -70.94, -82.88.

Synthesis Compound 6b

**5b** (201 mg, 0.48 mmol) and TFA (1 mL, 13.06 mmol) were dissolved in 5 mL of dry DCM under argon atmosphere. The mixture was stirred for 15 min and, then, solvent was removed under vacuum. The colourless oil was dissolved in 15 mL of AcOEt and the organic phase was washed with Na<sub>2</sub>CO<sub>3</sub> (sat) (2 x 10 mL) and NaCl (sat) (10 mL),

dried over anhydrous  $\text{MgSO}_4$  and filtered. After the evaporation, compound **6b** was obtained as a white powder (121 mg, 80 % yield).  $^1\text{H}$  NMR (300 MHz,  $\text{DMSO-}d_6$ )  $\delta$  8.02 (d,  $J = 8.4$  Hz, 2H), 7.77 (s, 2H), 7.74 (d,  $J = 8.4$  Hz, 2H), 4.62-4.50 (m, 1H), 2.84 – 2.69 (m, 1H), 1.85 (d,  $J = 10.9$  Hz, 1H), 1.80 – 1.54 (m, 3H), 1.48 – 1.18 (m, 4H).  $^{19}\text{F}$  NMR (282 MHz,  $\text{DMSO}$ )  $\delta$  -70.87, -82.72.

### Synthesis compound 2

A mixture of 4-nitrophenyl isothiocyanate (52 mg, 0.29 mmol) and **6b** (110 mg, 0.35 mmol) was stirred in 5 mL of pyridine under argon atmosphere for 2 days. Next, pyridine was removed under vacuum and the yellow oil was dissolved in 15 mL of  $\text{AcOEt}$ . The organic phase was washed with  $\text{HCl}$  1 M (10 mL),  $\text{NaHCO}_3$  (sat) (10 mL) and  $\text{NaCl}$  (sat) (10 mL), dried over anhydrous  $\text{MgSO}_4$  and filtered.  $\text{AcOEt}$  was removed under vacuum and the yellow powder was purified by chromatographic column using hexane:  $\text{AcOEt}$  as eluent (from 7:3 to 4:6). 68 mg of compound **2** as a yellow powder were obtained (47 % yield).  $^1\text{H}$  NMR (300 MHz,  $\text{DMSO-}d_6$ )  $\delta$  10.09 (s, 1H), 8.45 (d,  $J = 8.5$  Hz, 1H), 8.28-8.10 (m, 2H), 8.04 (d,  $J = 9.2$  Hz, 2H), 7.73 (d,  $J = 3.5$  Hz, 1H), 7.65 (d,  $J = 9.2$  Hz, 2H), 5.00 (dt,  $J = 10.1, 5.2$  Hz, 1H), 4.64 (m, 1H), 2.19-2.03 (m, 2H), 1.74 (m, 2H), 1.65 – 1.26 (m, 4H).  $^{19}\text{F}$  NMR (282 MHz,  $\text{DMSO}$ )  $\delta$  -70.45, -82.28.  $^{13}\text{C}$  NMR (126 MHz,  $\text{DMSO}$ )  $\delta$  178.0, 179.9, 179.6, 179.4, 165.1, 164.3, 146.3, 143.5, 141.7, 135.5, 132.9, 130.5, 130.1, 130.0, 128.8, 127.8, 125.2, 124.4, 122.1, 120.2, 118.2, 117.3, 115.5, 115.0, 92.36, 75.8, 74.9, 55.7, 54.9, 30.4, 30.3, 30.1, 23.6, 23.3. HRMS (ESI):  $m/z$  calculated for  $\text{C}_{22}\text{H}_{23}\text{F}_3\text{N}_3\text{O}_6\text{S}$  ( $\text{M}+1 + \text{H}_2\text{O}$ ): 514.1260; found: 514.1236 [ $\text{M}+1 + \text{MeOH}$ ] $^+$ .

### General procedure for GHB titration

In a 3 mL cuvette (1 cm of path of length), 2475  $\mu\text{L}$  of  $\text{DMSO}$  were mixed with 25  $\mu\text{L}$  of a 1 mM solution of the sensor in  $\text{DMSO}$ . After that, increasing quantities of  $\text{NaGHB}$  (from a 2,5 mM solution in  $\text{DMSO}$ ) were added until arriving to saturation point.

### Interference studies

In a 3 mL cuvette (1 cm of path length), 30  $\mu\text{L}$  of 1 mM solution of sensor in DMSO were mixed with each interferent (0.3% w/v citric acid, 0.01% w/v sodium ascorbate and 10% sucrose).and diluted to 3000  $\mu\text{L}$  with DMSO.

### **Real Samples Analysis**

#### Beverage samples

In first place, alcoholic drinks were contaminated with NaGHB in a 54 mM concentration. After that, an aliquot of 100  $\mu\text{L}$  was taken and mixed with 100  $\mu\text{L}$  of  $\text{NaHCO}_3$  0.4 mM. Then, 50  $\mu\text{L}$  of this solution was taken and mixed, at room temperature, with 300  $\mu\text{L}$  of sensor solution (1 mM in DMSO) and 650  $\mu\text{L}$  of DMSO. The same process was followed for the samples without GHB. The changes were observed immediately.

#### Urine samples

5 ml of synthetic urine was contaminated with increasing amounts of NaGHB 2, 3, 4, 6, 10 mM (for a final concentration of 10, 15, 20, 30 and 50 mM). The sample was passed through a C18 standard pre-column that later was washed with MeOH and  $\text{H}_2\text{O}$  and. All the phases were mixed and lyophilized. After that, the residue was resolved in 1 ml of water and an aliquot of 10  $\mu\text{L}$  was taken and mixed with 10  $\mu\text{L}$  of  $\text{NaHCO}_3$  1 mM. This solution was mixed, at room temperature, with 100  $\mu\text{L}$  of sensor solution (1 mM in DMSO) and 2380  $\mu\text{L}$  of DMSO. The changes were observed immediately.

### **Theoretical calculations**

All calculations presented have been carried out with the restricted formalism of Xu and Goddard X3LYP<sup>12</sup> DFT hybrid functional together with 6-31+G(d,p) split-valence basis set. To take into account the effect of the solvent, DMSO, PCM solvation model was used.<sup>13</sup> Over the optimized structures of the stationary points found, a frequency calculation was performed to ensure that no imaginary frequencies were present. To explore the electronic transitions responsible for

the UV-Vis spectra, vertical excitation energies were computed over X3LYP/6-31+G(d,p)/PCM(DMSO) optimized geometries through single-point TD-DFT<sup>14,15</sup> calculation in solution (30 states, singlets only) using non-equilibrium formalism at the same theory level. All calculations were carried out using Gaussian 09 rev. D.01<sup>16</sup> program package.

## Results and Discussion

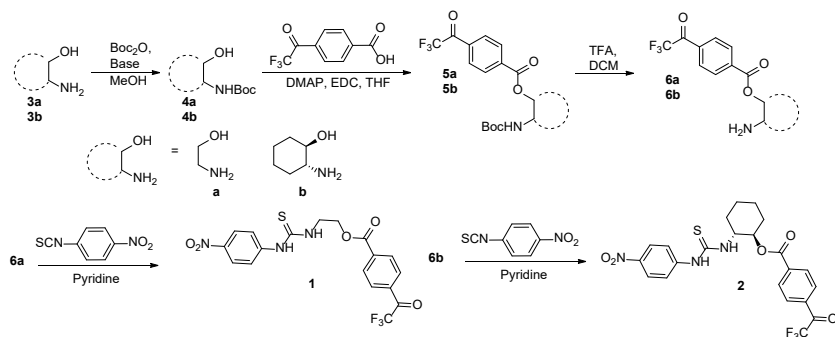
Compounds **1** and **2** were prepared following the pathways summarized in Scheme 1. The starting material in the synthesis of compound **1** was ethanolamine whereas trans-2-aminocyclohexanol was used for the preparation of compound **2**. In both synthetic pathways, the amine group in the starting aminoalcohol derivatives was converted into its corresponding Boc derivative.<sup>17</sup>

From these compounds, the esters of the 4-trifluoroacetyl benzoic acid were prepared using EDC as coupling agent.<sup>18</sup> The Boc-protected amines were then hydrolysed with trifluoroacetic acid and the corresponding free amines converted into the corresponding thioureas by reaction with 4-nitrophenylisothiocyanate.<sup>19</sup> The structure of chemosensors **1** and **2** were established using <sup>1</sup>H, <sup>19</sup>F and <sup>13</sup>C NMR spectroscopy and HRMS (see Supporting Information).

<sup>1</sup>H NMR studies show that, in DMSO-*d*<sub>6</sub> solutions, compound **1** appears as a mixture of two rotamers in a ratio around 1:5, meanwhile only one rotamer is observed in compound **2** in DMSO-*d*<sub>6</sub>. This different behaviour could be related to the rigidity induced by cyclohexyl ring in compound **2**. Additionally, a study in THF-*d*<sub>8</sub> was carried out which brought out in both chemosensors a mixture of rotamers in different ratios: around 1:5 for compound **1** and 0.7:1 in the case of compound **2**. The different results obtained for compound **2** depending on the solvent could be due to the higher viscosity of DMSO-*d*<sub>6</sub> when compare with THF- *d*<sub>8</sub>. In both solvents, NOESY experiments (Figures S3, S6, S9 and S12 in the Supporting Information) strongly suggest an *Z,Z* geometry for the major rotamer. In addition, <sup>19</sup>F NMR spectra indicate that the trifluoroacetyl group

appears partially as its corresponding hydrate form ( $\delta$  around -82 and -70 ppm for the hydrate and carbonyl form, respectively).

Finally, UV spectra of compounds **1** and **2** in DMSO solutions show absorption bands at 360 nm ( $\epsilon = 15970 \text{ M}^{-1} \text{ cm}^{-1}$ ) and 359 nm ( $\epsilon = 16700 \text{ M}^{-1} \text{ cm}^{-1}$ ), respectively.



**Scheme 1.** Synthetic pathway to prepare **1** and **2**

## Detection studies

UV-vis spectra of compounds **1** and **2** ( $10 \mu\text{M}$  in DMSO) show clear changes when GHB sodium salt ( $\text{NaGHB}$ ) ( $100 \mu\text{M}$ ) is present in the medium. Thus, whereas both probes show a band at 360 nm, in addition to this band, a new absorption band around 480 nm appears for both compounds in the presence of excess  $\text{NaGHB}$  (10 equiv.) with the immediate change of colour from yellow to dark orange (see Figure 1 for compound **1** and Figure S15 in the Supporting Information for compound **2**).

The appearance of this new band and the change of colour clearly indicate that, under these conditions,  $\text{NaGHB}$  interacts with the prepared sensors. In order to have more information about the interaction process,  $^1\text{H}$  and  $^{19}\text{F}$  NMR experiments were carried out.



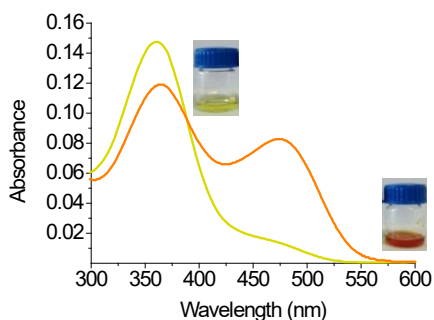


**Fig. 1.** (yellow) Spectrum of compound **1** (10  $\mu\text{M}$  in DMSO,  $\lambda=360$  nm), (orange) the same solution in presence of NaGHB (10 eq.) ( $\lambda_{\text{max}}=360$  nm,  $\lambda_{\text{max}}=475$  nm). Inside: visual changes observed in the sample from yellow (free probe) to orange (probe in presence of 10 eq. of NaGHB)

Both compounds exhibit substantial changes, both in  $^1\text{H}$  and  $^{19}\text{F}$  NMR spectra, after the addition of NaGHB.  $^1\text{H}$  NMR spectra indicate that the interaction between the NaGHB takes place with both the rotamers present in the solution as suggested by the disappearance of the signals corresponding to the other rotamer. On the other hand, the most important variation is induced for  $\text{H}_c$  and  $\text{H}_d$  signals (10.09 ppm and 8.45 ppm), as they become so broad singlets that they practically blend into the baseline (see Figure 2). In addition, the peak of  $\text{H}_b$  appears downfield shifted (from 7.80 ppm to 8.03 ppm) which is in accordance with the interaction between the thiourea group and the carboxylate group. The effect of this interaction affects  $\text{H}_a$ , in a lesser extent, as its signal is upfield shifted 0.03 ppm. The aliphatic signals confirm the presence of one rotamer as well. An upfield shift is observed for both signals corresponding to the methylene bound to the ester (from 4.48 ppm to 4.43 ppm) and for the methylene group linked to the thiourea nitrogen (from 3.94 ppm to 3.90 ppm).

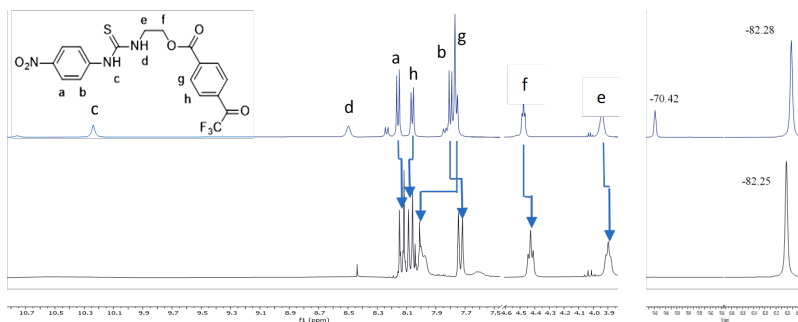


**Fig. 2.** Changes observed in  $^1\text{H}$  and  $^{19}\text{F}$  NMR spectra of **1** in presence of an excess of NaGHB in  $\text{DMSO-}d_6$

In the trifluoroacetyl-substituted aromatic ring,  $\text{H}_h$  is downfield shifted ( $\Delta\delta = 0.01$  ppm) whereas  $\text{H}_g$  is upshifted ( $\Delta\delta = 0.03$  ppm). These changes on the trifluoroacetyl ring suggest that the hemiacetal generation is possible. This suggestion is reinforced by the  $^{19}\text{F}$  NMR spectra, which show a clear difference when compound **1** interacts with GHB. Thus, whereas two peaks at  $-70.42$  ppm and  $-82.28$  ppm (ketone and hydrate of trifluoroacetyl group, respectively) appear in the spectrum of the probe, on addition of NaGHB, these two peaks disappear to generate a new signal at  $-82.25$  ppm. All these data clearly support the formation of the correspondent hemiacetal between trifluoromethylacetyl group of **1** and the alcohol group of NaGHB. Similar changes were obtained for compound **2** (see Supporting Information, Figures S16 and S17).

### Sensitivity studies

UV-vis titration experiments with NaGHB (from 0.1 eq. to saturation point) were carried out in  $10\ \mu\text{M}$  DMSO solutions of compounds **1** or **2** (Figure 3 and S18, respectively). From these experiments, a 1:1 stoichiometry for the complexes was determined and the corresponding complexation constants were established using the equation described in the Supporting Information. The limits of detection (LoD) for both compounds were determined as  $3 \cdot S_b/m$ , where  $S_b$  is the blank standard deviation and  $m$  is the slope obtained

during the titration. (Figure 4 and S19). These results are summarized in Table 1.

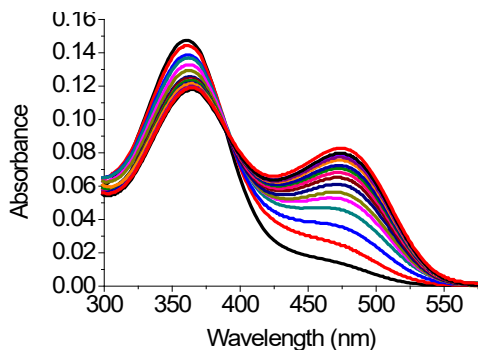


**Fig. 3.** Absorption titration spectra of **1** (10  $\mu\text{M}$ ) with increasing amounts of NaGHB (0-43  $\mu\text{M}$ ) in DMSO.

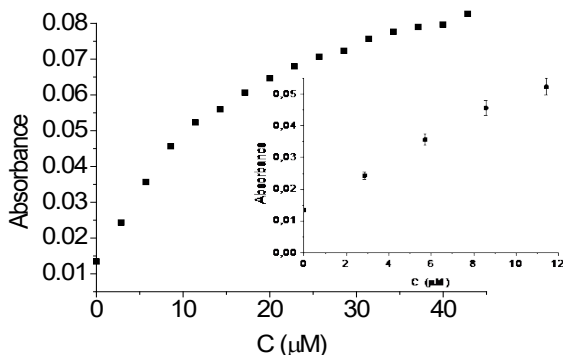


**Fig. 4.** Titration of **1** (10  $\mu\text{M}$ , DMSO  $\lambda = 475 \text{ nm}$ ) with increasing amounts of NaGHB (0-43  $\mu\text{M}$ ) in DMSO and its linear regression (0-12  $\mu\text{M}$ , inset)

**Table 1.** Limits of detection, complexation constants and wavelength shifts obtained for probes **1** and **2**.

	<b>1</b>	<b>2</b>
<b>LoD (<math>\mu\text{M}</math>)</b>	1.75	0.77
<b><math>K \cdot 10^{-3}</math></b>	$109 \pm 9$	$69 \pm 3$
<b>Wavelength shift (nm)</b>	From 360 to 475	From 359 to 485

The average amount of GHB used with recreational purposes is 10 mg/kg, a quantity much lower than that required to induced coma (50 mg/kg).<sup>20</sup> This fact implies that a person weighing 62 kg (the average body mass) has to intake 620 mg of GHB, at least, in a recreational environment. Therefore, the concentration in a standard volume of beverage is around 15 mM. This concentration is clearly higher than the LoD found for the reported sensors.

On the other hand, in relation to their possible forensic applications for detecting the drug in urine samples, it has been established that between 0-3 h after ingestion (when the peak concentration of GHB in urine appears) the concentration of GHB in urine after the intake of 10 mg/kg is around 0,3 mM which is higher than the LoD of the prepared sensors.<sup>21</sup>

As both detection media, soft drinks and urine, are aqueous solutions, the influence of water on the recognition and sensing events was evaluated. Thus, a titration in DMSO/water 95/5 was carried out (Figures S20 and S21). Under these conditions, sensibility is lower (LoD = 33  $\mu$ M), but even in these conditions, the probe is still capable of maintaining the coordination and detect the analyte in both cases, beverages and urine. In any case, 5% water is a percent higher than the usual required to detect the drug in real samples (see below).

### **Selectivity studies**

On one hand, we were interested in detecting GHB not only in alcoholic drinks but also in soft beverages and mixtures of soft beverages with alcoholic drinks. In these cases, the composition of soft drinks could have an important effect on the sensor response. For this reason, the selectivity of the probes toward the usual component of the soft beverages was evaluated. Usually these beverages include, in their composition, large amounts of citric acid and different sugars. In addition, minor amount of ascorbic acid is also a usual ingredient.<sup>22</sup> Due to this fact, the effect of these potential interferents on both probes was evaluated. Any of them, at the

concentrations usually found in drinks, induced any change in the spectra of either **1** or **2**. Therefore, it is possible to detect GHB in their presence (see Figure 5 for compound **1** and Supporting Information Figure S22 for compound **2**).

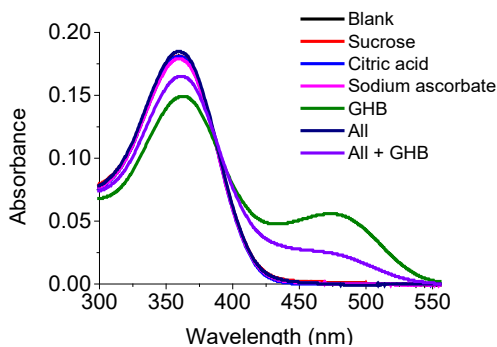


**Fig. 5.** Absorbance spectra of **1** (10  $\mu$ M in DMSO) in the presence of citric acid, sodium ascorbate, sucrose (at typical concentrations found in beverages) and NaGHB (1 eq.)

On the other hand, to carry out the detection in urine is important to know the selectivity of the probes in front of different hydroxyacids that can appear there.<sup>18</sup> In this sense, the selectivity of several different  $\omega$ -hydroxyacids was tested. As shown in Figure 6 and Figures S23-S25, compound **1** is mainly selective toward 4-hydroxybutyric and 5-hydroxypentanoic acids due to the spacer used in the sensor design.

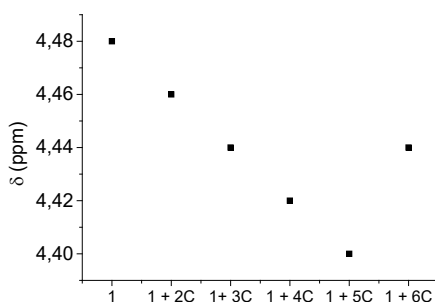


**Fig. 6.**  $^1\text{H}$  NMR spectra changes ( $-\text{O}-\text{CH}_2-$ ) of **1** in presence of  $\omega$ -hydroxyacids

### GHB determination in real samples

To test our probes under real conditions, different alcoholic drinks either pure or contaminated with known quantities of NaGHB were studied. These experiments were carried out in organic/ aqueous media (DMSO/water) at room temperature, mixing a known amount of sensor (300  $\mu$ M) with the sample, previously treated with 0.4 mM NaHCO<sub>3</sub> to ensure a slightly basic pH. All adulterated samples presented a 1.35 mM GHB concentration. In all cases, the colour changes were immediately appreciable when the drug was present, changing from yellow to orange (See Figure 7 for compound **1**, the results obtained with compound **2** are summarized in the Supporting Information, Figures S26 and S27).

UV-vis studies carried out with some beverages (rum-cola, vodka, and tonic water) showed clearly that the colour change was associated with the appearance of the absorption band at 480 nm. These data demonstrated that the sensing mechanism in the real sample was the same previously observed in organic media (see Supporting Information Figure S28). Recovery experiments were carried out and the obtained results are summarized in the Supporting Information Table S2.

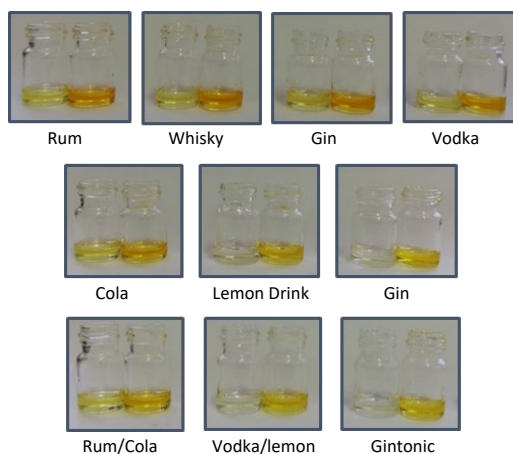


**Fig. 7.** Colour changes observed in real samples with compound **1**. In each image, the sample on the left corresponds to the pure beverage and on the right the same beverage contaminated with GHB (1.35 mM)

The experiments carried out in synthetic urine samples showed that the probe was able to detect the presence of the drug in this medium. However, a high concentration of the drug (at least 20 mM) was required to have a naked-eye detection as can be seen in Figure 8.

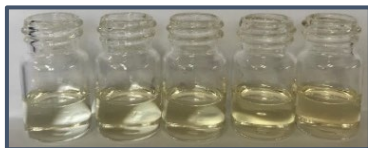


**Fig. 8.** Probe **1** 40  $\mu\text{M}$  in DMSO/water (99.9:0.01),  $\text{NaHCO}_3$  (4  $\mu\text{M}$ ) containing urine samples spiked with NaGHB (from left to right 0, 80, 120, 160 and 200  $\mu\text{M}$  in GHB)

These results indicate that the probe is able to detect GHB in synthetic urine. However, to use it as a visual probe, the real urine samples must be pre-concentrated before developing the test (see experimental section).

### Theoretical calculations

In order to gain insight in the GHB recognition mechanism of chemosensors **1** and **2**, some theoretical calculations were undertaken at X3LYP/6-31+G(d,p)/PCM(DMSO) level (see Supporting Information). Firstly, taking a reduced model of both chemosensors, namely 1-methyl-3-(4-nitrophenyl)thiourea, we studied the dihedral angle rotation around both NH-C thiourea bonds to obtain the *E* conformer from the *Z* one over the restricted singlet potential energy hypersurface. The barrier heights for that processes are about 6.5 ( $R_1\text{NH-C}$ ) and 17.2 kcal/mol ( $R_2\text{NH-C}$ ), respectively (relaxed PES scan, 12 points of  $15^\circ$  each one, see Supporting Information). Therefore, in the absence of steric interactions, the  $R_1\text{NH-C}$  bond is expected to be the only one implied in the thiourea conformational equilibrium. For compounds **1** and **2**, this *Z-E* interconversion barrier around  $R_1\text{NH-C}$  bond is even lower: 5.5 kcal/mol in both cases. Therefore, the calculations performed support the predominance of *Z,Z*- rotamer over the *E,Z*- one in both compounds. These data agree with the

<sup>1</sup>H NMR results where compounds **1** and **2** appear as a 1:5 and 0.7:1 ratio mixture being the main rotamer the *Z,Z*- one. This fact enables the chemosensors to establish readily an effective hydrogen-bond interaction through its *Z,Z*- conformer. Afterwards, the conformational equilibria in solution of both chemosensors, including the *E/Z* thiourea geometrical isomerism, was studied. For chemosensor **1**, the six different eclipsed and staggered conformers along the C-C ethylenic bond between the thiourea and ester units were considered together with rotamers around –CH<sub>2</sub>-O-C(=O)-Ar dihedral and the different *E,E*-, *E,Z*-, *Z,E*- and *Z,Z*- thiourea conformers. That yielded 32 starting structures which were subsequently fully optimized. Only five optimized structures (see Supporting Information) meet the criteria of being within 3 kcal/mol of the most stable structure, having an *Z,Z*- arrangement at the thiourea moiety and having a distance lower than 9 angstroms between trifluoroacetyl group and the thiourea moiety (maximum length of GHB chain). Following a similar procedure to search the most stable conformations of chemosensor **2** and taking into account that the ester and thiourea functional groups display an *1,2-anti* arrangement on the cyclohexane ring, which could yield diaxial *1,2-anti*- or diequatorial *1,2-anti*- diastereoisomers, respectively, we ended up with only two structures considering our three previous criteria. The simulated UV-Vis spectra of all these species (see Supporting Information) yields one band around 340-350 nm regardless of the chemosensor considered, which is in agreement with the experimental UV-Vis spectra of both chemosensors (see Figures 1 and 3).



## Chapter 2: GHB detection through the use of ditopic ligands

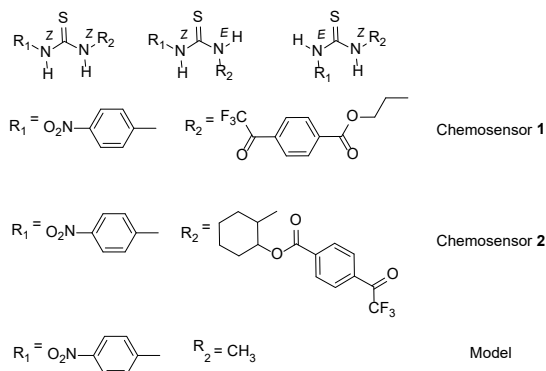


**Chart 3.** Possible rotamers depending on the thiourea geometrical isomerism of probes **1** and **2** and the model

Before studying the hydrogen bond interaction between the GHB and the thiourea moiety of chemosensors **1** and **2**, we analyzed it in a reduced model: 1-methyl-3-(4-nitrophenyl)thiourea) and butyric acid. Several scenarios were considered: the single and double hydrogen bond formation between the thiourea and both the acid or the corresponding carboxylate group and, in view of the relative acidity of the hydrogen atom of the thiourea nitrogen atom directly attached to the 4-nitrophenyl ring (N<sub>3</sub>), the simple and double hydrogen bond between the carboxylic acid group and the N-deprotonated thiourea (see Supporting Information). The stabilization experienced by the butyrate and the thiourea through a double hydrogen bond interaction was the higher one (17 kcal/mol) followed by the single hydrogen bond formation (13 kcal/mol) and the double hydrogen bond between the N<sub>3</sub>-deprotonated thiourea and the carboxylic acid (12 kcal/mol). Thus, taking into account this fact, together with the appropriate selection of the main conformation of chemosensors **1** and **2** done before, the influence of the hemiacetal formation in GHB complexation was evaluated. Several geometries in both GHB-derived chemosensors **1** and **2** were obtained. Those featuring a double hydrogen bond between carboxylate and the thiourea moiety showed a band centered at 380 nm in their simulated UV-Vis spectra (see Supporting Information). This band appeared at 430-440 nm at the geometries with a double hydrogen bond between the carboxylic acid the N<sub>3</sub>-

deprotonated thiourea (see Figure 9). This fact agrees with the experimental outcome: the addition of NaGHB shifts bathochromically the UV-Vis band of chemosensors **1** and **2** and due to an acid-base equilibrium with a concomitant hydrogen-bond formation.

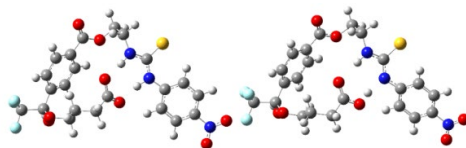


**Fig. 9.** Geometries of two conformers of **1-GHB** showing different double hydrogen bond types between GHB and thiourea moiety (carboxylate – thiourea at **1-GHB-a** on the left and carboxylic acid – N<sub>3</sub>-deprotonated thiourea at **1-GHB-f** on the right)

The last point studied was the specificity of the recognition process regarding the chain length of the hydroxyacid. To gain insight in this question, two series of compound **2** with linear hydroxyacids of increasing lengths (3 to 7 carbon atoms) attached were optimized: one where a double hydrogen bond between the hydroxyacid carboxylate and thiourea moiety was present and other with any hydrogen bond between these functional groups.

In each series, only the length of the hydroxyacid and no other parameters were modified. After the optimization of the structures, the energy difference between compounds with the same hydroxyacid length will account for the stabilization due to the hydrogen bond formation. As can be seen in Table S7 in Supporting Information, the stabilization due to the hydrogen bond formation at the 3-carbon hydroxyacid conformers is the lowest of all the series, which is maximum at the 4-carbon hydroxyacid compound so it can almost compensate the steric hindrance of the substituents coming closer. From that point, the difference is reduced as the hydroxyacid length increases. Therefore, the factor that defines the specificity of the chemosensors synthesized is the ability to accommodate the hydroxyacid into the spatial distance between trifluoroacetyl group and the thiourea moiety.

## **Conclusions**

In conclusion, we report herein two new probes bearing both: a thiourea moiety and a trifluoroacetyl group to detect GHB in real-time and in real-samples. In the presence of GHB, a marked colour change from yellow to orange for both probes was observed. We also demonstrate the influence of the chain length is the recognition process. Finally, in both cases, the limits of detection towards GHB are much lower than the usual GHB intake in recreational environments (around 15 mM in beverages). However, to detect the drug in urine samples, a previous preconcentration must be carried out to get concentrations around 30 mM.

## **Conflicts of interest**

There are no conflicts to declare.

## **Acknowledgements**

We thank the Spanish Government, MICINN funds (RTL2018-100910-B-C42) for financial support. S. R-N. is grateful to the Spanish Government for a fellowship. SCSIE (Universidad de Valencia) is gratefully acknowledged for all the equipment employed. NMR was registered at the U26 facility of ICTS "NAMBIOSIS" at the Universitat of València. The computational resources from the SIUV (Servei d'Informàtica, Universidad de Valencia) are gratefully acknowledged.

## **Notes and references**

[1] S. G. Smith, J. Chen, K. C. Basile, L. K. Gilbert, M. T. Merrick, N. Patel, M. Walling, A. Jain, The National Intimate Partner and Sexual Violence Survey (NISVS): 2010-2012 State Report. Atlanta, GA: National Center for Injury Prevention and Control, Centers for Disease Control and Prevention, 2017. <https://www.cdc.gov/violenceprevention/pdf/nisvs-statereportbook.pdf>.

*Chapter 2: GHB detection through the use of ditopic ligands*

- [2] Z. Nemeth, B. Kun, Z. Demetrovics, J. Psychopharmacol., 2010, 24, 1281.
- [3] C. L. Morris-Kukoski, Toxicol. Rev., 2004, 23, 33.
- [4] D. Zhai, Y. Q. E. Tan, W. Xu, Y-T. Chang, Chem. Commun., 2014, 50, 2904.
- [5] D. Zhai, B. K. Agrawalla, P. S .F. Eng, S.-C.Lee, W. Xua, Y.-T. Chang, Chem. Commun., 2013, 49, 6170.
- [6] W. Wang, Z.-Z. Dong, G. Yang, C.-H. Leung, S. Lin, D.-L. Ma, J. Mater. Chem. B, 2017, 5, 2739.
- [7] S. Rodríguez-Nuévalos, A. M. Costero, P. Arroyo, J. A. Sáez, M. Parra, F. Sancenón, R. Martínez Máñez, Chem Commun., 2020, 56, 12600.
- [8] D. T. Bravo; D. O. Harris, S. M. Parsons, J. Forensic Sci., 2004, 49, 379.
- [9] T. M. Godoy-Reyes, A. M. Costero, P. Gaviña, R. Martínez-Mañez, F. Sancenón, ACS Appl. Nano Mater., 2019, 2, 1367.
- [10] T. M. Godoy-Reyes, A. Llopis-Lorente, A. M. Costero, F. Sancenon, P. Gavina, R. Martinez-Mañez, Sensors and Actuators B-Chemical, 2018, 258, 829.
- [11] L. A. Juárez, A. Barba-Bon, A. M. Costero, R. Martínez-Mañez, F. Sancenón, M. Parra, P. Gaviña, M. C. Terencio, M. J. Alcaraz, Chemistry Eur. J., 2015, 21, 15468.
- [12] X. Xu, W. A. Goddard III, Proc. Natl. Acad. Sci. USA, 2004, 101, 2673.
- [13] G. Scalmani, M. J. Frisch, J. Chem. Phys., 2010, 132, 114110.
- [14] C. Adamo, D. Jacquemin, Chem. Soc. Rev., 2013, 42, 845.

*Chapter 2: GHB detection through the use of ditopic ligands*

- [15] A. D. Laurent, C. Adamo, D. Jacquemin, *Phys. Chem. Chem. Phys.*, 2014, 16, 14334.
- [16] Gaussian 09, Revision D.01, see complete citation in Supporting Information.
- [17] H. J. Lee, A. C. Jamison, T. Randall Lee, *Langmuir*, 2015, 31, 2136.
- [18] H.-G. Weinig, R. Krauss, M. Seidock, J. Bendig, U. Koert, *Chem. Eur. J.*, 2001, 7, 2075.
- [19] I. L. Kirby, M. B. Pitak, C. Wilson, P. A. Galea, S. J. Coles, *CrystEngComm.*, 2015, 17, 2815.
- [20] J. Royo-Isach, M. Magrané, R. Vilà, M.E. Capdevila, *Aten. Primaria*, 2004, 33, 516.
- [21] C. Huller, D. Thai, P. Jacob 3rd, J. E. Dyer, *J. Anal. Toxicol.*, 2006, 30, 360.
- [22] D. Kregiel, *BioMed Research International*, 2015, Article ID 128697.
- [23] M. Pazzi, S. Colella, E. Alladio, M. P. Puccinelli, G. Mengozzi, C. Medana, *Analytica*, 2020, 1, 14.



## **Supplementary material**

### **Heteroditopic chemosensor for detecting $\gamma$ -hydroxybutiric acid (GHB) in soft drinks and alcoholic beverages**

Silvia Rodríguez-Nuévalos<sup>a</sup>, Margarita Parra<sup>a,b,c</sup>, Salvador Gil<sup>a,b,c</sup>, Pablo Gaviña<sup>a,b,c</sup>, Pau Arroyo<sup>a,b</sup>, José A. Sáez<sup>a,b</sup>, Ana M. Costero<sup>a,b,c\*</sup>

<sup>a</sup>Instituto Interuniversitario de Investigación de Reconocimiento Molecular y Desarrollo Tecnológico (IDM). Universitat Politècnica de València, Universitat de València, Doctor Moliner 50, Burjassot, 46100, Valencia, Spain.

<sup>b</sup>Departamento de Química Orgánica, Universitat de València, Doctor Moliner 50, Burjassot, 46100, Valencia, Spain.

<sup>c</sup>CIBER de Bioingeniería, Biomateriales y Nanomedicina (CIBER-BBN) (Spain)

\* Correspondence: ana.costero@uv.es

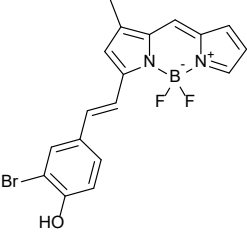
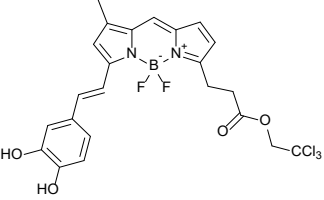
(See annexes I-V in CD)

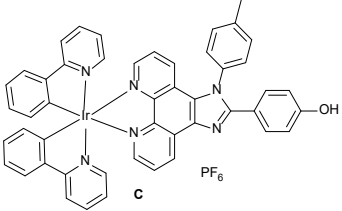
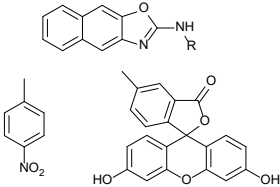
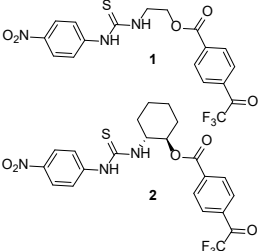




## Reported data and comparison

Table S1. Comparison with other sensors published

SENSOR	DETECTION	RECOGNITION	LoDs (mg/mL)	INTERFERENTS	REFERENCE
	FLUORESCENCE On-Off	Acid moiety by hydrogen bond	5	Some Acids	<i>Chem. Commun.</i> , <b>2014</b> , 50, 2904
	FLUORESCENCE Off-On Pre-treatment is required	No data available	10	No data available	<i>Chem. Commun.</i> , <b>2013</b> , 49, 6170-6172

 <p><b>c</b> PF<sub>6</sub></p>	<p>FLUORESCENCE</p> <p>On-Off</p>	<p>No data available</p>	<p>0.15</p>	<p>No data available</p>	<p><i>J. Mater. Chem. B</i>, <b>2017</b>, 5, 2739--2742</p>
	<p>COLOUR</p> <p>Yellow to red</p> <p>FLUORESCENCE</p> <p>Off-On</p>	<p>Deprotonation of acid moiety</p>	<p>0.04</p>	<p>Some Acids and sugars</p>	<p><i>Chem. Commun.</i>, <b>2020</b>, 56, 12600-12603</p>
 <p><b>1</b></p> <p><b>2</b></p>	<p>COLOUR</p> <p>Yellow to orange</p>	<p>Double recognition: Acid-base and hemiacetal formation</p>	<p>0.17</p>	<p>Some Acids and sugars</p>	<p><i>This work</i></p>

## NMR Spectra

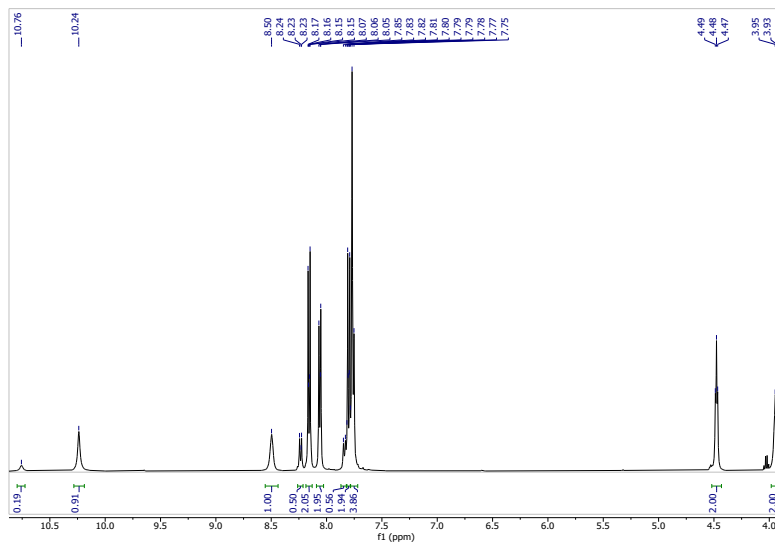


Figure S1. <sup>1</sup>H NMR spectrum of compound **1** in DMSO-*d*<sub>6</sub>.

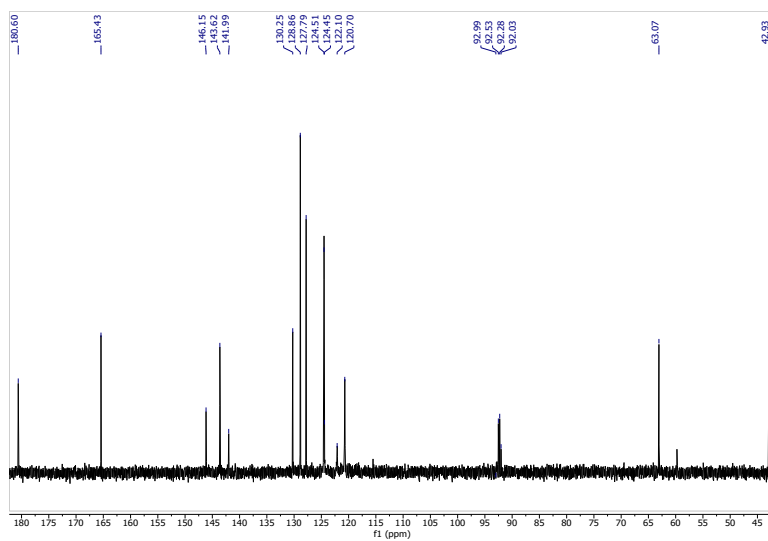


Figure S2. <sup>13</sup>C NMR spectrum of compound **1** in DMSO-*d*<sub>6</sub>.

## Chapter 2: GHB detection through the use of ditopic ligands

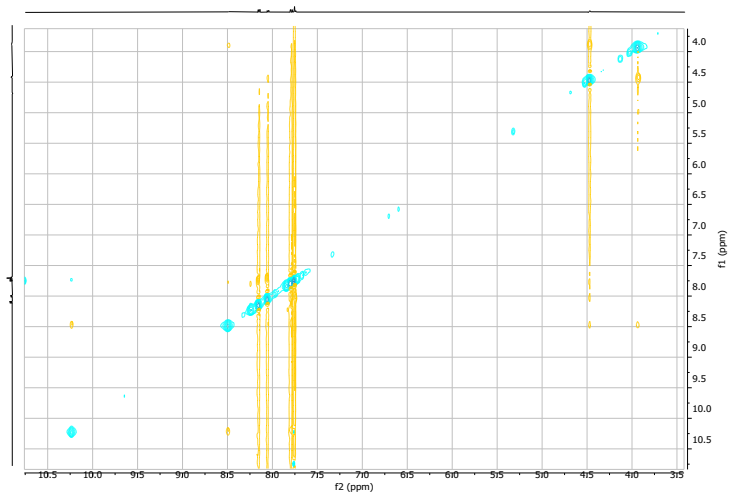


Figure S3. NOESY spectrum of compound 1 in DMSO- $d_6$ .

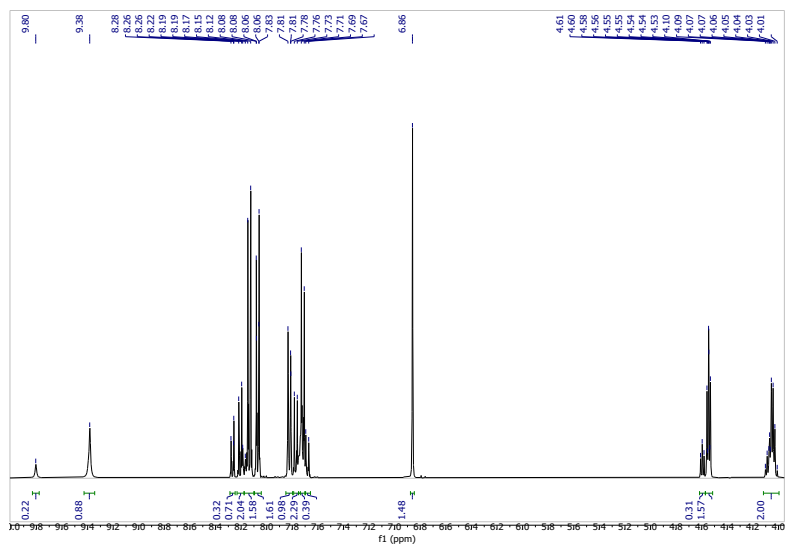
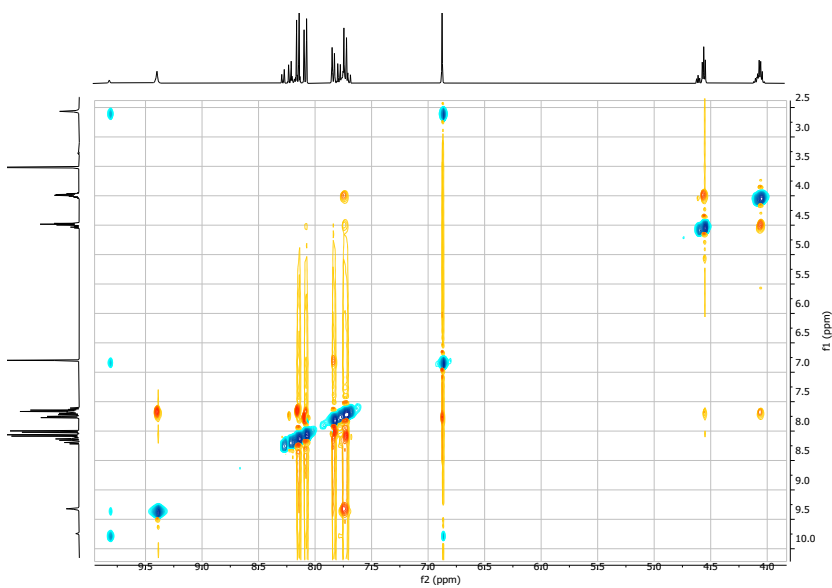
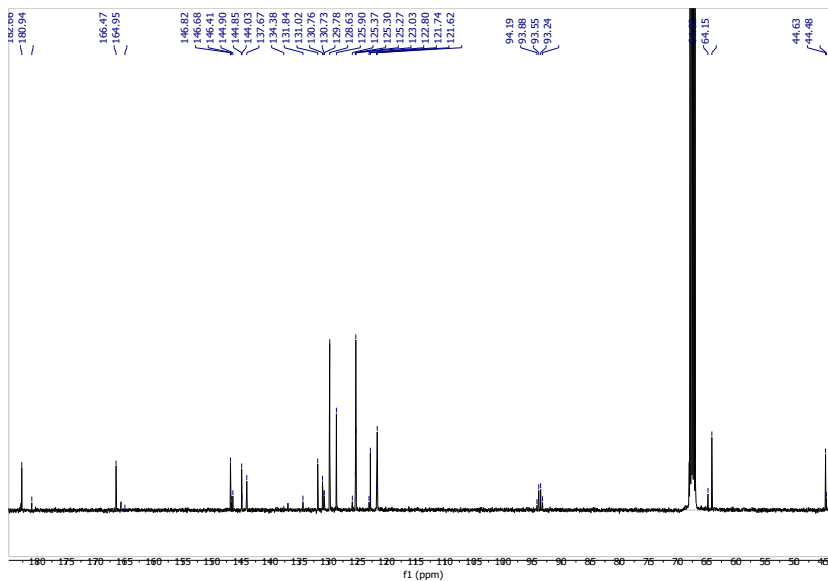


Figure S4.  $^1H$  NMR spectrum of compound 1 in THF- $d_8$ .

## Chapter 2: GHB detection through the use of ditopic ligands



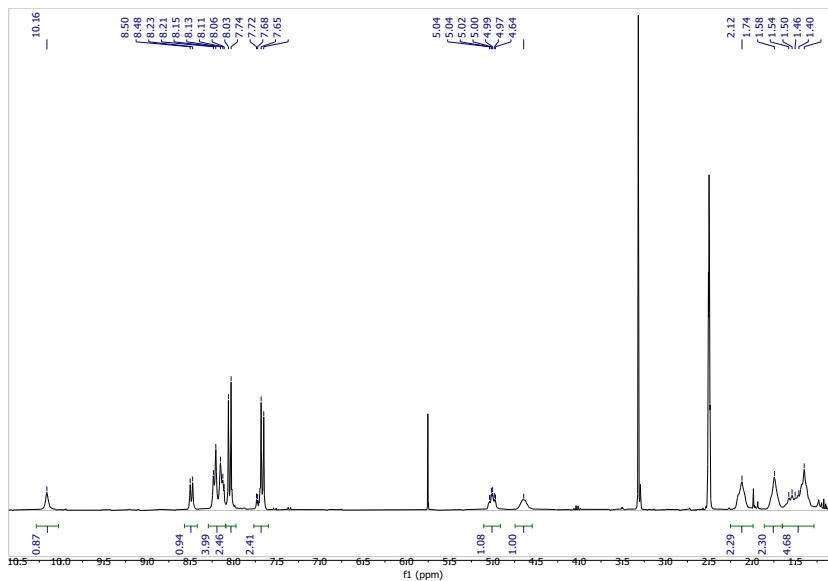


Figure S7.  $^1\text{H}$  NMR spectrum of compound **2** in  $\text{DMSO-}d_6$ .

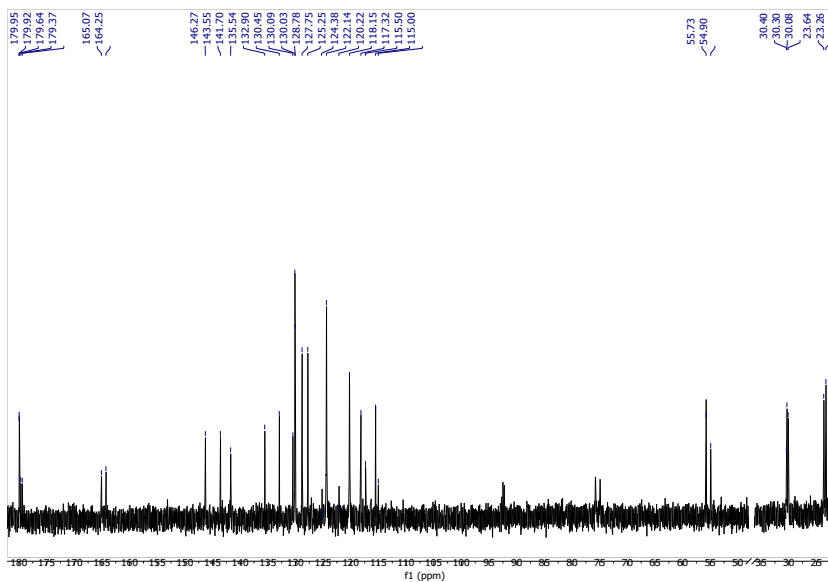


Figure S8.  $^{13}\text{C}$  NMR spectrum of compound **2** in  $\text{DMSO-}d_6$ .

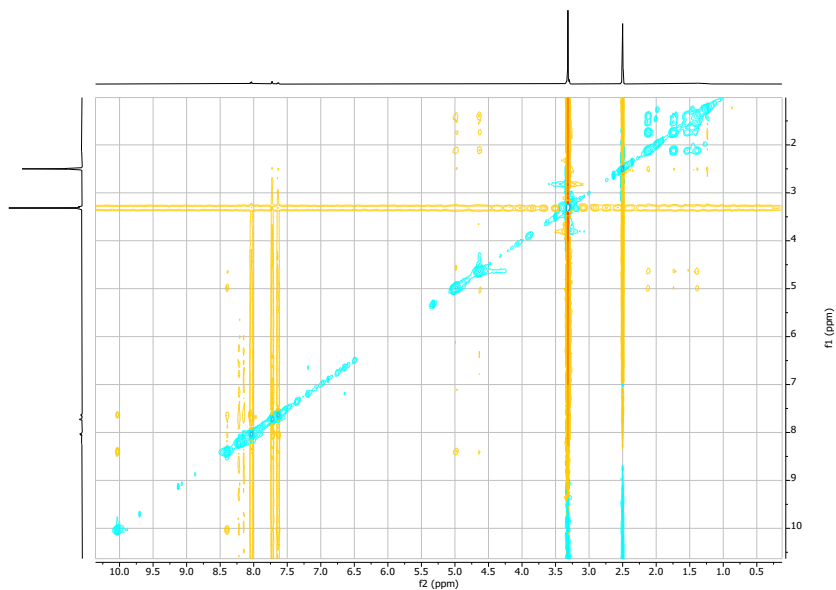


Figure S9. NOESY spectrum of compound **2** in DMSO- $d_6$ .

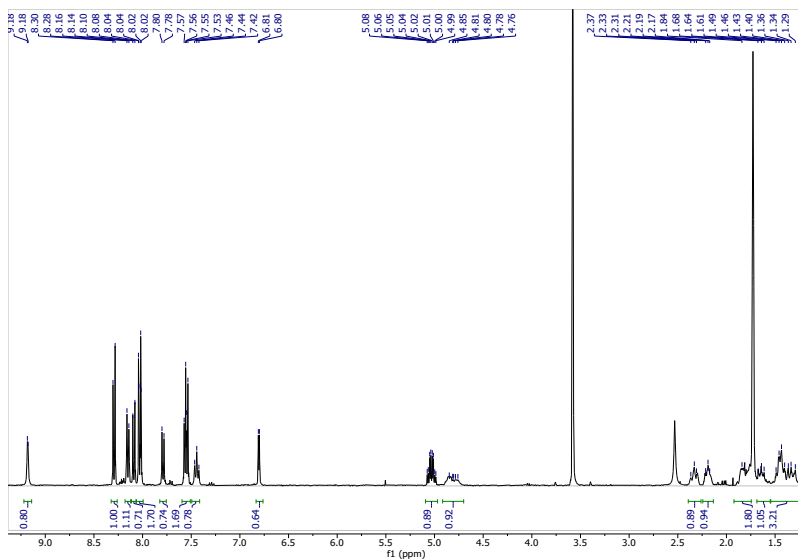


Figure S10.  $^1\text{H}$  NMR spectrum of compound **2** in THF- $d_3$ .

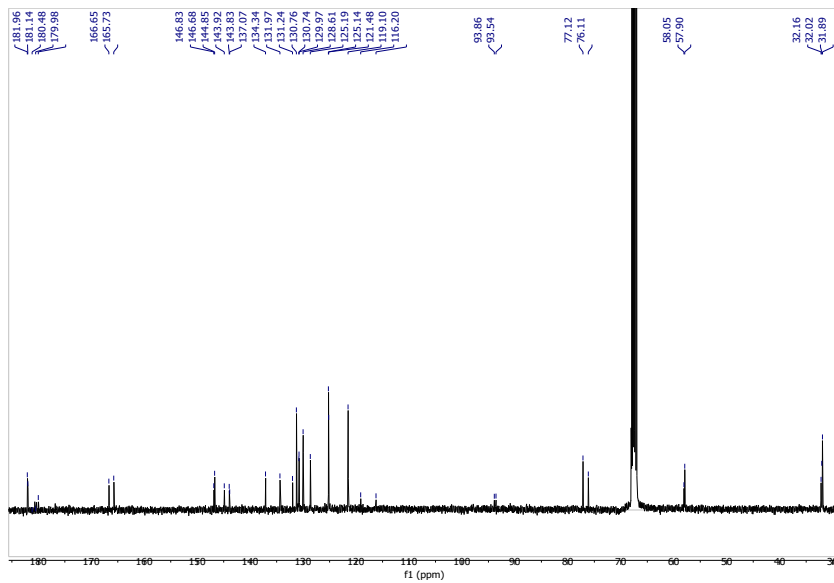


Figure S11.  $^{13}\text{C}$  NMR spectrum of compound 2 in  $\text{THF-}d_8$ .

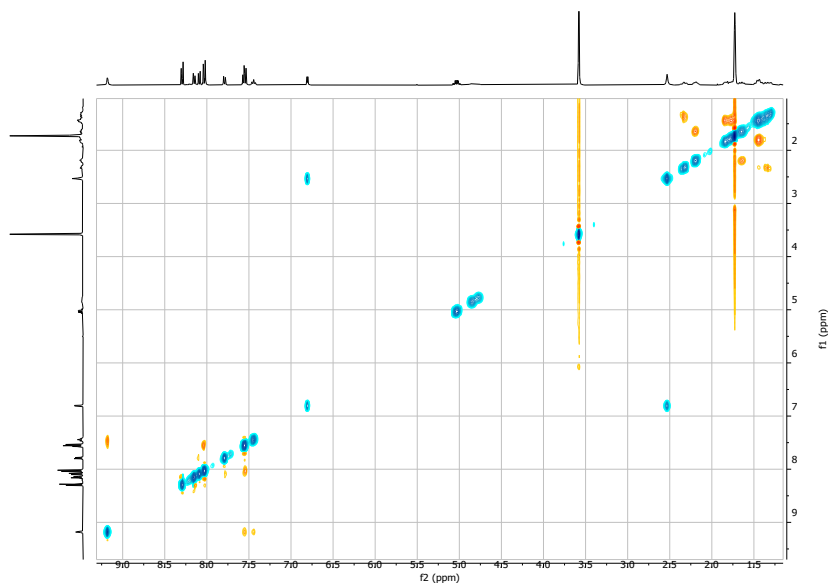


Figure S12. NOESY spectrum of compound 2 in  $\text{THF-}d_8$ .



## Mass Spectrometry Spectra

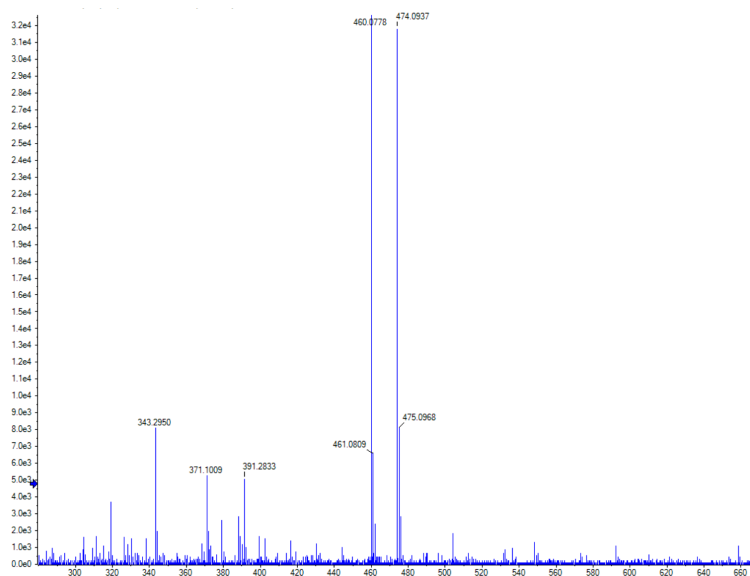


Figure S13. Mass Spectrum of compound 1.

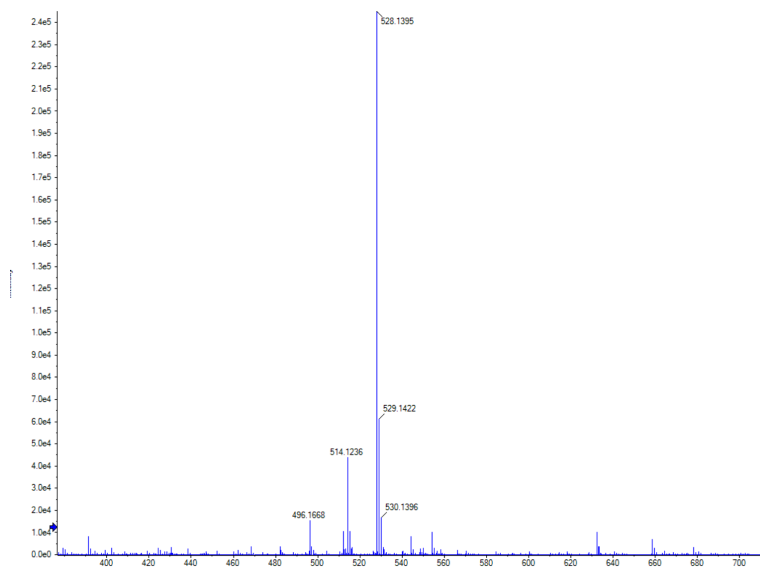
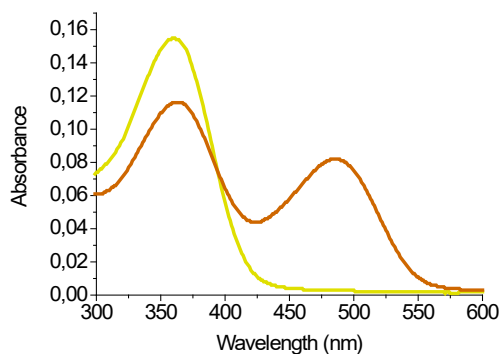


Figure S14. Mass Spectrum of compound 2.

## UV-Vis analysis



**Figure S15.** Changes observed in UV spectrum of compound **2** in presence of an excess of NaGHB.

## NMR Analysis

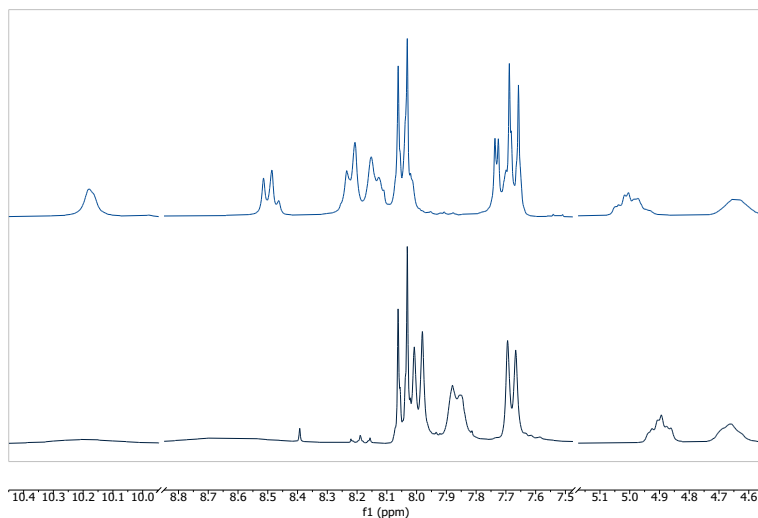


**Figure S16.** Changes observed in <sup>1</sup>H NMR spectrum of **2** in presence of an excess of GHB in DMSO-*d*<sub>6</sub>.

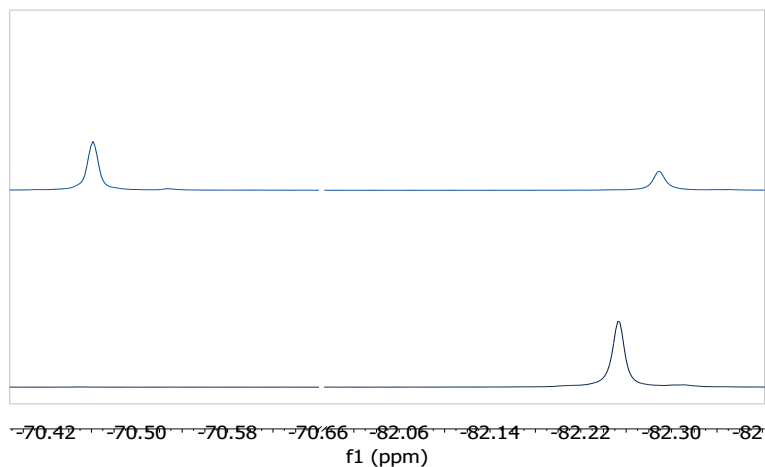


**Figure S17.** Changes observed in  $^{19}\text{F}$  NMR spectrum of **2** in presence of an excess of GHB in  $\text{DMSO-}d_6$ .

### UV-Vis titrations spectra

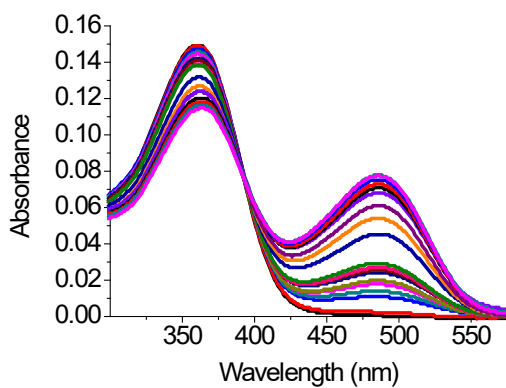


**Figure S18.** UV-visible spectra of probe **2** with increasing amounts of GHB (0–10 eq.) in DMSO ( $10\ \mu\text{M}$  of **2**)

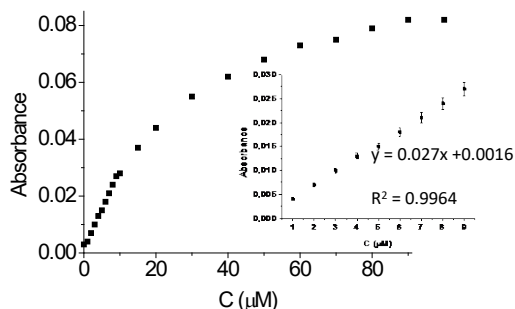


**Figure S19.** Changes in the absorbance at 485 nm of DMSO solutions of probe **2** upon the addition of increasing amounts of GHB

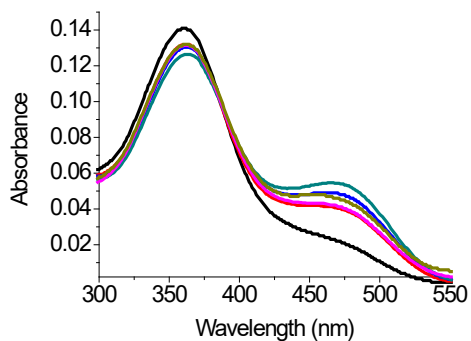


**Figure S20.** UV-visible changes of probe **1** with increasing amounts of GHB (0–21 eq.) in DMSO:H<sub>2</sub>O 95:5 media (10 μM of **1**).

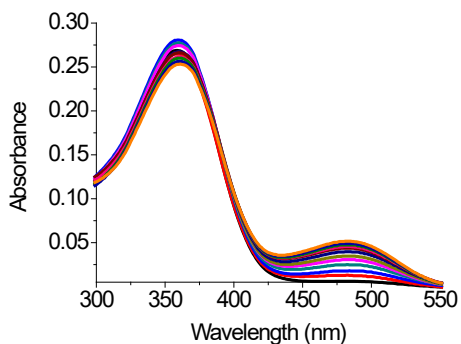


**Figure S21.** UV-visible changes of probe **2** with increasing amounts of GHB (0–42 eq.) in DMSO:H<sub>2</sub>O 95:5 media (10 μM of **2**).

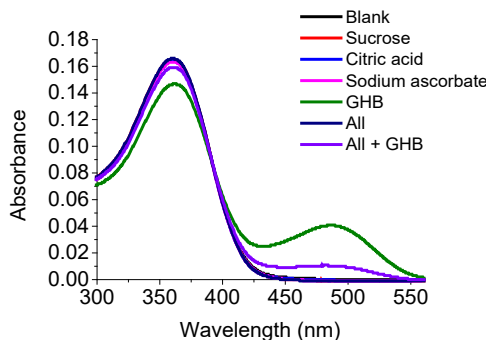


**Figure S22.** Absorbance spectra of **2** (10  $\mu\text{M}$  in DMSO) in the presence of citric acid, sodium ascorbate, sucrose (in real concentration present in beverages) and NaGHB (1 eq).

**Table S2.** Recovery and accuracy determination of the method to probe **1**. Recovery and accuracy of the method were calculated according to reference K. A. Rawat, R.K. Singhal, S. K. Kailasa, RSC Advances, 2016, 6, 32025.

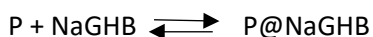
KNOWN CONCENTRATION ( $\mu\text{M}$ )	FOUND CONCENTRATION ( $\mu\text{M}$ )	RECOVERY % <sup>a</sup>	ACCURACY % <sup>b</sup>
5	4.48	89.50	-10,50

<sup>a</sup> % recovery (found concentration/known concentration) x 100

<sup>b</sup> % accuracy (found concentration – known concentration/known concentration) x 100

### Constant determination

The binding process can be described by the reaction



P= Probe, P@NaGHB = complex

The equilibrium constant was defined as  $K = \frac{[P@NaGHB]}{[P][NaGHB]}$

The analysis of the titration curves were done according to the following equation:[1]

$$\left[ \frac{C_P - C_{NaGHB}}{\Delta A} \right] + \left( \frac{\Delta A}{\Delta \epsilon^2} \right) = \left( \frac{1}{K \Delta \epsilon} \right) + \left[ \frac{(C_P + C_{NaGHB})}{\Delta \epsilon} \right]$$

where:

$C_P$  and  $C_{NaGHB}$  are the total probe and drug concentrations

$$\Delta A = A - \epsilon_P C_P$$

$\epsilon_P = \Delta A^0 / C_P$ ,  $A^0$  initial absorbance of NaGHB

$$\Delta \epsilon = \epsilon_{P@NaGHB} - \epsilon_P$$

Iteration were carried out using Origin 2000.

[1] Borja Díaz de Greñu, José García-Calvo, José Cuevas, Gabriel García-Herbosa,

Begoña Garía, Natalia Busto, Saturnino Ibeas, Tomás Torroba, Blanca Torroba, Antonio Herrera and Sebastian Pons, Chem. Sci., 2015, 6, 3757

## $\omega$ -hydroxyacids analysis

### NMR essays

A solution 100 mM of **1** and 100 mM of each  $\omega$ -hydroxyacid were prepared in DMSO- $d_6$ . 50  $\mu$ L of solution of **1** and 50  $\mu$ L of solution of each  $\omega$ -hydroxyacid were mixed and then diluted until 500  $\mu$ L with DMSO- $d_6$ .

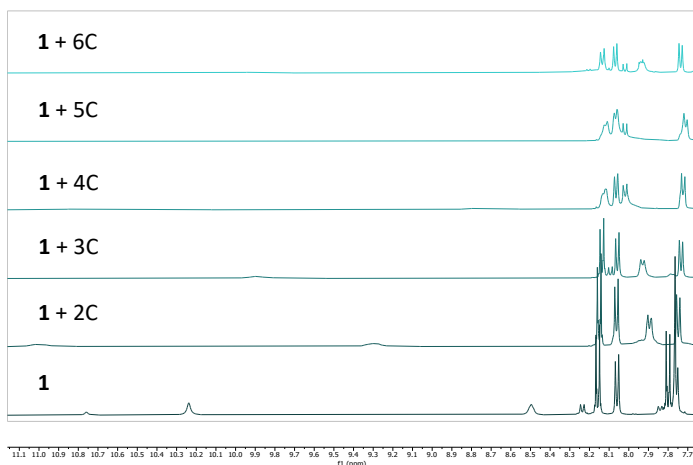


**Figure S23.** Changes observed in <sup>1</sup>H NMR spectrum of **1** in presence of 1 eq. of  $\omega$ -hydroxyacids of n carbon atoms in DMSO- $d_6$ .

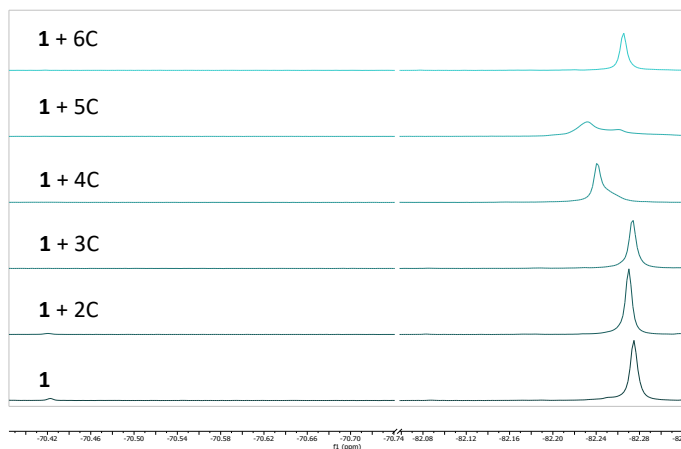


**Figure S24.** Changes observed in  $^{19}\text{F}$  NMR spectrum of **1** in presence of 1 eq of  $\omega$ -hydroxyacid in  $\text{DMSO-}d_6$ .

### UV-Vis essays

In a cuvette of 3 mL, 3  $\mu\text{L}$  of solution of **1** (100 mM in DMSO) and 9.9  $\mu\text{L}$  of solution of each  $\omega$ -hydroxyacid (100 mM in DMSO) were mixed and diluted until 3000  $\mu\text{L}$  with DMSO.

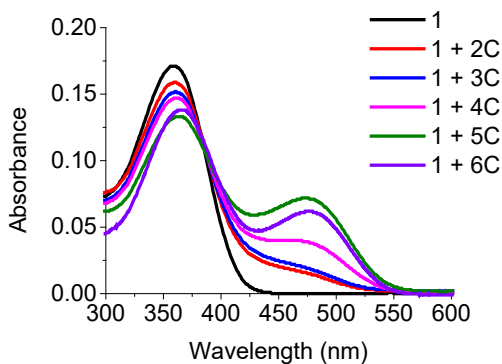


**Figure S25.** Changes observed in UV-Vis spectrum of **1** in presence of 3.3 eq. of  $\omega$ -hydroxyacids in DMSO.

## Real Samples Analysis

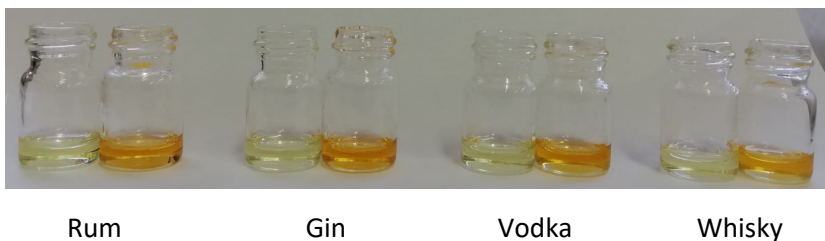


**Figure S26.** Colour changes observed in real samples with compound **2** (alcoholic drinks).



**Figure S27.** Colour changes observed in real samples with compound **2** (soft drinks and beverages).



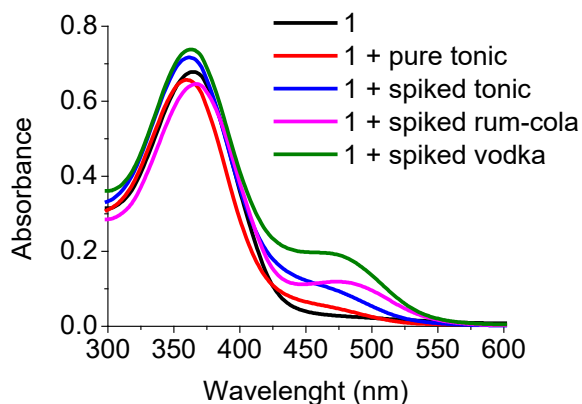


**Figure S28.** Changes observed in UV-Vis spectrum of 1 pure and in presence of spiked rum-cola, spiked vodka, spiked tonic and pure tonic. Sensor 60  $\mu\text{M}$  in DMSO in presence of GHB 0.75 mM in the spiked samples. (percent of water < 5%)

## Theoretical calculations

Complete reference for Gaussian09, Rev. D.01:

Gaussian 09, Revision D.01, M. J. Frisch, G. W. Trucks, H. B. Schlegel, G. E. Scuseria, M. A. Robb, J. R. Cheeseman, G. Scalmani, V. Barone, G. A. Petersson, H. Nakatsuji, X. Li, M. Caricato, A. Marenich, J. Bloino, B. G. Janesko, R. Gomperts, B. Mennucci, H. P. Hratchian, J. V. Ortiz, A. F. Izmaylov, J. L. Sonnenberg, D. Williams-Young, F. Ding, F. Lipparini, F. Egidi, J. Goings, B. Peng, A. Petrone, T. Henderson, D. Ranasinghe, V. G. Zakrzewski, J. Gao, N. Rega, G. Zheng, W. Liang, M. Hada, M. Ehara, K. Toyota, R. Fukuda, J. Hasegawa, M. Ishida, T. Nakajima, Y. Honda, O. Kitao, H. Nakai, T. Vreven, K. Throssell, J. A. Montgomery, Jr., J. E. Peralta, F. Ogliaro, M. Bearpark, J. J. Heyd, E. Brothers, K. N. Kudin, V. N. Staroverov, T. Keith, R. Kobayashi, J. Normand, K. Raghavachari, A. Rendell, J. C. Burant, S. S. Iyengar, J. Tomasi, M. Cossi, J. M. Millam, M. Klene, C. Adamo, R. Cammi, J. W. Ochterski, R. L. Martin, K. Morokuma, O. Farkas, J. B. Foresman, and D. J. Fox, Gaussian, Inc., Wallingford CT, 2016.

The following Supporting Information section, which contains the details of computational calculations performed in this work, has

been structured in the following subsections (which, in turn, has its own bibliographic references included at the end):

**Part 1** - Computational methods. In this section, computational details about the geometrical optimizations and the vertical excitation analysis are given.

**Part 2** - Figure of X3LYP/6-31G(d)/PCM(DMSO) energy barrier profiles along restricted singlet potential energy hypersurface (PES) of the dihedral angle of both NH-C bonds at the reduced 1-methyl-3-(4-nitrophenyl)thiourea going from *Z* to *E* rotamer (relaxed PES scan, 12 points, 15° each one at the corresponding dihedral angle).

**Part 3** -Figure of X3LYP/6-31G(d)/PCM(DMSO) energy barrier profiles along restricted singlet PES of the dihedral angle of both NH-C bonds of compound **1** (starting from one of its selected minimum-energy optimized conformations) going from *Z* to *E* rotamer (relaxed PES scan, 12 points, 15° each one at the corresponding dihedral angle).

**Part 4** -Figure of X3LYP/6-31G(d)/PCM(DMSO) energy barrier profiles along restricted singlet PES of the dihedral angle of both NH-C bonds of compound **2** (starting from one of its selected minimum-energy optimized conformations) going from *Z* to *E* rotamer (relaxed PES scan, 12 points, 15° each one at the corresponding dihedral angle).

**Part 5** -X3LYP/6-31+G(d,p)/PCM(DMSO) energies of the optimized structures for the different 32 starting rotamers found along the full-search of the PES for chemosensor **1**. Starting structures were the six different eclipsed and staggered conformers along the C-C ethylenic bond as well as the *E,E*-, *E,Z*-, *Z,E*- and *Z,Z*- thiourea conformers and rotamers around -CH<sub>2</sub>-O-C(=O)-Ar dihedral angle. Distances between C=O of trifluoromethyl acetate group and C=S thiourea carbon atoms are also depicted.

**Part 6** -X3LYP/6-31+G(d,p)/PCM(DMSO) energies of the optimized structures for the different 28 starting rotamers found along the full-search of the PES for chemosensor **2**. Starting structures were the different ester and thiourea diaxial 1,2-*anti*- or diequatorial 1,2-*anti*-diastereoisomers over the cyclohexane ring together with the

rotamers around  $-\text{CH}_2\text{-O-C(=O)-Ar}$  dihedral angle. Distances between C=O of trifluoromethyl acetate group and C=S thiourea carbon atoms are also depicted.

**Part 7** - Simulated UV-Vis spectra from the TD-DFT vertical excitation energies analysis of selected X3LYP/6-31+G(d,p)/PCM(DMSO) optimized geometries of rotamers of **1** at the same theory level (30 states, singlets only).

**Part 8** - Simulated UV-Vis spectra from the TD-DFT vertical excitation energies analysis of selected X3LYP/6-31+G(d,p)/PCM(DMSO) optimized geometries of rotamers of **2** at the same theory level (30 states, singlets only).

**Part 9** - X3LYP/6-31+G(d,p)/PCM(DMSO) energies of the optimized structures of **1-GHB** derivatives with hydrogen bonds between the thiourea and carboxylate moieties and between the N<sub>3</sub>-deprotonated thiourea and the carboxylic acid group.

**Part 10** - X3LYP/6-31+G(d,p)/PCM(DMSO) energies of the optimized structures of **2-GHB** derivatives with hydrogen bonds between the thiourea and carboxylate moieties and between the N<sub>3</sub>-deprotonated thiourea and the carboxylic acid group.

**Part 11** - Simulated UV-Vis spectra from the TD-DFT vertical excitation energies analysis of X3LYP/6-31+G(d,p)/PCM(DMSO) **1-GHB** optimized geometries at the same theory level (15 states, singlets only).

**Part 12** - Simulated UV-Vis spectra from the TD-DFT vertical excitation energies analysis of X3LYP/6-31+G(d,p)/PCM(DMSO) **2-GHB** optimized geometries at the same theory level (15 states, singlets only).

**Part 13** - X3LYP/6-31+G(d,p)/PCM(DMSO) energies of the optimized structures for chemosensor **2-GHB** with and without hydrogen bond between the hydroxyacid carboxylate and thiourea moiety with increasing hydroxyacid chain (3 to 7 carbon atoms).

**Part 14** – X3LYP/6-31+G(d,p)/PCM(DMSO) energies of butyric acid and 1-methyl-3-(4-nitrophenyl)thiourea in different hydrogen-bonded complexes in different protonation states.

**Annex I:** XYZ cartesian coordinates of the optimized energies of 32 starting rotamers of chemosensor **1**.

**Annex II:** XYZ cartesian coordinates of the optimized energies of 28 starting rotamers of chemosensor **1**.

**Annex III:** XYZ cartesian coordinates of the optimized energies of several **1-GHB** geometries bearing different hydrogen bonding modes between the thiourea and carboxylate moieties.

**Annex IV:** XYZ cartesian coordinates of the optimized energies of several **2-GHB** geometries bearing different hydrogen bonding modes between the thiourea and carboxylate moieties.

**Annex V:** XYZ cartesian coordinates of the optimized energies of the two **2-GHB** series (with and without hydrogen bond) with increasing hydroxyacid chain.

**Part 1** - Computational methods.

In order to gain insight in the behavior of chemosensors **1** and **2** with and without the presence of GHB, DFT calculations have been carried out using Gaussian09 rev. D01 program package[a] and GaussView 5 [b] was employed to visualize the results. The geometrical optimization was performed using the X3LYP hybrid DFT functional of Xu and Goddard[c] which accounts for the accurate description of nonbonding interactions as those we are dealing here with **1-GHB** and **2-GHB** structures. The double- $\zeta$  6-31+G(d,p) basis set[d] was used in the optimization of the real systems although for the sake of simplicity, 6-31G(d) basis set was used to perform the relaxed PES scan along the dihedral angle of both NH-C thiourea bonds at the reduced and complete models. To take into account the effect of the solvent, DMSO, PCM solvation model was used[e]. Frequency calculations were performed over optimized structures to properly characterize minima structures (no imaginary frequencies).

On the other hand, to explore the electronic transitions responsible for the UV-Vis spectra, vertical excitation energies were computed over X3LYP/6-31+G(d,p)/PCM(DMSO) geometries through single-point TD-DFT[f] calculations (15 states, singlets only) in solution using non-equilibrium formalism at the same theory level. Geometry details of all optimized geometries as well as excitation energies, oscillator strengths, spin and spatial symmetry,  $S^2$  and largest coefficients in the CI expansion for all TD-DFT vertical excitation energies computed for **1**, **2**, **1-GHB** and **2-GHB** geometries can be found in the different Annex sections.

[a] Gaussian 09, Revision D.01. See complete reference at the beginning of the theoretical calculations at the Supporting Information.

[b] GaussView, Version 5, Roy Dennington, Todd Keith, and John Millam, Semichem Inc., Shawnee Mission, KS, 2009.

[c] X. Xu, W. A. Goddard III, Proc. Natl. Acad. Sci. USA, 101 (2004) 2673-77.

[d] a) G. A. Petersson, A. Bennett, T. G. Tensfeldt, M. A. Al-Laham, W. A. Shirley, and J. Mantzaris, "A complete basis set model chemistry. I. The total energies of closed-shell atoms and hydrides of the first-row atoms," J. Chem. Phys., 89 (1988) 2193-218. b) G. A. Petersson and M. A. Al-Laham, "A complete basis set model chemistry. II. Open-shell systems and the total energies of the first-row atoms," J. Chem. Phys., 94 (1991) 6081-90. c) A. D. McLean and G. S. Chandler, "Contracted Gaussian-basis sets for molecular calculations. 1. 2nd row atoms, Z=11-18," J. Chem. Phys., 72 (1980) 5639-48. d) K. Raghavachari, J. S. Binkley, R. Seeger, and J. A. Pople, "Self-Consistent Molecular Orbital Methods. 20. Basis set for correlated wave-functions," J. Chem. Phys., 72 (1980) 650-54. e) J.-P. Blaudeau, M. P. McGrath, L. A. Curtiss, and L. Radom, "Extension of Gaussian-2 (G2) theory to molecules containing third-row atoms K and Ca," J. Chem. Phys., 107 (1997) 5016- 21. f) A. J. H. Wachters, "Gaussian basis set for molecular wavefunctions containing third-row atoms," J. Chem. Phys., 52 (1970) 1033. g) P. J. Hay, "Gaussian basis sets for molecular calculations – representation of 3D orbitals in transition-metal atoms," J. Chem. Phys., 66 (1977) 4377-84. h) K. Raghavachari and G. W. Trucks, "Highly correlated systems: Excitation energies of first row transition metals Sc-Cu," J. Chem. Phys., 91 (1989) 1062-65. i) R. C. Binning Jr. and L. A. Curtiss, 16 "Compact contracted basis-sets for 3rd-row atoms – GA-KR," J. Comp. Chem., 11 (1990) 1206-16. j) M. P. McGrath and L. Radom, "Extension of Gaussian-1 (G1) theory to bromine-

containing molecules,” J. Chem. Phys., 94 (1991) 511-16. k) L. A. Curtiss, M. P. McGrath, J.-P. Blaudeau, N. E. Davis, R. C. Binning Jr., and L. Radom, “Extension of Gaussian-2 theory to molecules containing third-row atoms Ga-Kr,” J. Chem. Phys., 103 (1995) 6104-13.

[e] G. Scalmani and M. J. Frisch, “Continuous surface charge polarizable continuum models of solvation. I. General formalism,” J. Chem. Phys., 132 (2010) 114110.

[f] a) C. Adamo and D. Jacquemin, “The calculations of excited-state properties with Time-Dependent Density Functional Theory,” Chem. Soc. Rev., 2013, 42, 845. b) A. D. Laurent, C. Adamo, D. Jacquemin, “Dye chemistry with time-dependent density functional theory,” Phys. Chem. Chem. Phys., 2014, 16, 14334-56.

**Part 2** –X3LYP/6-31G(d)/PCM(DMSO) energy profile of the dihedral bond rotation from *Z* to *E* rotamer for both NH-C thiourea bonds (N<sub>3</sub>H-C, left and N<sub>1</sub>H-C, right) at the reduced 1-methyl-3-(4-nitrophenyl)thiourea model. The energy difference between the first and the most energetic rotamer in the profile is 6.5 (N<sub>3</sub>H-C) and 17.2 kcal/mol (N<sub>1</sub>H-C), respectively.

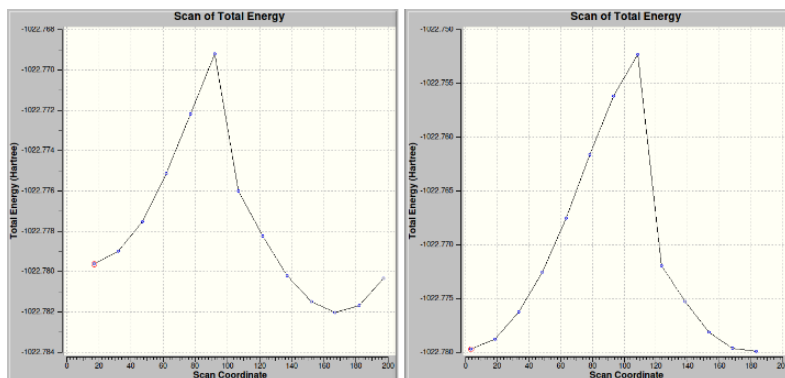


**Figure S29.** N<sub>3</sub>H-C (left) and N<sub>1</sub>H-C (right) energy profile of the dihedral bond-rotation from *Z* to *E* rotamer at 1-methyl-3-(4-nitrophenyl)thiourea.

**Part 3** –X3LYP/6-31G(d)/PCM(DMSO) energy profile of the dihedral bond rotation from *Z* to *E* rotamer for both NH-C thiourea bonds (N<sub>3</sub>H-C, left and N<sub>1</sub>H-C, right) at chemosensor **1**. The energy difference between the first and the most energetic rotamer in the profile is 5.5 (N<sub>3</sub>H-C) and 13.9 kcal/mol (N<sub>1</sub>H-C), respectively.

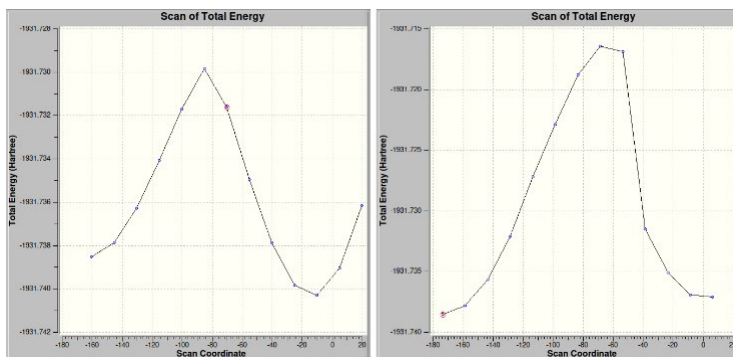


**Figure S30.** N<sub>3</sub>H-C (left) and N<sub>1</sub>H-C (right) energy profile of the dihedral bond-rotation from *Z* to *E* rotamer at chemosensor **1**.

**Part 4** –X3LYP/6-31G(d)/PCM(DMSO) energy profile of the dihedral bond rotation from *Z* to *E* rotamer for both NH-C thiourea bonds (N<sub>3</sub>H-C, left and N<sub>1</sub>H-C, right) at chemosensor **2**. The energy difference between the first and the most energetic rotamer in the profile is 5.5 (N<sub>3</sub>H-C) and 13.9 kcal/mol (N<sub>1</sub>H-C), respectively.

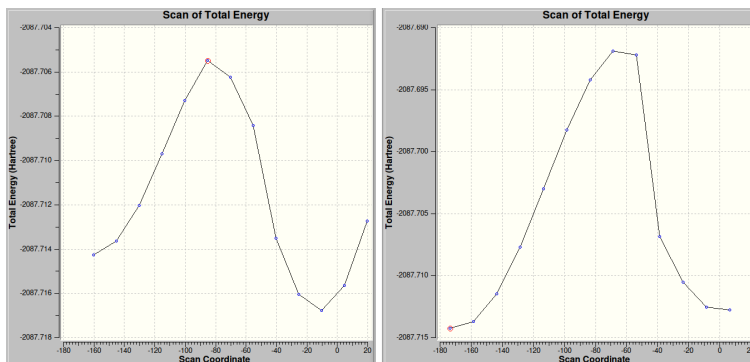


**Figure S31.** N<sub>3</sub>H-C (left) and N<sub>1</sub>H-C (right) energy profile of the dihedral bond-rotation from *Z* to *E* rotamer at chemosensor **2**.

**Part 5** - X3LYP/6-31+G(d,p)/PCM(DMSO) energy and (C=O)-(C=S) distance of the optimized structures of the rotamers found along the full-search of the PES for chemosensor **1**.

**Table S3.** X3LYP/6-31+G(d,p)/PCM(DMSO) energy (*E*, in hartrees), energy difference ( $\Delta E$ , in kcal/mol) with respect to the most stable structure and distance between C=O of trifluoromethyl acetate group and C=S thiourea carbon atoms ( $d_{(C=O)-(C=S)}$ , in angstroms) for the optimized structures of chemosensor **1** rotamers.

<b>Structure</b>	<b>E</b> (hartrees)	<b><math>\Delta E</math></b> (kcal/mol)	<b><math>d_{(C=O)-(C=S)}</math></b> (Å)
<b>1-conf1</b>	-1931,820057	10,6	8,14
<b>1-conf2</b>	-1931,833730	2,0	10,83
<b>1-conf3</b>	-1931,821545	9,6	8,08
<b>1-conf4</b>	-1931,835218	1,1	10,82
<b>1-conf5</b>	-1931,818129	11,8	7,93
<b>1-conf6</b>	-1931,831972	3,1	10,87
<b>1-conf7</b>	-1931,815870	13,2	8,67
<b>1-conf8</b>	-1931,829810	4,5	10,98
<b>1-conf9</b>	-1931,820038	10,6	9,40
<b>1-conf10</b>	-1931,834990	1,2	9,43
<b>1-conf11</b>	-1931,823127	8,7	9,39
<b>1-conf12</b>	-1931,836035	0,6	8,15
<b>1-conf13</b>	-1931,823717	8,3	9,11
<b>1-conf14</b>	-1931,833079	2,4	8,07
<b>1-conf15</b>	-1931,817851	12,0	9,22
<b>1-conf16</b>	-1931,831860	3,2	8,40
<b>1-conf17</b>	-1931,820042	10,6	9,22



*Chapter 2: GHB detection through the use of ditopic ligands*

<b>1-conf18</b>	-1931,834246	1,7	8,16
<b>1-conf19</b>	-1931,821940	9,4	9,40
<b>1-conf20</b>	-1931,836066	0,5	8,23
<b>1-conf21</b>	-1931,823759	8,3	9,13
<b>1-conf22</b>	-1931,834246	1,7	8,05
<b>1-conf23</b>	-1931,817851	12,0	9,22
<b>1-conf24</b>	-1931,831879	3,2	8,39
<b>1-conf25</b>	-1931,821427	9,7	9,42
<b>1-conf26</b>	-1931,835008	1,2	9,44
<b>1-conf27</b>	-1931,823127	8,7	9,39
<b>1-conf28</b>	-1931,836917	0,0	9,39
<b>1-conf29</b>	-1931,819072	11,2	9,36
<b>1-conf30</b>	-1931,833163	2,4	9,26
<b>1-conf31</b>	-1931,818218	11,7	9,83
<b>1-conf32</b>	-1931,832086	3,0	9,49

**Part 6** -X3LYP/6-31+G(d,p)/PCM(DMSO) energy and (C=O)-(C=S) distance of the optimized structures of the rotamers found along the full-search of the PES for chemosensor **2**.

**Table S4.** X3LYP/6-31+G(d,p)/PCM(DMSO) energy (E, in hartrees), energy difference ( $\Delta E$ , in kcal/mol) with respect to the most stable structure and distance between C=O of trifluoromethyl acetate group and C=S thiourea carbon atoms ( $d_{(C=O)-(C=S)}$ , in angstroms) for the optimized structures of chemosensor **2** rotamers.

<b>Structure</b>	<b>E</b> (hartrees)	<b><math>\Delta E</math></b> (kcal/mol)	<b><math>d_{(C=O)-(C=S)}</math></b> ( $\text{\AA}$ )
<b>2-conf1</b>	-2087,804293	12,1	7,20
<b>2-conf2</b>	-2087,805636	11,3	7,29
<b>2-conf3</b>	-2087,803340	12,7	7,03
<b>2-conf4</b>	-2087,800198	14,7	7,06
<b>2-conf5</b>	-2087,804254	12,1	7,24
<b>2-conf6</b>	-2087,805538	11,3	7,35
<b>2-conf7</b>	-2087,803070	12,9	7,05
<b>2-conf8</b>	-2087,800157	14,7	7,04
<b>2-conf9</b>	-2087,817794	3,6	10,52
<b>2-conf10</b>	-2087,819088	2,8	10,48
<b>2-conf11</b>	-2087,816545	4,4	10,57
<b>2-conf12</b>	-2087,813976	6,0	10,51
<b>2-conf13</b>	-2087,815185	5,3	8,49
<b>2-conf14</b>	-2087,817538	3,8	8,61
<b>2-conf15</b>	-2087,815219	5,2	8,38
<b>2-conf16</b>	-2087,807389	10,2	7,84
<b>2-conf17</b>	-2087,810663	8,1	8,32

<b>2-conf18</b>	-2087,812682	6,8	8,54
<b>2-conf19</b>	-2087,810178	8,4	8,32
<b>2-conf20</b>	-2087,803182	12,8	9,09
<b>2-conf21</b>	-2087,815893	4,8	8,43
<b>2-conf22</b>	-2087,817592	3,8	8,45
<b>2-conf23</b>	-2087,818135	3,4	8,56
<b>2-conf24</b>	-2087,811224	7,8	9,07
<b>2-conf25</b>	-2087,821879	1,1	8,63
<b>2-conf26</b>	-2087,823581	0,0	8,77
<b>2-conf27</b>	-2087,820226	2,1	8,84
<b>2-conf28</b>	-2087,817651	3,7	9,03

**Part 7** -Simulated UV-Vis spectra of selected optimized geometries of rotamers of **1**.

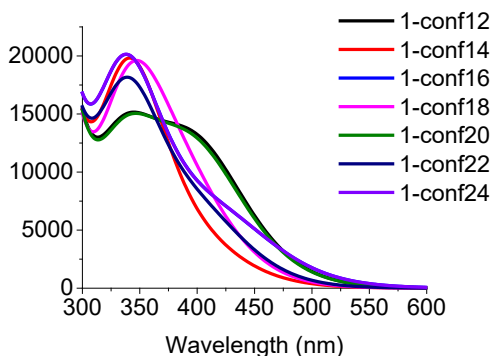


**Figure S32.** Simulated UV-Vis spectra from the TD-DFT vertical excitation energies analysis of selected X3LYP/6-31+G(d,p)/PCM(DMSO) optimized geometries of rotamers of **1** at the same theory level (15 states, singlets only).

Please, note that the main band is centered around 340-350 nm and that whenever N<sub>3</sub>H-C thiourea bond adopts an *E* conformation (see **1-conf12** and **1-conf20**), a shoulder at 390 nm appears, which is not seen at the experimental UV-Vis spectra, fact that agrees with the appearance of *Z,Z*-

rotamers (the ones that enables chemosensors to establish readily an effective hydrogen-bond interaction with the carboxylate of GHB) as the main ones.

**Part 8** -Simulated UV-Vis spectra of selected optimized geometries of rotamers of **2**.

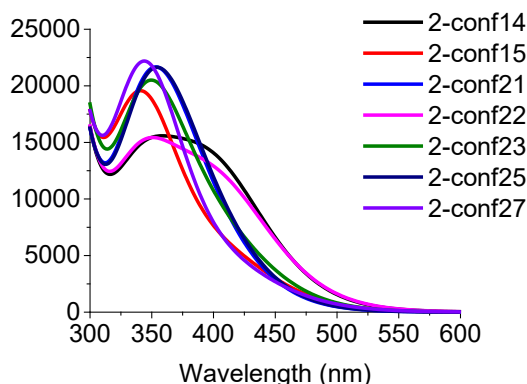


**Figure S33.** Simulated UV-Vis spectra from the TD-DFT vertical excitation energies analysis of selected X3LYP/6-31+G(d,p)/PCM(DMSO) optimized geometries of rotamers of **2** at the same theory level (15 states, singlets only).

Please, note that the main band is centered around 340-350 nm and that whenever  $N_3H-C$  thiourea bond adopts an *E* conformation (see **1-conf14** and **1-conf22**), a shoulder at 390 nm appears, which is not seen at the experimental UV-Vis spectra, fact that agrees with the appearance of *Z,Z*-rotamers (the ones that enables chemosensors to establish readily an effective hydrogen-bond interaction with the carboxylate of GHB) as the main ones.

**Part 9** - X3LYP/6-31+G(d,p)/PCM(DMSO) energies of the optimized structures of **1-GHB** derivatives with hydrogen bonds between the thiourea and carboxylate moieties and between the N<sub>3</sub>-deprotonated thiourea and the carboxylic acid group.

**Table S5.** X3LYP/6-31+G(d,p)/PCM(DMSO) energy (E, in hartrees), relative energy ( $\Delta E$ , in kcal/mol) and hydrogen-bond type, of the optimized structures of **1-GHB** derivatives with single/double hydrogen bonds between the thiourea and carboxylate or between the N<sub>3</sub>-deprotonated thiourea and the carboxylic acid group.

Structure	E (hartrees)	$\Delta E$ (kcal/mol)	Hydrogen-bond type
<b>1-GHB-a</b>	-2314,199679	0,00	double HB (carboxylate-thiourea)
<b>1-GHB-b</b>	-2314,191321	5,24	double HB (carboxylate-thiourea)
<b>1-GHB-c</b>	-2314,195948	2,34	double HB (carboxylate-thiourea)
<b>1-GHB-d</b>	-2314,184309	9,64	single HB (carboxylate-thiourea)
<b>1-GHB-e</b>	-2314,181783	11,23	double HB (carboxylic acid-N <sub>3</sub> -deprotonated thiourea)
<b>1-GHB-f</b>	-2314,190573	5,71	double HB (carboxylic acid-N <sub>3</sub> -deprotonated thiourea)
<b>1-GHB-g</b>	-2314,186472	8,29	double HB (carboxylic acid-N <sub>3</sub> -deprotonated thiourea)

**Part 10** - X3LYP/6-31+G(d,p)/PCM(DMSO) energies of the optimized structures of **2-GHB** derivatives with hydrogen bonds between the thiourea and carboxylate moieties and between the N<sub>3</sub>-deprotonated thiourea and the carboxylic acid group.

**Table S6.** X3LYP/6-31+G(d,p)/PCM(DMSO) energy (E, in hartrees), relative energy ( $\Delta E$ , in kcal/mol) and hydrogen-bond type, of the optimized structures of **2-GHB** derivatives with single/double hydrogen bonds between the thiourea and carboxylate or between the N<sub>3</sub>-deprotonated thiourea and the carboxylic acid group.

Structure	E (hartrees)	$\Delta E$ (kcal/mol)	Hydrogen-bond type
<b>2-GHB-a</b>	-2470,1733572	0,18	double HB (carboxylate-thiourea)
<b>2-GHB-b</b>	-2470,1736486	0,00	double HB (carboxylate-thiourea)
<b>2-GHB-c</b>	-2470,1715432	1,32	single HB (carboxylate-thiourea)
<b>2-GHB-d</b>	-2470,1664388	4,52	single HB (carboxylate-thiourea)
<b>2-GHB-e</b>	-2470,1646541	5,64	double HB (carboxylic acid-N <sub>3</sub> -deprotonated thiourea)
<b>2-GHB-f</b>	-2470,1651804	5,31	double HB (carboxylic acid-N <sub>3</sub> -deprotonated thiourea)
<b>2-GHB-g</b>	-2470,1660697	4,76	single HB (carboxylic acid-N <sub>3</sub> -deprotonated thiourea)
<b>2-GHB-h</b>	-2470,1586224	9,43	single HB (carboxylic acid-N <sub>3</sub> -deprotonated thiourea)

**Part 11** - Simulated UV-Vis spectra of selected optimized geometries of rotamers of **1-GHB** derivatives.

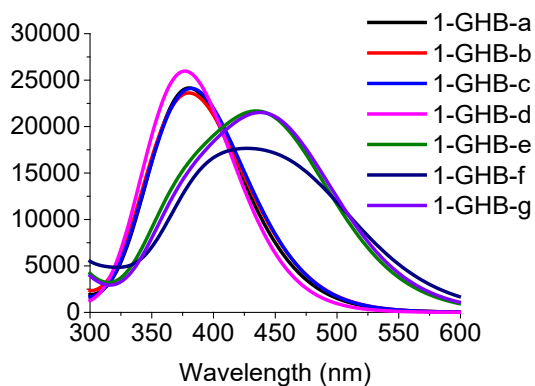


**Figure S34.** Simulated UV-Vis spectra from the TD-DFT vertical excitation energies analysis of selected X3LYP/6-31+G(d,p)/PCM(DMSO) optimized geometries of rotamers of **1-GHB** derivatives at the same theory level (15 states, singlets only).

Please, note that the main band is centered around 380 nm for species where the hydrogen bond takes place between the thiourea moiety and the carboxylate (**1-GHB-a** to **1-GHB-d**) regardless of the number of hydrogen bonds formed and the main band is centered around 430-440 nm for species where the hydrogen bond takes place between the N<sub>3</sub>-deprotonated thiourea and the carboxylic acid group (**1-GHB-e** to **1-GHB-g**).

**Part 12** - Simulated UV-Vis spectra of selected optimized geometries of rotamers of **2-GHB** derivatives.

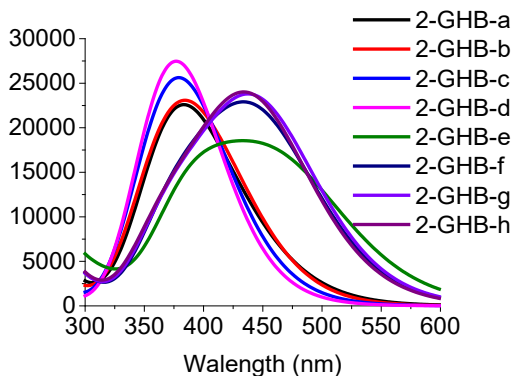


**Figure S35.** Simulated UV-Vis spectra from the TD-DFT vertical excitation energies analysis of selected X3LYP/6-31+G(d,p)/PCM(DMSO) optimized geometries of rotamers of **2-GHB** derivatives at the same theory level (15 states, singlets only).

Please, note that the main band is centered around 380 nm for species where the hydrogen bond takes place between the thiourea moiety and the carboxylate (**2-GHB-a** to **2-GHB-d**) regardless of the number of hydrogen bonds formed and the main band is centered around 430-440 nm for species where the hydrogen bond takes place between the  $N_3$ -deprotonated thiourea and the carboxylic acid group (**2-GHB-e** to **2-GHB-h**).



**Part 13** - X3LYP/6-31+G(d,p)/PCM(DMSO) absolute (E, in hartrees) and relative ( $\Delta E$ , in kcal/mol) of chemosensor **2-GHB-a** (double hydrogen bond between thiourea and carboxylate) and **2-GHB-a'** (no hydrogen bond, equivalent 1,2-trans cyclohexane ring substituents, Z,Z- thiourea and ester conformations) of increasing hydroxyacid chain.

**Table S7.** X3LYP/6-31+G(d,p)/PCM(DMSO) energy (E, in hartrees), relative energy ( $\Delta E$ , in kcal/mol) and hydrogen-bond type, of the optimized structures of **2-GHB** derivatives with (**2-GHB-a**) and without (**2-GHB-a'**) double hydrogen bonds between the thiourea and carboxylate of increasing hydroxyacid chain (3 to 7 carbon atoms, noted as XC) with equivalent conformations of cyclohexane ring substituents, thiourea moiety and ester group. Please, note that the lowest stabilization due to the hydrogen bond formation takes place at the 3-hydroxypropionate, is maximum at GHB and, from there, decreases.

Structure	E (hartrees)	$\Delta E(2\text{-GHB-a vs } 2\text{-GHB-a'})$ (kcal/mol)
<b>2-GHB-a(3C)</b>	-2430,872711	4,02
<b>2-GHB-a</b>	-2470,173357	0,09
<b>2-GHB-a(5C)</b>	-2509,467970	0,56
<b>2-GHB-a(6C)</b>	-2548,762117	1,50
<b>2-GHB-a(7C)</b>	-2588,057222	1,82
<b>2-GHB-a'(3C)</b>	-2430,879116	
<b>2-GHB-a'</b>	-2470,173500	
<b>2-GHB-a'(5C)</b>	-2509,468869	
<b>2-GHB-a'(6C)</b>	-2548,764502	
<b>2-GHB-a'(7C)</b>	-2588,060122	

**Part 14** –Stabilization of butyric acid and 1-methyl-3-(4-nitrophenyl)thiourea in different hydrogen-bonded complexes and protonation states.

**Table S8.** X3LYP/6-31+G(d,p)/PCM(DMSO) energy (E, in hartrees), relative energy ( $\Delta E$ , in kcal/mol) of butyric acid/butyrate, 1-methyl-3-(4-nitrophenyl)thiourea and  $N_3$ -deprotonated 1-methyl-3-(4-nitrophenyl)thiourea in different hydrogen-bonded complexes.

Structure	E (hartrees)	$\Delta E$ (kcal/mol)	Hydrogen bond
butyrate	-307,14534413		
butyric acid	-307,61249807		
1-methyl-3-(4-nitrophenyl)thiourea	-1022,82522452		
$N_3$ -deprotonated thiourea	-1022,35725196		
acid + thiourea <sub>conformation 1</sub>	-1330,44706964	-5,87	single hydrogen bond
acid + thiourea <sub>conformation 2</sub>	-1330,44612229	-5,27	single hydrogen bond
carboxylate thiourea <sub>conformation 1</sub>	+ -1329,99267431	-13,87	single hydrogen bond
carboxylate thiourea <sub>conformation 2</sub>	+ -1329,99140705	-13,08	single hydrogen bond
carboxylate thiourea <sub>conformation 3</sub>	+ -1329,99773512	-17,05	double hydrogen bond
carboxylate thiourea <sub>conformation 4</sub>	+ -1329,99773511	-17,05	double hydrogen bond
acid + $N_3$ -deprotonated thiourea	-1329,98884260	-11,98	double hydrogen bond

**Chapter 3: Colorimetric and  
fluorimetric GHB detection  
with benzoxazole derivatives**



### 3.1. Introduction

Heterocyclic compounds are cyclic chemical substances whose structures exhibit, at least, one heteroatom (usually nitrogen, oxygen or sulphur). They are commonly found in nature, playing besides indispensable roles to life. On one hand, some examples of their importance for human beings are their appearance in DNA (deoxyribonucleic acid) and RNA (ribonucleic acid), in some essential  $\alpha$ -aminoacids, such as histidine or tryptophan, or some vitamins or hormones. On the other hand, some highly known substances, such as penicillin or cocaine come naturally from fungi and plants, respectively (see Chart 3.1). Moreover, thanks to their key roles in life, they are widely employed with pharmaceutical purposes or as pesticides.<sup>69,70</sup>

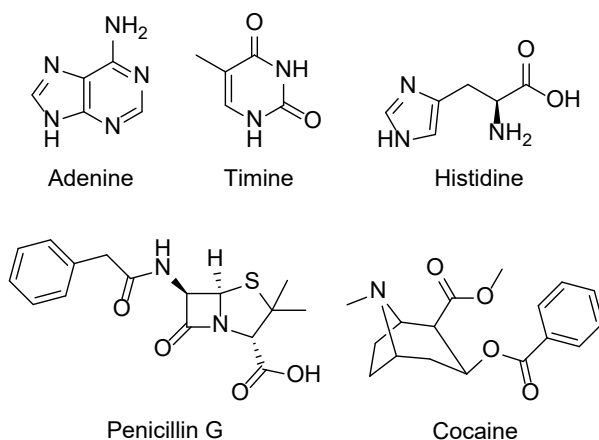


Chart 3.1. Some examples of natural products, which comprised a heterocycle in their structures

Benzoxazoles and their derivatives are included inside this huge and varied family. These heterocyclic compounds have been broadly explored due to their vast spectrum of biological activity.<sup>70-74</sup> Because of this feature, several synthetic methodologies to reach them have been developed.<sup>73-77</sup> Some examples of benzoxazoles are flunoxaprofen and boxazomycins, whose clinical properties are anti-inflammatory and antimicrobial, respectively (see Chart 3.2).

Chapter 3: Colorimetric and fluorimetric GHB detection with benzoxazole derivatives

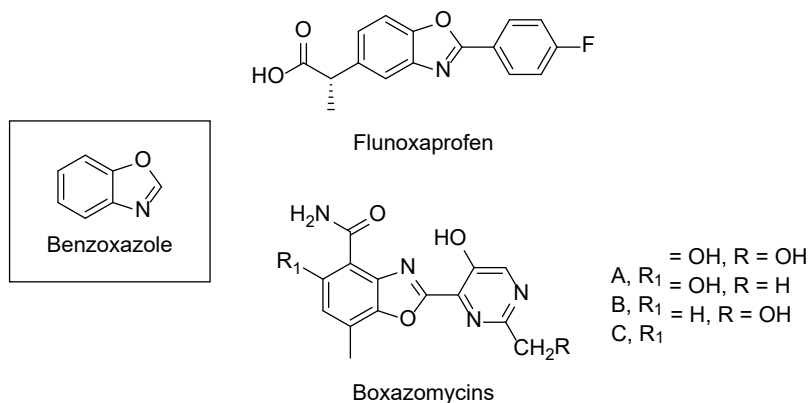


Chart 3.2. Basic structure of benzoxazole and some of its derivatives used in medicine.

These heterocycles also have been widely used in sensing field. Multiple sensors have been developed to detect cations such as Mg(II), Zn(II), Cd(II), Hg(II), Cu(II), Ni(II),<sup>78-85</sup> anions (CN<sup>-</sup> and F<sup>-</sup>),<sup>81,82</sup> both anions and cations either at the same time or separately<sup>82,84</sup> and neutral molecules such as cysteine and glutathione.<sup>86</sup>

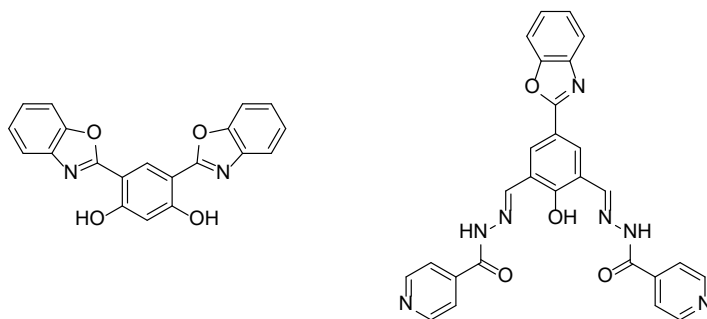


Chart 3.3. Some sensors, including benzoxazole moieties, described in the literature

Some of the sensors described in the literature with benzoxazole cores are shown in Chart 3.3. The first compound, a 2-(2'-hydroxyphenyl)benzoxazole (HBO) derivative, described by Abeywickrama and Pang was able to detect the anion fluoride. This family of compounds are well known since they easily undergo excited-state intramolecular proton transfer (ESIPT) and, as a result, they are very likely to exist in a tautomeric equilibrium between their

enol and keto forms. This event is interrupted in the presence of both cationic or anionic species. Thus, fluoride, able to establish an intermolecular hydrogen bond with the phenolic H, competed with the intramolecular one, which gave rise to the disappearance of the ESIPT phenomenon.<sup>82</sup> On the other hand, the second derivative showed in Chart 3.3 was capable of detecting not only Zn(II), but also pyrophosphate ion (PPI). According to the authors, the formed tetracoordinate complex of Zn(II) activated an intramolecular charge transference (ICT) with its concomitant fluorescence emission. Upon the addition of PPI, this emission disappeared as Zn(II) was no longer able to coordinate to the benzoxazole derivative, allowing to use the adduct ligand-Zn(II) to recognise PPI in a very competitive medium such cells.<sup>84</sup>

### 3.2. Chemosensors design

Regarding the large number of reports that exists in the bibliography related to not only benzoxazoles, but also their derivatives, we decided to synthesize a family of compounds which comprised this kind of heterocycles in their structure: 2-aminobenzoxazoles.

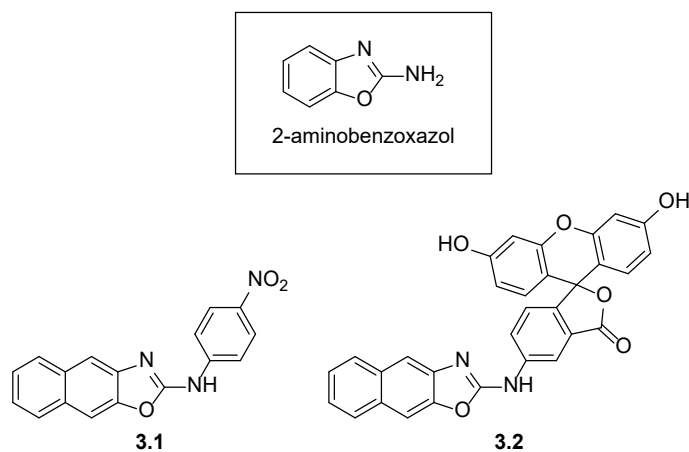


Chart 3.4. Structure of 2-aminobenzoxazole and the probes synthesised

*Chapter 3: Colorimetric and fluorimetric GHB detection with benzoxazole derivatives*

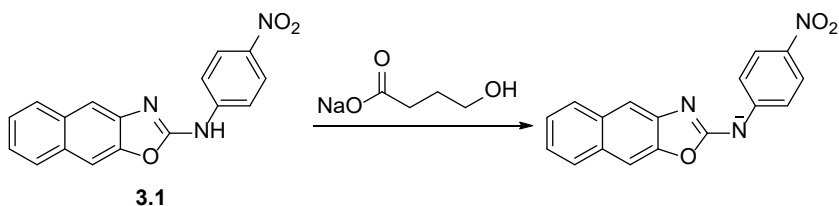
Additionally, to the best of our knowledge, this type of compounds had not been used to recognise carboxylates. For this reason, we designed two derivatives in order to detect GHB (see Chart 3.4). Both compounds contained in their structures a naphthoxazole ring and another aromatic moiety as signalling unit. *p*-Nitrophenyl and fluorescein were chosen as such since they were capable of providing significant changes in colour (probe **3.1**) and both colour and fluorescence (probe **3.2**).



### 3.3. Objectives

Considering the wide use of benzoxazoles and other similar heterocycles in the sensing field, including the recognition of anions, their well-established and easy synthesis available in the literature and the necessity of reliable and sensitive probes to detect GHB, the specific objectives proposed were:

- Synthesis of the designed chemosensors (**3.1** and **3.2**).
- Recognition studies using  $^1\text{H}$  NMR spectroscopy.
- Study of the probes optical properties in the absence and the presence of the analyte as well as the effect of the content of water in the medium.
- Assessment of their use in the detection of GHB in drinks and beverages.



Scheme 3.1. Paradigm of detection of GHB using the benzoxazole derivatives



### 3.4. Protection against chemical submission: Naked-eye detection of $\gamma$ -hydroxybutyric acid (GHB) in soft drinks and alcoholic beverages

Silvia Rodríguez-Nuévalos,<sup>a</sup> Ana M. Costero,\*<sup>a,b,c</sup> Pau Arroyo,<sup>b</sup> José A. Sáez<sup>b</sup>, Margarita Parra<sup>a,b,c</sup> Félix Sancenón<sup>a,c,d,e,f</sup> and Ramón Martínez-Máñez \*<sup>a,c,d,e,f</sup>

<sup>a</sup>Instituto Interuniversitario de Investigación de Reconocimiento Molecular y Desarrollo Tecnológico (IDM). Universitat Politècnica de València, Universitat de València, Doctor Moliner 50, Burjassot, 46100, Valencia, Spain.

<sup>b</sup>Departamento de Química Orgánica, Universitat de València, Doctor Moliner 50, Burjassot, 46100, Valencia, Spain.

<sup>c</sup>CIBER de Bioingeniería, Biomateriales y Nanomedicina (CIBER-BBN) (Spain)

<sup>d</sup>Unidad Mixta UPV-CIPF de Investigación en Mecanismos de Enfermedades y Nanomedicina, Universitat Politècnica de València, Centro de Investigación Príncipe Felipe, Valencia, Spain.

<sup>e</sup>Unidad Mixta de Investigación en Nanomedicina y Sensores, Universitat Politècnica de València, Instituto de Investigación Sanitaria La Fe, Valencia, Spain.

<sup>f</sup>Departamento de química, Universidad Politècnica de València, Camino de vera s/n 46022, Valencia, Spain

\* Correspondence: ana.costero@uv.es

**Received:** 7th August 2021

**Accepted:** 7th August 2021

*Chem. Commun.*, **2020**, *56*, 12600



## Abstract

Two new oxazole derivatives, able to detect  $\gamma$ -hydroxybutyric acid (GHB) in soft drinks and alcoholic beverages, by colour and fluorescence changes, are reported.

## Introduction

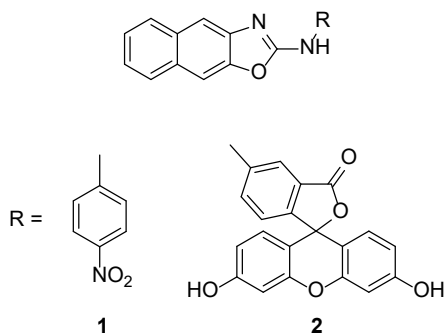
Chemical submission is an important social problem which, in many cases, is associated with sexual aggression. This type of aggression is known as drug facilitated sexual assault (DFSA). In fact, the use of chemical compounds able to manipulate the will of the persons with criminal goals has strongly increased in the last years. Compounds such as scopolamine, ketamine, rohypnol, xanax or  $\gamma$ -hydroxybutyric acid (GHB) can induce these effects. Among them, GHB is one of the most used as DFSA due to its physical and biological properties. GHB is a colourless and odourless liquid with a slightly salty taste that can be easily supplied in a drink without the victim perceiving it. Additionally, the effect after its intake is fast (15-30 min) and lasted periods of 6 to 8 hours. Finally, its detection in the body is difficult as GHB is quickly metabolized.<sup>1,2</sup> For all these reasons, the development of detection systems to prevent possible DFSA abuses is very desirable. In this sense, the preparation of colorimetric or fluorescent chemosensors to detect GHB is a research field of great interest.<sup>3</sup>

Chromo-fluorogenic chemosensors are extensively used for the detection of charged and neutral molecules and are excellent alternatives to classical analytical methods due to several functional features.<sup>4-8</sup> At this respect, these probes can detect the analyte in real-time, employ low cost instrumentations (in many cases, detection can be done by the naked eye) and not special skills are necessary to use them. In spite of these features, there are relatively few examples of chromo-fluorogenic chemosensors for GHB recognition. Recently, Chang *et al.* reported the use of two different borodipyromethene derivatives to detect GHB and its corresponding lactone (GHL).<sup>9,10</sup> The detection mechanism was, in both cases, based on hydrogen bonding interactions. On the other hand, Lin and co-workers prepared an Ir-complex whose luminescence was quenched

### Chapter 3: Colorimetric and fluorimetric GHB detection with benzoxazole derivatives

in the presence of GHB.<sup>11</sup> Bravo *et al.* detected GHB in drinks using the enzyme  $\beta$ -hydroxybutyrate dehydrogenase (GHB-DH).<sup>12</sup> The protocol proposed by these authors involves the enzymatic oxidation of GHB by  $\text{NAD}^+$  coupled with the reduction of a red-ox active dye. Finally, Baumes and co-workers used a colorimetric array to detect GHB and GHL in water.<sup>13</sup>

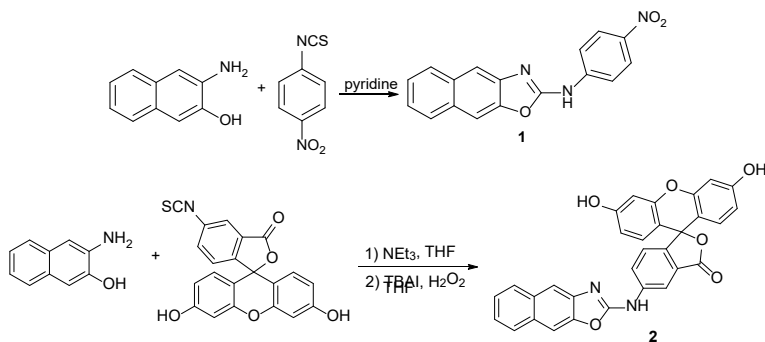
Taking into account the above mentioned facts and our interest in the design, synthesis and evaluation of optical chemosensors to sense different biologically active analytes such as nerve agent simulants, neurotransmitters or pollutant gases,<sup>14-16</sup> we report here the use of two naphthoxazole derivatives (Scheme 1) to detect GHB in both soft drinks and alcoholic beverages.



**Scheme 1.** Chemical structure of probes **1** and **2** for GHB detection.

Probes **1** and **2** were prepared from 3-amino-2-naphthol following the procedures described in Scheme 2. Compound **1** was synthesized in one step by stirring 3-amino-2-naphthol with 4-nitrophenylisothiocyanate in pyridine.<sup>17</sup> On the other hand, compound **2** was prepared from the same starting material but using fluorescein isothiocyanate and trimethylamine to isolate the corresponding thiourea that was subsequently transformed in the naphthoxazole derivative by using tetrabutylammonium iodide and hydrogen peroxide.<sup>18</sup> Compounds **1** and **2** were characterized using  $^1\text{H}$  and  $^{13}\text{C}$  NMR and HRMS (Figures S1-S6).

Chapter 3: Colorimetric and fluorimetric GHB detection with benzoxazole derivatives



**Scheme 2.** Synthetic pathway to prepare probes **1** and **2**.

Once **1** and **2** were fully characterised we studied the UV-visible and fluorescence properties of both probes in DMSO. Probe **1** (10  $\mu\text{M}$  in DMSO) shows an absorption band centred at 355 nm ( $\epsilon = 22880 \text{ M}^{-1} \text{ cm}^{-1}$ ) that confers a yellow colour to the solution. On the other hand, probe **2** (10  $\mu\text{M}$  in DMSO) shows an absorption band at 370 nm ( $\epsilon = 18935 \text{ M}^{-1} \text{ cm}^{-1}$ ) and presents in solution a pale yellow colour. Regarding emission features, probe **1** is non-emissive (probably due to the presence of an electron withdrawing nitro group in its structure) whereas **2** presents a weak fluorescence at 541 nm (when it is irradiated at 490 nm) ascribed to the neutral form of fluorescein.<sup>19</sup>

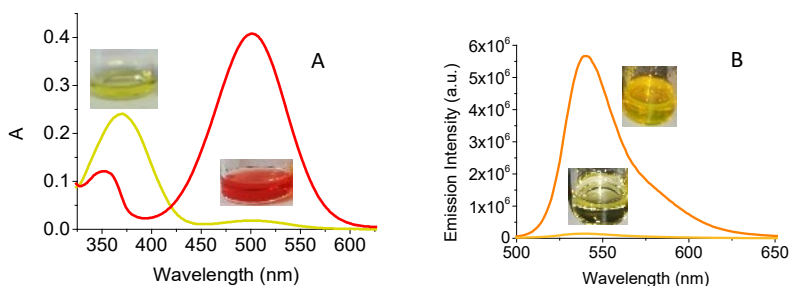


**Figure 1.** A) UV-visible spectra of probe **1** alone (yellow curve) and in the presence of GHB 10  $\mu\text{M}$  (red curve) in DMSO. B) Fluorescence of probe **2** alone (yellow curve) and in the presence of GHB 10  $\mu\text{M}$  (orange curve) in DMSO. The inset showed the colour changes observed in the presence of GHB for DMSO solutions of both probes.

### *Chapter 3: Colorimetric and fluorimetric GHB detection with benzoxazole derivatives*

Once assessed the spectroscopic characteristics of both probes, changes in the presence of GHB in DMSO were studied. Addition of GHB (10  $\mu\text{M}$ ) to DMSO solutions of probe **1** induced the appearance of a new absorption band centred at 500 nm with an associate clear colour change from yellow to red (Figure 1A). On the other hand, nearly the same behaviour was observed with probe N and addition of GHB (10  $\mu\text{M}$ ) also induced the appearance of a new absorption band centred at 490 nm (data not shown) resulting in a colour change from pale yellow to orange. However, in the case of probe **2**, a marked emission enhancement at 541 nm (excitation at 490 nm) was found (39-fold) in the presence of GHB (Figure 1B). UV-visible titrations, carried out with the addition of increasing amounts of GHB to DMSO solutions of probe **1**, showed the progressive decrease of the UV band at 355 nm and the concomitant appearance of the redshifted absorption at 500 nm (Figure 2A). From the titration profile shown in Figure 2B a limit of detection of 0.13  $\mu\text{M}$  for GHB was calculated as  $3 \cdot S_b/m$ , where  $S_b$  is the blank standard deviation and  $m$  is the slope.<sup>20</sup> On the other hand, addition of increasing quantities of GHB to DMSO solutions of probe **2** induced a progressive increase in the emission at 541 nm (excitation at 490 nm) as shown in Figure 2C. From the titration profile (Figure 2D) a limit of detection of 0.12  $\mu\text{M}$  for GHB was assessed.



Chapter 3: Colorimetric and fluorimetric GHB detection with benzoxazole derivatives

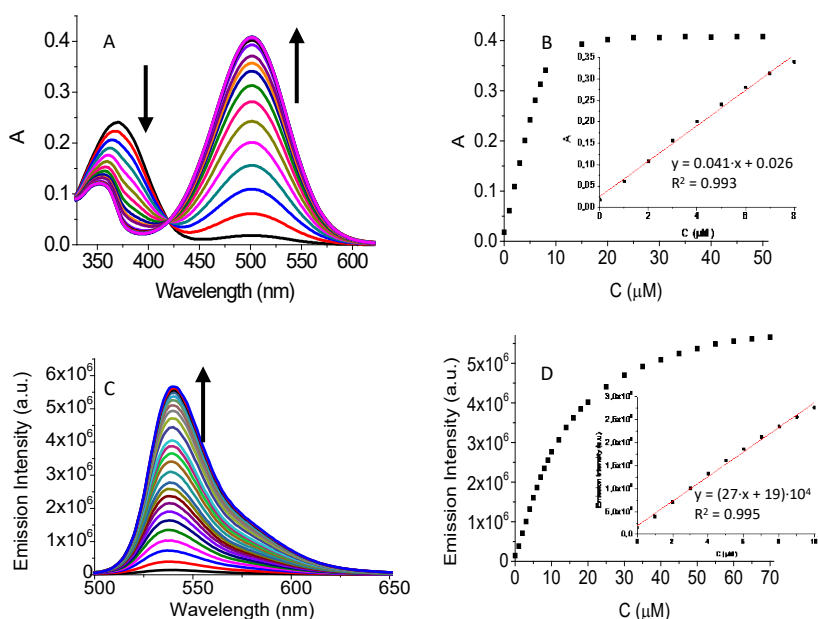


**Figure 2.** A) UV-visible changes of probe **1** (10  $\mu\text{M}$  in DMSO) with increasing amounts of GHB (0-5 eq.). B) Changes in the absorbance at 500 nm of DMSO solutions of probe **1** upon addition of increasing amounts of GHB. C) Fluorescence changes of probe **2** (10  $\mu\text{M}$  in DMSO) with increasing amounts of GHB (0-7eq.). D) Changes in the emission at 541 nm (excitation at 490 nm) of DMSO solutions of probe **2** upon addition of increasing amounts of GHB.

Dealing with the mechanism of the chromo-fluorogenic response observed in the presence of GHB, UV-visible titration of probe **1** (Figure 2A) showed the presence of an isosbestic point at 420 nm. This fact pointed to the presence of a single equilibrium between probe **1** and GHB. Besides,  $^1\text{H}$  NMR studies with probe **1** and increasing amounts of GHB (Figure S7) showed marked upfield shifts of all the signals of the aromatic protons in **1**. These changes are consistent with an increase electron density in the probe as a consequence of the recognition process. In addition, the signal at 11.64 ppm (ascribed to the NH group directly linked with the oxazole heterocycle and the benzene ring with a nitro in the para position) disappeared after addition of 0.1 eq. of GHB. Both facts pointed toward a deprotonation as the mechanism of the chromo-fluorogenic

response observed. To ensure this hypothesis, both NMR and UV-Vis spectra were registered after the addition of an excess of tetrabutylammonium hydroxide (TBAOH) and tetrabutylammonium fluoride (TBAF) and the same results were reached (see supplementary information, Figures S9 and S10). In addition, this explanation fits with the theoretical calculations included later in the text.

In order to further study the potential use of probes **1** and **2** in more realistic samples, we found that UV-visible titration of DMSO-water 95:5 v/v solutions of probe **1** with GHB was nearly the same than that observed in pure DMSO (Figure S8, ESI). Higher amounts of water (up to 20%) can also be used but the intensity of changes decreases as increasing quantities of water are used.

In the light of these results, we tested the response of probe **1** in the presence of different beverages. For this purpose, samples of different beverages were spiked with GHB sodium salt (12 mM) and pure beverages samples were also prepared for comparison. Then, 100  $\mu\text{L}$  of pure or GHB-containing beverage were mixed with 100  $\mu\text{L}$  of aqueous  $\text{NaHCO}_3$  solution (0.4 mM), to ensure a slight basic pH, at room temperature. 30  $\mu\text{L}$  of this mixture were added to a DMSO solution of probe **1** (50  $\mu\text{M}$ ) and a colour change was monitored immediately (Figure 3). Following the same procedure, probe **2** was studied but measuring fluorescence using a UV lamp for excitation (see also Figure 3). As could be seen in Figure 3 marked colour changes for the GHB-adulterated samples were observed in the presence of probe **1** whereas, also emission enhancement was seen when sensor **2** was used. The results obtained with other beverages are reported in the supplementary information (Figures S11-S16).

Chapter 3: Colorimetric and fluorimetric GHB detection with benzoxazole derivatives

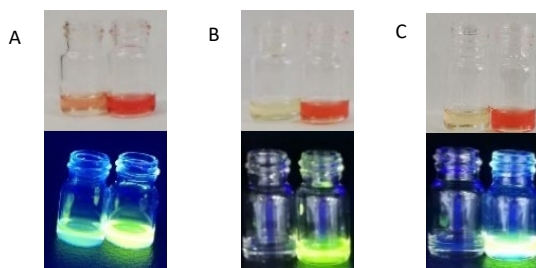
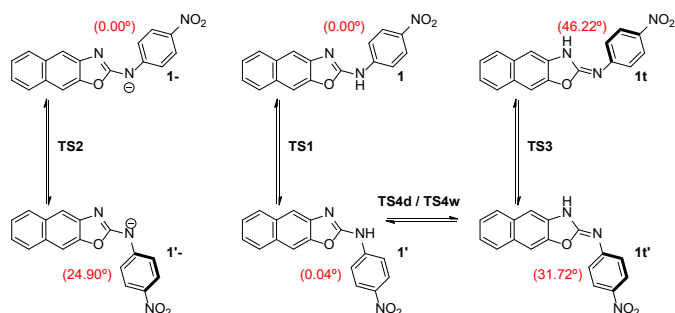


**Figure 3.** Up: Color changes observed with probe **1** in the presence of (A) whisky, (B) cola, (C) whisky/cola. Down: Fluorescence changes observed with probe **2** in the presence of (A) whisky, (B) cola, (C) whisky/cola. In both cases the left vial contained the drink whereas the right vial contained the beverage spiked with GHB.

In order to gain insight in the behaviour of **1** in presence of GHB, DFT calculations have been carried out using Gaussian09 rev. D01 program package<sup>21</sup> and GaussView 5<sup>22</sup> was employed to visualize the results. In this sense, structures of tautomers and conformers of **1** were considered (Scheme 3).



**Scheme 3.** Structure of the isomers obtained in the PES and transition states connecting them. In TS4, letters d and w indicate direct or water-mediated mechanism, respectively. In red, dihedral angle between naphthoxazole and p-aminonitrobenzene rings in the optimized geometries.

To do so, an exploration of the potential energy surface (PES) was carried out obtaining four main minima, which included **1**, the conformer **1'** (obtained through the rotation of the C-N bond between the naphthoxazole ring and the p-aminonitrobenzene moiety) and the tautomeric forms with the nitrogen atom of naphthoxazole ring protonated, **1t** and **1t'**. An extended discussion

about the PES has been moved to the ESI for brevity. Among these four computed isomers, the lower free energy structure corresponds to **1** by 1.43, 3.41 and 2.33 kcal/mol less than **1'**, **1t** and **1t'**, respectively. The lowest energy geometries of **1** and **1'** turned out to be planar, while **1t** and **1t'** had 46.22 and 31.72 degrees, respectively, between its two ring systems (see Scheme 3). With the purpose of studying the interaction between compound **1** and GHB, which is supposed to be an acid-base equilibrium to yield compound **1-**, as it has been pointed out by the experimental data, a thermodynamic cycle was performed to compute the pK<sub>a</sub> of both **1/1-** and GHB/GHB- species in DMSO using the procedure described in the ESI. These calculations yield a pK<sub>a</sub> of 10.4 for **1/1-** pair and a pK<sub>a</sub> of 11.3 for GHB/GHB-. The value of pK<sub>a</sub> computed for GHB/GHB- in DMSO is similar to that reported for acetic acid.<sup>23</sup> In the case of naphthoxazol amines, no bibliographic references of its acid-base behaviour in DMSO exist to our knowledge. Therefore, the proposed acid-base equilibrium between both acid-base pairs, in which **1** behaves as an acid and GHB- does as a base could occur under such conditions. In the same way, as previously proposed, **1-** presents a rotamer, **1'-**, which may be present in the medium (Scheme 3), that results 2.04 kcal/mol more energetic than **1-**.

Considering that the temperature of an alcoholic beverage may be between 5 and 25 °C and that acid-base reactions are considerably faster than both conformational changes and tautomerization reactions, we present here the study of the vertical excitation energies using the optimized geometries of **1** and **1-**. Additionally, bearing in mind the main species present in absence of GHB as well as in its presence of it, the Boltzmann distribution equation (1) on the relative energies obtained in the PES was applied. The results showed that the population of **1** and **1-** is around 90 and 97%, respectively, of the species present at 25 °C and, therefore, they can be considered as the main responsible for the shape of the UV-Vis spectra and, consequently, will be the only ones included in the UV-Vis spectra simulation analysis by TD-DFT calculations in solution phase.

$$N_i = e^{-\Delta E_i/RT} / \sum_n e^{-\Delta E_n/RT} \quad (1)$$

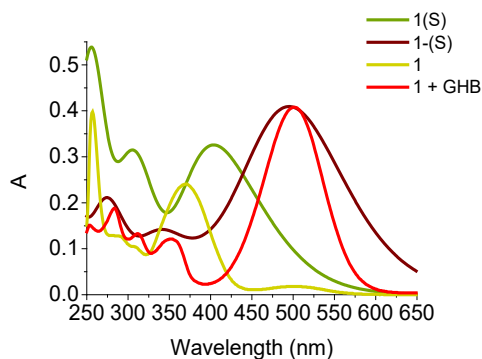


**Figure 4.** The simulated scaled spectra for **1** (green) and **1-** (garnet) in DMSO superimposed on the experimental spectra for **1** (yellow) and **1+GHB** (red) in DMSO.

Experimentally, the presence of GHB in a solution of **1** generates a bathochromic displacement of the  $\lambda_{\max}$  from 370 nm to 500 nm. In the case of the TD-DFT calculations, a  $\lambda_{\max}$  of 404 nm is observed for **1** in DMSO, while for the deprotonated species **1-** this band rises to 495 nm (Figure 4). The calculated electronic transitions responsible for the  $\lambda_{\max}$  are summarized in Figure 5. The main UV-Vis absorption band at 495 nm predicted for **1-** is mainly associated to an HOMO $\rightarrow$ LUMO excitation (2.4784 eV,  $f=0.9453$ , 500.05 nm; see ESI for further details). Electronic density in HOMO is delocalized over the whole molecular structure and upon excitation, it is mainly located over the *p*-aminonitrobenzene moiety (see Figure 5).

The good correlation found between the experimental and predicted UV-Vis spectra for **1-** supports the deprotonation of compound **1** in presence of GHB.

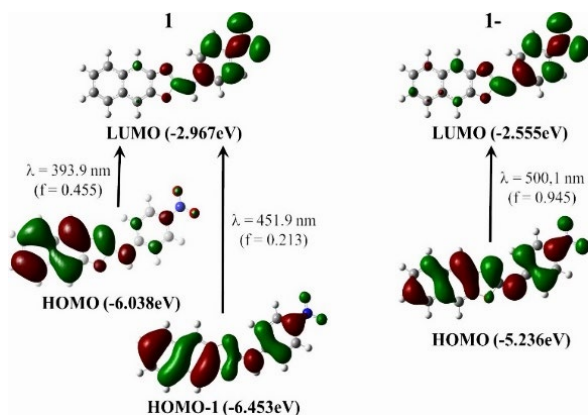


**Figure 5.** Representation of the canonical orbitals implied in the electronic transitions responsible for the  $\lambda_{\max}$  of simulated spectra of **1** and **1-**.

## Conclusions

In conclusion, we report herein two new probes based on the oxazole core to detect GHB in real-time and in real-samples. In the presence of GHB a marked color change from yellow to red for probe **1** and a remarkable emission enhancement for sensor **2** were observed. In both cases, the GHB limits of detection are much lower than the usual intake in recreational environments. DFT calculations and  $^1\text{H}$  NMR measurements indicated a GHB-induced deprotonation of the probes as a mechanism of the chromo-fluorogenic response observed. We believe that probe **2** might be suitable to be used in night clubs to test the purity of beverages due to its strong changes in fluorescence which can be easily observed with the lighting present in these places. This methodology improves what has already been described and it is simpler for its application.

## Acknowledgements

We thank the Spanish Government, MICINN funds (RTL2018-100910-B-C42 and RTI2018-100910-B-C41) and the Generalitat Valenciana (PROMETEO 2018/024) for financial support. S. R. -N. is grateful to the Spanish Government for a fellowship. SCSIE (Universidad de Valencia) is gratefully acknowledged for all the equipment employed. NMR was registered at the U26 facility of ICTS "NAMBIOISIS" at the

Universitat of València. The computational resources from the SIUV (Servei d'Informàtica, Universidad de Valencia) are gratefully acknowledged.

### Conflicts of interest

There are not conflicts to declare.

### References

1. E. E. Benarroch, *Neurology*, 2009, **72**, 282-286.
2. M. S. Okun, L. A. Boothby, R. B. Bartfield and P. L. Doering, *J. Pharm. Pharmaceut. Sci.*, 2001, **4**, 167-175.
3. F. P. Busardó, M. Gottardi, A. Tini, A. Minutillo, A. Sirignano, E. Marinelli and S. Zaami, *Current Drug Metabolism*, 2018, **19**, 1080-1085.
4. E. Garrido L. Pla, B. Lozano-Torres, S. El Sayed, R. Martinez-Mañez and F. Sancenon, *Chemistry Open*, 2018, **7**, 401-428.
5. Y. Liu and M. Bonizzoni, *J. Am. Chem. Soc.*, 2014, **136**, 14223-14229.
6. C. Wu, K. Vellaisamy, G. Yang, Z.-Z. Dong, C.-H. Leung, J.-B. Liu and D.-L. Ma, *Dalton Trans*, 2017, **46**, 6677-6682.
7. R. K. Mishra, K. Y. Goud, Z. Li, C. Moonla, M. A. Mohamed, F. Tehrani, H. Teymourian and J. Wang, *J. Am. Chem. Soc.*, 2020, **142**, 5991-5995.
8. M. A. Beatty, A. J. Selinger, Y. Li and F. Hof, *J. Am. Chem. Soc.*, 2019, **141**, 16763-16771.
9. D. Zhai, Y. Qiao, E. Tan, W. Xu and Y-T. Chang, *Chem Commun.*, 2014, **50**, 2904-2906.
10. D. Zhai, B. K. Agrawalla, P. S. F. Eng, S-C. Lee, W. Xua and Y-T. Chang, *Chem Commun.*, 2013, **49**, 6170-6172.
11. W. Wang, Z-Z. Dong, G. Yang, C-H. Leung, S. Lin and D-L. Ma, *J. Mat. Chem. B*, 2017, **8**, 2736-2742.

*Chapter 3: Colorimetric and fluorimetric GHB detection with  
benzoxazole derivatives*

12. D. Bravo, D. Harris and S. Parsons, *J. Forensic Sci.* 2004, **49**, 379-387.
13. L. A. Baumes, M. B. Sogo, P. Montes-Navajas, A. Corma, and H. Garcia, *Chem. Eur. J.*, 2010, **16**, 4489 – 4495.
14. E. Almenar, A.M. Costero, P. Gaviña, S. Gil, M. Parra, *R. Soc. Open sci.*, 2018, **5**, 171787-171792.
15. S. Rodríguez-Nuévalos, M. Parra, S. Ceballos, S. Gil and A. M. Costero, *J. Photochem. Photobiol A: Chemistry*, 2020, **388**, 112132.
16. L. A. Juarez, A. M. Costero, M. Parra, P. Gaviña, S. Gil, R. Martínez-Mañez and F. Sancenon, *Chem. Commun.*, 2017, **53**, 585-588.
17. I. L. Kirby, M. B. Pitak, C. Wilson, P. A. Gale and S. J. Coles, *CrystEngComm.*, 2015, **17**, 2815-2826.
18. V. K. Yadav, V P. Srivastava and L. D. S. Yadav, *Tetrahedron Letters*, 2018, **59**, 252–255.
19. X.-F. Zhang, *Photochem. Photobiol. Sci.*, 2010, **9**, 1261–1268.
20. M. Zhu, M. Yuan, X. Liu, J. Xu, J. Lv, C. Huang, H. Liu, Y. Li, S. Wand, D. Zhu, *Org. Lett.* 2008, **10**, 1481-1484
21. J. Frisch, et al., *Gaussian 09, Revision D.01*, Gaussian, Inc., Wallingford CT, 2016 (for the complete reference see ESI<sup>†</sup>).
22. GaussView, Version 5, Roy Dennington, Todd Keith, and John Millam, Semichem Inc., Shawnee Mission, KS, 2009.
23. I. M. Kolthoff, M. K. Chantooni Jr. and S. Bhowmik, *J. Am. Chem. Soc.*, 1968, **90**, 23-28.



## **Supplementary material**

### **Protection against chemical submission: Naked-eye detection of $\gamma$ -hydroxybutyric acid (GHB) in soft drinks and alcoholic beverages**

Silvia Rodríguez-Nuévalos,<sup>a</sup> Ana M. Costero,\*<sup>a,b,c</sup> Pau Arroyo,<sup>b</sup>  
José A. Sáez<sup>b</sup>, Margarita Parra<sup>a,b,c</sup>, Félix Sancenón<sup>a,c,d,e,f</sup> and  
Ramón Martínez-Máñez\*<sup>a,c,d,e,f</sup>

<sup>a</sup>Instituto Interuniversitario de Investigación de Reconocimiento Molecular y  
Desarrollo Tecnológico (IDM). Universitat Politècnica de València,  
Universitat de València, Doctor Moliner 50, Burjassot, 46100, Valencia,  
Spain.

<sup>b</sup>Departamento de Química Orgánica, Universitat de València, Doctor  
Moliner 50, Burjassot, 46100, Valencia, Spain.

<sup>c</sup>CIBER de Bioingeniería, Biometariables y Nanomedicina (CIBER-BBN) (Spain)

<sup>d</sup>Unidad Mixta UPV-CIPF de Investigación en Mecanismos de Enfermedades  
y Nanomedicina, Universitat Politècnica de València, Centro de Investigación  
Príncipe Felipe, Valencia, Spain.

<sup>e</sup>Unidad Mixta de Investigación en Nanomedicina y Sensores, Universitat  
Politècnica de València, Instituto de Investigación Sanitaria La Fe, Valencia,  
Spain.

<sup>f</sup>Departamento de química, Universidad Politècnica de València, Camino de  
vera s/n 46022, Valencia, Spain

\* Correspondence: ana.costero@uv.es

(See annexes I and II in the CD)

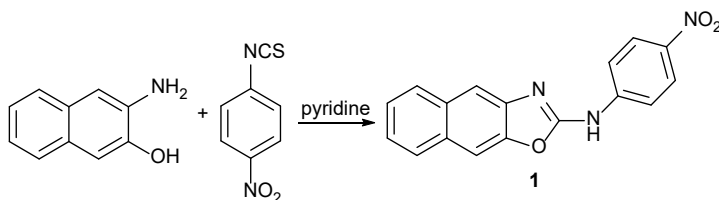


## **Material and methods**

The reagents employed in the synthesis were acquired in Sigma Aldrich and used without further purification.  $^1\text{H}$  NMR,  $^{13}\text{C}$  NMR and  $^{19}\text{F}$  NMR spectra were registered with Bruker Avance 300 MHz, 400 MHz or 500 MHz spectrophotometers, all of them referenced to solvent peak, DMSO( $d_6$ ) or THF( $d_8$ ). UV-Vis spectra were registered with a Shimadzu UV-2600 spectrophotometer, using a cuvette with 1 cm of path length. Fluorescent measures were carried out with a FluoroMax-4 Spectrofluorometer, employing a cuvette with 1 cm of path length. Mass spectrometry spectra were carried out with a TripleTOFTM 5600 LC/MS/MS System, with 2 gas sources (both to 35 psi), 450 °C and ion gas voltage of 5500 V. Origin 2020 was the program to plot titrations.

### **Synthesis of compounds**

#### **Synthesis compound 1**



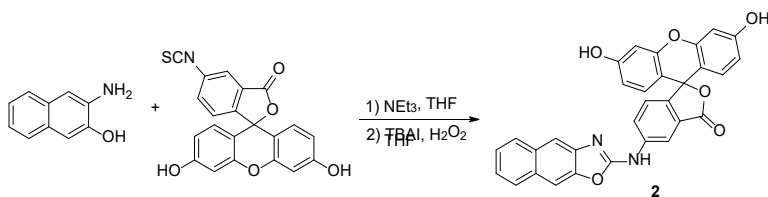
**Scheme S1.** Synthesis pathway to prepare compound 1

In 13 mL of pyridine, 202 mg (1.256 mmol) of 3-amino-2-naphthol were mixed with 191 mg (1.047 mmol) of 4-nitrophenyl isothiocyanate under argon atmosphere for 8 h at room temperature. Then, the solvent was removed to vacuum and the solid was solved in 35 mL of ethyl acetate. The organic phased was washed with 20 mL of an acidic aqueous solution (pH 5), 20 mL of  $\text{NaHCO}_3$  (sat) and 20 mL of  $\text{NaCl}$  (sat), dried over anhydrous  $\text{MgSO}_4$  and filtered. The solvent was removed and the crude was purified by chromatography column using a 6:4 Hexane:AcOEt mixture as eluent and silica gel as solid support. A yellow lightly orange was obtained in

Chapter 3: Colorimetric and fluorimetric GHB detection with benzoxazole derivatives

a 35 % of yield.  $^1\text{H}$  NMR (300 MHz, DMSO)  $\delta$  11.64 (s, 1H), 8.34 (d,  $J$  = 9.4 Hz, 2H), 8.13 – 7.94 (m, 6H), 7.62 – 7.27 (m, 2H).  $^{13}\text{C}$  NMR (75 MHz, DMSO)  $\delta$  158.36, 146.77, 144.62, 142.03, 141.66, 131.28, 129.96, 127.75, 127.68, 125.39, 124.64, 124.50, 117.67, 113.39, 105.06. HRMS:  $m/z$  calculated for  $\text{C}_{17}\text{H}_{12}\text{N}_3\text{O}_3$  ( $M + \text{H}$ ): 306.0879; found: 306.0877 [ $M + \text{H}$ ] $^+$ .

Synthesis compound 2



**Scheme S2.** Synthesis pathway to prepare compound 2

45 mg (0.283 mmol) of 3-amino-2-naphthol were mixed with 98 mg (0.283 mmol) of fluorescein-5-isothiocyanate in 3 mL of THF. Next, 50  $\mu\text{L}$  (0.359 mmol) of NEt<sub>3</sub> were added and the stirring was kept for 16 h to room temperature. Then, 34  $\mu\text{L}$  (0.565 mmol) of H<sub>2</sub>O<sub>2</sub> 30 % and 1 mg (0.003 mmol) of tetrabutylammonium iodide were added and the mixture was stirred for 24 h. Finally, the solvent was removed and the product was isolated as an orange powder without further purification in a 79 % of yield.  $^1\text{H}$  NMR (500 MHz, DMSO)  $\delta$  8.56 (d,  $J$  = 2.1 Hz, 1H), 8.08 – 7.93 (m, 6H), 7.60 – 7.39 (m, 2H), 7.30 (d,  $J$  = 8.4 Hz, 1H), 6.87 (s, 1H), 6.76 – 6.59 (m, 5H), 6.55 (dd,  $J$  = 8.7, 2.4 Hz, 3H).  $^{13}\text{C}$  NMR (126 MHz, DMSO)  $\delta$  151.47, 146.96, 139.19, 131.32, 129.74, 129.26, 128.03, 127.70, 127.54, 124.91, 124.52, 124.22, 112.74, 109.99, 104.71, 102.26. HRMS:  $m/z$  calculated for  $\text{C}_{31}\text{H}_{19}\text{N}_2\text{O}_6$  ( $M + \text{H}$ ): 515.1243; found: 515.1239 [ $M + \text{H}$ ] $^+$ .

## NMR Spectra

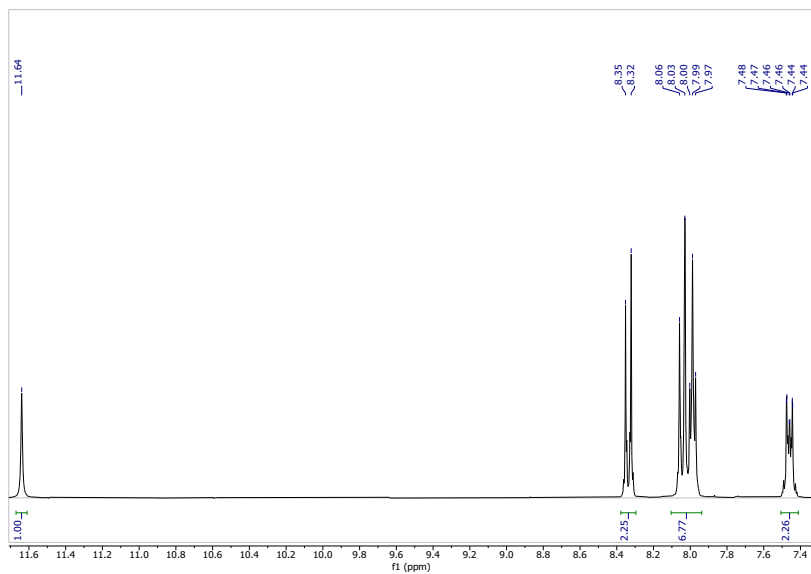


Figure S1. <sup>1</sup>H NMR of compound 1

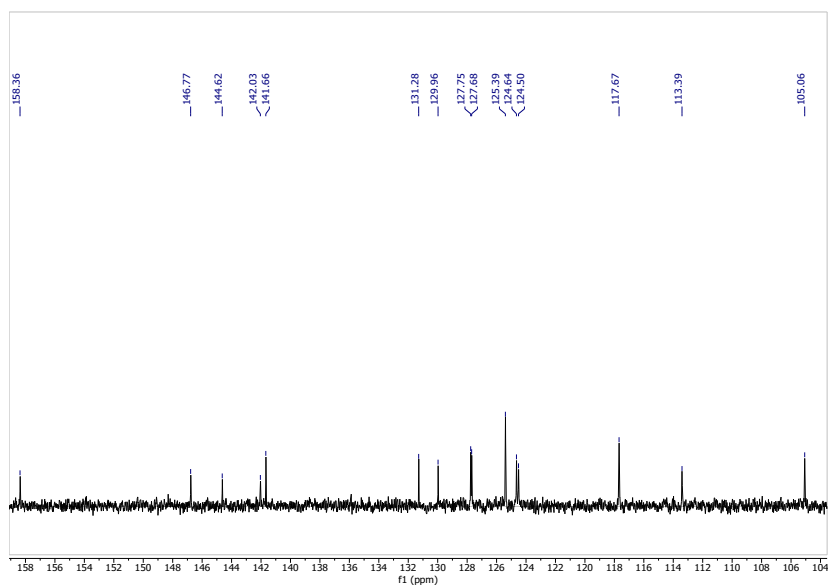


Figure S2. <sup>13</sup>C NMR of compound 1

Chapter 3: Colorimetric and fluorimetric GHB detection with benzoxazole derivatives

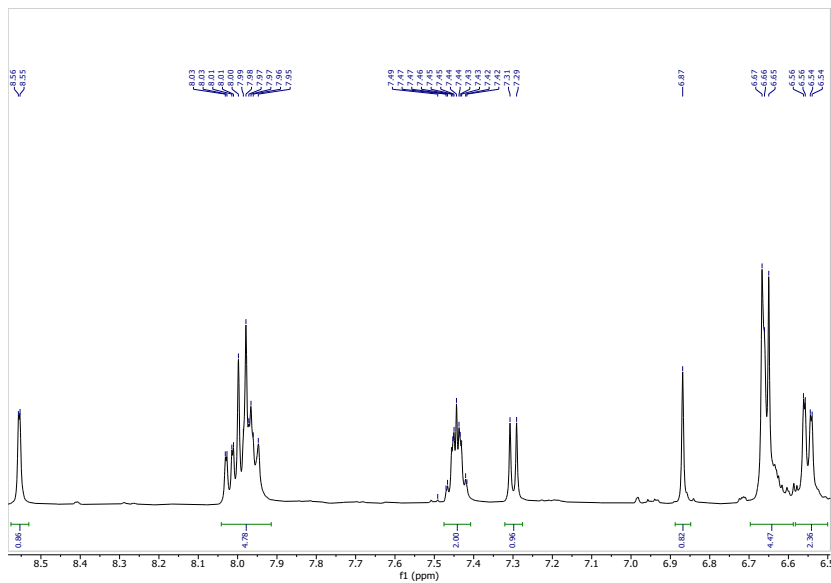


Figure S3. <sup>1</sup>H NMR of compound 2

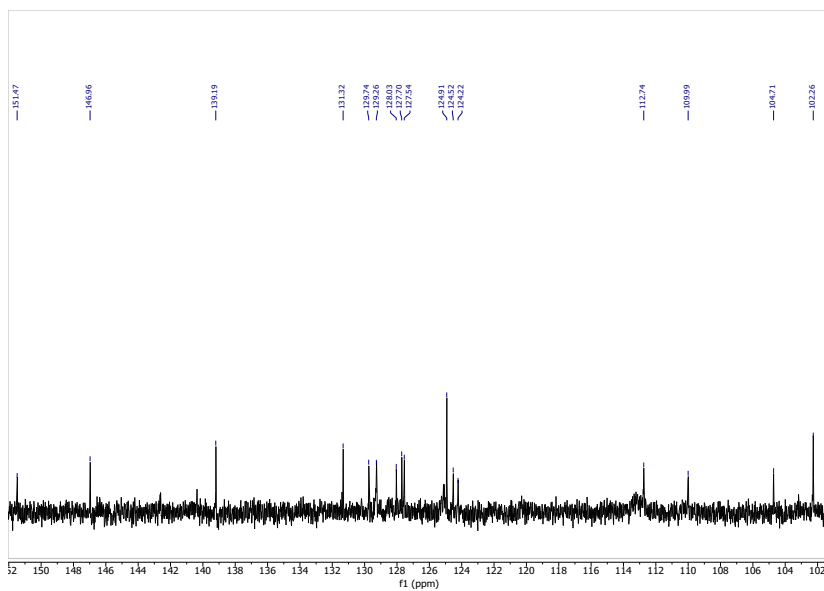


Figure S4. <sup>13</sup>C NMR of compound 2

## Mass Spectroscopy Spectra

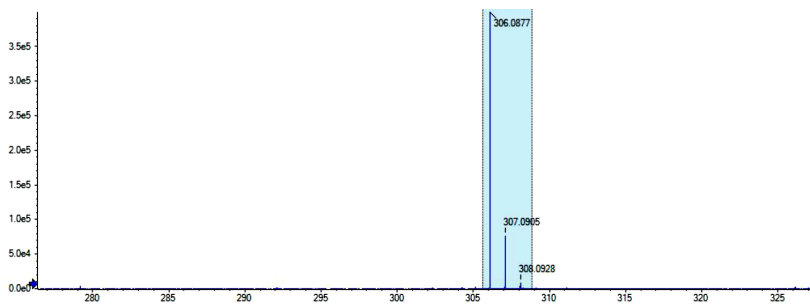


Figure S5. Mass Spectrum compound 1

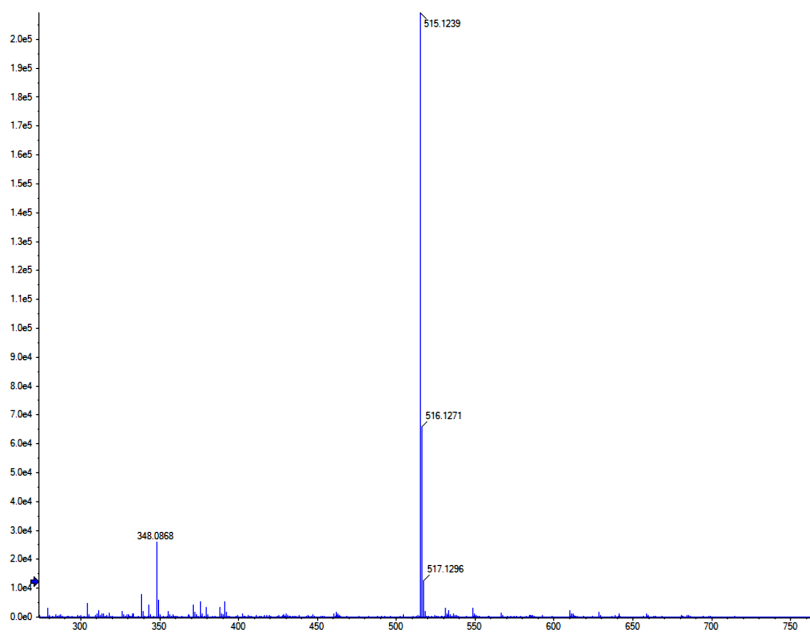


Figure S6. Mass Spectrum of compound 2

## Comparison methods

**Table S1.** Comparison of methods reported in literature

Derivative	BODIPY [1]	BODIPY [2]	Ir Complex [3]	Oxazole
<b>Interaction</b>	Hydrogen bonds	Hydrogen bonds	Not specified	Deprotonation
<b>Signal change</b>	Turn-off fluorescence	Turn-on fluorescence	Turn-off fluorescence	Chromogenic (1) or enhancement fluorescence (2)
<b>Determination</b>	Mixture 1:1 sample with sensor solution	Extraction with DCM and addition of water	Samples and sensor solved in water	Previous pretreatment with base
<b>C<sub>F</sub> sensor (μM)</b>	50	10	2.5	50
<b>C<sub>F</sub> GHB (mg/mL)</b>	5	10	0.15	0.045

## References

[1] D. Zhai, Y. Qiao, E. Tan, W. Xu and Y-T. Chang, *Chem Commun.*, 2014, 50, 2904-2906.

[2] D. Zhai, B. K. Agrawalla, P. S. F. Eng, S-C. Lee, W. Xua and Y-T. Chang, *Chem Commun.*, 2013, 49, 6170-6172.

[3] W. Wang, Z-Z. Dong, G. Yang, C-H. Leung, S. Lin and D-L. Ma, *J. Mat. Chem. B*, 2017, 8, 2736-2742.



## Titration

### NMR titration

A solution 10 mM of **1** and 200 mM of NaGHB were prepared in DMSO-*d*<sub>6</sub>. 400 μL were taken from the solution of **1** and increasing amounts of NaGHB were added, until a total volume of 500 μL.

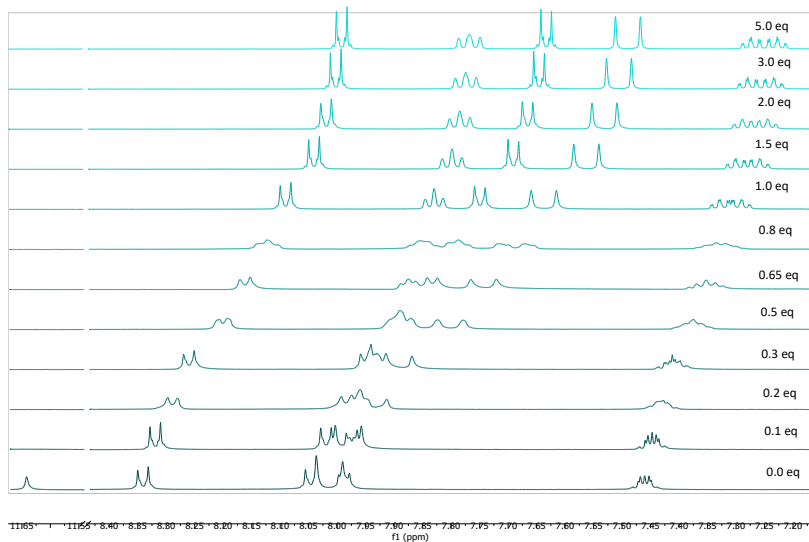


Figure S7. <sup>1</sup>H NMR studies of compound **1** in DMSO-*d*<sub>6</sub> with increasing amounts of GHB

### UV titration

In a 3 mL cuvette (1 cm of path of length), 2475 μL of DMSO were mixed with 25 μL of sensor from a 1 mM solution in DMSO. After that, increasing quantities of NaGHB were added from a 2,5 mM solution of NaGHB in DMSO until arriving to saturation point.

### Fluorescence titration

In a 3 mL cuvette (1 cm of path of length), 2475 μL of DMSO were mixed with 25 μL of sensor from a 1 mM solution in DMSO. Then, increasing quantities of NaGHB were added from a 2,5 mM solution of GHB in DMSO until arriving to saturation point. The samples were irradiated with a wavelength of 490 nm.

### Aqueous media titration

In a 3 mL cuvette (1 cm of path of length), 2350  $\mu\text{L}$  of DMSO were mixed with 125  $\mu\text{L}$  of deionized water and 25  $\mu\text{L}$  of sensor from a 1 mM solution in DMSO. After that, increasing quantities of NaGHB were added from a 2,5 mM solution of NaGHB in DMSO until arriving to saturation point.

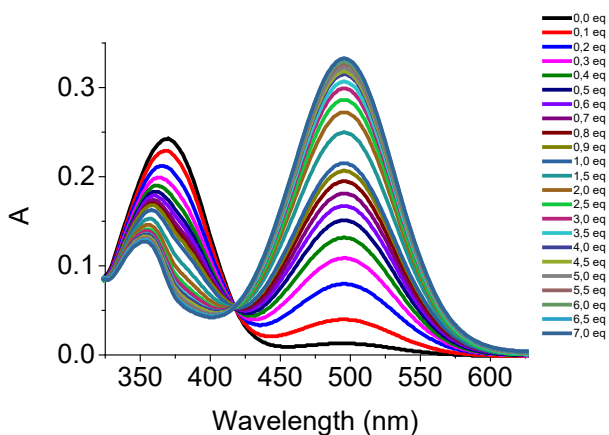


Figure S8. Titration of GHB with compound **1** in DMSO:H<sub>2</sub>O 95:5 media (10  $\mu\text{M}$  of **1**)

### Comparison with other bases

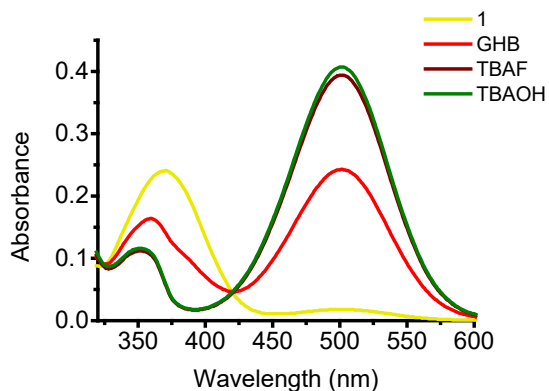
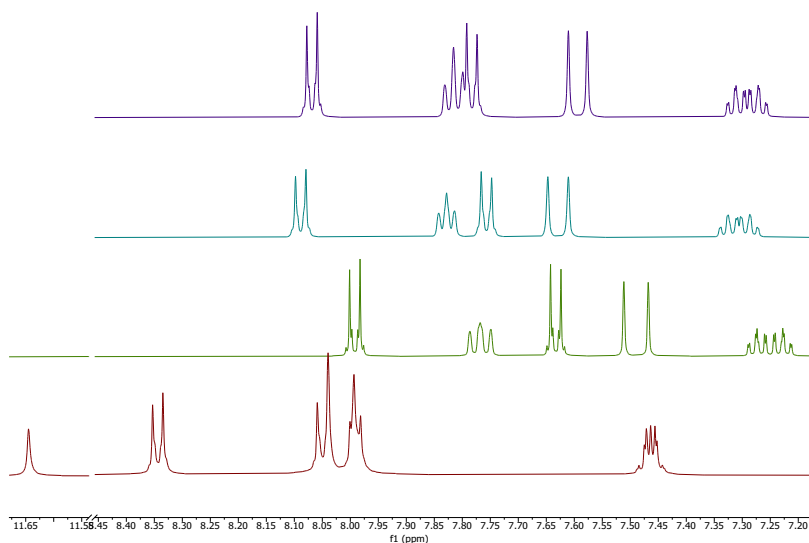


Figure S9. UV-Vis spectra variation of **1** (yellow) in DMSO with 0.5 eq of: GHB (red), TBAF (garnet) and TBAOH (green)



**Figure S10.**  $^1\text{H}$  NMR spectra variation of **1** (red) in  $\text{DMSO-}d_6$  with 0.5 eq of: GHB (green), TBAF (blue) and TBAOH (purple)

### Real Samples Analysis

In first place, the drinks were contaminated with NaGHB in a 12 mM concentration (except Gin tonic whose concentration was 20 mM). After that, an aliquot of 100  $\mu\text{L}$  was taken and mixed with 100  $\mu\text{L}$  of  $\text{NaHCO}_3$  0.4 mM, at room temperature. Then, 30  $\mu\text{L}$  of this solution was taken and mixed with 50  $\mu\text{L}$  of sensor (1 mM in DMSO) and 920  $\mu\text{L}$  of DMSO. Colour or fluorescence changes were observed immediately. The same process was followed for the samples without GHB.

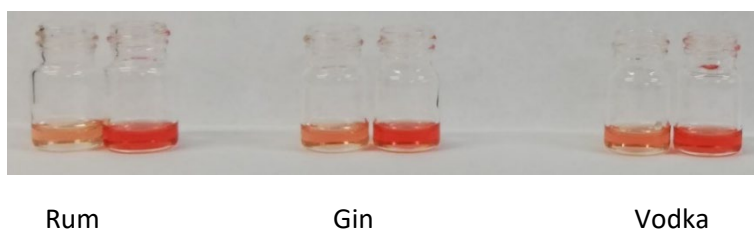


**Figure S11.** Colour change observed with alcoholic drinks using compound **1**

*Chapter 3: Colorimetric and fluorimetric GHB detection with benzoxazole derivatives*



Nestea

Beer

**Figure S12.** Colour change observed with soft drinks using compound **1**

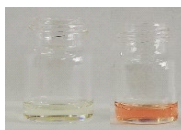


**Figure S13.** Colour change observed with a beverage (Gin Tonic) using compound **1**



Rum

Gin

Vodka

**Figure S14.** Fluorescent changes observed in compound **2** with real samples (alcoholic drinks)



Nestea

Beer

**Figure S15.** Fluorescent changes observed in compound **2** with real samples (soft drinks)



**Figure S16.** Colour change observed with a beverage (Gin Tonic) using compound **2**

## **Theoretical calculations**

The following Supporting Information section, which contains the details of computational calculations performed in this work, has been structured in the following subsections (which, in turn, has its own bibliographic references included at the end):

- Computational methods. In this section, computational details about the geometrical optimizations, the vertical excitation energy analysis and  $pK_a$  calculations are given.
- Potential energy surface (PES) full-search. In this section, geometry and relative energies of compounds **1** and **1-** as well as their conformers **1'** and **1'-** and tautomers **1t** and **1t'** together with the transition states leading to their interconversion will be described.
- Boltzmann distribution of species.
- Complete TD-DFT vertical excitation energies analysis. This will be done over all stationary points described in the previous sections, namely **1/1-**, **1'/1'-** and **1t/1t'**. Different DFT functionals and basis sets will be included used to predict the UV-Vis spectra starting from B3LYP/6-311++G(2df,2p)/PCM(DMSO) geometries.
- $pK_a$  calculations of the acid-base conjugate pairs **1/1-**, **1'/1'-** and **1t/1t'** through a thermodynamic cycle.
- Annex I: XYZ cartesian coordinates of the minima and TS geometries found along the PES.
- Annex II: Excitation energies, oscillator strengths, spin and spatial symmetry, the  $S^2$  and the largest coefficients in the CI expansion for all TD-DFT vertical excitation energies computed.

## **Computational Methods**

In order to gain insight in the behavior of **1** in presence of GHB, DFT calculations have been carried out using Gaussian09 rev. D01 program package [4] and GaussView 5 [5] was employed to visualize the results. In this sense, structures of **1** and **1-** were modeled. The geometrical optimization was performed using Becke3-Lee-Yang-Parr

hybrid functional (B3LYP) [6] with the split-valence triple- $\zeta$  6-311++G(2df,2p) basis set [7]. To take into account the effect of the solvent, DMSO, PCM solvation model was used [8]. Frequency calculations were performed over optimized structures to properly characterize minima and transition structures (none and a single imaginary frequency, respectively). On the other hand, to explore the electronic transitions responsible for the UV-Vis spectra, vertical excitation energies were computed over B3LYP/6-311++G(2df,2p)/PCM(DMSO) geometries through single-point TD-DFT [9] calculations (30 states, singlets only) in solution using non-equilibrium formalism at the same theory level. Geometry details as well as a full-search performed over the potential energy surface (PES) can be found in the corresponding section of this Electronic Supplementari Information. Finally, to compute  $pK_a$  of the acid-base conjugate pairs **1/1-** and **1'/1'**, the calculation scheme used by Ho via the thermodynamic cycle (MP2-TC) was reproduced [10]. In this scheme, a previous systematic conformer search was performed in both gas and solution phases to locate the global minimum energy structure of each species at the M06-2X/6-31+G(d) [11] level using an ultrafine grid. Solution phase calculations were carried within the SMD solvation model [12] using the default settings in Gaussian09. The corresponding thermal corrections to the Gibbs free energy were computed using a factor of 0.967 to scale the frequencies [13] and using the ideal gas molecular partition functions in conjunction with the rigid-rotor quasiharmonic oscillator (RR-QHO) approximation. In the QHO [14] approximation, vibrational frequencies that were lower than  $100\text{ cm}^{-1}$  were raised to  $100\text{ cm}^{-1}$  due to the breakdown of the harmonic oscillator model for low frequency vibrational modes. This was done with Goodvibes script [15] which, in addition, allowed to apply over the standard state calculations in Gaussian (1 atm and 298.15 K conditions) the appropriate corrections to ensure that all solution phase  $pK_a$ s are computed at a standard state of 1 mol/L. Single-point calculations at (RO)MP2/GTMP2Large theory level was performed on the M06-2X/6-31G+(d) optimised geometries. To compute the  $pK_a$  of each acid-base pair, we have employed the proton free energy  $AG^*_s(H^+)$  of -273.3 [16] kcal/mol, that is consistent with the parametrisation of the SMD model.

### *Chapter 3: Colorimetric and fluorimetric GHB detection with benzoxazole derivatives*

[4] Gaussian 09, Revision D.01, M. J. Frisch, G. W. Trucks, H. B. Schlegel, G. E. Scuseria, M. A. Robb, J. R. Cheeseman, G. Scalmani, V. Barone, G. A. Petersson, H. Nakatsuji, X. Li, M. Caricato, A. Marenich, J. Bloino, B. G. Janesko, R. Gomperts, B. Mennucci, H. P. Hratchian, J. V. Ortiz, A. F. Izmaylov, J. L. Sonnenberg, D. Williams-Young, F. Ding, F. Lipparini, F. Egidi, J. Goings, B. Peng, A. Petrone, T. Henderson, D. Ranasinghe, V. G. Zakrzewski, J. Gao, N. Rega, G. Zheng, W. Liang, M. Hada, M. Ehara, K. Toyota, R. Fukuda, J. Hasegawa, M. Ishida, T. Nakajima, Y. Honda, O. Kitao, H. Nakai, T. Vreven, K. Throssell, J. A. Montgomery, Jr., J. E. Peralta, F. Ogliaro, M. Bearpark, J. J. Heyd, E. Brothers, K. N. Kudin, V. N. Staroverov, T. Keith, R. Kobayashi, J. Normand, K. Raghavachari, A. Rendell, J. C. Burant, S. S. Iyengar, J. Tomasi, M. Cossi, J. M. Millam, M. Klene, C. Adamo, R. Cammi, J. W. Ochterski, R. L. Martin, K. Morokuma, O. Farkas, J. B. Foresman, and D. J. Fox, Gaussian, Inc., Wallingford CT, 2016.

[5] GaussView, Version 5, Roy Dennington, Todd Keith, and John Millam, Semichem Inc., Shawnee Mission, KS, 2009.

[6] a) A.D. Becke, *J.Chem.Phys.* 98 (1993) 5648-5652. b) C. Lee, W. Yang, R.G. Parr, *Phys. Rev. B* 37 (1988) 785-789. c) S.H. Vosko, L. Wilk, M. Nusair, *Can. J. Phys.* 58 (1980) 1200-1211. d) P.J. Stephens, F.J. Devlin, C.F. Chabalowski, M.J. Frisch, *J.Phys.Chem.* 98 (1994) 11623-11627.

[7] a) G. A. Petersson, A. Bennett, T. G. Tensfeldt, M. A. Al-Laham, W. A. Shirley, and J. Mantzaris, "A complete basis set model chemistry. I. The total energies of closed-shell atoms and hydrides of the first-row atoms," *J. Chem. Phys.*, 89 (1988) 2193-218. b) G. A. Petersson and M. A. Al-Laham, "A complete basis set model chemistry. II. Open-shell systems and the total energies of the first-row atoms," *J. Chem. Phys.*, 94 (1991) 6081-90. c) A. D. McLean and G. S. Chandler, "Contracted Gaussian-basis sets for molecular calculations. 1. 2nd row atoms, Z=11-18," *J. Chem. Phys.*, 72 (1980) 5639-48. d) K. Raghavachari, J. S. Binkley, R. Seeger, and J. A. Pople, "Self-Consistent Molecular Orbital Methods. 20. Basis set for correlated wave-functions," *J. Chem. Phys.*, 72 (1980) 650-54. e) J.-P. Blaudeau, M. P. McGrath, L. A. Curtiss, and L. Radom, "Extension of Gaussian-2 (G2) theory to molecules containing third-row atoms K and Ca," *J. Chem. Phys.*, 107 (1997) 5016-21. f) A. J. H. Wachters, "Gaussian basis set for molecular wavefunctions containing third-row atoms," *J. Chem. Phys.*, 52 (1970) 1033. g) P. J. Hay, "Gaussian basis sets for molecular calculations – representation of 3D orbitals in transition-metal atoms," *J. Chem. Phys.*, 66 (1977) 4377-84. h) K. Raghavachari and G. W. Trucks, "Highly correlated systems: Excitation energies of first row transition metals Sc-Cu," *J. Chem. Phys.*, 91 (1989) 1062-65. i) R. C. Binning Jr. and L. A. Curtiss, "Compact contracted basis-sets for 3rd-row atoms – GA-KR," *J. Comp. Chem.*, 11 (1990) 1206-16. j) M. P. McGrath and L. Radom, "Extension of Gaussian-1 (G1) theory to bromine-containing molecules," *J. Chem. Phys.*, 94 (1991) 511-16. k) L. A. Curtiss, M. P. McGrath, J.-P. Blaudeau, N. E. Davis, R. C. Binning Jr., and L. Radom, "Extension of Gaussian-2 theory to molecules containing third-row atoms Ga-Kr," *J. Chem. Phys.*, 103 (1995) 6104-13.

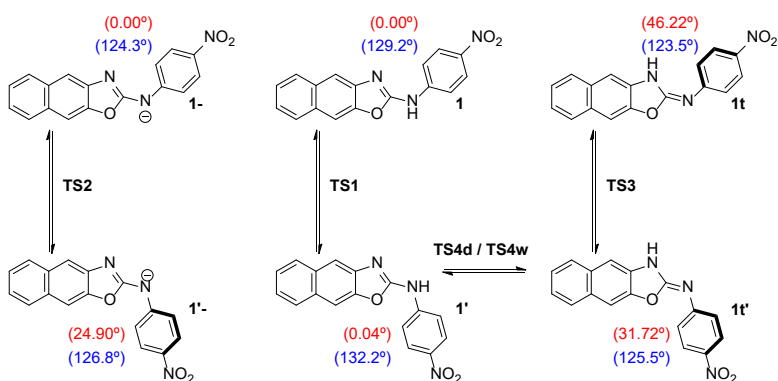
### *Chapter 3: Colorimetric and fluorimetric GHB detection with benzoxazole derivatives*

- [8] G. Scalmani and M. J. Frisch, "Continuous surface charge polarizable continuum models of solvation. I. General formalism," *J. Chem. Phys.*, 132 (2010) 114110.
- [9] a) C. Adamo and D. Jacquemin, "The calculations of excited-state properties with Time-Dependent Density Functional Theory," *Chem. Soc. Rev.*, 2013, 42, 845. b) A. D. Laurent, C. Adamo, D. Jacquemin, "Dye chemistry with time-dependent density functional theory," *Phys. Chem. Chem. Phys.*, 2014, 16, 14334-56.
- [10] J. Ho, "Are thermodynamic cycles necessary for continuum solvent calculation of pK<sub>a</sub>s and reduction potentials?," *Phys. Chem. Chem. Phys.*, 17 (2015) 2859.
- [11] Y. Zhao and D. G. Truhlar, "The M06 suite of density functionals for main group thermochemistry, thermochemical kinetics, noncovalent interactions, excited states, and transition elements: two new functionals and systematic testing of four M06-class functionals and 12 other functionals," *Theor. Chem. Acc.*, 120 (2008) 215-41.
- [12] A. V. Marenich, C. J. Cramer, and D. G. Truhlar, "Universal solvation model based on solute electron density and a continuum model of the solvent defined by the bulk dielectric constant and atomic surface tensions," *J. Phys. Chem. B*, 113 (2009) 6378-96.
- [13] M. K. Kesharwani, B. Brauer, and J. M. L. Martin, "Frequency and Zero-Point Vibrational Energy Scale Factors for Double-Hybrid Density Functionals (and Other Selected Methods): Can Anharmonic Force Fields Be Avoided?," *J. Phys. Chem. A*, 119 (2015), 1701-1714.
- [14] R. F. Ribeiro, A. V. Marenich, C. J. Cramer, and D. G. Truhlar, "Use of Solution-Phase Vibrational Frequencies in Continuum Models for the Free Energy of Solvation," *J. Phys. Chem. B*, 115 (2011) 14556-14562.
- [15] G. Luchini, J. V. Alegre-Requena, I. Funes-Ardoiz, R. S. Paton, "GoodVibes: Automated Thermochemistry for Heterogeneous Computational Chemistry Data", *F1000Research*, 291 (2020) 9. DOI: 10.12688/f1000research.22758.1.
- [16] C. P. Kelly, C. J. Cramer, D. G. Truhlar, "Single-ion solvation free energies and the normal hydrogen electrode potential in methanol, acetonitrile, and dimethyl sulfoxide", *J Phys Chem B.*, 111 (2007) 408-422.



### Potential energy surface (PES) full-search

Firstly, an exploration of the PES of the conformational and tautomeric equilibria involving compounds **1** and **1-** was performed at B3LYP/6-311++G(2df,2p)/PCM(DMSO) level. This search included the conformers **1'** and **1'-** obtained from **1** and **1-** through the rotation of the C-N bond between the naphthoxazole ring and *p*-aminonitrobenzene moiety and the tautomeric forms **1t** and **1t'**, with the proton on the naphthoxazole moiety instead of the nitrogen between the naphthoxazole moiety and *p*-aminonitrobenzene moiety (see Scheme S3). The transition state (TS) between each conformer/tautomer pair was also located and characterized.



**Scheme S3.** Scheme of the species located along the PES search of **1** and **1-** conformational and tautomeric equilibria and the TSs connecting them. In TS4, letters d and w indicate direct or water-mediated mechanism, respectively. In red, dihedral angle between naphthoxazole and *p*-aminonitrobenzene rings. In blue, C-N-C angle between two system rings.

The lowest energy geometries of **1**, **1'** and **1-** turned out to be almost planar (see dihedral angles between naphthoxazole and *p*-aminonitrobenzene rings depicted in red in Scheme S3) while **1'-**, **1t** and **1t'** had 24.9, 46.2 and 31.7 degrees between its two ring systems. The C-N-C angle between two system rings in the stationary points found, depicted in blue in Scheme S3 gives us an idea of the partial C-N double bond character between the naphthoxazole ring and the nitrogen. In this sense, at **1-**, **1'-**, **1t** and **1t'** optimized geometries this angle takes the values 124.3, 126.8, 123.5 and

125.5°, respectively, while at **1** and **1'**, this angle is 129.2 and 132.2°, respectively. The dihedral angle formed between the N-C<sub>p</sub> aminonitrobenzene bond and the naphthoxazol moiety plane at the corresponding TSs of the conformational equilibria between **1/1'**, **1-/1'-** and **1t/1t'** geometries, namely **TS1**, **TS2** and **TS3**, takes the values 87.2, 93.1 and 95.0°, respectively. Regarding the TS connecting **1'** and **1t'** through a tautomerization process (that has been studied both from the theoretical and experimental point of view on 2-aminobenzothiazole derivatives, see refs. [17] and [18]), one has to take into account that there is no equivalent TS between geometries **1** and **1t** since in these compounds hydrogen atom carried by the nitrogen atom between the two ring systems is not in a *syn*-coplanar rearrangement with the oxazol nitrogen atom (antarafacial shift). From that point, the location of the only transition state between **1'** and **1t'** can be made through a direct 1,3-hydride shift process through **TS4d** and through a process catalyzed by two water molecules (see reference [17] for the different catalysis with 1 to 3 water molecules) through **TS4w**. In the case of the latter, to evaluate the energy barrier of the water-catalyzed process, two molecular complexes had to be optimized, both formed by **1'** and **1t'** with two water molecules, namely **MC1'** and **MC1t'**. In the case of **TS4d**, the N<sub>naphthoxazol</sub>...H...N<sub>exocyclic</sub> bond distances were 1.331 and 1.418 angstroms, respectively, while the N<sub>naphthoxazol</sub>...H forming-bond and H...N<sub>exocyclic</sub> breaking-bond distances at **TS4w** were 1.126 and 1.121 angstroms, respectively. Geometries for all above discussed stationary points are depicted in Figure S17, although further details can be obtained at Annex I, where XYZ atomic coordinates are collected.

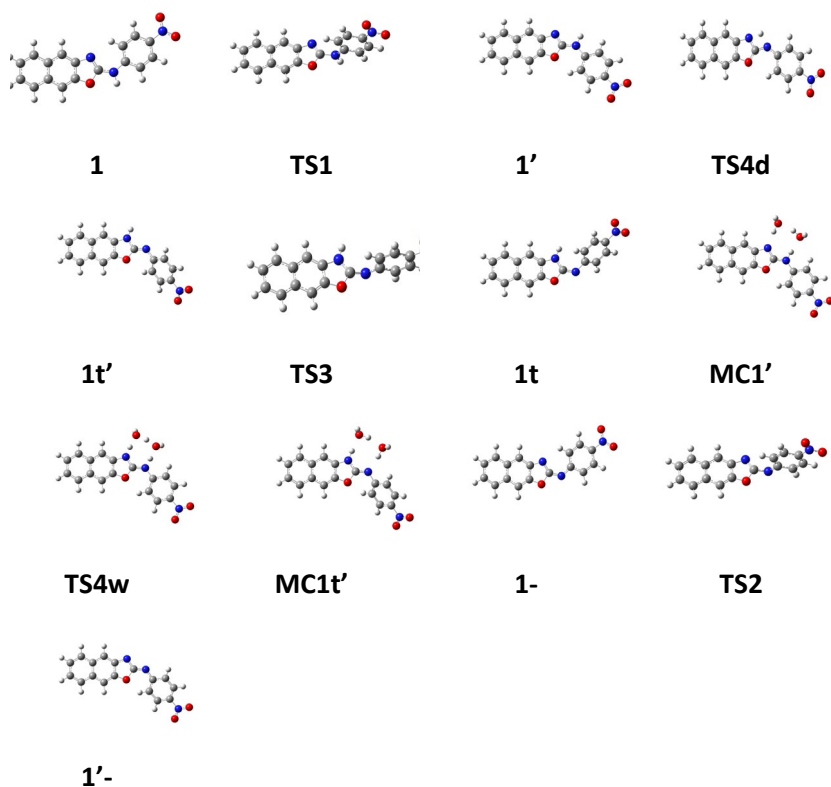


**Figure S17.** Geometries of the stationary points and the TSs found along the PES. For further details about these geometries (distances, angles, ...) please see Annex I, where XYZ atomic coordinates are depicted.

Once some remarkable geometrical details of the stationary points found along the PES had been shown, it is time to discuss the energy aspects of the PES. Among the six computed geometries, the most stable conformers are **1**, **1-** and **1t'** (1.5, 1.8 and 1.0 kcal/mol more stable respectively than their corresponding conformers **1'** and **1'-** and **1t**). In addition, the interconversion between conformers **1** and **1'**, **1-** and **1'-** and **1t** and **1t'** takes place through the corresponding TSs, namely **TS1**, **TS2** and **TS3**, that are located 8.2, 5.9 and 9.7 kcal/mol above the most stable structure of each pair. Regarding the tautomeric equilibria between **1'** and **1t'** that connects **1/1'** and **1t/1t'** rotamer pairs, direct and water-catalyzed processes were studied. In the direct process without catalysis, the energy barrier is

52.7 kcal/mol from the the most stable conformer **1t'**. The water-catalyzed process, taking as the energy reference the molecular complexes **MC1'** and **MC1t'**, the energy barrier is 17.4 kcal/mol. Therefore, the catalysis of two water molecules lowers the barrier of the process by 35.3 kcal/mol. Taking into account the thermal corrections to enthalpies and entropies (computed at 25 °C and 1 atm and scaling the frequencies by a factor of 0.96 [10]) to yield the Gibbs free energy of each stationary point, do not modify the conclusions discussed above. In fact, the exothermic or endothermic character of each conformational or tautomeric process is kept over the Gibbs PES and the value of the free energy barriers of the different processes through **TS1**, **TS2**, **TS3** is lower than 1.1 kcal/mol. The major variation comes with **TS4d** and **TS4w** were the free barriers are lowered to 50.35 kcal/mol and 14.33 kcal/mol but, as can be seen, conclusions are the same as previously stated. The absolute electronic and free Gibbs energies, together with the relative energies of every process are collected in Table S2 and the free energy profile is depicted in Figure S18.

**Table S2.** Absolute electronic and free Gibbs energies (computed at 298.15 K and 1 atm and scaling frequencies by 0.96) of the stationary points found along the PES full-search. Please, note that compound **1** has been used as reference in the relative electronic and free Gibbs energies. \*In the case of water-catalyzed process through **TS4w**, the most stable molecular complex, **MC1'**, has been used as reference to compute the barrier of the tautomerization process. Boltzmann distribution according to the Eq. 1 has been included.

Structure	E (hartree)	$\Delta E$ (kcal/mol)	G (hartree)	$\Delta G$ (kcal/mol)	Boltzmann distribution (%)
<b>1</b>	-1044,6466	0,00	-1044,4518	0,00	89.92
<b>TS1</b>	-1044,6335	8,23	-1044,4386	8,27	
<b>1'</b>	-1044,6442	1,53	-1044,4495	1,43	8.03
<b>TS4d</b>	-1044,5602	54,20	-1044,3715	50,35	
<b>1t'</b>	-1044,6417	3,07	-1044,4481	2,33	1.76
<b>TS3</b>	-1044,6262	12,79	-1044,4316	12,67	
<b>1t</b>	-1044,6401	4,08	-1044,4463	3,41	0.28

<b>MC1'</b>	-1197,6037	0,00*	-1197,3695	0,00*	
<b>TS4w</b>	-1197,5760	17,36	-1197,3467	14,33	
<b>MC1t'</b>	-1197,6007	1,88	-1197,3674	1,31	
<b>1-</b>	-1044,1788	0,00	-1043,9979	0,00	96.91
<b>TS2</b>	-1044,1694	5,90	-1043,9866	7,07	
<b>1'-</b>	-1044,1760	1,80	-1043,9946	2,04	3.09

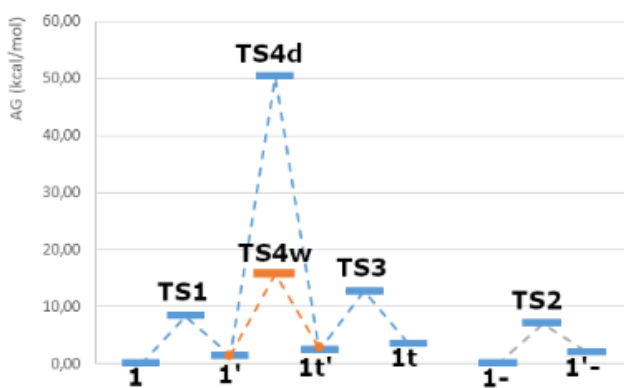


**Figure S18.** Free energy profile of the different conformational/tautomerization processes found along the PES. Please, note that **MC1'** has moved over compound **1'** (and **MC1t'** over **1t'**) to show the difference in the free energy profile between the direct non-catalyzed process through **TS4d** and the water-catalyzed process through **TS4w**.

[17] D. H. Reid, Organic Compounds of Sulphur, Selenium, and Tellurium, Volume 2, Chemical Society, 1973. ISBN 0851862691.

[18] Wazzan, N., Safi, Z., Al-Barakati, R. et al. DFT investigation on the intramolecular and intermolecular proton transfer processes in 2-aminobenzothiazole (ABT) in the gas phase and in different solvents. Struct Chem 31, 243–252 (2020).

### Boltzmann distribution of species

Considering that the temperature of an alcoholic beverage may be between 5 and 25 °C and that the acid-base reaction is considerably faster than the conformational changes and tautomerization reactions, we analyze the relative abundance using the Boltzmann distribution equation 1 on the relative free energies at 298.15 K (see below) of the protonated compounds **1** and **1'** and its corresponding tautomers, **1t** and **1t'**, respectively. In the same way, considering that in presence of GHB, the deprotonation of **1** occurs, the free energy of conformers **1-** and **1'-** was taken and equation 1 was also applied to them at the same temperature. The results, collected in Table S2, showed that the population of **1** and **1-** is around 90 and 97%, respectively, of the species present and therefore they can be considered the main responsible for the shape of the UV-Vis spectra in absence and in presence of GHB, respectively. Anyway, the maxima of simulated UV-Vis bands of **1'**, **1t**, **1t'** and **1'-** differ a few nanometers from **1** and **1-** and therefore would only result in a slight broadening of the experimental bands (see later).

### Complete TD-DFT vertical excitation energies analysis

Starting from the B3LYP/6-311++(2df,2p)/PCM(DMSO) optimized geometries for all the stationary points found along the PES, namely **1**, **1'**, **1t'**, **1t**, **1-** and **1'-**, single-point TD-DFT calculations at the same theory level were performed in DMSO solution using non-equilibrium formalism which are the ones presented in the main communication. Further single-point TD-DFT calculations in DMSO solution using B3LYP/6-311++(2df,2p)/PCM(DMSO) optimized geometries were also made using different hybrid DFT functionals (X3LYP [19], PBE0 [20] and CAM-B3LYP [21]) as well as B3LYP functional combined with different triple- $\zeta$  quality basis sets as Ahlrichs and coworkers Def2TZVPD [22-23] and Truhlar and Papajak "calendar" basis set jul-cc-pV(T+d)Z [24] that were downloaded from [www.basissetexchange.org](http://www.basissetexchange.org) [25] for the H, C, N and O elements for comparative purposes. In all calculations submitted, the state of interest was the first one and only the first 30 singlet excited states were considered using keywords root=1, nstates=30, singlets.

### Chapter 3: Colorimetric and fluorimetric GHB detection with benzoxazole derivatives

Excitation energies, oscillator strengths, spin and spatial symmetry, the  $\langle S^2 \rangle$  and the largest coefficients in the CI expansion for all TD-DFT calculations classified by DFT functional and basis set used have been collected in Annex II.

From all the TD-DFT calculations computed by Gaussian09, GaussView can generate UV-Vis plots using the excitation energies and the oscillator strength for each excited state. Collection of the TD-DFT UV-Vis plots for absorbance values ranging from 250 to 650 nm for compounds **1**, **1'**, **1t'**, **1t**, **1-** and **1'-** together with that obtained experimentally for compound **1** and compound **1** in presence of GHB (scaling the simulated spectra absorbance to fit that found experimentally taking the absorbance value of the highest band allows us to compare different DFT functionals (B3LYP, X3LYP, PBE0 and CAM-B3LYP) and several triple- $\zeta$  quality basis sets (6-311++(2df,2p), Def2TZVPD and jul-cc-pV(T+d)Z) with the same DFT functional (B3LYP) in Figures S17 to Figures S22. Oscillator strengths for each TD-DFT UV-Vis plots have been omitted for the sake of simplicity and only absorbances (in arbitrary units) have been plotted.

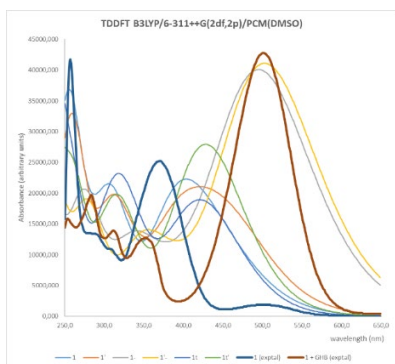


**Figure S19.** Single-point TDDFT B3LYP/6-311++(2df,2p)/PCM(DMSO) over B3LYP/6-311++(2df,2p)/PCM(DMSO) geometry.

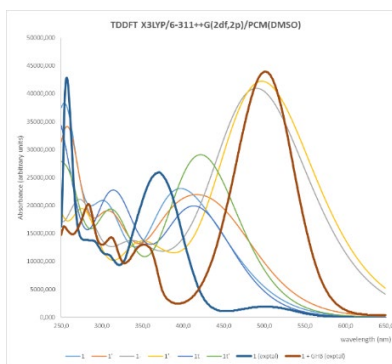


**Figure S20.** Single-point TDDFT X3LYP/6-311++(2df,2p)/PCM(DMSO) over B3LYP/6-311++(2df,2p)/PCM(DMSO) geometry.

Chapter 3: Colorimetric and fluorimetric GHB detection with benzoxazole derivatives

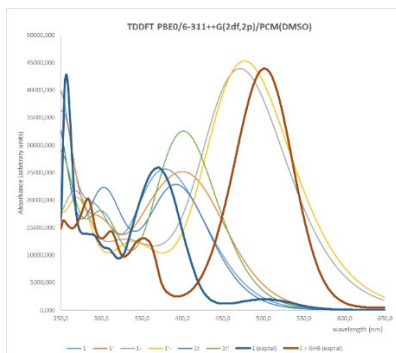


**Figure S21.** Single-point TDDFT PBE0/6-311++(2df,2p)/PCM(DMSO) over B3LYP/6-311++(2df,2p)/PCM(DMSO) geometry.

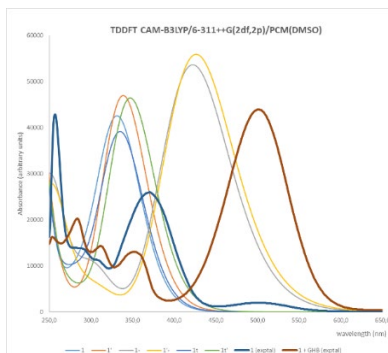


**Figure S22.** Single-point TDDFT CAM-B3LYP/6-311++(2df,2p)/PCM(DMSO) over B3LYP/6-311++(2df,2p)/PCM(DMSO) geometry.

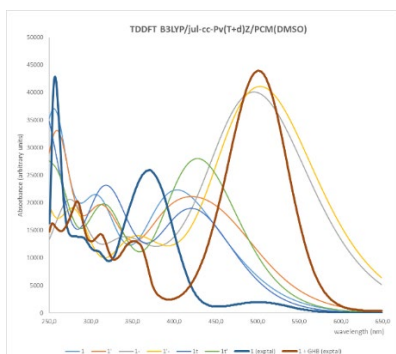


**Figure S23.** Single-point TDDFT B3LYP/jul-cc-Pv(T+d)Z/PCM(DMSO) over B3LYP/6-311++(2df,2p)/PCM(DMSO) geometry.

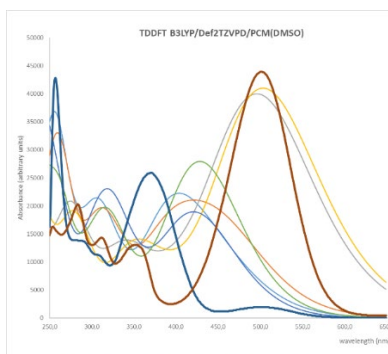


**Figure S24.** Single-point TDDFT B3LYP/Def2TZVPD/PCM(DMSO) over B3LYP/6-311++(2df,2p)/PCM(DMSO) geometry.



### Chapter 3: Colorimetric and fluorimetric GHB detection with benzoxazole derivatives

As can be seen, the most accurate overall match between  $\lambda_{\max}$  between experimental and simulated UV-Vis plots for all the species depicted are those from TD-DFT B3LYP/6-311++G(2df-2p)/PCM(DMSO) calculations (see Figure S19), although not far away from those reported for X3LYP (second best match, see Figure S20) and PBE0 (see Figure S21) DFT functionals. The functional with the poorest match is CAM-B3LYP (see Figure S22). Also, when comparing the same method (B3LYP) with different basis sets (6-311++G(2df,2p), jul-cc-Pv(T+d)Z and Def2TZVPD, see Figures S19, S23 and S24), almost no difference between the computed UV-Vis plots can be seen.

[19] X. Xu and W. A. Goddard III, "The X3LYP extended density functional for accurate descriptions of nonbond interactions, spin states, and thermochemical properties," Proc. Natl. Acad. Sci. USA, 101 (2004) 2673-77.

[20] C. Adamo and V. Barone, "Toward reliable density functional methods without adjustable parameters: The PBE0 model," J. Chem. Phys., 110 (1999) 6158-69.

[21] T. Yanai, D. Tew, and N. Handy, "A new hybrid exchange-correlation functional using the Coulomb-attenuating method (CAM-B3LYP)," Chem. Phys. Lett., 393 (2004) 51-57.

[22] F. Weigend and R. Ahlrichs, "Balanced basis sets of split valence, triple zeta valence and quadruple zeta valence quality for H to Rn: Design and assessment of accuracy," Phys. Chem. Chem. Phys., 7 (2005) 3297-305.

[23] F. Weigend, "Accurate Coulomb-fitting basis sets for H to Rn," Phys. Chem. Chem. Phys., 8 (2006) 1057-65.

[24] E. Papajak, J. Zheng, H. R. Leverentz and D. G. Truhlar, "Perspectives on Basis Sets Beautiful: Seasonal Plantings of Diffuse Basis Functions," J. Chem. Theory and Comput., 7 (2011) 3027.

[25] A New Basis Set Exchange: An Open, Up-to-date Resource for the Molecular Sciences Community. Benjamin P. Pritchard, Doaa Altarawy, Brett Didier, Tara D. Gibson, Theresa L. Windus. J. Chem. Inf. Model. 2019, 59(11), 4814-4820.

#### **pKa calculations of the acid-base conjugate pairs 1/1-, 1'/1'- and 1t/1t' through a thermodynamic cycle**

Finally, in order to find out the interaction between compound **1** and GHB, which is supposed to be an acid-base equilibria to yield compound **1-** as has been pointed out by the experimental data, a

Chapter 3: Colorimetric and fluorimetric GHB detection with benzoxazole derivatives

thermodynamic cycle was performed to compute the  $pK_a$  of both **1/1-** and GHB/GHB<sup>-</sup> species in DMSO using the methodology described in the reference [7] of computational methods section in order to evaluate the feasibility of the acid-base process.

To carry on these calculations, first of all, a thorough conformation search over GHB and GHB<sup>-</sup> species at M062X/6-31+G(d) level both in gas phase and in solvent (SMD, solvent DMSO) was performed in order to select the most stable conformations. To do so, several starting candidates where the dihedral angles of the C-C and C-O bonds have been rotated were fully optimized until the most stable structure was found (see Figure S25).

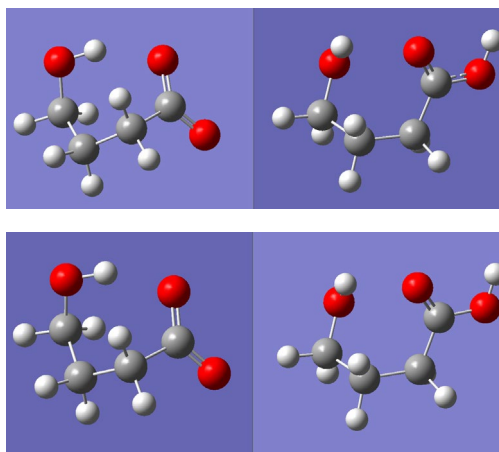


**Figure S25.** Most stable conformations found for GHB-/GHB pair in DMSO solvent (up) and in gas phase (down).

After this step, an optimization of all stationary points (**1**, **1-**, **1'**, **1'-**, **1t** and **1t'**) was performed at M062X/6-31+G(d) level both in gas phase and in solvent (SMD, solvent DMSO) starting from different geometries to be sure that the lowest energy conformer of the corresponding species had been found. Finally, over the optimized gas phase and solvent geometries of the most stable conformers of the aforementioned species, the corresponding thermal corrections to the Gibbs free energy were computed at 298.15 K and 1 atm using a factor of 0.967 to scale the frequencies using the ideal gas molecular partition functions in conjunction with the rigid-rotor

*Chapter 3: Colorimetric and fluorimetric GHB detection with  
benzoxazole derivatives*

quasiharmonic oscillator (RR-QHO) approximation. This was done with Goodvibes script which, in addition, allowed to apply over the standard state calculations in Gaussian the appropriate corrections to ensure that all solution phase  $pK_a$ s are computed at a standard state of 1 mol/L.

Finally, over the optimized M062X/6-31+G(d) gas phase geometries, single point calculations at the (RO)MP2/GTMP2Large theory level were performed. Finally, to compute the  $pK_a$  of each acid-base pair, we have employed the proton free energy  $AG^*_s(H^+)$  of -273.3 kcal/mol.

$pK_a$  was computed through a thermodynamic cycle (TC) using these equations:

$$pK_a = (\Delta G^*_{soln} / RT \ln(10))$$

Where:

$$\Delta G^*_{soln} = \Delta G^*_{soln} (TC) = \Delta E^L_{soln} + \Delta G^{soln,L}_{corr} + G^*_{soln}(H^+) + \Delta E^H_{gas} - \Delta E^L_{gas}$$

Where:

$$\Delta E^X_Y = E^X_Y (A^-) - E^X_Y (AH)$$

Where X superscript refers to (RO)MP2/GTMP2Large energy when it equals to H (high level calculations) and to M062X/6-31+G(d) energy when it equals to L (low level calculations) and Y subscript refers to gas phase optimized geometry when it equals to "gas" or to solvent phase geometry when it equals to "soln".

And where:

$$\Delta G^{soln,L}_{corr} = \Delta G^{gas}_{corr} - \Delta G^{soln}_{corr}$$

The results of all these calculations are collected in the following Table S3:

*Chapter 3: Colorimetric and fluorimetric GHB detection with benzoxazole derivatives*

**Table S3:** “Low level” M062X/6-31+G(d) and “high level” M062X/6-31+G(d)/gas phase//(RO)MP2/GTMP2Large calculation results over **1**, **1-**, **1'**, **1'-**, **1t**, **1t'**, GHB and GHB<sup>-</sup> minimum-energy geometries.

Species	E <sup>L</sup> <sub>soln</sub> (hartree)	E <sup>H</sup> <sub>gas</sub> (hartree)	E <sup>L</sup> <sub>gas</sub> (hartree)	G <sup>soln,L</sup> <sub>corr</sub> (hartree)
<b>1-</b>	-1043,46175841	-1041,7313	-1043,38877017	0,186534
<b>1</b>	-1043,92994532	-1042,2488	-1043,90252410	0,200172
<b>1t</b>	-1043,92255735	-1042,2385	-1043,89252962	0,199082
<b>1'-</b>	-1043,45839550	-1041,7256	-1043,38280982	0,187047
<b>1'</b>	-1043,92680469	-1042,2451	-1043,89906003	0,201494
<b>1t'</b>	-1043,92262142	-1042,2399	-1043,89465108	0,199231
GHB <sup>-</sup>	-382,31902611	-381,6959	-382,23164084	0,078718
GHB	-382,78635260	-382,2394	-382,77191902	0,089027

These calculations yield the following pK<sub>a</sub>s in DMSO for the corresponding acid-base pairs: 10.4 for **1/1-**, 7.4 for **1t/1-**, 10.0 for **1'/1'-**, 8.7 for **1t'/1'-** and 11.3 for GHB/GHB<sup>-</sup>. Therefore, taking into account that both the free energy profile and Boltzmann population analysis yields **1** and **1-** as the major products, the difference between the pK<sub>a</sub>s of **1/1-** and GHB/GHB<sup>-</sup> systems (10.4 and 11.3, respectively), which is 0.9 units, accounts for the presence of compound **1-** in equilibrium with **1** in presence of GHB in DMSO solvent and, therefore, for the change in the UV-Vis

## **Chapter 4: Colorimetric detection of GHB using gold nanoparticles**



## 4.1 Introduction

### 4.1.1. Nanomaterials

Nanomaterials (NMs) or Nanotechnology are terms which have become very popular among scientists and society, as well. The prefix nano-, which derives from Greek, means “*very short man*”, giving an idea of how little these materials are. Even though there are several definitions of NMs, depending on the source consulted, one of the most accepted ones is that from ISO (International Organization for Standardization). They define NMs as a material that comprises, at least, one of its external dimensions in the nanoscale (1-100 nm) or possesses a surface or internal structure in this same scale (see Figure 4.1).<sup>87,88</sup>

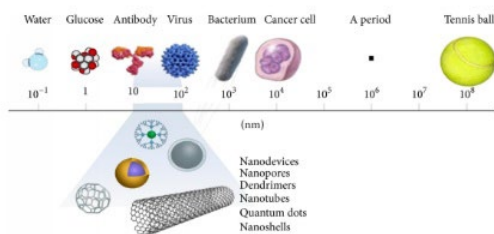


Figure 4.1. Comparison of large-sized materials with NMs<sup>88</sup>

These materials have been receiving more and more attention during the last few decades thanks to their tuneable size and shape and unique properties.<sup>87</sup> Among all these NMs, metal nanoparticles (NPs) are involved in a very active research field thanks to their very appealing size and shape-dependent properties. Since they are nano-objects, which show all their three external dimensions in the nanoscale, they have led interesting applications in several different fields such as catalysis and sensing. Thus, gold nanoparticles (AuNPs) have been widely studied and employed.<sup>87,89,90</sup>

### 4.1.2. Gold Nanoparticles

Thanks to the different properties that some metals show as a bulk or as NPs, AuNPs show exceptional optical properties due to an interesting and advantageous phenomenon called Surface Plasmon Resonance (SPR). When the nanoscale is governing, the most external electrons (conduction electrons) undergo a quantic confinement. As a result, for a concrete domain of electromagnetic waves, these electrons displace from their original positions, creating a dipole. The restoring force is the attraction between nuclei and electrons, generating a coherent oscillation of the electrons (see Figure 4.2). Consequently, an absorption band known as plasmonic band is observed. The position and width of this band depends on the solvent, the morphology and the size of the NPs. For instance, a colloidal solution formed by spherical AuNPs with a 20-nanometer diameter generates a plasmonic band with an absorption maximum around 520 nm, providing a red solution. Usually, those AuNPs with diameters between 9 and 99 nm show an absorption maximum range from 517 to 575 nm. On the other hand, when these metallic nanoparticles aggregate, their electronic clouds interact and overlap, resulting in a hypsochromic band shift from red to blue, since they are behaving as a larger particle. It is true that this phenomenon shows a huge importance in Au, but also other conducting metals such as Ag or Cu exhibit this same optical property.<sup>89–98</sup>

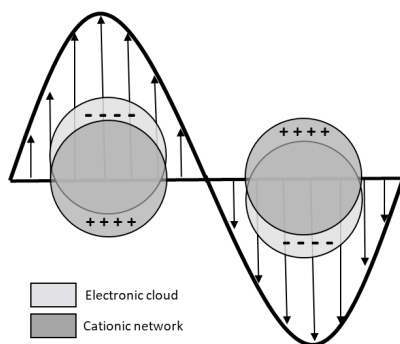


Figure 4.2. Schematic description of electronic cloud displacements in nanoparticles under the effect of an electromagnetic wave



Additionally, not only their remarkable optoelectronic properties, but also their easy preparation, high surface-to-volume ratio and their exceptional biocompatibility make AuNPs excellent ligands.<sup>89</sup> For these reasons, over the last years, the synthetic techniques of AuNPs have improved to such extent that now scientists are able to obtain a broad range of sizes and shapes (Figure 4.3).<sup>89–95</sup>

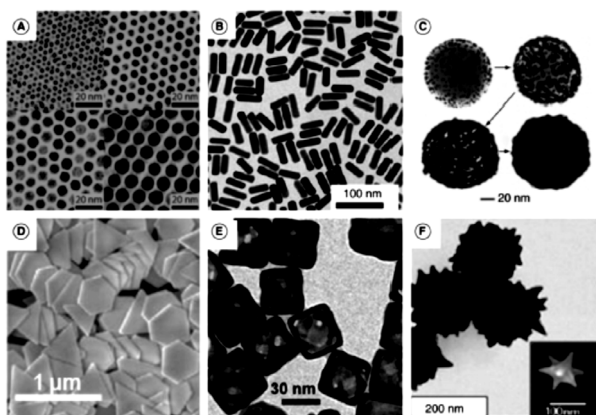
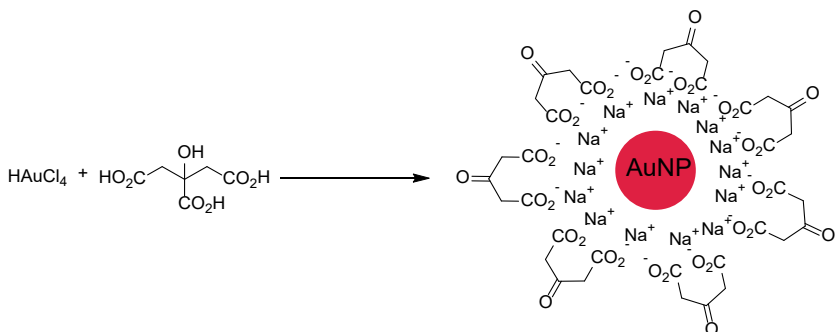


Figure 4.3. Transmission electron micrograph of (a) gold nanoparticles, (b) gold nanorods, (c) gold nanoshells, (d) gold nanoprisms, (e) gold nanocages and (f) gold nanostars.<sup>95</sup>

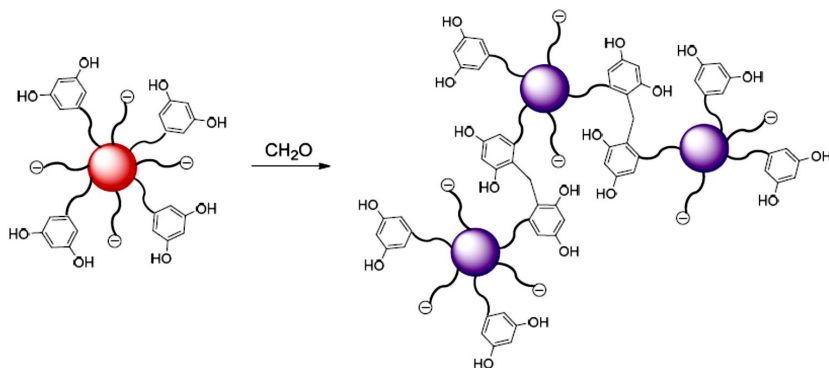
In order to synthesise AuNPs, two different approach can be carried out: “top down” or “bottom up”. The first one consists of breaking methodically a bulk state Au to generate AuNPs of wished dimensions, controlling the particle formation using a pattern. However, this method shows some drawbacks such as the lack of complete control of both size and shape as well as subsequent functionalization. In the second alternative, “bottom up”, AuNPs are synthesised from individual molecules, being necessary a biological or chemical reduction. In this latter, many reducing agents such as borohydrides, aminoboranes, hydrazines, citric acid, sulphites and so on have been widely investigated. After reduction, an additional stabilization step is required. Among all the different ways to synthesise AuNPs, the most explored is the Turkevich-Frens method in which citrate is used as both stabilizing and reducing agent.<sup>90–95</sup>



Scheme 4.1. Schematic view of Turkevich-Frens synthesis

Once the AuNPs are formed, to exchange partially that citrate layer for other organic molecules is relatively easy. This fact allows scientists to change the surrounding chemical environment through functionalization of their surface with many different ligands with the aim of using these NMs as sensors.<sup>89–95</sup> Due to the fact that these AuNPs are spherical and colloidal particles, some of the most common techniques employed to characterize them are Transmission Electron Microscopy (TEM) and Z-potential determination, which allow scientists to know their shape and size in the absence or presence of solvent, respectively.

Considering their extensive application not only in chemical, but also biological sensing, an extensive range of sensors has been developed to be potentially applied in industry or medical fields, e.g. in food safety or as theranostics systems.<sup>90,99,100</sup> One example of a sensor that could be applied in industry is the AuNPs developed to detect formaldehyde, as a pollutant gas that can be released from materials which contains it.<sup>101</sup> The authors describe the sensing process as a condensation reaction between resorcinol derivative and formaldehyde, promoting AuNPs closeness and their aggregation, inducing a displacement of SPR and an observable colour change.



Scheme 4.2. Paradigm of detection of formaldehyde by means of using resorcinol functionalised AuNPs<sup>101</sup>

## 4.2. Ligands Designed

Taking into account all the information provided above, two ligands were designed to detect both the carboxylate and the hydroxyl group present in GHB. One of them (**L1**) was synthesised with a benzoxazole moiety,<sup>102</sup> whereas the second one (**L2**) included a phenanthroline group, in order to interact with the carboxylate and the hydroxyl group, respectively (see Chart 4.1).<sup>103</sup> Both ligands contain, at least, a sulphur atom to anchor the ligands to the AuNPs.

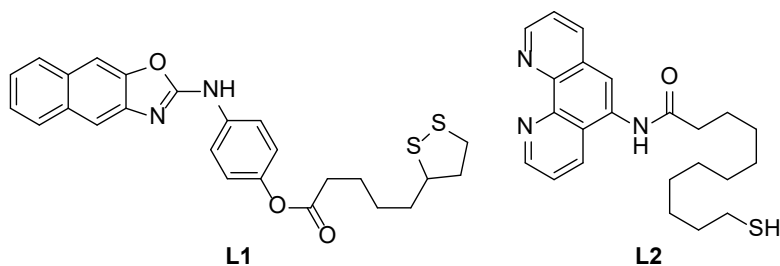
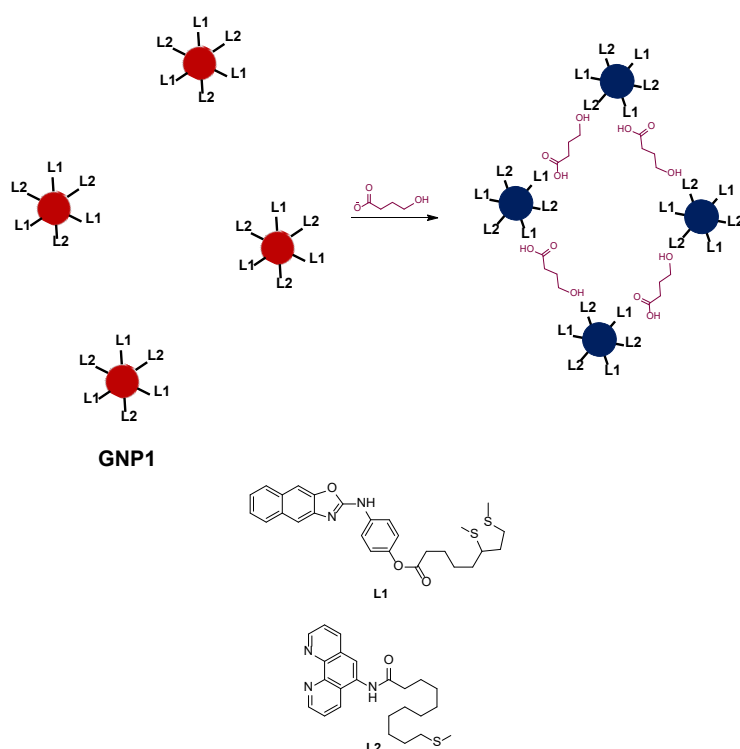


Chart 4.1. Chemical structure of the synthesized ligands

### 4.3. Objectives

Considering the different properties of AuNPs in terms of their aggregation, the main goal of this chapter was to obtain AuNPs with two different functional groups in order to recognise both the hydroxyl and the carboxylate groups present in GHB. To do so, three specific objectives were defined:

- Design and synthesis of **L1** and **L2** in order to reach the wished complementary between ligands and analyte.
- Synthesis of citrate-capped AuNPs and optimization of their functionalization with both ligands at the same time (**GNP1**).
- Analysis of experimental conditions (solvent, temperature and time) to detect GHB.



Scheme 4.3. Recognition proposal of GHB using **GNP1**

#### **4.4. Bifunctionalized gold nanoparticles for the colorimetric detection of the drug $\gamma$ -hydroxybutyric acid (GHB) in beverages**

Silvia Rodríguez-Nuévalos<sup>1</sup>, Ana M. Costero<sup>1,2,\*</sup>, Salvador Gil<sup>1,2</sup>,  
Margarita Parra<sup>1,2</sup>, Pablo Gaviña<sup>1,2,\*</sup>

1) Instituto Interuniversitario de Investigación de Reconocimiento Molecular y Desarrollo Tecnológico (IDM). Universidad Politècnica de València, Universitat de València, Doctor Moliner 50, Burjassot, 46100, Valencia, Spain; e-mail: pablo.gavina@uv.es

2) CIBER de Bioingeniería, Biomateriales y Nanomedicina (CIBER-BBN) (Spain).

\* Correspondence: pablo.gavina@uv.es; Tel.: +34 963543740

**Received:** 20th May 2021

**Accepted:** 22th June 2021

*Chemosensors*, **2021**, 9(7), 160-169



## **Abstract**

The increase in the number of drug-facilitated sexual assault (DFSA) cases in recent years, has become a major concern. Consequently, there is a need to develop methods for the real-time detection of these substances. We report herein a colorimetric chemosensor for the real-time in-situ detection of the “date rape” drug GHB. The sensor is based on gold nanoparticles functionalized with both, a 2-aminonaphthoxazole and phenanthroline derivative. Its ability to act as “naked-eye” colorimetric sensor for the detection of the drug in soft drinks and alcoholic beverages has been studied. The detection process is based on the double recognition of both the hydroxyl and the carboxylate groups present in GHB, which triggers the aggregation of the AuNPs with the resulting change in the colour of the solution.

## **Introduction**

According to the European Monitoring Centre for Drugs and Drug Addiction (EMCDDA), the number of cases of ‘drug-facilitated sexual assaults’ (DFSA) has increased in recent years. Six European countries have carried out population surveys in order to know the extent of this problem and the results have shown that around 20% of women had experienced some sexual assault during their adulthood. However, the exact number of cases remains unknown due to the lack of efficient monitoring systems to detect this situation. The most commonly used drugs in DFSA are central nervous systems depressants such as alcohol, benzodiazepines, ketamine or  $\gamma$ -hydroxybutyric acid (GHB) [1]. Apart from alcohol, GHB is one of the most used drugs for two main reasons. First, it is an odourless and colourless compound that exhibits a slight salty taste in water solution, so it can be easily delivered to the victims without them realizing it [2]. Second, its detection after consumption is elusive since it is fast metabolized in the body ( $C_{\max}$  is reached 20-40 min after its ingestion). It is eliminated from plasma with a half-life of 30-50 min and only small amounts of this substance can be recovered from victim’s urine (1-5% of the dose). Thus, the drug detection time is very short (3-10 h) [3]. For the above reasons, it is highly desirable

and necessary to develop efficient detection systems to prevent this type of aggressions as well as to detect them in a reasonable short time after they have taken place.

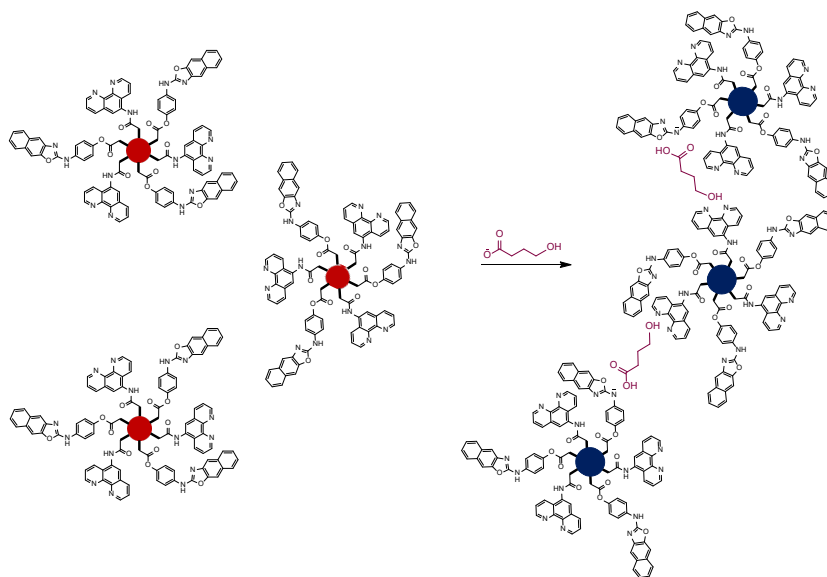
GHB detection methods are being widely studied but most are based on chromatographic [4, 5] and spectroscopic methods [6] that, demonstrating high sensitivity, usually require complicated samples treatments. The use of optical sensors is usually a simple and much faster alternative [7]. These probes can detect the analyte in real-time and not special skills are necessary to use them. Despite this, only a few chromo-fluorogenic chemosensors for GHB recognition have been described, with very diverse approaches [8- 12]. The latest system published by Xing and col. [13] is based on a specific enzymatic reaction of GHB that generates NADH, which facilitates the reduction of Au (III) to give rise to AuNPs, producing a colour change.

Gold nanoparticles (AuNPs) have received a great attention over the past years as scaffolds to prepare chemosensors to sense different analytes. Their usefulness is based on their optoelectronic properties, being one of the most remarkable their surface plasmon resonance (SPR) [14]. The SPR absorption band can be modified by different factors such as AuNPs shape, size or aggregation state. Thus, under an appropriate stimulus, well dispersed AuNPs can aggregate, which results in a bathochromic shift of the SPR absorption band with the corresponding change in the colour of the solution from red (dispersed) to blue (aggregated). This colour change usually can be observed naked eye. This fact, in addition to their biocompatibility as well as their easy surface functionalization with many different types of organic molecules, have converted AuNPs in a common and useful material to develop rapid, economic and selective colorimetric sensors [15].

Taking all this into account and the expertise of our group in the development of chemosensors based on functionalized AuNPs [16,17], here we report a selective and efficient method to detect GHB in beverages. The sensing protocol is based on the use of AuNPs doubly functionalized with two different ligands to recognize the functional groups present in GHB: a carboxylate and an alcohol



group. The recognition units chosen were a 2-aminonaphthoxazole moiety, capable of interacting with the carboxylate groups [18] and a phenanthroline group to interact with the hydroxyl group of GHB [19, 20]. We expected that GHB would trigger the aggregation of the gold nanoparticles through a double recognition process. The recognition paradigm is showed in the Scheme 1.



**Scheme 1.** Proposed paradigm for GHB recognition with sensor **GNP1**.

## Materials and Methods

The reagents employed in the synthesis were acquired in Sigma Aldrich and used without further purification.  $^1\text{H}$  NMR and  $^{13}\text{C}$  NMR spectra were registered in Bruker Avance 300 MHz or 500 MHz spectrophotometers, all of them referenced to solvent peak,  $\text{DMSO}(d_6)$ . UV-Vis spectra were registered in a Shimadzu UV-2600 spectrophotometer, using a cuvette with 1 cm of path length. All measurements were carried out at room temperature. Images of transmission electron microscopy were taken with JEOL-1010 transmission electron microscopy operating at 100 kV. Z potential and DLS values were measured in a Malvern Zetasizer ZS, for 3 times in 10-25 cycles. Mass spectrometry spectra were carried out with a TripleTOFTM 5600 LC/MS/MS System, with 2 gas sources (both to

35 psi), 450 °C and ion gas voltage of 5500 V. Origin 2020 was the program to plot titrations.

### Synthesis of the ligands

#### Synthesis of 3

In a 50 mL 3 neck round bottom flask, 201 mg of 3-amino-2-naphthol (1.26 mmol) were dissolved in 9 mL of pyridine under an argon atmosphere. Then, 180  $\mu$ L of 1-isothiocyanato-4-methoxybenzene were added and the mixture was kept stirring over night at room temperature. After that, the solvent was removed, and the brown oil obtained was dissolved in 30 mL of AcOEt. Then, the organic phase was washed with 15 mL of 1% aqueous HCl, 15 mL of saturated aqueous NaHCO<sub>3</sub> and 15 mL of saturated aqueous NaCl, successively. The organic phase was dried over anhydrous MgSO<sub>4</sub>, filtered and the solvent removed to vacuum. The reaction crude was purified by chromatography column, using silica gel as stationary phase and Hexane:AcOEt from 7:3 to 5:5 as eluent. 350 mg of compound **3** were obtained as a brown solid in 96% yield. <sup>1</sup>H NMR (300 MHz, DMSO)  $\delta$  10.48 (s, 1H), 10.06 (s, 1H), 9.16 (s, 1H), 8.84 (s, 1H), 7.74 – 7.60 (m, 2H), 7.39 (d, J = 9.0 Hz, 2H), 7.35 – 7.22 (m, 2H), 7.19 (s, 1H), 6.95 (d, J = 9.0 Hz, 2H), 3.76 (s, 3H).

#### Synthesis of 4

In a 25 mL 2 neck round bottom flask, 181 mg of **3** (0.56 mmol) were dissolved in 5 mL of THF. Then, 127  $\mu$ L of H<sub>2</sub>O<sub>2</sub> 30 % (1.12 mmol) and 3 mg of TBAI (0.008 mmol) were added. The stirring was kept overnight at room temperature. Then, the solvent was removed, and the brown oil obtained was dissolved in 15 mL of AcOEt. The organic phase was washed with 15 mL of deionized water, dried over anhydrous MgSO<sub>4</sub> and filtered. After removing solvent, 160 mg of compound **4** were obtained as a brown solid (99% yield). <sup>1</sup>H NMR (500 MHz, DMSO)  $\delta$  10.67 (s, 1H), 7.97 – 7.91 (m, 2H), 7.90 (s, 1H), 7.81 (s, 1H), 7.71 (d, J = 9.0 Hz, 1H), 7.45 – 7.37 (m, 2H), 7.00 (d, J = 9.0 Hz, 2H), 3.76 (s, 3H). <sup>13</sup>C NMR (126 MHz, DMSO)  $\delta$  159.61, 155.02, 147.15, 143.07, 131.47, 131.31, 129.45, 127.63, 127.38, 124.37, 123.89, 119.69, 114.28, 111.89, 104.35, 55.27.

### Synthesis of 5

In a 100 mL round bottom flask, 59 mg of compound **4** (0.20 mmol) were dissolved in 3 mL of DCM and cooled at 0 °C. Then, 820 µL of BBr<sub>3</sub> (0.82 mmol) were added dropwise. The reaction temperature was risen to room temperature and the stirring kept overnight. After that, 15 mL of deionized water were added, and the stirring was kept for 15 min. DCM was removed and compound **5** was extracted with AcOEt (3 x 15 mL). The organic phase was washed with 15 mL of saturated aqueous NaCl, dried over MgSO<sub>4</sub>, filtered and the solvent was removed to vacuum. Compound **5** was obtained as a brown solid (60 mg, 99% gross yield). <sup>1</sup>H NMR (300 MHz, DMSO) δ 10.52 (s, 1H), 9.24 (s, 1H), 7.97 – 7.88 (m, 2H), 7.88 (s, 1H), 7.77 (s, 1H), 7.57 (d, J = 9.0 Hz, 2H), 7.45 – 7.37 (m, 2H), 6.81 (d, J = 9.0 Hz, 2H). <sup>13</sup>C NMR (126 MHz, DMSO) δ 159.77, 153.14, 147.22, 143.31, 131.32, 129.95, 129.38, 127.60, 127.34, 124.31, 123.80, 119.93, 115.47, 111.69, 104.23.

### Synthesis of L1

In a 50 mL 2 neck round bottom flask, under argon atmosphere, 46 mg of (±)-α-lipoic acid (0.22 mmol), 10 mg of DMAP (0.081 mmol) and 40 µL of EDC were solved in 2 mL of dry THF. The stirring was kept for 1 h at room temperature. Then, 60 mg of **5** were solved in 4 mL of dry THF and added to the previous mixture. The reaction was stirred overnight at room temperature. After that, the solvent was removed, and the resulting brown oil was solved in 15 mL of AcOEt. Then, the organic phase was washed with 10 mL of acid aqueous solution (pH 4), 10 mL of saturated aqueous NaHCO<sub>3</sub> and 10 mL of saturated aqueous NaCl. The organic phase was dried over anhydrous MgSO<sub>4</sub>, filtered and the solvent removed to vacuum. The reaction crude was purified by chromatography column, using silica gel as stationary phase and Hexane:AcOEt 7:3 as eluent. 51 mg of **L1** were obtained as a brown powder (51% yield). <sup>1</sup>H NMR (500 MHz, DMSO) δ 10.93 (s, 1H), 8.00 – 7.89 (m, 3H), 7.86 (s, 1H), 7.84 (d, J = 9.0 Hz, 2H), 7.48 – 7.39 (m, 2H), 7.17 (d, J = 9.0 Hz, 1H), 3.67 – 3.60 (m, 1H), 3.22 – 3.16 (m, 1H), 3.15 – 3.08 (m, 2H), 2.58 (t, J = 7.3 Hz, 2H), 2.45 – 2.38 (m, 1H), 1.94 – 1.84 (m, 1H), 1.76 – 1.55 (m, 4H), 1.51 – 1.41 (m,

2H).  $^{13}\text{C}$  NMR (126 MHz, DMSO)  $\delta$  171.91, 159.31, 149.62, 147.03, 145.53, 145.50, 142.84, 136.13, 135.99, 131.31, 129.61, 127.67, 127.49, 124.44, 124.07, 123.91, 122.35, 122.32, 118.87, 112.36, 104.55, 56.06, 38.14, 34.05, 33.29, 28.08, 24.14. HRMS:  $m/z$  calculated for  $\text{C}_{25}\text{H}_{25}\text{N}_2\text{O}_3\text{S}_2$  (M + H): 465.1307; found: 465.1301  $[\text{M} + \text{H}]^+$ .

### Synthesis of L2

In a 50 mL 2 neck round bottom flask, 100 mg of 11-mercaptoundecanoic acid (0.46 mmol) were solved in 10 mL of dry DCM. Then, 40  $\mu\text{L}$  of  $\text{SOCl}_2$  (0.47 mmol) were added and the mixture was heating to reflux for 6 h. After that, the stirring was kept overnight to room temperature. Next, the solvent was removed to vacuum and 158 mg of  $\text{K}_2\text{CO}_3$  (1.15 mmol) and 2 mL of acetone were added to the crude of reaction. After 15 min, 89 mg of 1,10-phenanthroline-5-amine (0.46 mmol) and 2 mL of acetone were added to the previous mixture and the stirring was kept for 4 h. Then, the solid was filtered at vacuum, resuspended in 10 mL of water deionized and 10 mL of AcOEt for 15 min and filtered at vacuum. Finally, 60 mg of **L2** were obtained as a light brown powder (30% yield).  $^1\text{H}$  NMR (500 MHz, DMSO)  $\delta$  10.24 (s, 1H), 9.10 (dd,  $J = 4.3, 1.6$  Hz, 1H), 9.01 (dd,  $J = 4.3, 1.7$  Hz, 1H), 8.65 (dd,  $J = 8.4, 1.7$  Hz, 1H), 8.44 (dd,  $J = 8.1, 1.8$  Hz, 1H), 8.17 (s, 1H), 7.81 (dd,  $J = 8.4, 4.3$  Hz, 1H), 7.74 (dd,  $J = 8.1, 4.3$  Hz, 1H), 2.86 (t,  $J = 7.2$  Hz, 0.7H), 2.83 – 2.77 (m, 0.3H), 2.66 (t,  $J = 7.2$  Hz, 1H), 2.54 (t,  $J = 7.3$  Hz, 2H), 1.77 – 1.63 (m, 3H), 1.58 (p,  $J = 7.2$  Hz, 1H), 1.46 – 1.12 (m, 12H).  $^{13}\text{C}$  NMR (126 MHz, DMSO)  $\delta$  172.55, 149.89, 149.32, 145.66, 143.54, 135.96, 131.92, 128.13, 124.69, 123.67, 122.88, 119.89, 38.15, 37.89, 35.96, 34.05, 28.88, 28.86, 28.81, 28.75, 28.56, 28.50, 28.21, 27.70, 27.66, 25.26. HRMS:  $m/z$  calculated for  $\text{C}_{46}\text{H}_{57}\text{N}_6\text{O}_2\text{S}_2$  (M + H): 789.3984; found: 789.3967  $[\text{M} + \text{H}]^+$ .

## **Synthesis of the functionalized gold nanoparticles (AuNPs)**

### Synthesis of citrate-capped gold nanoparticles (citrate-GNPs)

Prior to use, the whole material was washed with aqua regia and dried at 120 °C in an oven for 24 h. In a 250 mL 3 neck round bottom flask, 39.4 mg of HAuCl<sub>4</sub> (0.1 mmol) were dissolved in 100 mL of milliQ water and boiled. Then, a solution of 114.1 mg of trisodium citrate dihydrate (0.38 mmol) in 10 mL of milliQ water was quickly added and the resulting mixture was boiled and vigorously stirred for 30 min. After that, the mixture was cooled to room temperature and the AuNPs were preserved until their use in the fridge at 4 °C.

### Synthesis of GNP1

In a 25 mL round bottom flask, 3900 µL of milliQ water were mixed with 21 µL of aqueous NaOH 0.5 M for 1 min. Then, 2100 µL of the previously prepared AuNPs were added. Then, **L1** (15 µL, 0.5 mM) and **L2** (15 µL, 0.32 mM) were added simultaneously, and the stirring was kept for 1 h. Next, the mixture was diluted with 6 mL of milliQ water and centrifuged for 10 min at 10500 rpm. Then, the supernatant was discarded and replaced by 6 mL of milliQ water.

### Exchange of buffer

3 mL of **GNP1** were diluted with 3 mL of milliQ water, divided in six Eppendorf (1 mL of mixture per Eppendorf) and centrifuged at 10500 rpm for 10 min. The supernatants were discarded and replaced by 1 mL of buffer (1 mM Phosphate pH 6.5, 7.5 and 8.5) or deionized water. The solutions were kept in the fridge at 4 °C for 5 days.

## **UV-Vis measurements**

### GHB titration

Prior to measure, each solution of NaGHB was prepared from 1 M aqueous NaGHB solution. Concentrations ranged from 0 to 100 mM. 400 µL of each solution were mixed with 400 µL of **GNP1** in a 1 mL cuvette and, after an incubation period of two min, the UV-Vis spectra were registered.

### AcONa/EtOH vs GHB

In a 1 mL cuvette, 400  $\mu\text{L}$  of **GNP1** were mixed with 400  $\mu\text{L}$  of 70 mM aqueous AcONa/EtOH or 70 mM aqueous NaGHB and, after an incubation period of two min, the UV-Vis spectra were registered.

### Interferent measurements

In a 1 mL cuvette, 400  $\mu\text{L}$  of **GNP1** were mixed with 400  $\mu\text{L}$  each interferent (0.3% w/v citric acid and 0.01% w/v sodium ascorbate) and, after an incubation period of two min, the UV-Vis spectra were registered.

### **Real Samples**

Previously, beverage samples were adulterate with NaGHB, in a 70 mM concentration. Then, 100  $\mu\text{L}$  of sample were mixed with 100  $\mu\text{L}$  of **GNP1**, at room temperature. The same process was followed for the samples without GHB. The changes were observed immediately.

## **Results and Discussion**

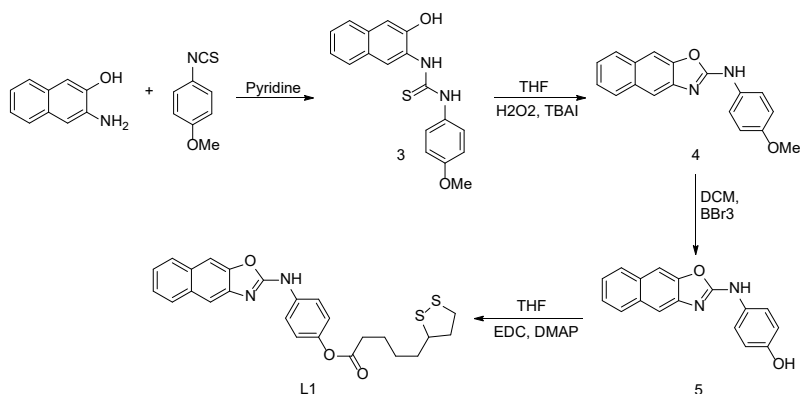
### **AuNPs preparation**

The structure and synthesis of both recognition units (**L1** and **L2**) to be anchored onto the gold surface are depicted in Scheme 2 and Scheme 3 respectively. Ligand **L1** consists of a lipoic acid derivative incorporating a 2-aminonaphthoxazole moiety. First, thiourea **3** was prepared by reaction between 3-amino-2-naphthol and isothiocyanate-4-methoxy-benzene in pyridine [21]. Then, **3** was treated with  $\text{H}_2\text{O}_2$  in presence of a catalytic amount of TBAI to obtain the naphthoxazole derivative **4** [22]. Demethylation of **4** with  $\text{BBr}_3$  in DCM gave rise to phenol **5**. Finally, esterification between **5** and lipoic acid in the presence of EDC and a catalytic amount of DMAP led to ligand **L1** (Scheme 2) which incorporates a disulfide group to anchor the ligand to the gold surface [23].

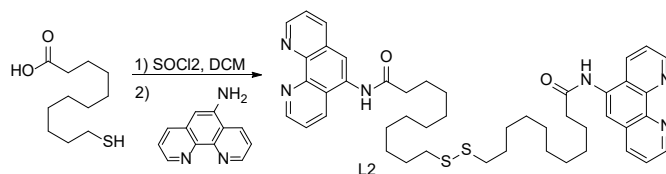
**L2**, incorporating two 5-amido-1,10-phenanthrolines connected through a disulfide bridge, was synthesized as depicted in Scheme 3. 11-mercaptopundecanoic acid was converted in its correspondent acid

chloride derivative using  $\text{SOCl}_2$  in DCM. Then, the **L2** was obtained by reaction with 5-amino-1,10-phenanthroline. Under the reaction conditions, the disulfide bond was spontaneously formed by oxidation of the thiols.

On the other hand, AuNPs were prepared following the method of Turkevich-Frens, which provides AuNPs whose diameters range from 15 to 150 nm [24]. Firstly, citrate-stabilized gold nanoparticles (citrate-GNPs) were prepared by reducing tetrachloro-auric acid with trisodium citrate in boiling water. Secondly, the functionalization of the citrate-GNPs with ligands **L1** and **L2** to obtain **GNP1** was optimized by varying the quantity of gold nanoparticles, the amount of both ligands, and the reaction and the centrifugation time (see supporting information).



**Scheme 2.** Synthetic pathway designed to obtain **L1**.



**Scheme 3.** Synthetic pathway designed to obtain **L2**.

The diameter of **GNP1**, determined from TEM images (Figure 1), was 18 nm. Data from DLS (Dynamic Light Scattering) and zeta-potential corresponding to citrate-GNP (the gold nanoparticles citrate-capped)

diluted to 35%) and **GNP1** are summarized in Table 1 (**GNP1** distribution size is shown in Supplementary Materials).

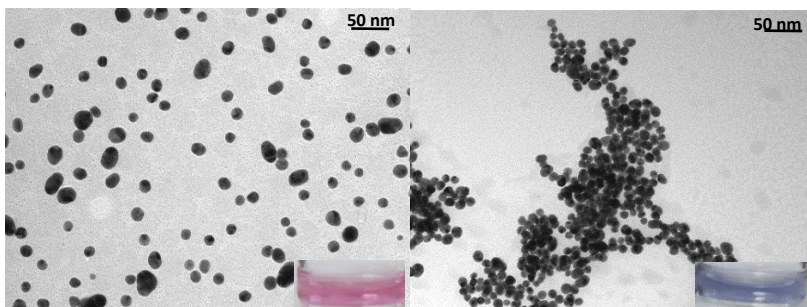


**Figure 1.** Changes induced in the aggregation of GNP1 in presence of GHB.

**Table 1.** Size and zeta-potential measured for citrate-GNP and GNP1 in deionized water.

Material	Size (nm) TEM Images	Size (nm) DLS	Z Potential (mV)
<b>citrate-GNP</b>	-----	$24.2 \pm 1.6$	$-29.2 \pm 0.9$
<b>GNP1</b>	$18 \pm 2$	$25.2 \pm 0.3$	$-37 \pm 2$

**GNP1** has a hydrodynamic diameter slightly higher than citrate-GNP which can be related to the ligand interchange. The small change observed can be related to the low functionalization of **GNP1**. On the other hand, Z-potential of **GNP1** is also higher than this value for **citrate-GNP**. This data indicated a higher stabilization of **GNP1** when compare with the nanoparticles without functionalization.

The concentration of **GNP1** turned out to be  $(5.7 \pm 0.4) \cdot 10^{-10}$  M. This was calculated from UV-Vis spectra measurements, considering  $6.01 \cdot 10^8 \text{ M}^{-1} \cdot \text{cm}^{-1}$  as an estimated molar extinction coefficient [25].

The stability of GNP1 in different media was evaluated. Several buffer solutions (1 mM phosphate, pH 6.5, 7.5 and 8.5) and deionized water were used, and the suspensions were kept in the fridge for 5 days. After this time, only the suspensions in deionized water remained dispersed (Supplementary Materials Figure S8). In consequence, this was the medium used in the sensing experiments.



### Sensing experiments

In order to verify the detection ability of sensor **GNP1** towards GHB, a preliminary UV-vis study was developed. **GNP1** exhibits an absorption band centred at 525 nm in the UV-vis spectrum, which is in accordance with the SPR band of dispersed gold nanoparticles of ca 20 nm diameter [15]. Addition of an excess of GHB, after 2 min of incubation time, promoted the aggregation of the nanoparticles with a bathochromic shift of the plasmon band to 643 nm and a clear change in the colour of the solution from red to blue (Figure 2). The position of the maximum in the UV-Vis spectrum, in addition to the colour change, strongly suggest that aggregation of **GNP1** was taking place. This was further supported by TEM images that clearly showed the aggregation (Figure 1).

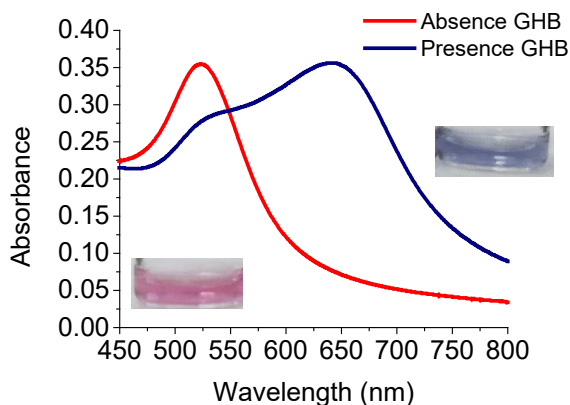


**Figure 2.** **GNP1** UV-Vis spectra variation in absence and presence of 100 mM of GHB, using deionized water as solvent.

UV-vis titrations of **GNP1** using increasing amounts of GHB were made in deionized water (see Figure 3). A decrease of the band at 525 nm and an enhancement of the band at 643 nm was observed as the concentration of GHB increased. These changes induced a gradual change in the colour of the suspension, which could be observed naked eye.

The probe showed a linear response from 16 mM to 28 mM. From these data and using the expression:  $LoD = 3 \cdot S_b/m$  (where  $S_b$  is the

standard deviation of the blank and  $m$  is the slope) a value of  $LoD = 1.12$  mM was determined. At this point, it is noteworthy to remark that the average amount of GHB necessary to facilitate anesthesia, leading to severe confusional episodes and coma is 50 mg/kg [26]. It means that a person who weighs 62 kg (the average body mass) has to intake about 3100 mg of GHB to promote a coma state. That implies an approximate concentration of 90 mM, a higher value than the  $LoD$  found.

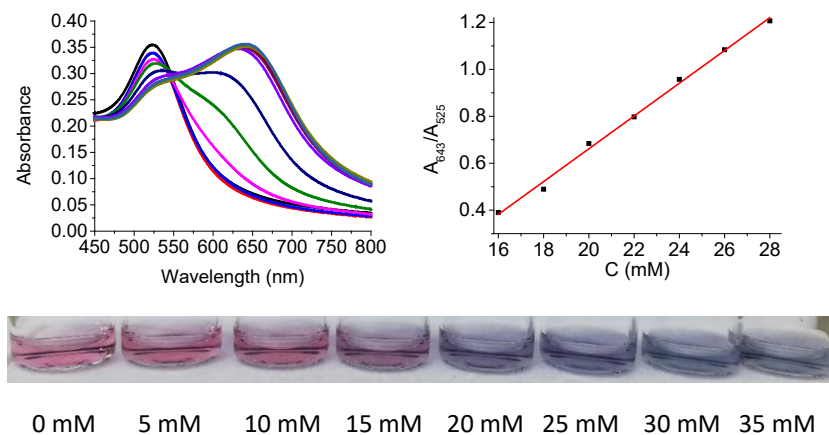


**Figure 3.** (Top) Titration of GHB ranging from 0 mM to 35 mM with **GNP1** (left) and its linear regression (right,  $y = (0.0698 \pm 0.0019) \cdot x - 0.74 \pm 0.04$ ,  $R^2 = 0.996$ ) using deionized water as solvent. (Bottom) Colorimetric changes observed during the titration.

To demonstrate that both, the hydroxyl and the carboxylate groups of GHB are simultaneously involved in the aggregation process, the responses of the sensor in presence of GHB (35 mM) and a mixture of AcONa and EtOH (35 mM each) was evaluated (see Supplementary Materials Figure S9). A slight change was observed in UV-Vis spectrum of **GNP1** when the mixture AcONa/EtOH is added but it was not as remarkable as the response induced by GHB. This result reinforces the interaction of both functional groups with the receptors units de-signed.

As the main aim of this work was to test **GNP1** in beverages, the response in presence of citric acid and sodium ascorbate was

#### Chapter 4: Colorimetric detection of GHB using gold nanoparticles

evaluated, as these compounds are present in soft drinks, where their concentrations are usually around 0.3% w/v and 0.01% w/v, respectively [27]. Citric acid, due to its acidity, caused a destabilising interaction because negative charges which surrounded **GNP1** were partially neutralized, promoting its rapid aggregation. On the other hand, sodium ascorbate had the opposite effect, acting as a stabilising agent. So, when both compounds are together (in the described concentrations), ascorbic acid counteracts partially the negative effect of citric acid allowing the detection of GHB (see Supplementary Materials Figure S10).

The last step was to test sensor **GNP1** in real samples. For this, detection of GHB in some beverages such as alcoholic drinks and soft drinks (alone and mixed with some distilled drink) was studied. Initially, the samples were spiked with GHB (70 mM final concentration) and mixed with **GNP1** at room temperature (for further details see "Section 2"). In all the tested cases, the changes were immediately observed by naked eye. The results were satisfactory, as can be seen in Figure 4, and it was possible to distinguish between clean samples and samples adulterated with GHB (35 mM final concentration). Apart from orange soda and whisky, other samples were tested and compiled in the Supplementary Materials Figure S11.



**Figure 4.** Colour changes in real samples. Please notice in all cases, the vials are grouped in pairs and the first vial contains the clean sample; meanwhile, the second one contains the spiked sample.

The visual observation of the drug in beverages clearly suggests that the system could be easily modified to be used onsite. In this sense, a kit for personal safety to be used in recreational environments could be envisaged. This kit would be formed by an Eppendorf containing the AuNPs suspension and a simple instructions sheet (an example is

included in Supplementary Materials Figure S12). The addition of a drop of the beverage to the container, followed by the colour observation, would permit the user to know if the beverage has been contaminated with GHB.

## **Conclusions**

In conclusion, we report herein a colorimetric sensor (**GNP1**) for the quick and easy detection of GHB by naked eye in both aqueous solutions and real samples. Sensor **GNP1** consists of an aqueous dispersion of gold nanoparticles functionalised with two different ligands, a 2-aminonaphthoxazole derivative, capable of interacting with carboxylate groups and a phenanthroline terminated ligand, which can bind to hydroxyl groups. These ligands can recognise both functional groups present in GHB giving rise to an aggregation process, which in turns results in a clear colour change of the solution from red to blue and a bathochromic shift of the SPR band in the UV-vis spectrum. The LoD here reported (1.12 mM) is considerable smaller than the quantity necessary of GHB to induce a severe confusion (90 mM).

## **Supplementary Materials**

The following are available online at <https://www.mdpi.com/article/10.3390/chemosensors9070160/s1>. Figure S1. <sup>1</sup>H NMR spectrum of L1. Figure S2. <sup>13</sup>C NMR spectrum of L1. Figure S3. <sup>1</sup>H NMR spectrum of L2. Figure S4. <sup>13</sup>C NMR spectrum of L2. Figure S5. Mass Spectrometry Spectrum of L1. Figure S6. Mass Spectrometry Spectrum of L2. Figure S7. GNP1 DLS size distribution. Figure S8. GNP1 stability in different buffers. Figure S9. UV-visible changes of sensor GNP1 with 35 mM GHB and a 35 mM mixture of AcONa/EtOH using water deionised as solvent. Figure S10. Absorbance spectra of GNP1 in the presence of citric acid, sodium ascorbate, in the real concentration present in beverages, and NaGHB (35 mM). Figure S11. Colour changes in real sample. Figure S12. Instructions sheet for an on-site safety kit based on GHB detection.

### **Author Contributions**

Conceptualization, A.M.C.; methodology, S.R.-N.; characterization, S.G.; sources, M.P.; writing—review and editing, S.R.-N., A.M.C. and M.P.; supervision, P.G. All authors have read and agreed to the published version of the manuscript.

### **Funding**

This research was funded by Spanish Government, MICINN funds (RTL2018- 100910-B-C42) and Ministry of Health, Consumer Affairs and Social Welfare Project 2020I040 PNSD 2020 and the Generalitat Valenciana (PROMETEO 2018/024).

### **Acknowledgments**

S. R.-N. is grateful to the Spanish Government for a fellowship. SCSIE (Universidad de Valencia) is gratefully acknowledged for all the equipment used. NMR was registered at the U26 facility of ICTS “NAMBIOSIS” at the Universitat of València. gratefully acknowledged.

### **Conflicts of Interest**

The authors declare no conflict of interest regarding the publication of this paper.

### **References**

1. Olszewski, D. Sexual assaults facilitated by drugs or alcohol. *Drugs: education, prevention, policy* 2019, 16, 39-52.
2. Nemeth, Z.; Kun, B.; Demetrovics, Z. Gamma-hydroxybutyrate (GHB): an emerging substance of abuse. *J. Psychopharmacol.* 2010, 24, 1281-1287.
3. Busardò, F.P.; Jones, A.W. GHB Pharmacology and Toxicology: Acute Intoxication, Concentrations in Blood and Urine in Forensic Cases and Treatment of the Withdrawal Syndrome. *Current Neuropharmacology* 2015, 13, 47-70.

#### *Chapter 4: Colorimetric detection of GHB using gold nanoparticles*

4. Davis, K.E.; Hickey, L.D.; Goodpaster, J.V. Detection of [n.611]-hydroxybutyric acid (GHB) and [n.611]-butyrolactone (GBL) in alcoholic beverages via total vaporization solid-phase microextraction (TV-SPME) and gas chromatography-mass spectrometry. *Journal of Forensic Sciences* 2021, 66, 846-853.
5. Jin, S.; Ning, X.; Cao, J.; Wang, Y. Simultaneous Quantification of  $\gamma$ -Hydroxybutyrate,  $\gamma$ -Butyrolactone, and 1,4-Butanediol in Four Kinds of Beverages. *International Journal of Analytical Chemistry* 2020, 8837743.
6. Jin, S.; Ning, X.; Cao, J.; Wang, Y. Food safety risk assessment of gamma-butyrolactone transformation into dangerous gamma-hydroxybutyric acid in beverages by quantitative  $^{13}\text{C}$ -nuclear magnetic resonance technique. *Journal of Food Quality* 2020, 8846214.
7. Garrido, E.; Pla, L.; Lozano-Torres, B.; El Sayed, S.; Martinez-Mañez, R.; Sancenon, F. Chromogenic and Fluorogenic Probes for the Detection of Illicit Drugs. *Chemistry Open* 2018, 7, 401-428.
8. Zhai, D.; Qiao, Y.; Tan, E.; Xu, W.; Chang, Y-T. Development of a fluorescent sensor for illicit date rape drug GHB. *Chem Commun.* 2014, 50, 2904-2906.
9. Zhai, D.; Agrawalla, B.K.; Eng, P.S.F.; Lee, S-C.; Xua, W.; Chang, Y-T. Development of a fluorescent sensor for an illicit date rape drug – GBL. *Chem Commun.* 2013, 49, 6170-6172.
10. Wang, W.; Dong, Z-Z.; Yang, G.; Leung, C-H.; Lin S.; Ma, D-L. A long-lived iridium(iii) chemosensor for the real-time detection of GHB. *J. Mat. Chem. B* 2017, 8, 2736-2742.
11. Bravo, D.; Harris D.; Parsons, S. Reliable, sensitive, rapid and quantitative enzyme-based assay for gamma-hydroxybutyric acid (GHB). *J. Forensic Sci.* 2004, 49, 379-387.
12. Baumes, L.A.; Sogo, M.B.; Montes-Navajas, P.; Corma, A.; Garcia, H. A Colorimetric Sensor Array for the Detection of the Date-Rape

Drug  $\gamma$ -Hydroxybutyric Acid (GHB): A Supramolecular Approach. *Chem. Eur. J.*, 2010, 16, 4489 – 4495.

13. Hu, M.; Han, Q.; Xing, B. Metallic nanoparticle-enabled sensing of a drug-of-abuse: an attempt at forensic application. *ChemBioChem*. 2020, 21, 2512-2517.

14. Mayer†, K.M.; Hafner, J. H. Localized Surface Plasmon Resonance Sensors. *Chem. Rev.* 2011, 111, 3828–3857.

15. Priyadarshinia, E.; Pradhana, N. Gold nanoparticles as efficient sensors in colorimetric detection of toxic metal ions: A re-view. *Sensors and Actuators B* 2017, 238, 888–902.

16. Godoy-Reyes, T.M.; Costero, A.M.; Gaviña, P.; Martínez-Máñez, R.; Sancenón, F. Colorimetric detection of normetanephrine, a pheochromocytoma biomarker, using bifunctionalised gold nanoparticles. *Analytica Chimica Acta* 2019, 1056, 146-152.

17. Martí, A.; Costero, A.M.; Gaviña, P.; Parra, M. Selective colorimetric NO(g) detection based on the use of modified gold nanoparticles using click Chemistry. *Chem. Commun.* 2015, 51, 3077-3079.

18. Rodríguez-Nuévalos, S.; Costero, A.M.; Arroyo, P.; Sáez, J.A.; Parra, M.; Sancenón F.; Martínez-Máñez, R. Protection against chemical submission: naked-eye detection of  $\gamma$ -hydroxybutyric acid (GHB) in soft drinks and alcoholic beverages. *Chem. Commun.* 2020, 56, 12600-12603.

19. Mazik, M.; Hartmann A.; Jones, P.G. Highly Effective Recognition of Carbohydrates by Phenanthroline-Based Receptors:  $\alpha$ - versus  $\beta$ -Anomer Binding Preference. *Chem. Eur. J.*, 2009, 15, 9147-9159.

20. Talwelkar, M.; Pedireddi, V. R. -B(OH)<sub>2</sub> versus -OH in supramolecular synthesis: molecular complexes of 4-hydroxyphenylboronic acid with aza-donor compounds. *Tetrahedron Letters* 2010, 51, 6901-6905.

21. Kirby, I.L.; Pitak, M.B.; Wilson, C.; Galea, P.A.; Coles, S.J. Electron density distribution studies as a tool to explore the behaviour of

thiourea-based anion receptors. *Cryst. Eng. Comm.* 2015, 17, 2815–2826.

22. Yadav, V. K.; Srivastava, V.P.; Yadav, L.D.S. Iodide catalyzed synthesis of 2-aminobenzoxazoles via oxidative cyclodesulfurization of phenolic thioureas with hydrogen peroxide. *Tetrahedron Lett.* 2018, 59, 252–255.

23. Weinig, H.-G.; Krauss, R.; Seidock, M.; Bendig, J.; Koert, U. Molecular Signal Transduction by Conformational Transmission: Use of Tetrasubstituted Perhydroanthracenes as Transducers. *Chem. Eur. J.* 2001, 7, 2075-2088.

24. Zhao, P.; Li, N.; Astruc, D. State of the art in gold nanoparticle synthesis. *Coord. Chem. Rev.* 2013, 257, 638-665.

25. Liu, X.; Atwater, M.; Wang, J.; Huo, Q. Extinction coefficient of gold nanoparticles with different sizes and different capping ligands. *Colloids Surf. B Biointerfaces* 2007, 58, 3-7.

26. Royo-Isaach, J.; Magrané, M.; Vilà, R.; Capdevila, M.E. El «éxtasis líquido» (GHB): ¿una droga de uso recreativo? *Clínica biopsicosocial del consumidor y algunas propuestas terapéuticas.* *Aten Primaria* 2004, 33, 516-20.

27. Kregiel, D. Health Safety of Soft Drinks: Contents, Containers, and Microorganisms. *BioMed Research International* 2015 Article ID 128697.



## **Supplementary Information**

### **Bifunctionalized gold nanoparticles for the colorimetric detection of the drug $\gamma$ -hydroxybutyric acid (GHB) in beverages**

Silvia Rodríguez-Nuévalos<sup>1</sup>, Ana M. Costero<sup>1,2,\*</sup>, Salvador Gil<sup>1,2</sup>, Margarita Parra<sup>1,2</sup>, Pablo Gaviña<sup>1,2,\*</sup>

- 1) Instituto Interuniversitario de Investigación de Reconocimiento Molecular y Desarrollo Tecnológico (IDM). Universidad Politècnica de València, Universitat de València, Doctor Moliner 50, Burjassot, 46100, Valencia, Spain; e-mail: pablo.gavina@uv.es
- 2) CIBER de Bioingeniería, Biomateriales y Nanomedicina (CIBER-BBN) (Spain).

\* Correspondence: pablo.gavina@uv.es; Tel.: +34 963543740



## NMR Spectra

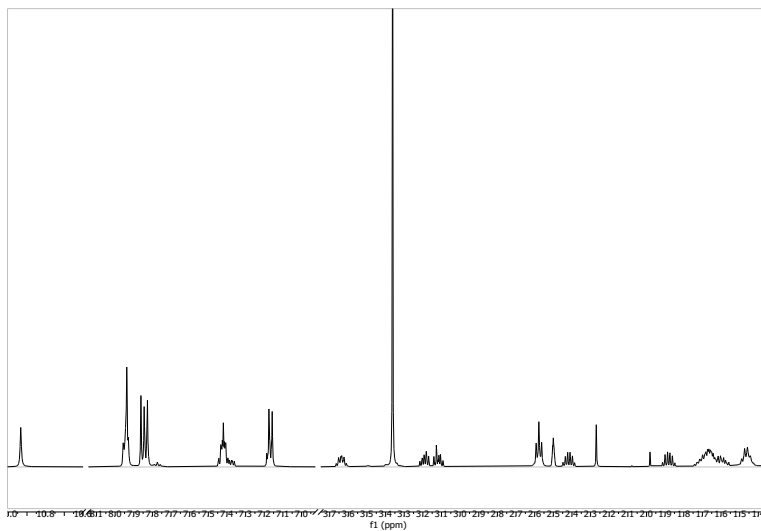


**Figure S1.** <sup>1</sup>H NMR spectrum of L1

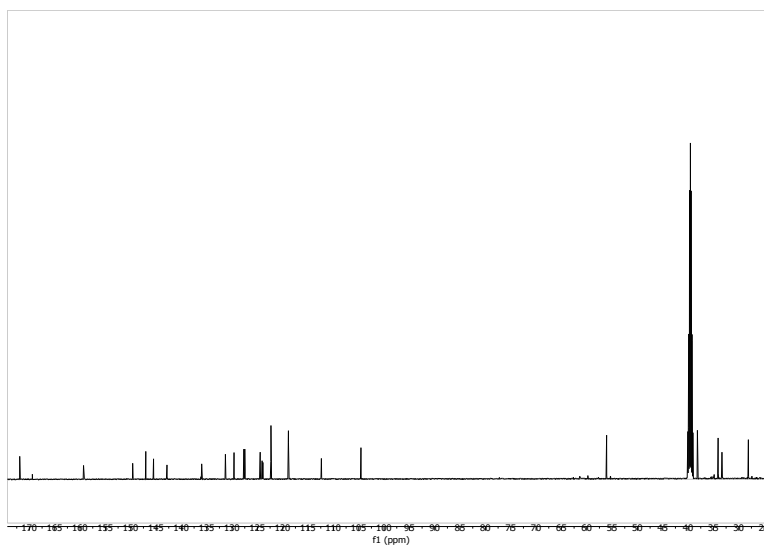


**Figure S2.** <sup>13</sup>C NMR spectrum of L1

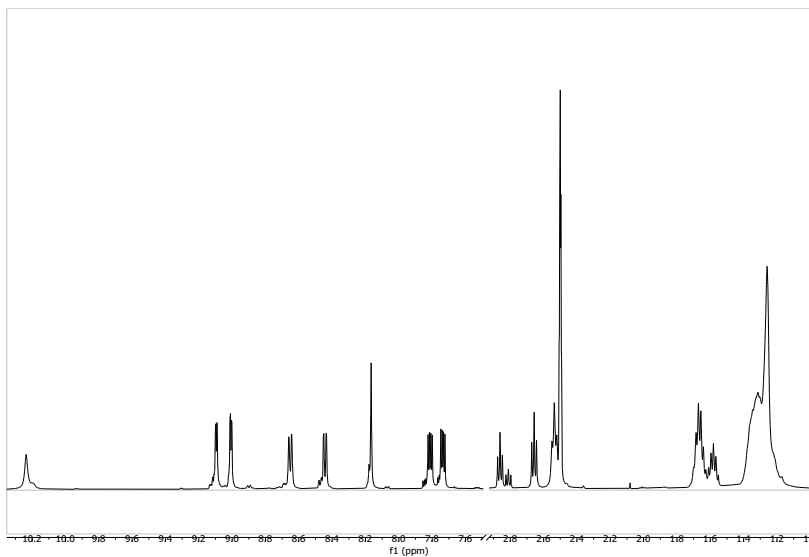


Figure S3.  $^1\text{H}$  NMR spectrum of L2

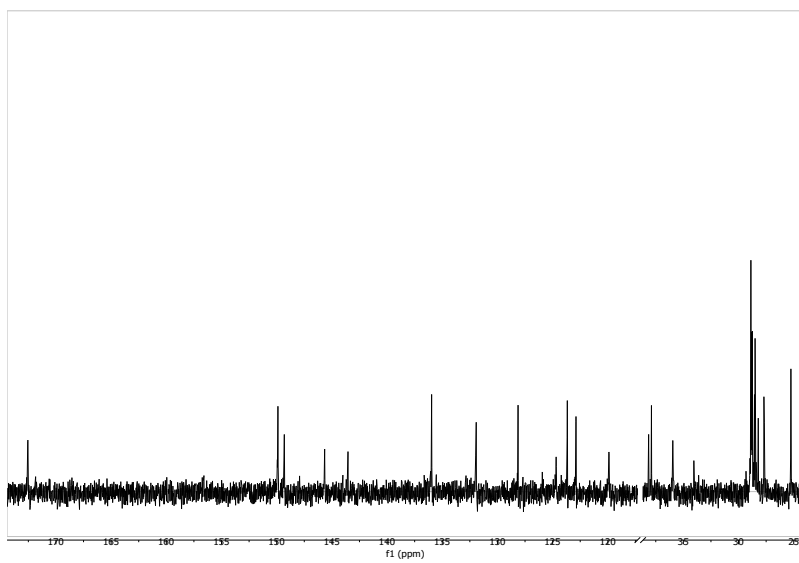


Figure S4.  $^{13}\text{C}$  NMR spectrum of L2

## Mass Spectrometry Spectra

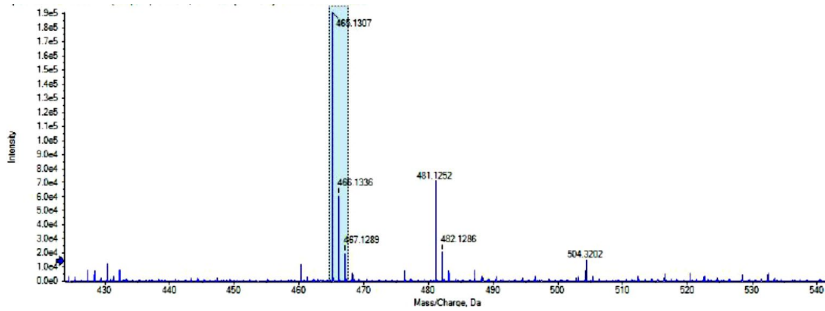


Figure S5. Mass Spectrometry Spectrum of L1

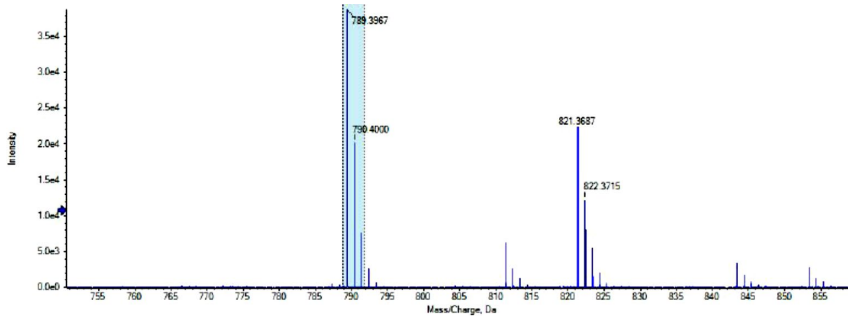


Figure S6. Mass Spectrometry Spectrum of L2

## GNP1 Characterization

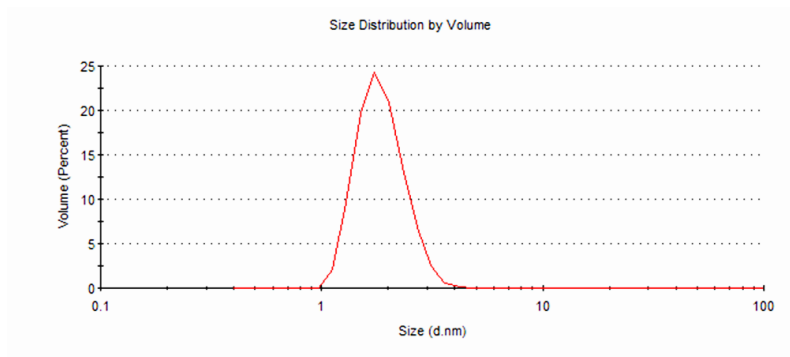


Figure S7. GNP1 DLS size distribution

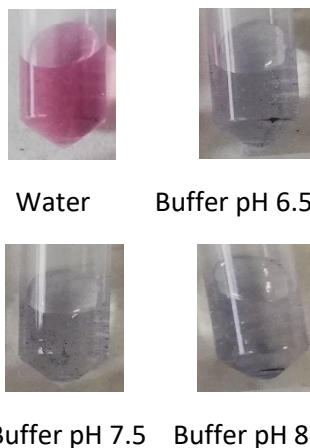


Figure S8. GNP1 stability in different buffers

### UV-Vis Spectra

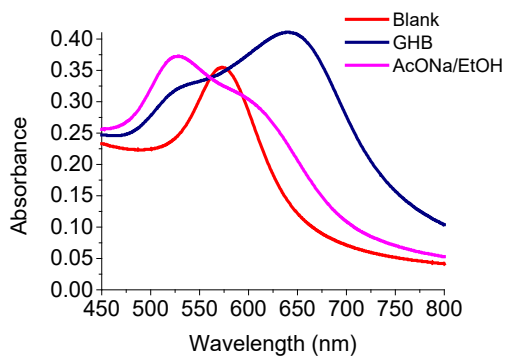
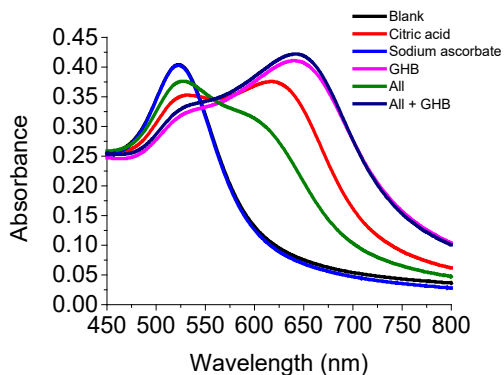


Figure S9. UV-visible changes of sensor GNP1 with 35 mM GHB and a 35 mM mixture of AcONa/EtOH using water deionised as solvent.

## Chapter 4: Colorimetric detection of GHB using gold nanoparticles



**Figure S10.** Absorbance spectra of **GNP1** in the presence of citric acid, sodium ascorbate, in the real concentration present in beverages, and NaGHB (35 mM).

### Real samples



**Figure S11.** Colour changes in real samples



**Figure S12.** Instruction sheet for an on-site safety kit based on GHB detection





**Chapter 5: GHB and synthetic  
cathinones detection using  
BODIPY derivatives**



## 5.1. Introduction

### 5.1.1. BODIPY core

Over the last few decades, the design synthesis and study of new fluorescent compounds is a research field in continuous expansion owing to their application in different areas such as medicine, clinical diagnosis, materials science or environment. Among all of them, BODIPYs (4,4-difluoro-4-bora-3a,4a-diaza-s-indacenes) have been growing in popularity. The first BODIPY reported in the literature was in 1968, by Treibs and Kreuzer.<sup>104</sup> From now then, the interest in these compounds has done nothing, but augment. This has been possible thanks to their extraordinary and almost unique photophysical properties such as large molar absorption coefficients, usual high quantum yields, their absorption, excitation and emission spectra in the visible range, redox behaviour, robustness against light and chemicals, significantly low tendency towards self-aggregation in solution and fluorescence lifetimes in the nanosecond range.<sup>104–113</sup> Structural differences among BODIPY, dipyrromethene and dipyrromethane cores as well as their IUPAC numbering are depicted in Chart 5.1. Even though the numbering is different, the  $\alpha$ ,  $\beta$  and *meso* positions are still the same between BODIPYs and dipyrromethenes.<sup>105</sup>

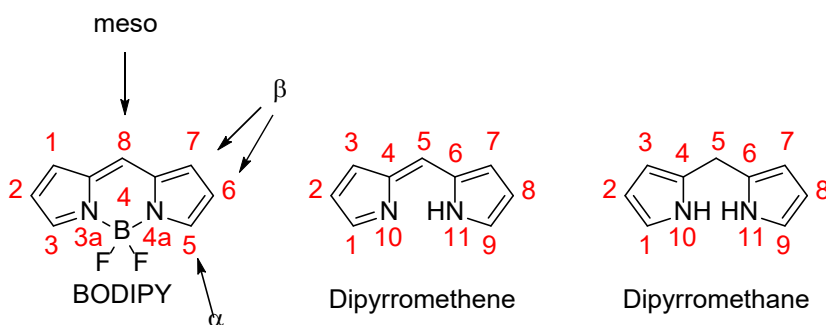
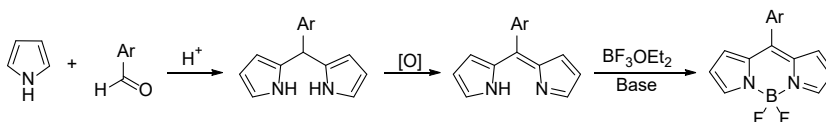


Chart 5.1. Chemical structures of BODIPY, dipyrromethene and dipyrromethane cores and their numberings

### 5.1.2. Synthesis and postfunctionalization

The synthetic approach to obtain these dyes can be grouped in two categories: prefunctionalization and postfunctionalization. The first one consists of the use of a pyrrole with the appropriate functionalization to synthesise the BODIPY, whereas the second approach implies the functionalization when the BODIPY is already synthesised. Even though these different procedures can be competitive, normally they are quite complementary. Thanks to both approaches, a large variety of BODIPY derivatives is accessible to scientists.<sup>104–114</sup> The synthetic pathways followed in order to obtain BODIPYs are highly related to the well-known porphyrins chemistry. One example of this is shown in Scheme 5.1.<sup>105</sup>



Scheme 5.1. Example of a synthetic route to obtained BODIPY derivatives

The condensation of aldehydes with pyrrole under acidic catalysis generates the dipyrromethane derivate. A second oxidation stage is required to obtain the dipyrromethene core. Finally, the boron bridge is introduced by addition of BF<sub>3</sub>OEt<sub>2</sub> in the presence of a base. Even though a large amount of synthesis has been described using aldehydes, it is not compulsory to use them. Gradually, the number of synthesis using acid chlorides or anhydrides have increased.<sup>104–114</sup>

On the other hand, BODIPYs reactivity can be explained based on their different resonance structures. As can be seen in Chart 5.2, positions 1, 3, 5, 7 and 8 are prone to undergo nucleophilic aromatic substitutions (S<sub>N</sub>Ar), whereas positions 2 and 6 will suffer electrophilic aromatic substitutions (S<sub>E</sub>Ar).

Chapter 5: GHB and synthetic cathinones detection using BODIPY derivatives

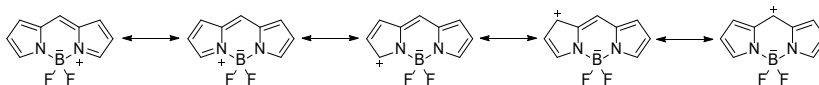


Chart 5.2. Resonance structures depicted to explain the reactivity of the different positions in BODIPYs

Additionally, an extensive range of procedures to halogenate the core,<sup>115</sup> to form carbon-carbon bonds,<sup>116</sup> Knoevenagel condensations<sup>117</sup> and so on<sup>118–121</sup> has been developed over the years, providing scientific community with a vast versatility of pathways to obtain a very broad family of fluorescent dyes. Some of these reactions are indicated in Chart 5.3.

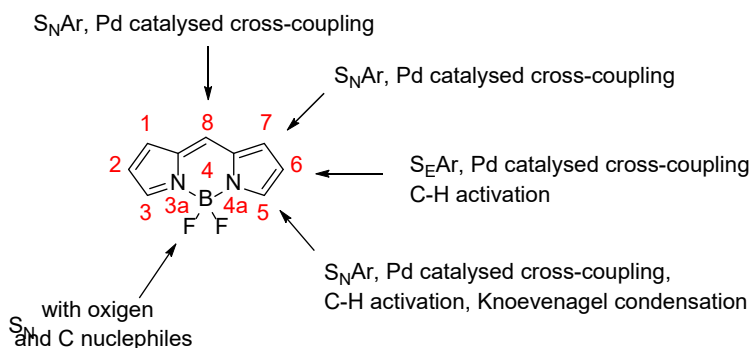
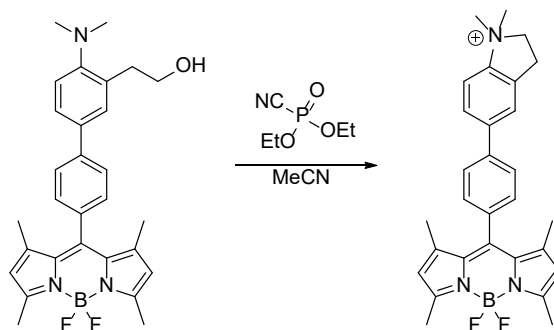


Chart 5.3. Summary of some of the most relevant postfunctionalization carried out on the BODIPY core<sup>105</sup>

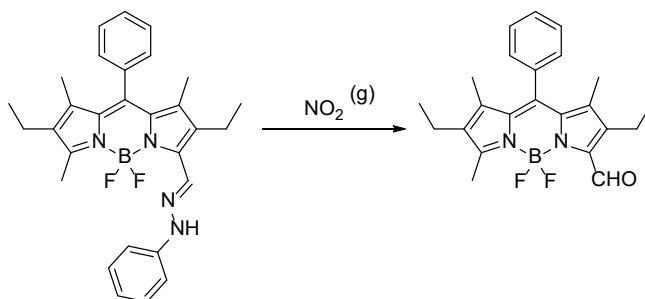
All these characteristics explain the wide use of these fluorophores in the development of chemosensors.<sup>122,123</sup> As an example, one of these sensors is discussed below. Chart 5.4 shows the chemical structure of one sensor developed to detect nerve agent simulants such as DCNP (Diethylcyanophosphonate) and DFP (Diisopropylfluorophosphate) and its detection reaction.<sup>124</sup> The authors described the sensing process through the interruption of an ICT process. Initially, the amino group is able to donate charge to the BODIPY core, generating a quenching of the fluorescence. When this BODIPY was in the presence of DCNP or DFP, a cyclization process took place. The hydroxyl group reacted with the nerve agent simulants generating a

phosphate group that underwent a  $S_N2$  generating an ammonium derivative with the consequent deactivation of the ICT process.



Scheme 5.2. Detection reaction of a nerve agent simulant (DCNP) using a chemodosimeter based on a BODIPY core<sup>124</sup>

Another example of a probe containing a BODIPY core is the one depicted in Scheme 5.3.<sup>125</sup> The authors reported a chemosensor able to detect  $\text{NO}_2$  by means of an oxidative cleavage of the hydrazone moiety, obtaining the aldehyde derivative. As a result, they observed a hypsochromic shift in the lowest energy band in the UV-Visible spectrum.



Scheme 5.3. Detection reaction of  $\text{NO}_2$  (g) using a BODIPY derivative as chemodosimeter<sup>125</sup>

## 5.2. Chemosensors design

Regarding the vast versatility and availability of these derivatives, two sensors were developed to detect not only GHB, but also cathinones. These probes were designed with a hydrazone moiety in their structures (see Chart 5.4). On one hand, on the basis of the potential acid-base behaviour that these BODIPY derivatives could show, they were expected to interact with the carboxylate group present in GHB through an acid-base reaction. On the other hand, concerning to SCs detection, we took advantage of three factors. The first one, the ability of hydrazones to coordinate Cu(II);<sup>126,127</sup> the second one, the capability of cathinones to reduce Cu(II) to Cu(I)<sup>51</sup> and finally, the different behaviour that ligands show towards Cu(II) or Cu(I) coordination.<sup>128,129</sup> Consequently, all these factors combined would allow us to recognise indirectly SCs.

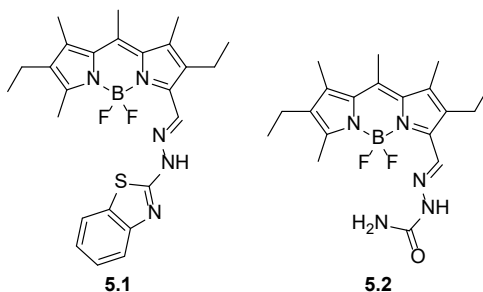
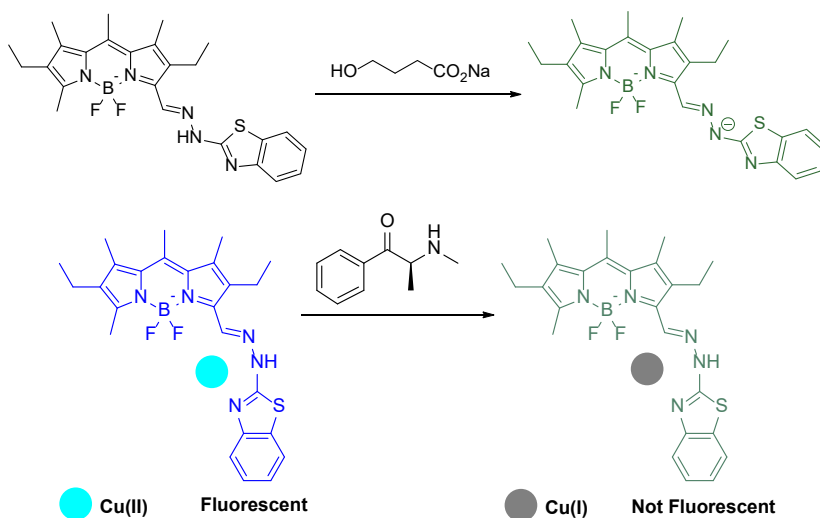


Chart 5.4. Probes designed to detect GHB and/or SCs

### 5.3. Objectives

Regarding the exceptional optical properties of BODIPY derivatives and their synthetic versatility, the main goal was to create, at least, a probe able to detect both drugs at the same time: GHB and SCs. For that reason, five specific objectives were set.

- Synthesis of two hydrazone BODIPY derivatives (compounds **5.1** and **5.2**).
- Study of their acid-base properties and, therefore, to analyse their viability as probes for GHB detection.
- Assessment of the different complexation behaviour towards Cu(I) and Cu(II) in different solvents.
- Pursuit of the optimal conditions to carry out the reduction of Cu(II) to Cu(I) using SCs and, thus, to detect them.
- Evaluate the possibility of using those latter experimental conditions to recognise both analytes.



Scheme 5.4. Detection proposal of GHB and SCs



## 5.4. Colorimetric and fluorescent hydrazone-BODIPY probes for the detection of $\gamma$ -hydroxybutyric acid (GHB) and cathinones

Silvia Rodríguez-Nuévalos<sup>a,b</sup>, Ana M. Costero<sup>a,b,c</sup>, Margarita Parra<sup>a,b,c</sup>, Salvador Gil<sup>a,b,c</sup>, Pau Arroyo<sup>a,b</sup>, Jose A. Sáez\*<sup>a,b</sup>, Pablo Gaviña\*<sup>a,b,c</sup>, Paola Ceroni<sup>d</sup>, Andrea Fermi<sup>d</sup>

<sup>a</sup>Instituto Interuniversitario de Investigación de Reconocimiento Molecular y Desarrollo Tecnológico (IDM). Universitat Politècnica de València, Universitat de València, Doctor Moliner 50, Burjassot, 46100, Valencia, Spain.

<sup>b</sup>Departamento de Química Orgánica, Universitat de València, Doctor Moliner 50, Burjassot, 46100, Valencia, Spain.

<sup>c</sup>CIBER de Bioingeniería, Biomateriales y Nanomedicina (CIBER-BBN) (Spain)

<sup>d</sup>Dipartimento di Chimica "G. Ciamician", Università di Bologna, Via Selmi, 2, 40126 Bologna (Italy)

\* Correspondence: pablo.gavina@uv.es; Tel.: +34 963543740,  
jose.a.saez@uv.es; Tel.: +34 963544202

**Received:** 27th July 2022

**Accepted:** 14th September 2022

*Dyes and Pigments 207 (2022) 110757*



## **Abstract**

Consumption and abuse of drugs is a general problem, which concerns our entire society. In some cases, drugs are used for recreational purposes; but in others, they are used to commit crimes such as Drug-Facilitated Sexual Assault (DFSA). In other cases, this consumption alters the consumer mood in such a way that risky situations can rise. In any case, detection of drugs in different environment is worthwhile. Here, two new chromogenic and fluorescent probes are reported. Detection of both cathinone derivatives and  $\gamma$ -hydroxybutyric acid (GHB) can be carried out with naked-eye with limits of detection of 0.4  $\mu\text{M}$  and 0.3  $\mu\text{M}$  for GHB and 2.00  $\mu\text{M}$  for cathinone. Selectivity in the presence of other drugs has been tested. Sensing mechanisms have been studied using different spectroscopic techniques and they have been also corroborated through theoretical calculations.

## **Introduction**

Over the last years, the number of drug users in our society has increased alarmingly. According to the statistics from European Monitoring Centre for Drugs and Drug Addiction (EMCDDA), around 97 million people aged 15-64 in European Union (EU), almost the third of the population, have consumed illicit drugs at some moment of their lives [1]. Related to this latter issue, it is also considerably worrying the quick emergence of illegal substances known as New Psychoactive Substances (NPS). NPS consist of a noticeably extensive range of uncontrolled and illegal drugs. Not only their consumption has increased in the last three decades, but also their easy replacement for another derivative and their illegal trafficking. In fact, in 2015, 34,000 seizures in EU took place, which implied 4.6 tonnes of seized NPS [2]. In this sense, the importance of synthetic cathinones (SCs) has risen in the last 10 years.

Synthetic cathinones, commonly known as “bath salts”, are substances chemically related to cathinone (Figure 1), a stimulant drug found in the khat plant. The synthetic variants of cathinone can be more potent as drugs than the parent natural compound and, in some cases, much more dangerous due to their cardiac and

neurological effects. Some examples of SCs are ephedrone, 3,4-MDPHP (3',4'-methylenedioxy- $\alpha$ -pyrrolidinohexiophenone), MPHP (4'-methyl- $\alpha$ -pyrrolidinohexiophenone) and MDMC (3,4-methylenedioxy-*N*-methylcathinone). The qualitative identification of these drugs is usually carried out by the Zimmermann test, which uses 1,3-dinitrobenzene in basic medium to induce a colour change by the formation of a Meisenheimer complex. However, this test is non-specific giving rise to many false positive responses. Therefore, the preparation of more selective sensors to detect these compounds is a hot field in the sensing area [3].

On the other hand, another drug that is generating significantly troublesome situations to law enforcement agencies and authorities is  $\gamma$ -hydroxybutyric acid (GHB or liquid ecstasy). GHB (Figure 1), a natural product generated during the  $\gamma$ -aminobutyric acid (GABA) metabolism, is involved in the regulation of a high number of neurotransmitters such as GABA, dopamine or 5-hydroxytryptamine. However, this little fatty acid is also an illicit drug whose use has increased considerably. In 2020, GHB was reported as the fifth most consumed drug by Euro-DEN Plus hospitals [4]. This substance was found in 35% of critical care admissions and 11% of drug acute intoxications, highlighting how easy is to overdose during its consumption. The number of seizures of GHB in Europe also rose to 2000. Furthermore, this compound is implicated in other criminal acts, such as Drug-Facilitated Sexual Assault (DFSA). In that respect, GHB is one of the drugs known as “rape drugs” [5]. Usually, these substances are added to the victims’ drinks without their consent, undermining thus their will after ingesting them since they are not able to notice their presence in the drinks. Due to this fact, the number of reports in literature regarding the detection of GHB has increased in the last few years [6, 7]. SCs are also likely to be found as “rape drugs” [8].

From this perspective, we focused our effort and attention on the development of chemosensors to detect these drugs: GHB and SCs. In that regard, the use of optical molecular sensors has proved to be very useful, reliable and inexpensive systems for a large number of analytes detection [9,10]. Following our experience in this field [11-13], we now report the preparation and evaluation of two new dyes

based on a 4,4-difluoro-4-bora-3a,4a-diaza-s-indacene (borodipyrromethene or BODIPY) moiety functionalized in the alpha position (Figure 1). Functionalization has been chosen, on one hand, to explore the acid-base properties of the compounds and their application in GHB detection. On the other hand, the capability of hydrazones to complex Cu(II) salts [14] combined with the well-established redox properties of cathinones, able to reduce Cu(II) to Cu(I), prompted us to study the possibility of using the prepared compounds in combination with Cu(II) to also detect these drugs [15].

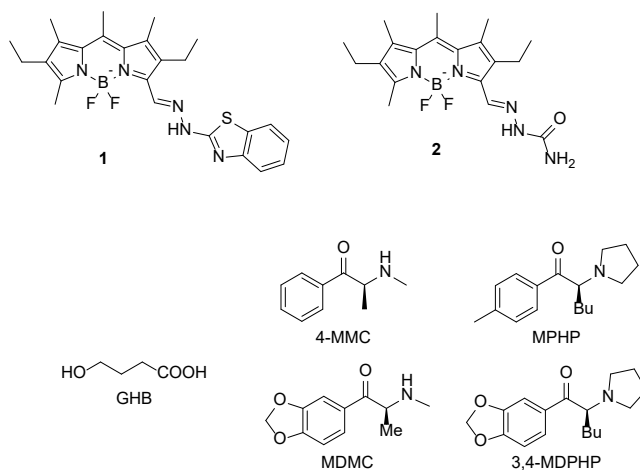


Figure 1. New prepared probes and structures of selected drugs.

## 2. Material and Methods

### 2.1. Materials

The reagents employed in the synthesis were acquired from Sigma Aldrich and used without further purification.  $^1\text{H}$  NMR,  $^{13}\text{C}$  NMR and  $^{19}\text{F}$  NMR spectra were registered with Bruker Avance 300 MHz or 500 MHz spectrometers, all of them referenced to solvent peak, DMSO( $d_6$ ). All photophysical analysis was carried out in air-equilibrated DMSO or MeCN at 298 K, unless otherwise specified. UV-vis absorption spectra were recorded with a PerkinElmer  $\lambda$ 40 spectrophotometer or Shimadzu UV-2600 using quartz cells with path length of 1.0 cm. Luminescence spectra were performed with a

PerkinElmer LS-50 or FluoroMax-4 Spectrofluorometer. Lifetimes shorter than 10  $\mu$ s were measured with an Edinburgh FLS920 spectrofluorometer using time-correlated single-photon counting (TCSPC) technique. Quantum yields were determined with the method of Demas and Crosby [16] using Rhodamine B and Rhodamine 101 as standards ( $\phi_{fl}$  = 0.7, 0.915, in MeOH and EtOH, respectively). The estimated experimental errors were 2 nm on the band maximum, 5% on the molar absorption coefficient and luminescence lifetime and 20% on emission quantum yields. Mass spectrometry spectra were carried out with a TripleTOFTM 5600 LC/MS/MS System, with 2 gas sources (both to 35 psi), 450 °C and ion gas voltage of 5500 V. Origin 2020 was the program used to plot titrations and to calculate complexation constants.

## 2.2. Synthesis of compounds 1 and 2

The synthesis of chemosensors **1** and **2** is summarized in Scheme 1.

### 2.2.1. Synthesis of 2,6-diethyl-1,3,5,7,8-pentamethyl-4,4-difluoro-4-bora-3a,4a-diaza-s-indacene (**3**) [17]

2.2 mL (16.30 mmol) of 3-ethyl-2,4-dimethyl-1H-pyrrole were dissolved in 8 mL of dry DCM under inert atmosphere. 3.44 mL (48.38 mmol) of acetyl chloride were added dropwise and the mixture was refluxed for 75 min. Then, the mixture was poured over 40 mL of hexane and solvents were removed under vacuum. The red oil was dissolved in 92 mL of dry DCM under inert atmosphere and 12 mL (86.10 mmol) of  $NEt_3$  were added. After stirring 10 min at room temperature, 12 mL (97.23 mmol) of  $BF_3OEt_2$  were added dropwise and the stirring was kept for 2 h at room temperature. Then, the solvent was removed and the crude was purified by chromatographic column, using hexane:AcOEt 9:1 as eluent. Compound **3** was obtained as an orange solid (1.98 g, 76% yield).  $^1H$  NMR (300 MHz,  $CDCl_3$ )  $\delta$  2.60 (s, 3H), 2.49 (s, 3H), 2.40 (q, J = 7.6 Hz, 4H), 2.33 (s, 3H), 1.04 (t, J = 7.6 Hz, 6H).  $^{13}C$  NMR (126 MHz,  $CDCl_3$ )  $\delta$  151.95, 139.86, 136.47, 132.50, 131.80, 17.26, 17.09, 15.05, 14.52, 12.51.

2.2.2. Synthesis of 2,6-diethyl-1,5,7,8-tetramethyl-4,4-difluoro-4-bora-3a,4a-diaza-s-indacene-3-carbaldehyde (4) [18]

300 mg (0.94 mmol) of compound **3** were dissolved in 8.5 mL of THF and cooled to 0 °C. Then, a solution of 1.074 g (4.71 mmol) of DDQ in 2 mL of THF were added dropwise and, after that, 3.5 mL of THF were added. The mixture was stirred while it was leading to warm slowly to room temperature. The solvent was removed under vacuum and the crude was purified by chromatographic column, using hexane:AcOEt 8:2 as eluent. Compound **4** was isolated as an orange powder (221 mg, 71% yield). <sup>1</sup>H NMR (300 MHz, CDCl<sub>3</sub>) δ 10.34 (t, J = 2.1 Hz, 1H), 2.82 (q, J = 7.5 Hz, 2H), 2.71 (s, 3H), 2.61 (s, 3H), 2.45 (q, J = 7.6 Hz, 2H), 2.40 (s, 3H), 2.34 (s, 3H), 1.09 (m, 6H). <sup>13</sup>C NMR (126 MHz, CDCl<sub>3</sub>) δ 186.01, 163.99, 142.02, 141.91, 138.88, 137.43, 136.93, 132.01, 17.80, 17.62, 17.17, 14.98, 14.63, 14.33, 13.50, 13.16.

2.2.3. Synthesis of compound 1

100 mg (0.30 mmol) of compound **4** were mixed with 65 mg (0.39 mmol) of 2-hydrazinobenzothiazole and 26 mg (0.32 mmol) of sodium acetate in 13 mL of EtOH and refluxed overnight. The solvent was removed under vacuum and the crude was purified by chromatographic column using hexane:AcOEt 7:3. After drying at 40 °C for 1 day, compound **1** was isolated as a dark green powder (99 mg, 68% yield). <sup>1</sup>H NMR (500 MHz, DMSO-*d*<sub>6</sub>) δ 12.63 (s, 1H), 8.56 (s, 1H), 7.93 – 7.70 (m, 1H), 7.49 (s, 1H), 7.31 (t, J = 7.6 Hz, 1H), 7.13 (t, J = 7.6 Hz, 1H), 2.89 (q, J = 7.3 Hz, 2H), 2.70 (s, 3H), 2.48 (s, 3H), 2.43 (q, J = 7.5 Hz, 2H), 2.38 (s, 3H), 1.18 (t, J = 7.3 Hz, 3H), 1.02 (t, J = 7.5 Hz, 3H). <sup>13</sup>C NMR (126 MHz, DMSO-*d*<sub>6</sub>) δ 155.53, 141.20, 139.43, 135.86, 134.10, 133.05, 126.08, 121.94, 121.67, 118.15, 115.50, 17.90, 17.01, 16.41, 14.60, 14.33, 14.23, 13.25, 12.51. <sup>19</sup>F NMR (471 MHz, DMSO-*d*<sub>6</sub>) δ -137.95, -138.01, -138.09, -138.15. HRMS (ESI<sup>+</sup>): *m/z* calcd for C<sub>25</sub>H<sub>29</sub>BF<sub>2</sub>N<sub>5</sub>S [M+H]<sup>+</sup>: 480.2210; found: 480.2190. UV-Vis: λ<sub>max</sub> (DMSO) = 584 nm. Fluorescence emission (DMSO): λ<sub>max</sub> = 616 nm (λ<sub>exc</sub> = 500 nm), φ<sub>fl</sub>: 0.39, τ: 2.5 ns.

#### 2.2.4. Synthesis of compound 2

100 mg (0.30 mmol) of compound **4** were mixed with 72 mg (0.65 mmol) of semicarbazide hydrochloride and 79 mg (0.97 mmol) of sodium acetate in 12 mL of EtOH. The mixture was refluxed for 3 h and, after cooling, was filtered under vacuum and dried at 40 °C for 1 day. 104 mg of compound **2** were obtained as a pink solid (83% yield). <sup>1</sup>H NMR (500 MHz, DMSO-*d*<sub>6</sub>) δ 10.68 (s, 1H), 8.30 (s, 1H), 2.73 (q, J = 7.4 Hz, 2H), 2.69 (s, 3H), 2.45 (s, 3H), 2.41 (q, J = 7.6 Hz, 2H), 2.37 (s, 3H), 2.35 (s, 0H), 1.10 – 0.96 (m, 6H). <sup>13</sup>C NMR (126 MHz, DMSO-*d*<sub>6</sub>) δ 156.10, 155.15, 141.44, 141.35, 139.25, 135.92, 133.94, 133.61, 132.82, 132.30, 131.89, 118.15, 115.50, 17.77, 17.01, 16.40, 14.62, 14.21, 14.05, 13.27, 12.46. <sup>19</sup>F NMR (471 MHz, DMSO-*d*<sub>6</sub>) δ -138.25, -138.31, -138.39, -138.45. HRMS (ESI<sup>+</sup>): *m/z*, calcd for C<sub>19</sub>H<sub>27</sub>BF<sub>2</sub>N<sub>5</sub>O [M + H]<sup>+</sup>: 390.2282; found: 390.2268. UV-Vis: λ<sub>max</sub> (DMSO)= 559 nm. Fluorescence emission (DMSO): λ<sub>max</sub>= 580 nm (λ<sub>exc</sub>= 450 nm), φ<sub>fl</sub>: 0.94, τ: 4.7 ns.

### **2.3. Sensing Experiments**

#### 2.3.1. NaGHB detection

In a 3 mL quartz cell (1 cm of path length), 2410 μL of DMSO were mixed with 90 μL of sensor from a 139 μM solution in DMSO. After that, increasing quantities of NaGHB were added from a 1.25 mM solution in DMSO until saturation point was reached.

#### 2.3.2. Interferents measurements (NaGHB)

In a 3 mL quartz cell (1 cm of path length), 90 μL of 139 μM solution of sensor in DMSO were mixed with each interferent (0.3% w/v citric acid, 0.01% w/v sodium ascorbate and 10% sucrose) and diluted until 2500 μL with DMSO.

#### 2.3.3. Real samples (NaGHB)

Initially, drinks were spiked in a 12 mM concentration of NaGHB. Next, an aliquot of 50 μL of each drink was mixed with 50 μL of NaHCO<sub>3</sub> (1 mM in H<sub>2</sub>O). 50 μL of this latter mixture were taken and added to a second mixture of 900 μL of DMSO and 50 μL of the



sensor (1 mM in DMSO). The whole process was carried out at room temperature and the described changes took place immediately.

#### 2.3.4. Copper complexation and cathinone detection

##### *2.3.4.1. Copper(II) titrations*

In a 3 mL quartz cell (1 cm of path length), 2410  $\mu\text{L}$  of MeCN were mixed with 90  $\mu\text{L}$  of sensor from a 139  $\mu\text{M}$  solution in MeCN. After that, increasing quantities of  $\text{Cu}(\text{OTf})_2$  were added from a 1.25 mM solution in MeCN until saturation point was reached.

##### *2.3.4.2. Copper(I) titrations*

In a 3 mL quartz cell (1 cm of path length), 2220  $\mu\text{L}$  of DMSO were mixed with 100  $\mu\text{L}$  of ultra pure water and 180  $\mu\text{L}$  of sensor from a 139  $\mu\text{M}$  solution in DMSO. After that, increasing quantities of CuBr were added from a 2.5 mM solution in DMSO, with a 3-min period of incubation after each addition, until arriving to saturation point.

#### 2.3.5. Cathinone titrations

In a 3 mL quartz cell (1 cm of path length), 2220  $\mu\text{L}$  of DMSO were mixed with 100  $\mu\text{L}$  of ultra pure water  $\text{H}_2\text{O}$ , 180  $\mu\text{L}$  of sensor from a 139  $\mu\text{M}$  solution in DMSO and 80  $\mu\text{L}$  of  $\text{Cu}(\text{OTf})_2$  from a 1.25 mM solution in DMSO. After that, increasing quantities of ephedrone were added from a 2.5 mM solution in ultra pure water, with a 5-min period of incubation after each addition, until arriving to saturation point.

#### 2.3.6. Interferents measurements (SCs)

In a 3 mL quartz cell (1 cm of path of length), 2220  $\mu\text{L}$  of DMSO were mixed with 100  $\mu\text{L}$  of ultra pure water, 180  $\mu\text{L}$  of sensor from a 139  $\mu\text{M}$  solution in DMSO and 80  $\mu\text{L}$  of  $\text{Cu}(\text{OTf})_2$  from a 1.25 mM solution in DMSO. After that, 1 equiv. of ephedrone, NaGHB, SCs or other abuse drugs were added, with a 5-min period of incubation after each addition.

### 2.3.7. Computational methods

The geometrical optimization of compounds **1** and **2** together with their deprotonated counterparts at the *meso* (**1m** and **2m**) and hydrazone NH positions (**1n** and **2n**) starting from different conformations for their hydrazone side-chain (-**conf<sub>x</sub>**, where x is the conformation number) have been carried out using Gaussian16 rev. A03 program package [19] with the hybrid M062X functional of Truhlar and Zhao [20] using the split-valence triple- $\zeta$  6-311+G(2d,2p) basis set [21-31]. At those conformations of compound **1** where a 1,4-*syn*-periplanar arrangement of nitrogen atoms of its side-chain is able to coordinate Cu(I) cation (-**cu**), the optimization has been carried out using Ahlrichs and coworkers DEF2TZVP basis set [32,33] over the metal centre. To take into account the effect of the solvent, DMSO, SMD solvation model was used [34]. Frequency calculations were performed over optimized structures to properly characterize minima structures (no imaginary frequencies).

To explore the electronic transitions responsible for the UV-vis spectra, vertical excitation energies were computed over M062X/6-311+G(2d,2p)/SMD(DMSO) (DEF2TZVP over Cu(I) when present) geometries through single-point TD-DFT [35,36] calculations (15 states, singlets only) in solution using non-equilibrium formalism at the same theory level. From all the TD-DFT calculations submitted, GaussView [37] was used to visualize the results and generate the UV-vis plots using the excitation energies and the oscillator strength for each excited state.

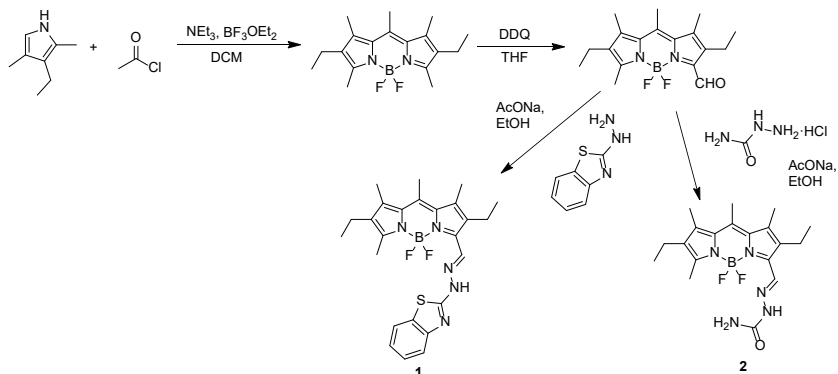
## **3. Results and discussion**

### **3.1. Synthesis and optical properties of BODIPY-probes**

Although there are several methods to synthesize BODIPYs [38], compounds **1** and **2** were synthesized as it is described in Scheme 1. In first place, 3-ethyl-2,4-dimethyl pyrrole was refluxed with acetyl chloride and TFA in DCM.  $\text{NEt}_3$  and  $\text{BF}_3\text{OEt}_2$  were added consecutively and, after purification, derivative **3** was isolated [30]. The synthesis of compound **4** was carried out through a selective oxidation of **3** using DDQ in THF at 0 °C. Finally, derivatives **1** and **2** were synthesized

Chapter 5: GHB and synthetic cathinones detection using BODIPY derivatives

using the appropriate hydrazine derivatives in the presence of AcONa in refluxing EtOH. The structures of compounds **1** and **2** were established by HRMS and  $^1\text{H}$ ,  $^{19}\text{F}$  and  $^{13}\text{C}$  NMR spectroscopy (see supporting information, Figures S1-S6).



Scheme 1. Synthetic pathway to prepare compounds **1** and **2**.

Once compounds **1** and **2** were obtained, their optical properties were studied in MeCN and DMSO ( $5\ \mu\text{M}$  both). Derivative **1** showed an absorption band centred at 584 nm and an emission band centred at 616 nm in DMSO ( $\lambda_{\text{ex}} = 500\ \text{nm}$ ). In this solvent, compound **1** presented a low intensity absorption band with maximum at 717 nm, most likely attributed to its deprotonated form. On the other hand, compound **2** exhibited an absorption band centred at 559 nm and an emission profile centred at 580 nm ( $\lambda_{\text{ex}} = 450\ \text{nm}$ ). The optical properties of both compounds studied in MeCN showed similar absorption and emission bands and, in any case, no significant solvatochromic effect was observed (see supporting information, Figures S7-S10). High quantum yields were determined and lifetimes were measured in both solvents. Results obtained in DMSO are summarized in Table 1 (see Table S1 for ones in MeCN), which agree with those found in literature [39].

Table 1. Absorption and emission maximums, quantum yields and lifetimes of compounds **1** and **2** in DMSO.

COMPOUND	$\lambda_{\text{abs}}$ (nm)	$\lambda_{\text{em}}$ (nm)	$\phi$	$\tau$ (ns)
<b>1</b>	584	616	0.39	2.5
<b>2</b>	559	580	0.94	4.7

### 3.2. Acid-base properties and GHB detection

The acid-base properties of compounds **1** and **2** were evaluated in DMSO solution with different bases: TBAOH, AcONa, DABCO and  $\text{NEt}_3$ . Neither DABCO nor  $\text{NEt}_3$  gave rise to significant modifications in absorption or fluorescence emission (see Figure S11). On the other hand, strong changes in colour and fluorescence emission were observed for compound **1** with TBAOH and AcONa, while compound **2** showed less intense ones. As can be seen in Figure S11, the lowest energy absorption band, corresponding to the BODIPY core, disappeared after the addition of 1 equiv. of TBAOH in the case of compound **1** and decreased significantly for compound **2**, being the effect on **1** stronger than in **2**. In addition to this effect, in the case of compound **1** the absorption band peaked at 717 nm increased in intensity, whilst for compound **2** a new band appeared at lower wavelength (355 nm). A strong quenching of fluorescence was observed for both probes upon the base addition (see Figure S12).

These results indicated that whereas the anion generated from compound **1** led to an enhancement of the conjugation of the BODIPY core, resulting in a bathochromic shift of the main absorption band, that originated from compound **2** disrupted this conjugation, since an hypsochromic effect was observed. This opposite behaviour suggested that **1** underwent a deprotonation at the hydrazone NH, giving rise to an increase in the electronic delocalization of the molecule, whereas **2** was deprotonated at the methyl group at the *meso* position of the BODIPY (Figure 2), thereby justifying the loss of conjugation.

Chapter 5: GHB and synthetic cathinones detection using BODIPY derivatives

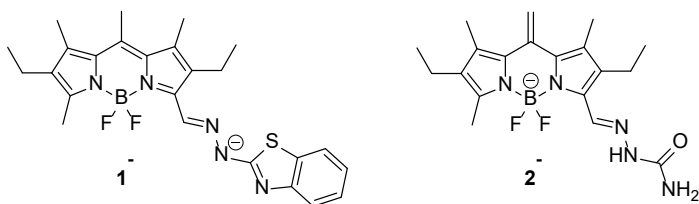


Figure 2. Proposed anions generated by probes **1** and **2** in presence of TBAOH.

This hypothesis was tested using both experimental and theoretical data. Thus, NMR spectra were registered for both probes with and without the presence of 1 equiv. of TBAOH. When the base is placed with compound **2**, several changes were observed in both  $^1\text{H}$  and  $^{13}\text{C}$  NMR spectra: (a) only three signals (2.20, 2.13 and 2.10 ppm) of the methyl groups directly bond to the BODIPY core appeared instead of the four signals of the initial compound, (b) a couple of peaks at 5.05 ppm corresponding to two olefinic hydrogens appeared and (c) a signal around 101 ppm in the  $^{13}\text{C}$  NMR spectrum corresponding to an olefinic carbon appeared (see Figures 3 and S13), which clearly accords with the anion structure proposed in Figure 2.

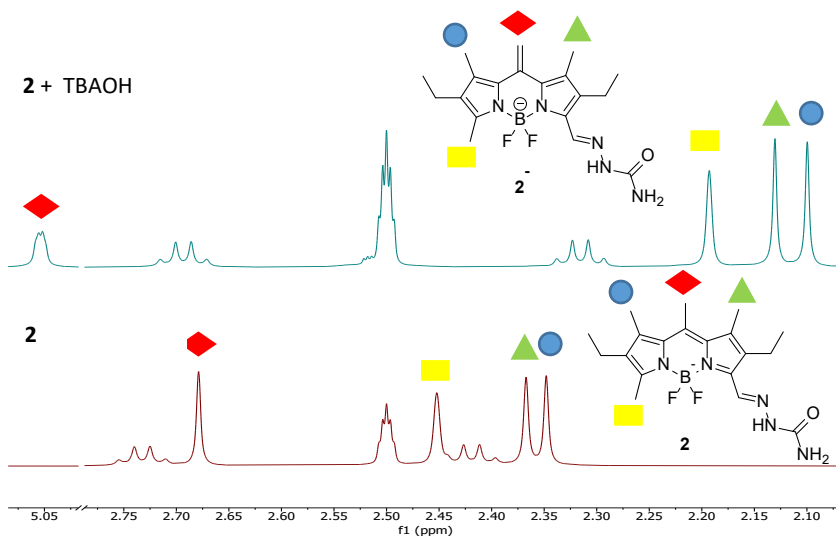


Figure 3. Changes observed in  $^1\text{H}$  NMR spectra of compound **2** ( $\text{DMSO}-d_6$ ) upon the addition of 1 equiv. of TBAOH (showed from 5.10 to 2.0 ppm).

By contrast, in the case of compound **1**, the greatest portion of deprotonation took place at the NH of the hydrazone group since the signal around 12.66 ppm in the  $^1\text{H}$  NMR spectrum disappeared completely. At the same time, a small portion of compound **1** was also deprotonated at the *meso* position as a pair of peaks around 5.10 ppm were observed (see Figure S14).

To confirm these results, the acid-base properties of compounds **1** and **2** were studied through theoretical calculations, computing the  $\text{pK}_a$  of selected positions in both molecules in DMSO. Whereas in compound **2** the H in *meso* position was, by far, the most acidic one; in compound **1** there were two H with similar calculated acidity (Figure 4). The slightly most acidic one was the H from the NH of the hydrazone group, which was in agreement with NMR experiments and UV-vis spectra since the largest deprotonation in that position has been demonstrated by the complete disappearance of the NH peak in the  $^1\text{H}$  NMR spectrum and the bathochromic shift of the main band observed in UV-vis spectra. Experimental maximum absorption bands shifts were compared to theoretical ones (see Table S2).

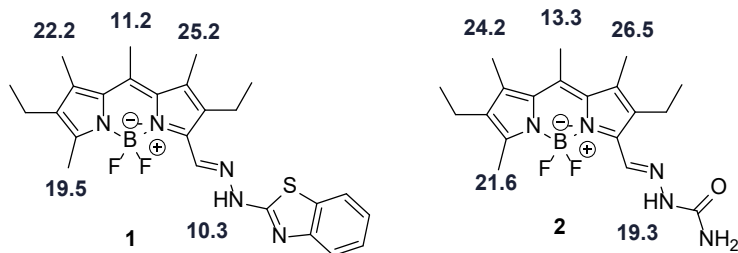


Figure 4. Calculated  $\text{pK}_a$  of selected positions at each BODIPY-derivative in DMSO

Next, the utility of the new probes in detecting NaGHB was explored. To do that, absorption and emission titrations using both compounds were carried out (see Figure 5 for absorption changes and Figure S15 for emission ones). As can be observed in Figure 5A, addition of increasing amounts of NaGHB to a 5  $\mu\text{M}$  DMSO solution of compound **1** induced a linear decrease of the absorption band at 584 nm with a concomitant increase in the band at 717 nm. The increase of this band is responsible for the colour change observed in the solution

(from purple to green). In the case of compound **2**, the decrease of the band at 559 nm was observed with the simultaneous increase of the band at 355 nm, with its corresponding colour disappearance.

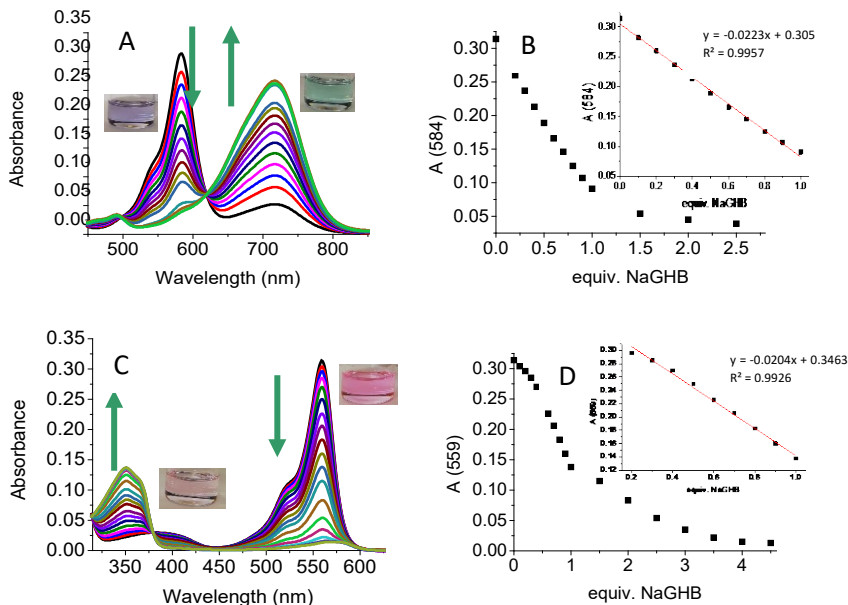


Figure 5. A) Absorption changes observed in probe **1** (5 μM in DMSO) with increasing amounts of NaGHB (0 – 2.5 equiv.). B) Changes in absorbance at 584 nm of probe **1** upon the addition of increasing amounts of NaGHB and its linear regression. C) UV-Visible spectra changes observed for compound **2** (5 μM in DMSO) with increasing amounts of NaGHB (0 – 4.5 equiv.).

D) Absorption changes at 559 nm of compound **2** upon the addition of increasing amounts of NaGHB and its linear regression.

From the titration experiments carried out, the limits of detection (LoD) could be determined, using the expression:  $LoD = \frac{3 \cdot S_b}{m}$ , where  $S_b$  is the blank standard deviation and  $m$  the slope. The values obtained were 0.4 μM for compound **1** and 0.3 μM for compound **2**. It should be noted that these values are considerably lower than the amount of GHB necessary to induce severe effects (50 mg·kg<sup>-1</sup>), which is around 75 mM (assuming an average weight of 62 kg in a standard volume of 330 mL) [40].

Aiming at exploring the possible usability of the sensor in beverages, several interferences present in these media (citric acid, sodium ascorbate and sucrose at their usual concentration in drinks were analysed in presence and absence of NaGHB (see Figure S16 for absorption changes for compounds **1** and **2** and Figure S17 for fluorescence changes). No significant absorption changes were observed in any case, after the addition of the interferences, and both compounds were still capable of detecting NaGHB in a much lower concentration than that usually used in a recreational environment [40].

With these promising results in mind, we decided to test compounds **1** and **2** in real samples, in order to ensure their use to detect GHB in drinks. For this reason, some soft drinks were spiked with NaGHB (12 mM). An aliquot of each one was slightly neutralised with NaHCO<sub>3</sub> and mixed with the sensor (100 μM in DMSO). The changes in the emission intensity were immediately observed at room temperature under a common UV lamp. Results for compound **1** are shown in Figure 6. Those for compound **2** are summarised in supporting information (Figure S18).



Figure 6. Changes in emission of probe **1** in the presence of NaGHB in soft drinks. Notice that left vial means non-spiked drink, whilst the right vial stands for the spiked ones.

### 3.3. Copper complexation and cathinone detection

Going a step further, the utility of the new probes in detecting SCs was explored. First, studies of Cu(II) and Cu(I) complexation with ligands **1** and **2** in different solvents were carried out (see Figures S19-S20 in supporting information for the studies carried out in MeCN). These studies showed that whereas compound **2** did not exhibit any interaction with either Cu(II) or Cu(I) in DMSO, compound **1** showed different behaviour depending on the cation. Thus, Cu(II)



gave rise to little changes, especially in absorbance, whereas Cu(I) induced notable changes in both the absorption and the emission spectra of compound **1** (see Figure S21). A bathochromic shift of the absorption band from 584 nm to 632 nm as well as a fluorescence emission quenching was observed for **1** in the presence of an excess of Cu(I) (Figure 7). This different behaviour could be used to detect cathinones since it has been described in the literature that these compounds are suitable reducing agents for Cu(II) [15]. In a first stage, complexation of compound **1** with Cu(I) was carefully studied. Thus, we carried out titration experiments with increasing amounts of Cu(I), observing the formation of a 1:1 complex, whose association constant was determined as  $9.22 \cdot 10^4 \text{ M}^{-1}$  [41]. The starting point of the titration (black line) showed a less intense absorption of the band centred at 717 nm most likely due to the presence of some water.

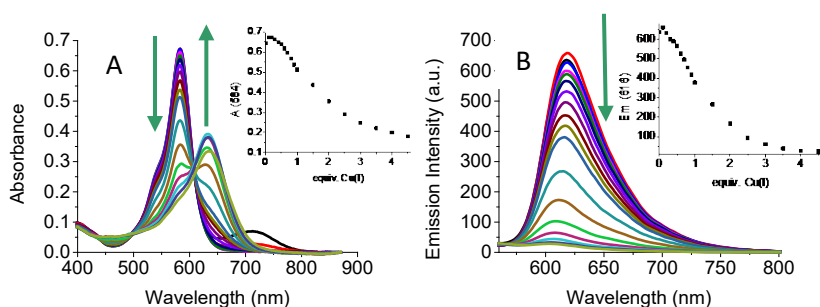


Figure 7. A) Absorption and (B) emission ( $\lambda_{\text{ex}} = 500 \text{ nm}$ ) changes observed for compound **1** ( $10 \mu\text{M}$  in DMSO:H<sub>2</sub>O 96:4) after the addition of increasing quantities of CuBr (0 – 4.5 equiv.) and their reaction profiles at 584 nm and 616 nm, respectively (insets).

Since different results were obtained during the complexation studies of Cu(II) and Cu(I) in DMSO, we decided to explore the detection of ephedrone through the reduction of a salt of Cu(II) in the presence of probe **1**. To do so, sensing conditions were optimized and the measurements were carried out using  $10 \mu\text{M}$  of compound **1**, 4 equiv. of Cu(OTf)<sub>2</sub>, a mixture of DMSO:H<sub>2</sub>O 96:4 as solvent and an incubation period of 5 min.

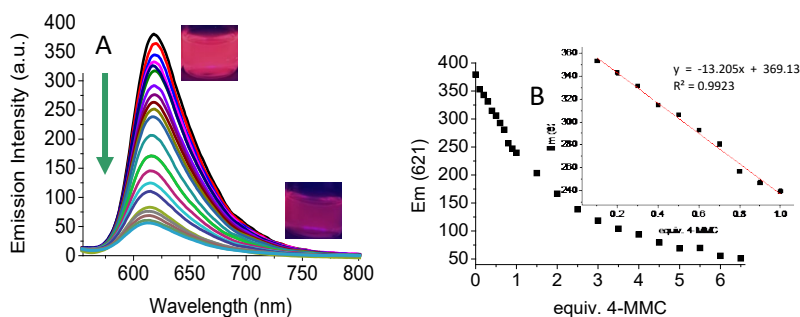


Figure 8. A) Emission changes observed for probe **1** (10  $\mu$ M in DMSO:H<sub>2</sub>O 96:4, 4 equiv. of Cu(OTf)<sub>2</sub>,  $\lambda_{\text{ex}}$  = 500 nm) with increasing quantities of ephedrone (0 – 6.5 equiv.). B) Changes in fluorescence for probe **1** (10  $\mu$ M in DMSO:H<sub>2</sub>O 96:4, 4 equiv. of Cu(OTf)<sub>2</sub>,  $\lambda_{\text{exc}}$  = 500 nm) upon the addition of increasing amounts of ephedrone (0 – 6.5 equiv.).

As can be observed in Figure 8, the addition of increasing amounts of ephedrone to a mixture of compound **1** and Cu(II) resulted in a progressive fluorescence emission quenching of **1**. From the titration results (Figure 8B), a LoD of 2.0  $\mu$ M was found (see Figure S22 for absorption titration results). Since a potential application of this probe could be the identification of SCs in seized materials, the visual observation of the fluorescence quenching under a simple and portable UV-lamp would allow the enforcement officers in few minutes to discover whether or not those substances are SCs.

To verify whether the mixture of compound **1** and Cu(II) was a useful sensor for the detection of other cathinones, the behaviour of several SCs such as: 3,4-MDPHP, MPPH and MDMC was studied under the previous experimental conditions. Emission changes are shown in Figure 9 (see Figure S23 for absorption changes).

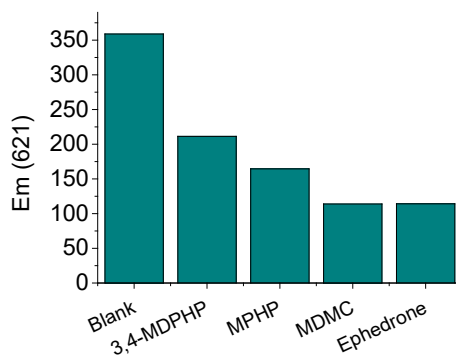


Figure 9. Emission changes for probe **1** at 621 nm (10  $\mu$ M in DMSO:H<sub>2</sub>O 96:4, 4 equiv. of Cu(OTf)<sub>2</sub>,  $\lambda_{ex}$  = 500 nm) upon the addition of 2 equiv. of SCs.

As can be seen, the response promoted by the presence of 2 equiv. of ephedrone is similar to the rest of SCs, highlighting the potential application of compound **1** to detect any SCs. It is also noteworthy that, regardless of the type of substitution present in cathinone core as well as the type of amine (primary, secondary or tertiary) they present, these SCs are able to reduce Cu(II) to Cu(I) and the subsequent Cu(I) formed can be detected by probe **1**.

As compound **1** was able to recognize separately GHB and cathinone, we tried to detect GHB using the new established conditions, i.e. in the presence of Cu(II) and a mixture of 96:4 of DMSO:H<sub>2</sub>O. Satisfactory results were obtained since compound **1** demonstrated that was capable not only of detecting NaGHB alone, but also when both drugs were simultaneously present (absorption and emission changes are summarised in Figure S24). These results highlighted that the presence of Cu(II) did not affect the NaGHB detection and extends the scope of the prepared sensor.

Finally, other abuse drugs such as benzodiazepines, scopolamine and ketamine were tested as potential interferents (Figures 10 and S25). No remarkable changes were observed in the presence of any of them. Only the mixture of NaGHB and ephedrone gave rise to a significant response, even in the presence of the other drugs.

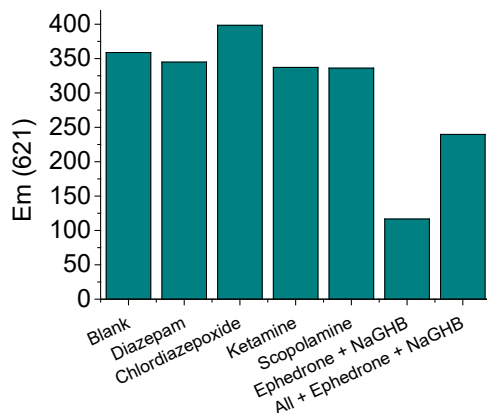


Figure 10. Fluorescence spectra changes of probe **1** at 621 nm (10  $\mu\text{M}$  in DMSO:H<sub>2</sub>O 96:4, 4 equiv. of Cu(OTf)<sub>2</sub>,  $\lambda_{\text{ex}}$  = 500 nm) upon the addition of 1 equiv. of other abuse drugs.

#### 4. Conclusions

Two novel compounds (**1** and **2**) based on a BODIPY-hydrazone core have been prepared and their photophysical properties studied in two different solvents: DMSO and MeCN. The acid-base properties of both compounds were evaluated by spectroscopic techniques and the observed results corroborated by theoretical calculations. These probes can be used to detect NaGHB through an acid-base reaction. In presence of this drug, both probes showed a significant quenching fluorescence that can be easily observed under a laboratory UV lamp or with the typical light in pubs or discos and a change of colour that can be appreciated with naked-eye. The LoD determined were 0.4  $\mu\text{M}$  for compound **1** and 0.3  $\mu\text{M}$  for compound **2**, making them suitable to point out the presence of GHB in spiked drinks. Additionally, the different complexation behaviour of compound **1** toward Cu(I) and Cu(II) salts in DMSO makes it suitable to detect SCs. The sensing mechanism in this case is based on the capability of cathinones to reduce Cu(II) to Cu(I). The limit of detection determined was 2.0  $\mu\text{M}$ . In this case, the detection of SCs could be focused on the identification of seized materials, since the quenching of the fluorescence is readily noticed using a laboratory UV lamp. Finally, the mixture of **1** and Cu(II) is also capable to detect SCs NaGHB simultaneously.

## Acknowledgements

Grant RTI2018-100910-B-C42 funded by MCIN/AEI/10.13039/501100011033 and, by “ERDF A way of making Europe”, Project 2020I040 PNSD 2020, funded by the Spanish Ministry of Health, Consumer Affairs and Social Welfare and grant INNVA2/2021/2, funded by Generalitat Valenciana (AVI) and “ERDF A way of making Europe” are gratefully acknowledged. SCSIE (Universitat de València) is gratefully acknowledged for all the equipment employed. NMR was registered at the U26 facility of ICTS “NANBIOSIS” at the Universitat of València. The computational resources from the SIUV (Servei d’Informàtica, Universitat de València) are gratefully acknowledged. S. R-N. is grateful to the Spanish Government for a fellowship.

**Conflicts of Interest:** The authors declare no conflict of interest. The funders had no role in the design of the study; in the collection, analyses, or interpretation of data; in the writing of the manuscript, or in the decision to publish the results.

## Appendix A. Supplementary data

### References

- [1] OECD/European Union (2020), “Illicit drug consumption among adults”, in Health at a Glance: Europe 2020: State of Health in the EU Cycle, OECD Publishing, Paris. <https://doi.org/10.1787/fc8a3fcf-en>
- [2] European Monitoring Centre for Drugs and Drug Addiction (2022), New psychoactive substances: 25 years of early warning and response in Europe. An update from the EU Early Warning System (June 2022), Publications Office of the European Union, Luxembourg.
- [3] A. Shafi, A.J. Berry, H. Sumnall, D.M. Wood, D.K. Tracy, New psychoactive substances: a review and updates, *Ther. Adv. Psychopharmacol.* 10 (2020) 1–21. <https://doi.org/10.1177/2045125320967197>

- [4] European Monitoring Centre for Drugs and Drug Addiction (2022), European Drug Report 2022: Trends and Developments, Publications Office of the European Union, Luxembourg.
- [5] F.P. Busardò, M.R. Vari, A. di Trana, S. Malaca, J. Carlier, N.M. di Luca, Drug-facilitated sexual assaults (DFSA): a serious underestimated issue, *Eur Rev Med Pharmacol Sci.* 23 (2019) 10577-10587. doi: 10.26355/eurrev\_201912\_19753.
- [6] 4 (a) W. Wang, Z.-Z. Dong, G. Yang, C.-H. Leung, S. Lin, D.-L. Ma, A long-lived iridium(III) chemosensor for the real-time detection of GHB, *J. Mat. Chem. B* 5 (2017) 2739-2742. <https://doi.org/10.1039/C6TB03396B>
- [7] M.J. Bennett B.S., R.R. Steiner M.S., Detection of Gamma-Hydroxybutyric Acid in Various Drink Matrices via AccuTOF-DART, *J. Forensic Sci.* 54 (2009) 370-375. <https://doi.org/10.1111/j.1556-4029.2008.00955.x>
- [8] K. S.Hagan, L. Reidy, Detection of synthetic cathinones in victims of sexual assault. *Forensic Sci. Int.* 257 (2015) 71-75. <https://doi.org/10.1016/j.forsciint.2015.07.040>
- [9] N. Anzar, S. Suleman, S. Parvez, J. Narang, A review on Illicit drugs and biosensing advances for its rapid detection, *Process Biochem.* 113 (2022) 113-124. <https://doi.org/10.1016/j.procbio.2021.12.021>
- [10] A.M. Costero, M. Parra, S. Gil, P. Gaviña, BODIPY Core as Signaling Unit in Chemosensor Design in: BODIPY Dyes - A Privilege Molecular Scaffold with Tunable Properties, J. Bañuelos-Prieto, R. Sola Llano (Eds.), IntechOpen (London), 2019, chapter 2. <https://doi.org/10.5772/intechopen.75220>
- [11] S. Rodríguez-Nuévalos, M. Parra; S. Gil; P. Gaviña; P. Arroyo; J.A. Sáez; A.M. Costero, Heteroditopic chemosensor for detecting  $\gamma$ -hydroxybutyric acid (GHB) in soft drinks and alcoholic beverages, *Analyst* 146 (2022) 5601-5609. <https://doi.org/10.1039/D1AN01084K>

- [12] S. Rodríguez-Nuévalos, A.M. Costero, S. Gil, M. Parra; P. Gaviña, Bifunctionalized gold nanoparticles for the colorimetric detection of the drug  $\gamma$ -hydroxybutyric acid (GHB) in beverages, *Chemosensors* 9 (2021) 160. <https://doi.org/10.3390/chemosensors9070160>
- [13] S. Rodríguez-Nuévalos, A.M. Costero, P. Arroyo, J.A. Sáez, M. Parra, F- Sancenón, R. Martínez-Mañez, Protection against chemical submission: naked-eye detection of  $\gamma$ -hydroxybutyric acid (GHB) in soft drinks and alcoholic beverages, *Chem. Commun.* 56 (2020) 12600-12603. <https://doi.org/10.1039/D0CC05387B>
- [14] V. Vrdoljak, G. Pavlovic, N. Maltar-Strmeckic, M. Cindric, Copper(II) hydrazone complexes with different nuclearities and geometries: synthetic methods and ligand substituent effects, *New J. Chem.* 40 (2016) 9263-9274. <https://doi.org/10.1039/C6NJ01036A>
- [15] M. Philp, R. Shimmon, M. Tahtouh, S. Fu, Development and validation of a presumptive color spot test method for the detection of synthetic cathinones in seized illicit materials, *Forensic Chem.* 1 (2016) 39-50. <https://doi.org/10.1016/j.forc.2016.06.001>
- [16] G.A. Crosby, J.N. Demas, Measurement of photoluminescence quantum yields. Review, *J. Phys. Chem.* 75 (1971) 991-1024. <https://doi.org/10.1021/j100678a001>
- [17] L. Yang, R. Simionescu, A. Lough, H. Yan, Some observations relating to the stability of the BODIPY fluorophore under acidic and basic conditions, *Dyes and Pigm.* 46 (2017) 264-267. <https://doi.org/10.1016/j.dyepig.2011.03.027>
- [18] X-F. Zhang, BisBODIPY as PCT-based halogen free photosensitizers for highly efficient excited triplet state and singlet oxygen formation: Tuning the efficiency by different linking positions, *Dyes Pigm.* 146 (2017) 491-501. <https://doi.org/10.1016/j.dyepig.2017.07.051>

[19] Gaussian 16, Revision A.03, M.J. Frisch, G.W. Trucks, H.B. Schlegel, G.E. Scuseria, M.A. Robb, J.R. Cheeseman, G. Scalmani, V. Barone, G.A. Petersson, H. Nakatsuji, X. Li, M. Caricato, A.V. Marenich, J. Bloino, B.G. Janesko, R. Gomperts, B. Mennucci, H.P. Hratchian, J.V. Ortiz, A.F. Izmaylov, J.L. Sonnenberg, D. Williams-Young, F. Ding, F. Lipparini, F. Egidi, J. Goings, B. Peng, A. Petrone, T. Henderson, D. Ranasinghe, V.G. Zakrzewski, J. Gao, N. Rega, G. Zheng, W. Liang, M. Hada, M. Ehara, K. Toyota, R. Fukuda, J. Hasegawa, M. Ishida, T. Nakajima, Y. Honda, O. Kitao, H. Nakai, T. Vreven, K. Throssell, J.A. Montgomery Jr.; J.E. Peralta, F. Ogliaro, M.J. Bearpark, J.J. Heyd, E.N. Brothers, K.N. Kudin, V.N. Staroverov, T.A. Keith, R. Kobayashi, J. Normand, K. Raghavachari, A.P. Rendell, J.C. Burant, S.S. Iyengar, J. Tomasi, M. Cossi, J.M. Millam, M. Klene, C. Adamo, R. Cammi, J.W. Ochterski, R.L. Martin, K. Morokuma, O. Farkas, J.B. Foresman, D.J. Fox, Gaussian, Inc., Wallingford CT, 2016.

[20] Y. Zhao, D. G. Truhlar, The M06 suite of density functionals for main group thermochemistry, thermochemical kinetics, noncovalent interactions, excited states, and transition elements: two new functionals and systematic testing of four M06-class functionals and 12 other functionals, *Theor. Chem. Acc.* 120 (2008) 215-241. DOI: 10.1007/s00214-007-0310-x.

[21] G.A. Petersson, A. Bennett, T.G. Tensfeldt, M.A. Al-Laham, W.A. Shirley, J. Mantzaris, A complete basis set model chemistry. I. The total energies of closed-shell atoms and hydrides of the first-row atoms, *J. Chem. Phys.* 89 (1988) 2193-2218. <https://doi.org/10.1063/1.455064>

[22] G.A. Petersson, M.A. Al-Laham, A complete basis set model chemistry. II. Open-shell systems and the total energies of the first-row atoms, *J. Chem. Phys.* 94 (1991) 6081-6090. <https://doi.org/10.1063/1.460447>



- [23] A.D. McLean, G.S. Chandler, Contracted Gaussian-basis sets for molecular calculations. I. Second row atoms, Z=11-18, J. Chem. Phys. 72 (1980) 5639-5648. <https://doi.org/10.1063/1.438980>
- [24] K. Raghavachari, J.S. Binkley, R. Seeger, J.A. Pople, Self-Consistent Molecular Orbital Methods. 20. Basis set for correlated wave-functions, J. Chem. Phys. 72 (1980) 650-654. <https://doi.org/10.1063/1.438955>
- [25] P. Blaudeau, M.P. McGrath, L.A. Curtiss, L. Radom, Extension of Gaussian-2 (G2) theory to molecules containing third-row atoms K and Ca, J. Chem. Phys. 107 (1997) 5016-5021. <https://doi.org/10.1063/1.474865>
- [26] A.J.H. Wachters, Gaussian basis set for molecular wavefunctions containing third-row atoms, J. Chem. Phys. 52 (1970) 1033. <https://doi.org/10.1063/1.1673095>
- [27] P.J. Hay, Gaussian basis sets for molecular calculations – representation of 3D orbitals in transition-metal atoms, J. Chem. Phys. 66 (1977) 4377-4384. <https://doi.org/10.1063/1.433731>
- [28] K. Raghavachari, G.W. Trucks, Highly correlated systems: Excitation energies of first row transition metals Sc-Cu, J. Chem. Phys. 91 (1989) 1062-1065. <https://doi.org/10.1063/1.457230>
- [29] R.C. Binning Jr., L. A. Curtiss, Compact contracted basis-sets for 3rd-row atoms – GA-KR, J. Comp. Chem. 11 (1990) 1206-1216. <https://doi.org/10.1002/jcc.540111013>
- [30] M.P. McGrath, L. Radom, Extension of Gaussian-1 (G1) theory to bromine-containing molecules, J. Chem. Phys., 94 (1991) 511-516. <https://doi.org/10.1063/1.460367>
- [31] L.A. Curtiss, M P. McGrath, J.-P. Blaudeau, N.E. Davis, R.C. Binning Jr., L. Radom, Extension of Gaussian-2 theory to molecules

containing third-row atoms Ga-Kr, *J. Chem. Phys.* 103 (1995) 6104-6113. <https://doi.org/10.1063/1.470438>

[32] F. Weigend, R. Ahlrichs, Balanced basis sets of split valence, triple zeta valence and quadruple zeta valence quality for H to Rn: Design and assessment of accuracy, *Phys. Chem. Chem. Phys.* 7 (2005) 3297-3305. <https://doi.org/10.1039/B508541A>

[33] F. Weigend, Accurate Coulomb-fitting basis sets for H to Rn, *Phys. Chem. Chem. Phys.* 8 (2006) 1057-1065. <https://doi.org/10.1039/B515623H>

[34] A.V. Marenich, C.J. Cramer, D.G. Truhlar, Universal solvation model based on solute electron density and a continuum model of the solvent defined by the bulk dielectric constant and atomic surface tensions, *J. Phys. Chem. B*, 113 (2009) 6378-6396. <https://doi.org/10.1021/jp810292n>

[35] C. Adamo, D. Jacquemin, The calculations of excited-state properties with Time-Dependent Density Functional Theory, *Chem. Soc. Rev.* 42 (2013) 845-856. <https://doi.org/10.1039/C2CS35394F>

[36] A.D. Laurent, C. Adamo, D. Jacquemin, Dye chemistry with time-dependent density functional theory, *Phys. Chem. Chem. Phys.* 16 (2014) 14334-14356. <https://doi.org/10.1039/C3CP55336A>

[37] GaussView, Version 5, Roy Dennington, Todd Keith, and John Millam, Semichem Inc., Shawnee Mission, KS, 2009.

[38] N. Boens, B. Verbelen, M. J. Ortiz, L. Jiao, W. Dehaen, Synthesis of BODIPY dyes through postfunctionalization of the boron dipyrromethene core, *Coord. Chem. Rev.* 399 (2019), 213024. <https://doi.org/10.1016/j.ccr.2019.213024>.

[39] J. Bañuelos, BODIPY dye the most versatile fluorophore ever? *Chem. Rec.* 16 (2016) 335-348. <https://doi.org/10.1002/tcr.201500238>

*Chapter 5: GHB and synthetic cathinones detection using BODIPY derivatives*

[40] C. Huller, D. Thai, P. Jacob III, J. E. Dyer, GHB Urine Concentrations After Single-Dose Administration in Humans, *J. Anal. Toxicol.* 30 (2006) 360-364. <https://doi.org/10.1093/jat/30.6.360>

[41] B. Diaz de Greñu, Detection and discrimination of organic contaminants and metabolites of high environmental impact by means of fluorogenic probes, PhD Thesis, University of Burgos (Spain), 2014.



## Supplementary information

### Colorimetric and fluorescent hydrazone-BODIPY probes for the detection of $\gamma$ -hydroxybutyric acid (GHB) and cathinones

Silvia Rodríguez-Nuévalos<sup>a,b</sup>, Ana M. Costero<sup>a,b,c</sup>, Margarita Parra<sup>a,b,c</sup>, Salvador Gil<sup>a,b,c</sup>, Pau Arroyo<sup>a,b</sup>, Jose A. Sáez<sup>\*a,b</sup>, Pablo Gaviña<sup>\*a,b,c</sup>, Paola Ceroni<sup>d</sup>, Andrea Fermi<sup>d</sup>

<sup>a</sup>Instituto Interuniversitario de Investigación de Reconocimiento Molecular y Desarrollo Tecnológico (IDM). Universitat Politècnica de València, Universitat de València, Doctor Moliner 50, Burjassot, 46100, Valencia, Spain.

<sup>b</sup>Departamento de Química Orgánica, Universitat de València, Doctor Moliner 50, Burjassot, 46100, Valencia, Spain.

<sup>c</sup>CIBER de Bioingeniería, Biomateriales y Nanomedicina (CIBER-BBN) (Spain)

<sup>d</sup>Dipartimento di Chimica "G. Ciamician", Università di Bologna, Via Selmi, 2, 40126 Bologna (Italy)

\* Correspondence: pablo.gavina@uv.es; Tel.: +34 963543740,  
jose.a.saez@uv.es; Tel.: +34 963544202

(See XYZ cartesian coordinates of optimized structures in CD)



## NMR Characterization

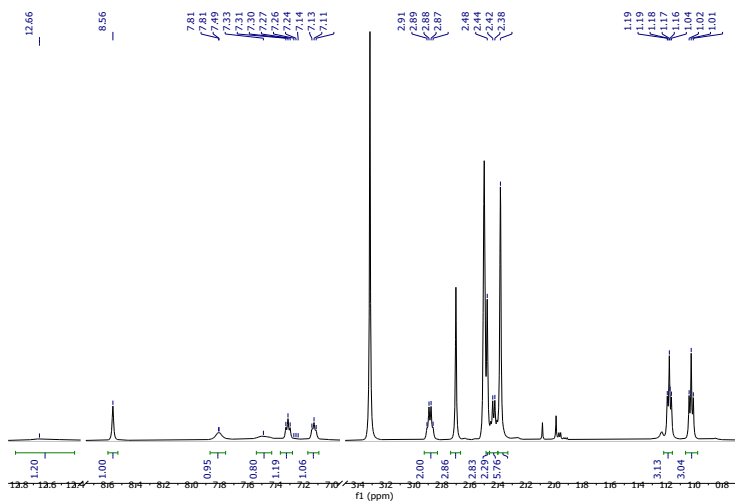


Figure S1. <sup>1</sup>H NMR spectrum of compound **1** in DMSO-*d*<sub>6</sub>.

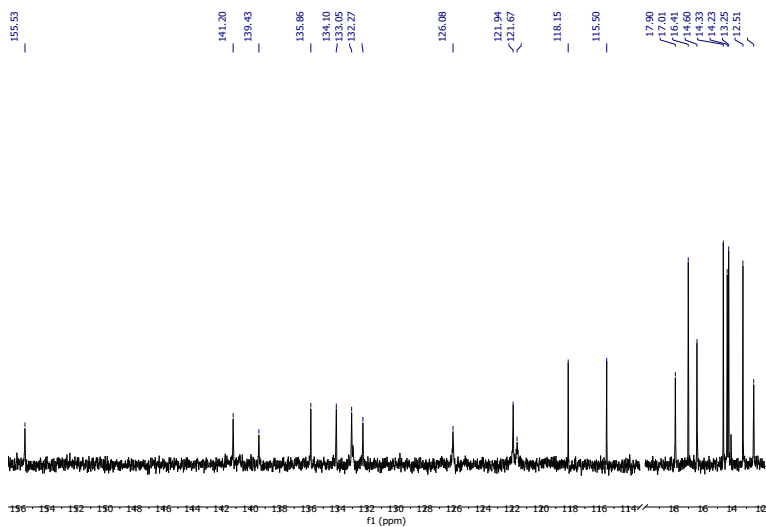


Figure S2. <sup>13</sup>C NMR spectrum of compound **1** in DMSO-*d*<sub>6</sub>.

Chapter 5: GHB and synthetic cathinones detection using BODIPY derivatives

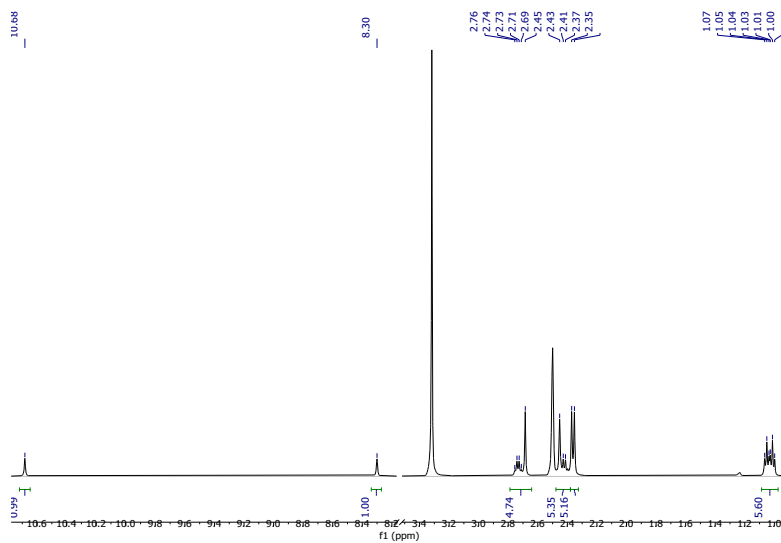


Figure S3.  $^1\text{H}$  NMR spectrum of compound **2** in  $\text{DMSO-}d_6$ .

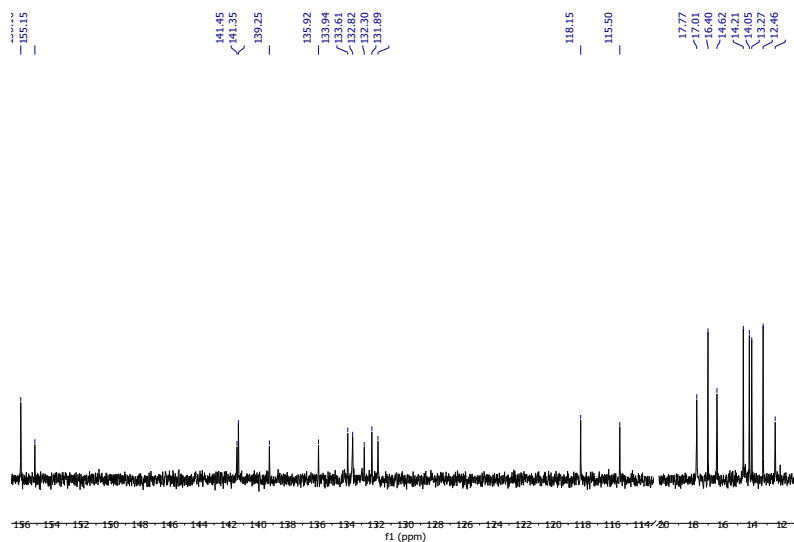


Figure S4.  $^{13}\text{C}$  NMR spectrum of compound **2** in  $\text{DMSO-}d_6$ .



## HRMS Characterization

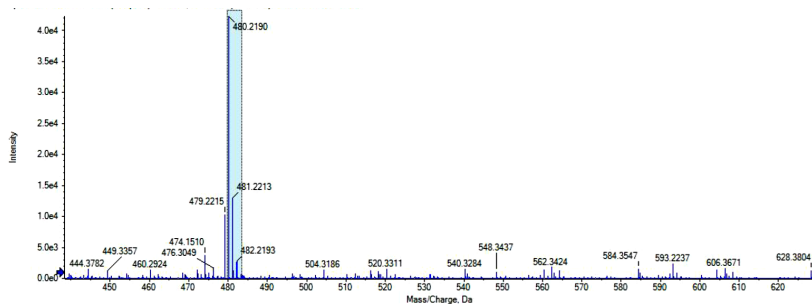


Figure S5. Mass Spectra of compound 1.

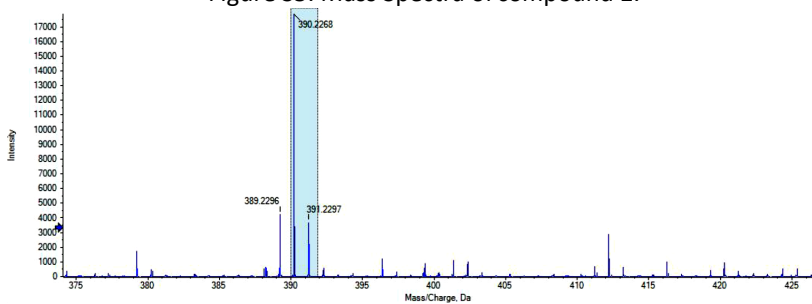


Figure S6. Mass Spectra of compound 2.

## Absorption and Fluorescence Characterization

Table S1. Absorption and emission maximums, quantum yields and lifetimes of compounds 1 and 2 in MeCN.

SOLVENT	MeCN				
	COMPOUND	$\lambda_{\text{abs}}$ (nm)	$\lambda_{\text{em}}$ (nm)	$\phi$	$\tau$ (ns)
	1	573	600	0.73	3.3
	2	552	573	0.96	5.6

Chapter 5: GHB and synthetic cathinones detection using BODIPY derivatives

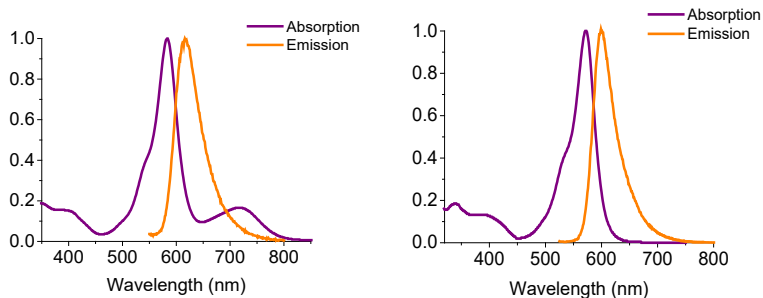


Figure S7. A) Normalized absorption and emission spectra of compound 1 in DMSO ( $\lambda_{\text{ex}} = 500$  nm). B) Normalized absorption and emission spectra of compound 1 in MeCN ( $\lambda_{\text{ex}} = 515$  nm).

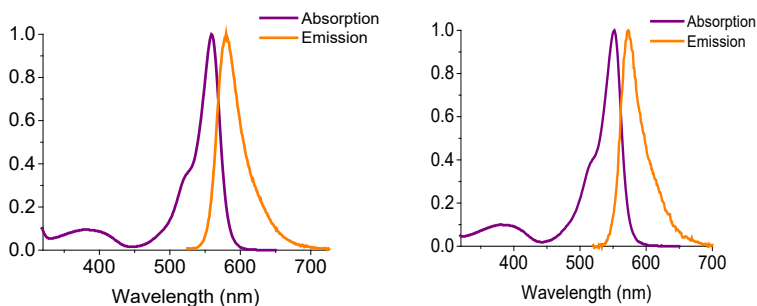


Figure S8. A) Normalized absorption and emission spectra of compound 2 in DMSO ( $\lambda_{\text{ex}} = 450$  nm). B) Normalized absorption and emission spectra of compound 2 in MeCN ( $\lambda_{\text{ex}} = 513$  nm).

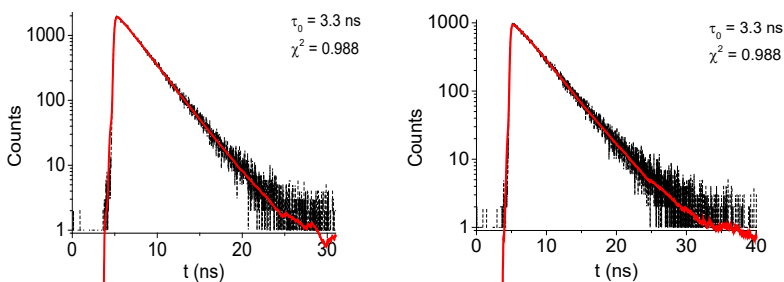


Figure S9. A) Fluorescence decay of compound 1 in DMSO at  $\lambda_{\text{em}} = 615$  nm. B) Fluorescence decay of compound 1 in MeCN at  $\lambda_{\text{em}} = 602$  nm.

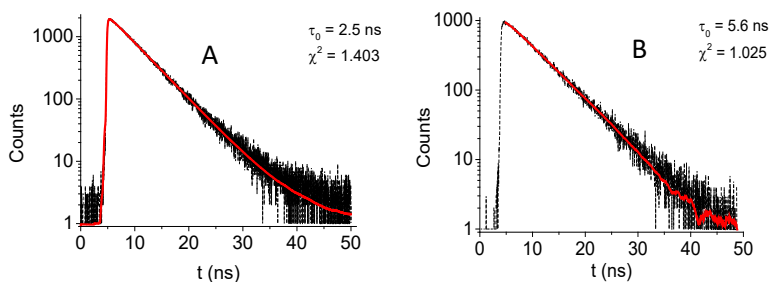


Figure S10. A) Fluorescence decay of compound **2** in DMSO at  $\lambda_{em} = 580$  nm. B) Fluorescence decay of compound **2** in MeCN at  $\lambda_{em} = 576$  nm.

### Acid-base properties and NaGHB detection

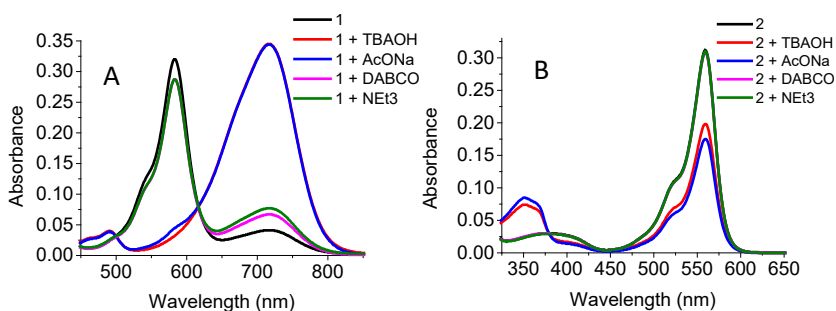


Figure S11. Absorption changes observed for (A) probe **1** (5  $\mu$ M in DMSO) and (B) probe **2** (5  $\mu$ M in DMSO) upon the addition of 2 equiv. of different bases.

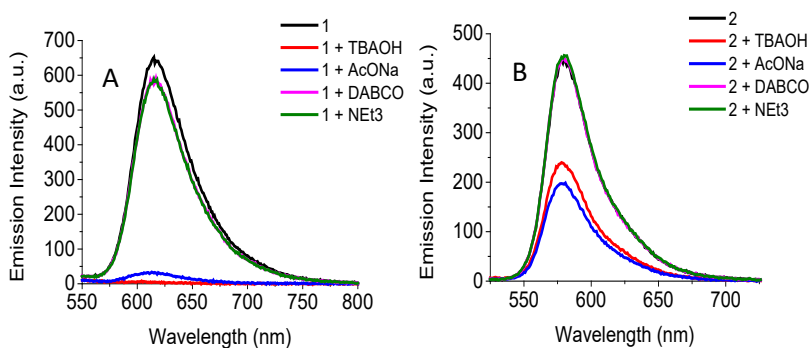
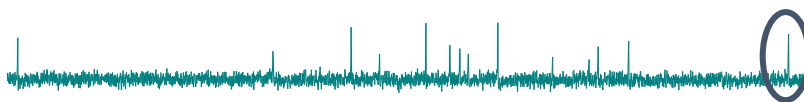


Figure S12. Emission changes observed for (A) probe **1** (5  $\mu$ M in DMSO,  $\lambda_{ex} = 500$  nm) and (B) probe **2** (5  $\mu$ M in DMSO,  $\lambda_{ex} = 450$  nm) upon the addition of 2 equiv. of different bases.

**2** + TBAOH



**2**

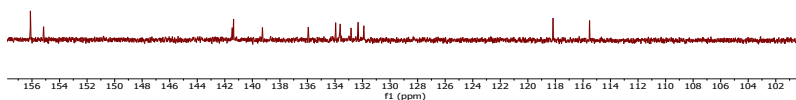
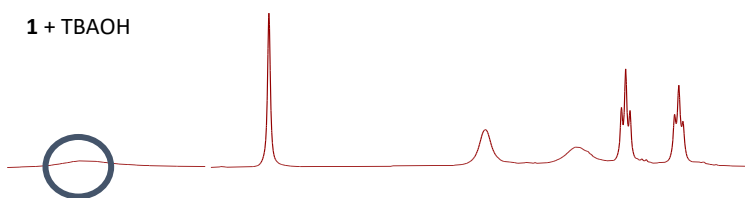


Figure S13. Changes observed in  $^{13}\text{C}$  NMR spectra of compound **2** ( $\text{DMSO-}d_6$ ) upon the addition of 1 equiv. of TBAOH.

**1** + TBAOH



**1**

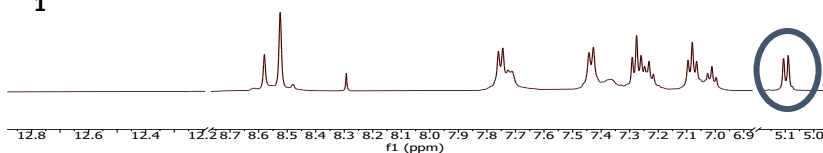


Figure S14. Changes observed in  $^1\text{H}$  NMR spectra of compound **1** ( $\text{DMSO-}d_6$ ) upon the addition of 1 equiv. of TBAOH.

Table S2. Comparison of experimental and theoretical shift maximum bands for compounds **1** and **2** upon the addition of 1 equiv. of TBAOH.

COMPOUND	Experimental Shift (nm)	Theoretical Shift(nm)
<b>1</b>	133	77
<b>2</b>	204	159

### NaGHB detection

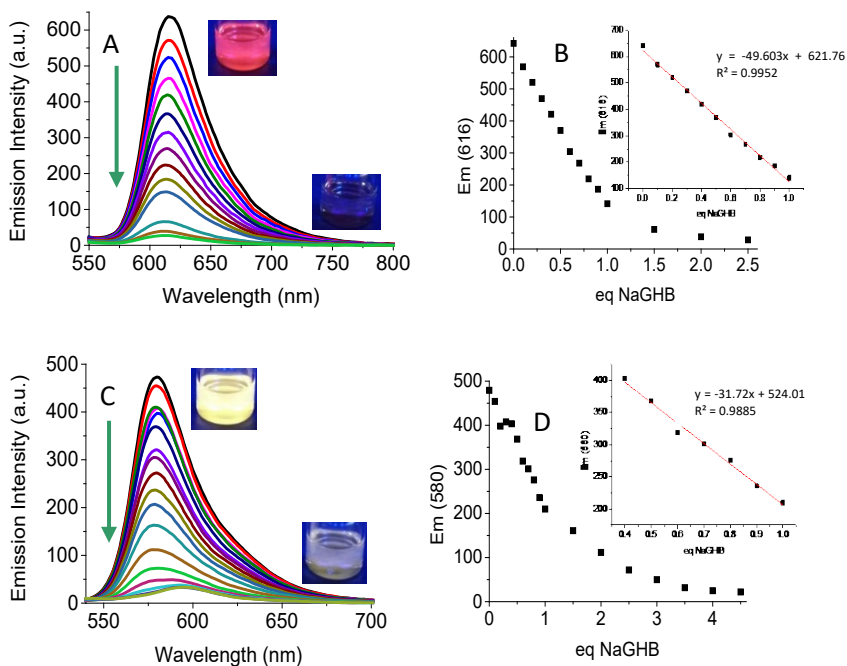


Figure S15. A) Fluorescence changes observed of probe 1 (5 μM in DMSO, λ<sub>ex</sub> = 500 nm) with increasing quantities of NaGHB (0 - 2.5 equiv.). B) Changes in fluorescence at 616 nm of probe 1 upon the addition of increasing amounts of NaGHB and its linear regression. C) Emission spectra changes observed for compound 2 (5 μM in DMSO, λ<sub>ex</sub> = 450 nm) with increasing quantities of NaGHB (0 - 4.5 equiv.). D) Emission changes at 580 nm of compound 2 upon the addition of increasing amounts of NaGHB and its linear regression.

### Interferents measurements (NaGHB)

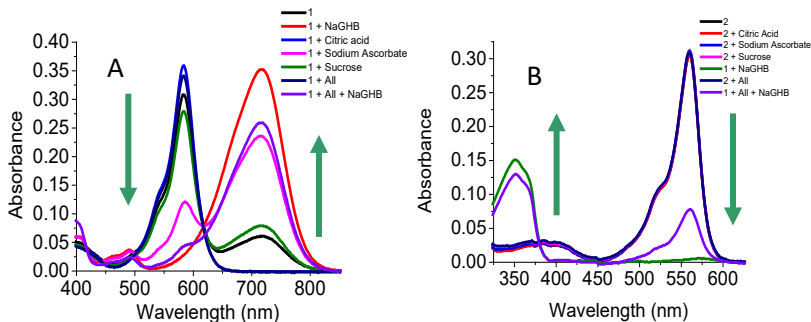


Figure S16. A) Absorption spectra of **1** (5 μM in DMSO) in the presence of citric acid, sodium ascorbate, sucrose (0.3%, 0.01% and 10% wt/v, respectively) and NaGHB (0.51 mM). B) Absorption spectra of **2** (5 μM in DMSO) in the presence of citric acid, sodium ascorbate, sucrose (0.3%, 0.01% and 10% wt/v, respectively) and NaGHB (0.51 mM).

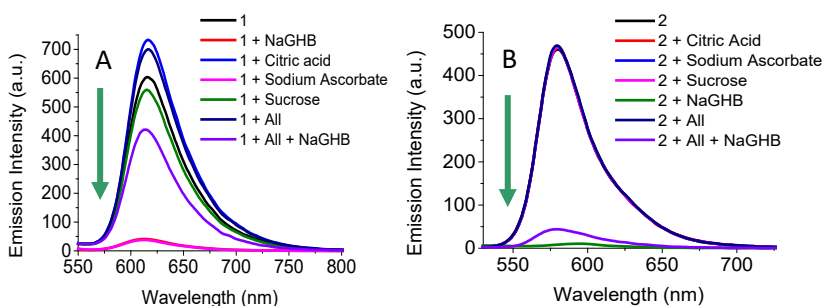


Figure S17. A) Emission spectra of **1** (5 μM in DMSO,  $\lambda_{ex} = 500$  nm) in the presence of citric acid, sodium ascorbate, sucrose (0.3%, 0.01% and 10% wt/v, respectively) and NaGHB (0.51 mM). B) Emission spectra of **2** (5 μM in DMSO,  $\lambda_{ex} = 450$  nm) in the presence of citric acid, sodium ascorbate, sucrose (0.3%, 0.01% and 10% wt/v, respectively) and NaGHB (0.51 mM).



Figure S18. Changes in emission of probe **2** in the presence of NaGHB in soft drinks. Please notice that left vial means non-spiked drink, whilst the right vial stands for the spiked ones.

## Copper complexation and cathinone detection

### Copper) studies

#### Copper(II) titrations

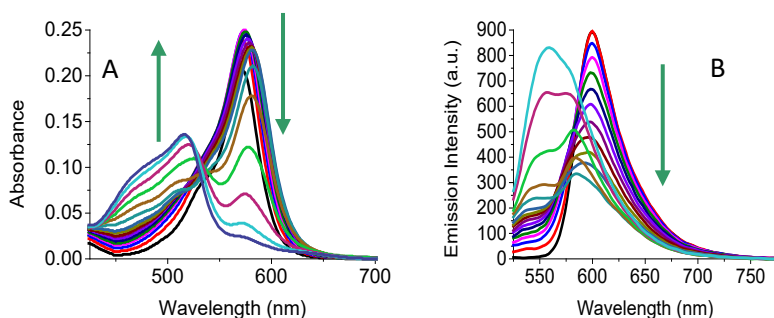


Figure S19. A) UV-Visible spectra changes of compound **1** ( $5 \mu\text{M}$  in MeCN) and (B) fluorescent spectra changes ( $5 \mu\text{M}$  in MeCN,  $\lambda_{\text{ex}} = 515 \text{ nm}$ ) upon the addition of increasing amounts of  $\text{Cu}(\text{OTf})_2$  (0 – 8 equiv.).

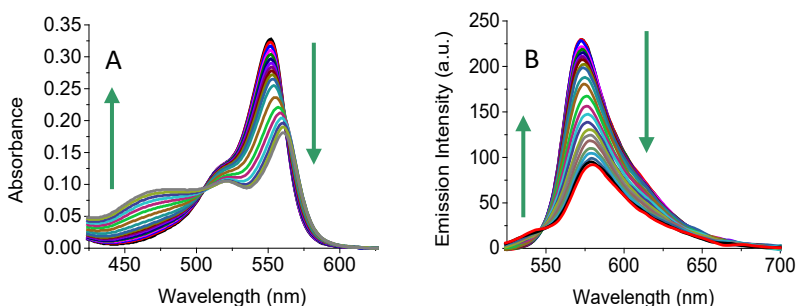


Figure S20. A) UV-Visible spectra changes of compound **2** ( $5 \mu\text{M}$  in MeCN) and (B) fluorescent spectra changes ( $5 \mu\text{M}$  in MeCN,  $\lambda_{\text{ex}} = 513 \text{ nm}$ ) upon the addition of increasing amounts of  $\text{Cu}(\text{OTf})_2$  (0 – 10 equiv.) of compound **2**.

Chapter 5: GHB and synthetic cathinones detection using BODIPY derivatives

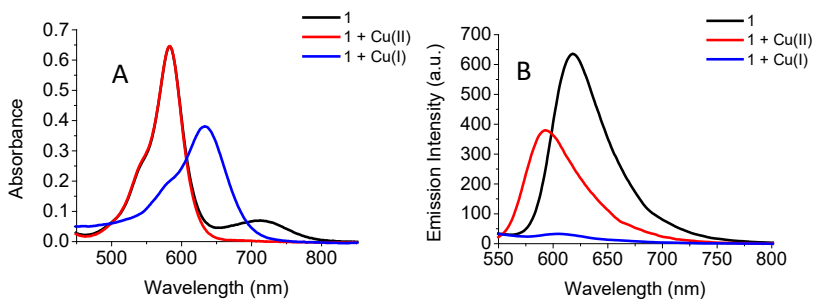


Figure S21. A) UV-Visible spectra changes of compound **1** (10  $\mu$ M in DMSO:H<sub>2</sub>O 96:4) and (B) fluorescent spectra changes ( $\lambda_{\text{ex}} = 500$  nm) upon the addition of 4 equiv. of Cu(OTf)<sub>2</sub> (red line) or 4 equiv. of CuBr (blue line).

Copper(I) titrations

Table S3. Comparison of experimental and theoretical shift maximum bands for compounds **1** and **2** upon the addition of Cu(I).

COMPOUND	Experimental Shift (nm)	Theoretical Shift (nm)
<b>1</b>	48	57

**Synthetic Cathinones detection**

Ephedrone titration

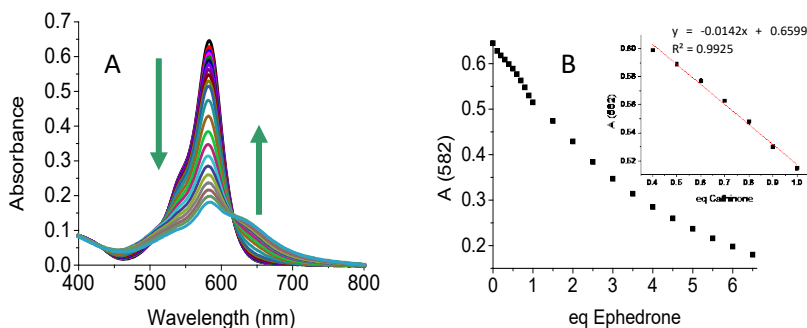


Figure S22. A) Absorption changes observed for probe **1** (10  $\mu$ M in DMSO:H<sub>2</sub>O 96:4, 4 equiv. of Cu(OTf)<sub>2</sub>) with increasing amounts of ephedrone (0 – 6.5 equiv.). B) Changes in absorbance at 582 nm for probe **1** (10  $\mu$ M in DMSO:H<sub>2</sub>O 96:4, 4 equiv. of Cu(OTf)<sub>2</sub>), upon the addition of increasing amounts of ephedrone (0 – 6.5 equiv.) and its linear regression.



Interferents measurements (SCs)

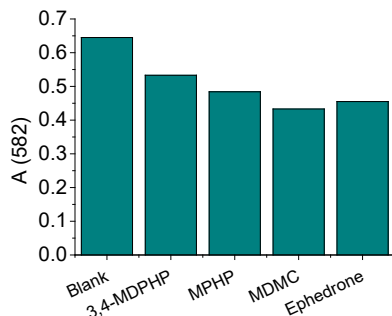


Figure S23. Absorption changes for probe **1** at 582 nm (10  $\mu$ M in DMSO:H<sub>2</sub>O 96:4, 4 equiv. of Cu(OTf)<sub>2</sub>,  $\lambda_{ex}$  = 500 nm) upon the addition of 2 equiv. of SCs.

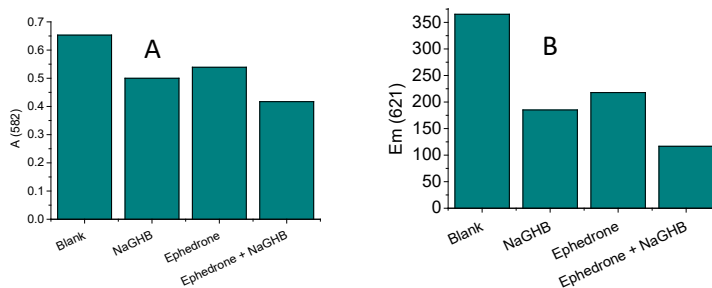


Figure S24. Absorption changes observed at 582 nm (A) and emission changes registered at 621 nm (B) for probe **1** (10  $\mu$ M in DMSO:H<sub>2</sub>O 96:4, 4 equiv. of Cu(OTf)<sub>2</sub>,  $\lambda_{ex}$  = 500 nm) upon the addition of 1 equiv. of ephedrone and NaGHB.

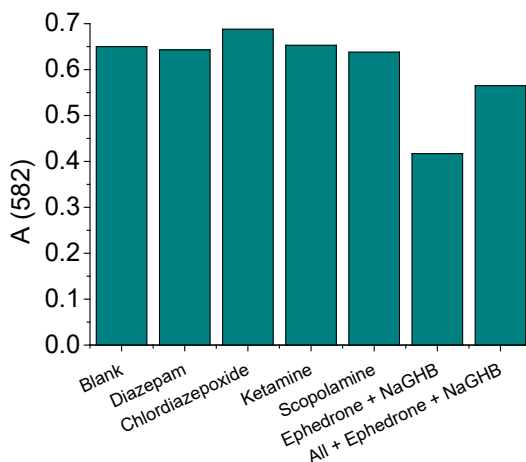


Figure S25. UV-Visible spectra changes for probe **1** at 582 nm (10  $\mu\text{M}$  in DMSO:H<sub>2</sub>O 96:4, 4 equiv. of Cu(OTf)<sub>2</sub>,  $\lambda_{\text{ex}}$  = 500 nm) upon the addition of 1 equiv. of other abuse drugs.

## Theoretical calculations

The following Supporting Information section contains the details of computational calculations performed in this work structured in these two subsections (the first one has its own bibliographic references included at the end):

- Computational methods. In this section, computational details about the geometrical optimizations, the vertical excitation energy analysis and pK<sub>a</sub> calculations are given.
- Optimized structures. XYZ cartesian coordinates of the optimized structures of the conformers of compounds **1** and **2** together with their deprotonated counterparts at M062X/6-311+G(2d,2p)/SMD(DMSO) level and XYZ cartesian coordinates of the optimized structures of the conformers of the complex formed between **1** and Cu(I) at M062X/6-311+G(2d,2p)/DEF2TZVP(Cu)/SMD(DMSO) level.

### Computational methods

The energy results of these calculations as well as the energy difference between them are depicted in Tables S4, S5 and S6.

Table S4. Energies ( $E$ , in hartrees) of the optimized conformations (-conf $x$ , where  $x$  is the conformation number) of **1** and its deprotonated counterparts at the meso (**1m**) and hydrazone NH (**1n**) positions together with their energy difference ( $\Delta E$ , in kcal/mol) at M062X/6-311+G(2d,2p)/SMD(DMSO) level.

Structure	Energy (hartree)	$\Delta E$ (kcal/mol)
<b>1-conf1</b>	-1866,08077522	8,3
<b>1-conf2</b>	-1866,08427163	6,1
<b>1-conf3</b>	-1866,07726000	10,5
<b>1-conf4</b>	-1866,08021700	8,7
<b>1-conf5</b>	-1866,09403021	0,0
<b>1-conf6<sup>a</sup></b>	-1866,08883106	3,3
<b>1-conf7</b>	-1866,08925002	3,0
<b>1-conf8<sup>a</sup></b>	-1866,08466000	5,9
<b>1m-conf1</b>	-1865,61167260	6,1
<b>1m-conf2</b>	-1865,61106567	6,5
<b>1m-conf3</b>	-1865,60770157	8,6
<b>1m-conf4</b>	-1865,60734271	8,8
<b>1m-conf5</b>	-1865,62142756	0,0
<b>1m-conf6<sup>a</sup></b>	-1865,61633345	3,2
<b>1m-conf7</b>	-1865,61680923	2,9
<b>1m-conf8<sup>a</sup></b>	-1865,61211719	5,8
<b>1n-conf1</b>	-1865,62184415	0,0
<b>1n-conf2</b>	-1865,60309344	11,8
<b>1n-conf3</b>	-1865,61462738	4,6
<b>1n-conf4<sup>a</sup></b>	-1865,60966668	7,7
<b>1n-conf5</b>	-1865,62188382	0,0
<b>1n-conf6<sup>a</sup></b>	-1865,61556246	4,0

Chapter 5: GHB and synthetic cathinones detection using BODIPY derivatives

<b>1n-conf7</b>	-1865,61463721	4,5
<b>1n-conf8<sup>a</sup></b>	-1865,60970002	7,6

<sup>a</sup> - these conformations show 1,4-*syn* periplanar arrangement of nitrogen atoms on its side-chain able to coordinate Cu(I) cation.

Table S5. Energies (E, in hartrees) of the optimized conformations (-confx, where x is the conformation number) of **2** and its deprotonated counterparts at the meso (**2m**) and hydrazone NH (**2n**) positions together with their energy difference ( $\Delta E$ , in kcal/mol) at M062X/6-311+G(2d,2p)/SMD(DMSO) level.

Structure	Energy (hartree)	$\Delta E$ (kcal/mol)
<b>2-conf1<sup>a</sup></b>	-1313,31765114	8,1
<b>2-conf2<sup>a</sup></b>	-1313,32826658	1,4
<b>2-conf3<sup>a</sup></b>	-1313,33050486	0,0
<b>2-conf4</b>	-1313,32044881	6,3
<b>2-conf5</b>	-1313,31650915	8,8
<b>2m-conf1<sup>a</sup></b>	-1312,84721937	6,2
<b>2m-conf2<sup>a</sup></b>	-1312,85495286	1,4
<b>2m-conf3<sup>a</sup></b>	-1312,85713778	0,0
<b>2m-conf4</b>	-1312,84632902	6,8
<b>2m-conf5</b>	-1312,84420630	8,1
<b>2n-conf1<sup>a</sup></b>	-1312,82217006	13,7
<b>2n-conf2<sup>a</sup></b>	-1312,84050069	2,2
<b>2n-conf3<sup>a</sup></b>	-1312,84405653	0,0
<b>2n-conf4<sup>a</sup></b>	-1312,82814738	10,0
<b>2n-conf5</b>	-1312,82261915	13,5

<sup>a</sup> - these conformations show 1,4-*syn* peryplanar arrangement of nitrogen atoms on its side-chain able to coordinate Cu(I) cation.

Table S6. Energies ( $E$ , in hartrees) of the optimized conformations (-conf $x$ -cu, where  $x$  is the conformation number) of the complex formed between **1** and Cu(I) and its deprotonated counterparts at the meso (**1m**) and hydrazone NH (**1n**) positions together with their energy difference ( $\Delta E$ , in kcal/mol) at M062X/6-311+G(2d,2p)/SMD(DMSO) level (DEF2TZVP basis set was used over Cu(I)).

Structure	Energy (hartree)	$\Delta E$ (kcal/mol)
<b>1-conf6-cu</b>	-3506,49049551	0,0
<b>1-conf8-cu</b>	-3506,49033288	0,1
<b>1m-conf6-cu</b>	-3506,02201578	1,5
<b>1m-conf8-cu</b>	-3506,02435975	0,0
<b>1n-conf4-cu</b>	-3506,02680089	0,9
<b>1n-conf6-cu</b>	-3506,02818815	0,0
<b>1n-conf8-cu</b>	-3506,02666646	1,0

Collection of the TD-DFT UV-Vis plots for absorbance values ranging from 300 to 800 nm for all the computed geometries ranging from the most stable ones until those 4.0 kcal/mol above in the energy scale are presented in Figures S26, S27 and S28 for compound **1** and its deprotonated counterparts and in Figures S29, S30 and S31 for compound **2** and its deprotonated counterparts.

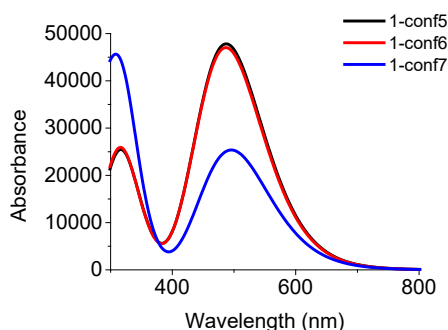


Figure S26. Single-point TDDFT M062X/6-311+(2d,2p)/SMD(DMSO) over the geometry optimized at the same theory level for compound **1**.

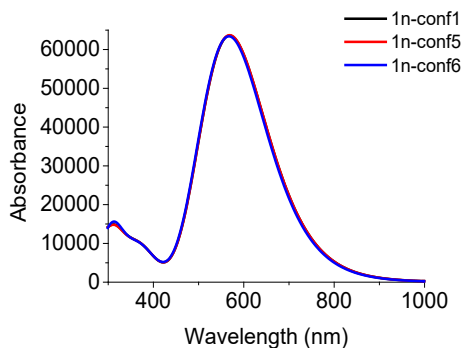


Figure S27. Single-point TDDFT M062X/6-311+(2d,2p)/SMD(DMSO) over the geometry optimized at the same theory level for compound **1n** (compound **1** deprotonated at the hydrazone NH position).

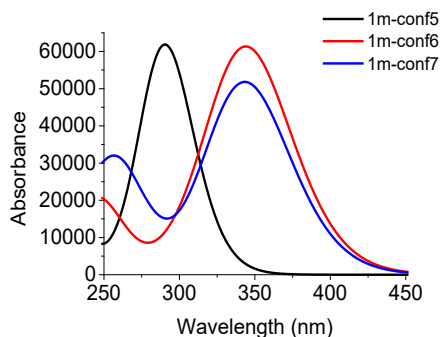


Figure S28. Single-point TDDFT M062X/6-311+(2d,2p)/SMD(DMSO) over the geometry optimized at the same theory level for compound **1m** (compound **1** deprotonated at the BODIPY meso position).

As can be seen, a bathochromic effect of *ca.* 90 nm in the UV-Vis spectra of compound **1** in presence of a base able to deprotonate the hydrazone NH hydrogen atom is predicted, which is in agreement with the experimental results. Deprotonation of the *meso* position in **1** leads to the disappearance of the band centred around 570 nm leaving a band centred around 350 nm which is already present in the initial compound.

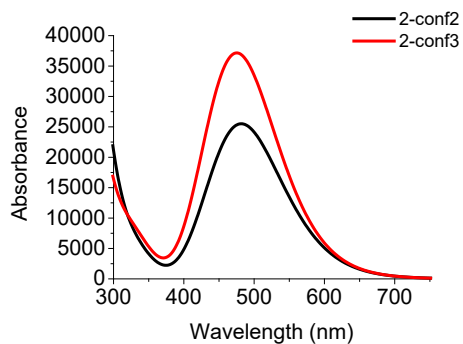


Figure S29. Single-point TDDFT M062X/6-311+(2d,2p)/SMD(DMSO) over the geometry optimized at the same theory level for compound **2**.

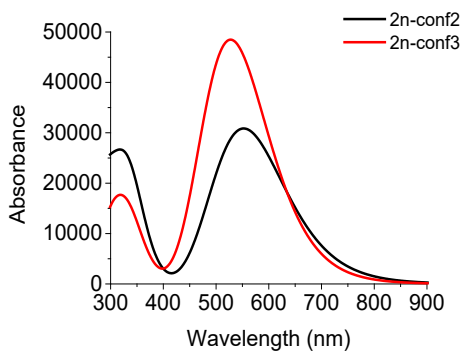


Figure S30. Single-point TDDFT M062X/6-311+(2d,2p)/SMD(DMSO) over the geometry optimized at the same theory level for compound **2n** (compound **2** deprotonated at the hydrazone NH position).

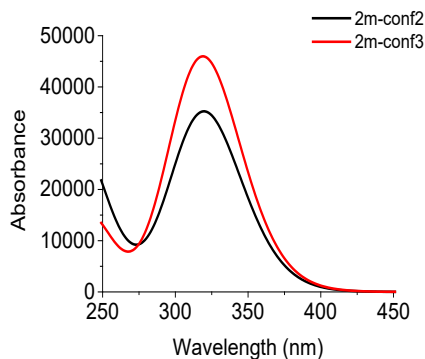


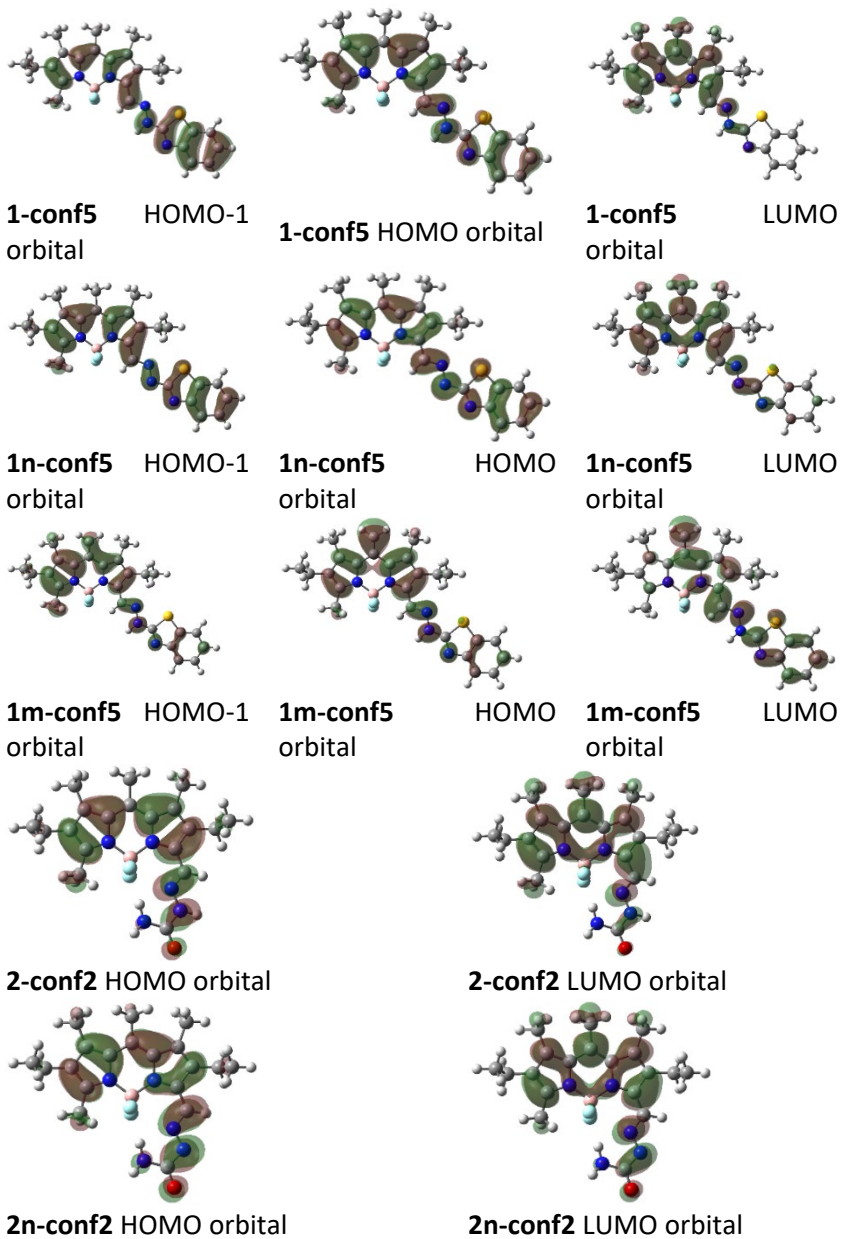
Figure S31. Single-point TDDFT M062X/6-311+(2d,2p)/SMD(DMSO) over the geometry optimized at the same theory level for compound **2m** (compound **2** deprotonated at the BODIPY meso position).

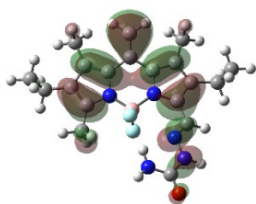
As can be seen, a bathochromic effect of *ca.* 75 nm in the UV-vis spectra of compound **2** in presence of a base able to deprotonate the hydrazone NH hydrogen atom is predicted, which is in agreement with the experimental results. Deprotonation of the *meso* position in **2** leads to the disappearance of the band centred around 550 nm leaving a band centred around 320 nm which is already present in the initial compound around 280 nm.

Anyway, in both **1** and **2** compounds, deprotonation of the most acidic hydrazone NH position leads to a bathochromic effect on the band centred around 480-500 nm and, in the case of the deprotonation over the *meso* position, the band disappears. Taking a look at the oscillator strengths and the molecular orbitals implied in main band regarding compounds **1** and **2**, those are HOMO-1, HOMO and LUMO in the case of compound **1** and HOMO and LUMO in the case of compound **2** (see Figure S32 where canonical orbitals with 0.02 isosurface value are presented).

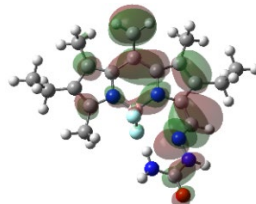


Chapter 5: GHB and synthetic cathinones detection using BODIPY derivatives





**2m-conf2** HOMO orbital



**2m-conf2** LUMO orbital

Figure S32. Canonical orbitals of compounds **1** and **2** and their deprotonated counterparts at the hydrazone NH and meso positions which are implied in the highest UV-Vis absorbance band of the TD-DFT simulated spectra each compound (0.02 isosurface value).

In the case of the complex of compound **1** with Cu(I) and its deprotonated counterparts in the hydrazone NH and *meso* positions, collection of the TD-DFT UV-visible plots for absorbance values ranging from 300 to 800 nm is presented in Figures S33, S34 and S35.

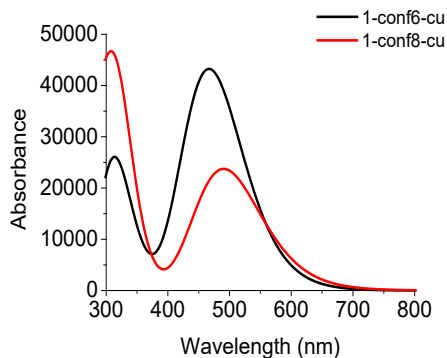


Figure S33. Single-point TDDFT M062X/6-311+(2d,2p)-DEF2TZVP/SMD(DMSO) over the geometry optimized at the same theory level for complex **1:Cu(I)**.

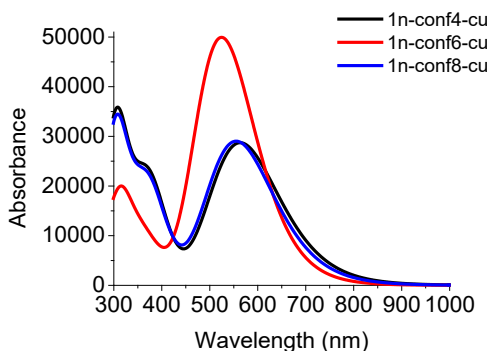


Figure S34. Single-point TDDFT M062X/6-311+(2d,2p)-DEF2TZVP/SMD(DMSO) over the geometry optimized at the same theory level for complex **1n:Cu(I)**.

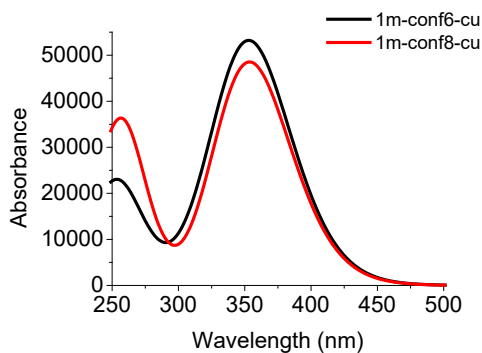


Figure S35. Single-point TDDFT M062X/6-311+(2d,2p)-DEF2TZVP/SMD(DMSO) over the geometry optimized at the same theory level for complex **1m:Cu(I)**.

As can be seen, there is no substantial change in the position of the band when comparing the UV-Vis absorption spectra of species **1m** and its **1m:Cu(I)** complex (see Figure S35) but a clear decrease of the intensity of the main UV-vis band around 500 nm respect the secondary one around 300 nm in both **1** and **1n** compounds is registered when these species form a complex with Cu(I) (see Figures S26 and S27).

To compute the  $pK_a$  value of several selected positions of compounds **1** and **2**, we reproduced the calculation scheme used by Ho *via* a thermodynamic cycle (MP2-TC) [1]. To do so, a previous systematic

conformational search was performed in both gas and solution phase to locate the global minimum energy structure of each species at the M062X/6-31+G(d) level using an ultrafine grid. Solution phase calculations were carried out in DMSO within the SMD solvation model using the default settings in Gaussian16. The corresponding thermal corrections to the Gibbs free energy were computed using a factor of 0.967 to scale the frequencies [2] and using the ideal gas molecular partition functions in conjunction with the rigid-rotor quasiharmonic oscillator (RR-QHO) approximation. In the QHO [3] approximation, vibrational frequencies that were lower than  $100\text{ cm}^{-1}$  were raised to  $100\text{ cm}^{-1}$  due to the breakdown of the harmonic oscillator model for low frequency vibrational modes. This was done with Goodvibes script [4] which, in addition, allowed to apply over the standard state calculations in Gaussian (1 atm and 298.15 K conditions), the appropriate corrections to ensure that all solutions phase  $\text{pK}_a$ s are computed at a standard state of 1 mol/L. Single-point calculations at (RO)MP2/GTMP2 Large theory level were performed on the M062X/6-31G+(d) optimized geometries. To compute the  $\text{pK}_a$  of each acid-base pair, we have employed the proton free energy  $\Delta G^*_s(\text{H}^+)$  of  $-273.3\text{ kcal/mol}$  [5], that is consistent with the parametrisation of the SMD model.

Finally,  $\text{pK}_a$  was computed through a thermodynamic cycle (TC) using this equation:  $\text{pK}_a = (\Delta G^*_{\text{soln}} / R \cdot T \cdot \ln(10))$

Where:  $\Delta G^*_{\text{soln}} = \Delta G^*_{\text{soln}}(\text{TC}) = \Delta E^L_{\text{soln}} + \Delta G^{\text{soln,L}}_{\text{corr}} + G^*_{\text{soln}}(\text{H}^+) + \Delta E^{\text{H}}_{\text{gas}} - \Delta E^L_{\text{gas}}$

And, also, where:  $\Delta E^X_Y = E^X_Y(\text{A}^-) - E^X_Y(\text{AH})$ ; in this equation, X superscript refers to (RO)MP2/GTMP2 Large energy when it equals to H (high level calculations) and to M062X/6-31+G(d) energy when it equals to L (low level calculations) and Y subscript refers to gas phase optimized geometry when it equals to "gas" or to solvent phase geometry when it equals to "soln".

And where:  $\Delta G^{\text{soln,L}}_{\text{corr}} = \Delta G^{\text{gas}}_{\text{corr}} - \Delta G^{\text{soln}}_{\text{corr}}$

Chapter 5: GHB and synthetic cathinones detection using BODIPY derivatives

The results of all these calculations are collected in the following Table S7.

Table S7. "Low level" M062X/6-31+G(d) and "high level" M062X/6-31+G(d)/gas phase//((RO)MP2/GTMP2Large calculation results over compounds **1** and **2** and the corresponding deprotonated species at selected positions.

Structure	$E_{\text{soln}}^L$ (hartree)	$E_{\text{gas}}^H$ (hartree)	$E_{\text{gas}}^L$ (hartree)	$G^{\text{soln,L,corr}}$ (hartree)
<b>1</b>	-1865,65158597	-1862,77529500	-1865,61712931	0,420735
<b>1n</b>	-1865,18309869	-1862,25084690	-1865,09390605	0,409308
<b>1m</b>	-1865,17978324	-1862,25489253	-1865,09883917	0,407101
<b>1a</b>	-1865,15973178	-1862,23123052	-1865,07888787	0,407340
<b>1b</b>	-1865,16476000	-1862,23076348	-1865,07774973	0,407040
<b>1c</b>	-1865,15223584	-1862,22155290	-1865,06869094	0,406717
<b>2</b>	-1312,94865690	-1310,84613730	-1312,91229310	0,369215
<b>2n</b>	-1312,46596498	-1310,30068864	-1312,37155955	0,359584
<b>2m</b>	-1312,47620447	-1310,32513450	-1312,39330119	0,359626
<b>2a</b>	-1312,45582313	-1310,30127160	-1312,37308430	0,359301
<b>2b</b>	-1312,46083662	-1310,30053986	-1312,37166042	0,359415
<b>2c</b>	-1312,44940507	-1310,29319464	-1312,36447405	0,358452

The  $pK_a$  values of selected positions corresponding to the calculation results of Table S7 are depicted in Figure S36:

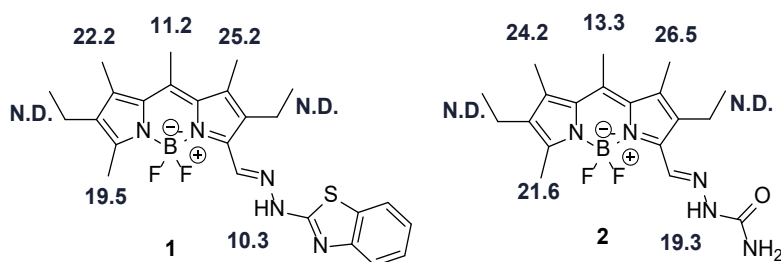


Figure S36. Computed  $pK_a$  values of selected positions of compounds **1** and **2**.

*Chapter 5: GHB and synthetic cathinones detection using BODIPY derivatives*

- [1] J. Ho, "Are thermodynamic cycles necessary for continuum solvent calculation of pK<sub>a</sub>s and reduction potentials?", *Phys. Chem. Chem. Phys.*, 17 (2015) 2859.
- [2] M. K. Kesharwani, B. Brauer, and J. M. L. Martin, "Frequency and Zero-Point Vibrational Energy Scale Factors for Double-Hybrid Density Functionals (and Other Selected Methods): Can Anharmonic Force Fields Be Avoided?", *J. Phys. Chem. A*, 119 (2015), 1701-1714.
- [3] R. F. Ribeiro, A. V. Marenich, C. J. Cramer, and D. G. Truhlar, "Use of Solution-Phase Vibrational Frequencies in Continuum Models for the Free Energy of Solvation", *J. Phys. Chem. B*, 115 (2011) 14556-14562.
- [4] G. Luchini, J. V. Alegre-Requena, I. Funes-Ardoiz, R. S. Paton, "GoodVibes: Automated Thermochemistry for Heterogeneous Computational Chemistry Data", *F1000Research*, 291 (2020) 9. DOI: 10.12688/f1000research.22758.1.
- [5] C. P. Kelly, C. J. Cramer, D. G. Truhlar, "Single-ion solvation free energies and the normal hydrogen electrode potential in methanol, acetonitrile, and dimethyl sulfoxide", *J Phys Chem B.*, 111 (2007) 408-422.

## **Chapter 6: Conclusions**





Over the past of the years, a considerable increase in the number of sensors in the literature has been observed. Among them, the development of optical chemosensors has been key due to their ease of use and the low-cost instrumentation that they require.

In this thesis, the main goal has been to detect GHB in real samples such as drinks and beverages. For this purpose, we have designed, synthesized and evaluated several chemosensors. One of them has also showed the capability to detect synthetic cathinones.

In chapter 2, two heteroditopic ligands have been reported. Meanwhile the host units were the same for both probes, a thiourea moiety and the trifluoroacetyl group, the linker was different. This fact allowed us to study the rigidity effect in the recognition event. In both cases, the probes demonstrated their ability to detect GHB not only in a pure organic solvent (DMSO), but also in a mixture of DMSO:H<sub>2</sub>O. Additionally, these chemosensors were tested in spiked drinks, providing quite satisfactory results.

In chapter 3, two benzoxazole derivatives have been described for the very first time as recognition units for carboxylates. Their easy synthesis and highly sensitive response towards GHB detection was reported. In this chapter, the effect of the content of water in the medium was also analysed. Both sensors could stand high quantities of it. Moreover, a great number of different spiked drinks and beverages with GHB were tested and, in every case, the probes demonstrated their capability to detect this analyte in real samples.

In chapter 4, the use of AuNPs has been explored. To do so, two different ligands were synthesized to recognise both functional groups present in GHB and anchored to the AuNPs. The detection experiments were carried out in aqueous dissolution. Even though the quantities of GHB detected with this system were higher than those reported in previous chapters, it was possible to test it in real samples, with moderate results.

In chapter 5, two new hydrazones based on a BODIPY core have been reported. These sensors proved to be able to detect GHB in an organic medium and in spiked drinks. Moreover, one of them

(compound **5.1**) also proved to be capable of detecting synthetic cathinones through the reduction of a Cu(II) salt. It was assessed the possibility of detecting both drugs using the same detection conditions, providing us with very satisfactory results.

Finally, from the work in collaboration with ScienceFlow, we have created NoSUM, a personal use kit to detect GHB in drinks. In this project, we carried out some workshops in a university environment to increase students' awareness of DFSA and how to act in case they got involved in one of them. Additionally, we provided them with some kits to test them in real situations. The preliminary data obtained from surveys showed us mainly when and why students used their kits and how they found their use.

Con el paso de los años, se ha observado un incremento considerable del número de sensores moleculares en la bibliografía. Entre ellos, el desarrollo de quimiosensores ópticos ha sido clave debido a su facilidad de uso y a la instrumentación de bajo coste que requieren.

En esta tesis, el principal objetivo ha sido detectar GHB en muestras reales como, por ejemplo, bebidas y combinados. Para este propósito, hemos diseñado, sintetizado y evaluado varios quimiosensores. Uno de ellos ha mostrado también la capacidad de detectar catinonas sintéticas.

En el capítulo 2, se ha presentado dos ligandos heteroditópicos. Mientras que las dos unidades receptoras eran las mismas para ambos, una unidad de tipo tiourea y un grupo trifluoroacetilo, la unidad espaciadora era diferente. Este hecho nos permitió estudiar el efecto de la rigidez del sistema durante el reconocimiento. En ambos casos, las sondas demostraron su habilidad para detectar GHB no solo en un disolvente orgánico puro, sino que también en una mezcla DMSO:H<sub>2</sub>O. Además, estos quimiosensores fueron probados en bebidas adulteradas y proporcionaron resultados bastante satisfactorios.

En el capítulo 3, se ha descrito dos derivados de benzoxazol como unidades de reconocimiento de carboxilatos por primera vez. Se describió su sencilla síntesis y se observó una excelente respuesta en la detección de GHB. En este capítulo, el efecto del contenido de agua en el medio también se evaluó. Ambos sensores soportaron elevados contenidos de la misma. Además, un gran número de bebidas y combinados adulterados con GHB fueron analizados y, en todos los casos, las sondas demostraron su capacidad de detectar este analito en las muestras reales estudiadas.

En el capítulo 4, se exploró el uso de AuNPs. Para ello, se sintetizó dos ligandos diferentes para reconocer ambos grupos funcionales presentes en el GHB y se anclaron a las AuNPs. Los experimentos de detección se llevaron a cabo en disolución acuosa. A pesar de que las cantidades detectadas con este sistema fueron mayores que aquellas detectadas en el capítulo anterior, fue posible testarlo con muestras reales, con resultados aceptables.

En el capítulo 5, se ha estudiado dos nuevas hidrazonas basadas en un sistema BODIPY. Estos sensores demostraron ser capaces de detectar GHB en un medio orgánico y en bebidas adulteradas. Además, una de ellas (el compuesto **5.1**) también demostró ser capaz de detectar catinonas sintéticas a través de la reducción de una sal de Cu(II). También fue evaluada la posibilidad de detectar ambas drogas al mismo tiempo con resultados muy satisfactorios.

Finalmente, a partir de la colaboración con ScienceFlow, hemos creado NoSUM, un kit de uso personal para detectar GHB en bebidas. En este proyecto, se han llevado a cabo algunos talleres en un ambiente universitario para hacer que el estudiantado tome conciencia de los DFSA y cómo actuar en caso de que se encuentre involucrado en uno de ellos. Además, les hemos proporcionado algunos kits para que puedan probarlos en situaciones reales. Los datos preliminares obtenidos a partir de las encuestas nos mostraron principalmente cuándo y por qué los usaron.

## References



1. Folgar MI, Taboada CS, Boubeta AR, Alías A, McCartan K. Drug-facilitated sexual assault and chemical submission. *Psychology, Society and Education*. 2017;9(2):263-282. doi:10.25115/psye.v9i2.701
2. Crocq MA. *Historical and Cultural Aspects of Man's Relationship with Addictive Drugs*. 2007;9:355-361. doi:10.31887/DCNS.2007.9.4/macrocq
3. World drug report 2015. CHAPTER I STATUS AND TREND ANALYSIS OF ILLICIT DRUG MARKETS. Accessed in May 2022. [https://www.unodc.org/documents/wdr2015/WDR15\\_Drug\\_use\\_health\\_consequences.pdf](https://www.unodc.org/documents/wdr2015/WDR15_Drug_use_health_consequences.pdf)
4. NCDAS: Substance Abuse and Addiction Statistics [2022]. Accessed in May 2022. <https://drugabusestatistics.org/>
5. Emcdda. Informe Europeo sobre Drogas. doi:10.2810/862853. Accessed in May 2022. [https://www.emcdda.europa.eu/data/stats2020/gps\\_en](https://www.emcdda.europa.eu/data/stats2020/gps_en)
6. B Poyen, Rodor F, Jouve-Bestagne MH, Galland MC, Lots R, Jouglard J. Amnesia and behavior disorders of criminal appearance after ingestion of benzodiazepines. *Therapie*. 1982;37(6):675-678.
7. Cruz A, Quintela O, López-Rivadulla M. Sumisión química: epidemiología y claves para su diagnóstico. *Med. Clin*. 2008;131:783-789. doi: 10.1016/S0025-7753(08)75505-2
8. Unodc. Guidelines for the Forensic Analysis of Drugs Facilitating Sexual Assault and Other Criminal Acts. Accessed in May 2018. [https://www.unodc.org/documents/scientific/forensic\\_analysis\\_of\\_drugs\\_facilitating\\_sexual\\_assault\\_and\\_other\\_criminal\\_acts.pdf](https://www.unodc.org/documents/scientific/forensic_analysis_of_drugs_facilitating_sexual_assault_and_other_criminal_acts.pdf)
9. European Monitoring Centre for Drugs and Drug Addiction. *Sexual Assaults Facilitated by Drugs or Alcohol*. Accessed in November 2021. [https://www.emcdda.europa.eu/drugs-library/sexual-assaults-facilitated-drugs-or-alcohol\\_en](https://www.emcdda.europa.eu/drugs-library/sexual-assaults-facilitated-drugs-or-alcohol_en)

10. Grela A, Gautam L, Cole MD. A multifactorial critical appraisal of substances found in drug facilitated sexual assault cases. *Forensic Sci Int.* 2018;292:50-60. doi:10.1016/j.forsciint.2018.08.034
11. Sonone SS, Jadhav S, Singh Sankhla M. A forensic aspect on drug facilitated sexual assault. *Forensic Res Criminol Int J.* 2021;9(2):59–63. doi:10.15406/frcij.2021.09.00341
12. Prescription CNS Depressants DrugFacts | National Institute on Drug Abuse (NIDA). Accessed in May 2022. <https://nida.nih.gov/publications/drugfacts/prescription-cns-depressants>
13. Busardò FP, Vari MR, di Trana A, Malaca S, Carlier J, di Luca NM. Drug-Facilitated Sexual Assaults (DFSA): A Serious Underestimated Issue. *Eur Rev Med Pharmacol Sci.* 2019;23:10577-10587. doi:10.26355/eurrev\_201912\_19753
14. Busardò FP, Jones AW. GHB Pharmacology and Toxicology: Acute Intoxication, Concentrations in Blood and Urine in Forensic Cases and Treatment of the Withdrawal Syndrome. *Curr. Neuropharmacol.* 2015;13:47-70. doi:10.2174/1570159X13666141210215423.
15. Corkery JM, Loi B, Claridge H, et al. Gamma hydroxybutyrate (GHB), gamma butyrolactone (GBL) and 1,4-butanediol (1,4-BD; BDO): A literature review with a focus on UK fatalities related to non-medical use. *Neurosci Biobehav Rev.* 2015;53:52-78. doi:10.1016/j.neubiorev.2015.03.012
16. Benarroch EE.  $\gamma$ -Hydroxybutyric acid and its relevance in neurology. *Neurology.* 2009;72(3):282-286. doi:10.1212/01.WNL.0000341945.28830.88
17. Hassan Z, Bosch OG, Singh D, et al. Novel psychoactive substances-recent progress on neuropharmacological mechanisms of action for selected drugs. *Front Psychiatry.* 2017;8:152-172. doi:10.3389/fpsy.2017.00152
18. Schep LJ, Knudsen K, Slaughter RJ, Vale JA, Mégarbane B. The clinical toxicology of gamma-hydroxybutyrate, gamma-butyrolactone and



- 1,4-butanediol. *Clin Toxicol.* 2012;50(6):458-470. doi:10.3109/15563650.2012.702218
19. Németh Z, Kun B, Demetrovics Z. The involvement of gamma-hydroxybutyrate in reported sexual assaults: A systematic review. *J. Psychopharmacol.* 2010;24(9):1281-1287. doi:10.1177/0269881110363315
  20. Okun MS, Boothby LA, Baterfield RB, Doering PL. GHB: An Important Pharmacologic and Clinical Update. *J. Pharm. Pharm. Sci.* 2001;4:167-175. PMID: 11466174
  21. Morris-Kukoski CL. *GHB SYMPOSIUM Bridging the Clinical-Analytical Gap. Toxicol. Rev.* 2004;23:33-43. doi:1176-2551/04/0001-0033/\$31.00/0
  22. What are NPS? Accessed in May 2022. <https://www.unodc.org/LSS/Page/NPS>
  23. Specka M, Kuhlmann T, Sawazki J, et al. Prevalence of Novel Psychoactive Substance (NPS) Use in Patients Admitted to Drug Detoxification Treatment. *Front Psychiatry.* 2020;11:569-577. doi:10.3389/fpsy.2020.00569
  24. Zawilska JB. *Current Topics in Neurotoxicity. Synthetic Cathinones Novel Addictive and Stimulatory Psychoactive Substances.* 1<sup>st</sup> Edition. Springer International Publishing. 2018. doi:10.1007/978-3-319-78707-7
  25. Dasgupta A. *Alcohol, Drugs, Genes and the Clinical Laboratory: An Overview for Healthcare and Safety Professionals. Designer drugs including bath salts and spices.* 1<sup>st</sup> Edition. Academic Press. 2016. doi:10.1016/B978-0-12-805455-0.00003-8
  26. Shafi A, Berry AJ, Sumnall H, Wood DM, Tracy DK. New psychoactive substances: a review and updates. *Ther Adv Psychopharmacol.* 2020;10:1-21. doi:10.1177/2045125320967197
  27. Karch SB. Cathinone Neurotoxicity ("The "3Ms"). *Curr Neuropharmacol.* 2015;13(1):21-25. doi:10.2174/1570159X13666141210225009

28. Lehn MJ. *Supramolecular Chemistry. Concepts and Perspectives*. 1<sup>st</sup> Edition. 1995. doi:10.1002/ange.19951072130
29. Wallace KJ, Broome JH. *Light in Forensic Science: Issues and Applications. Supramolecular Approach in Detecting Drugs of Abuse: Optical Sensors*. 1<sup>st</sup> Edition. Royal Society of Chemistry. 2018. doi:10.1039/9781788010344-00333
30. Kim K. *Cucurbiturils and Related Macrocycles*. 1<sup>st</sup> Edition. Royal Society of Chemistry. 2019.. doi:10.1039/9781788015967
31. Ebralidze II, Laschuk NO, Poisson J, Zenkina OV. *Colorimetric Sensors and Sensor Arrays. In: Nanomaterials Design for Sensing Applications*. 1<sup>st</sup> Edition. Elsevier; 2019. doi:10.1016/B978-0-12-814505-0.00001-1
32. Dongare PR, Gore AH. Recent Advances in Colorimetric and Fluorescent Chemosensors for Ionic Species: Design, Principle and Optical Signalling Mechanism. *ChemistrySelect*. 2021;6(23):5657-5669. doi:10.1002/slct.202101090
33. Qian RC, Long YT. Wearable Chemosensors: A Review of Recent Progress. *ChemistryOpen*. 2018;7(2):118-130. doi:10.1002/open.201700159
34. Martínez-Máñez R, Sancenón F. New advances in fluorogenic anion chemosensors. *J Fluoresc*. 2005;15(3):267-285. doi:10.1007/s10895-005-2626-z
35. Wu J, Kwon B, Liu W, Anslyn E v., Wang P, Kim JS. Chromogenic/Fluorogenic Ensemble Chemosensing Systems. *Chem Rev*. 2015;115(15):7893-7943. doi:10.1021/cr500553d
36. Wu D, Sedgwick AC, Gunnlaugsson T, Akkaya EU, Yoon J, James TD. Fluorescent chemosensors: the past, present and future. *Chem Soc Rev*. 2017;46(23):7105-7123. doi:10.1039/C7CS00240H
37. Zhai D, Elton Tan YQ, Xu W, Chang YT. Development of a fluorescent sensor for illicit date rape drug GHB. *Chem. Comm..* 2014;50(22):2904-2906. doi:10.1039/c3cc49603a

38. Zhai D, Agrawalla BK, Eng PSF, Lee SC, Xu W, Chang YT. Development of a fluorescent sensor for an illicit date rape drug – GBL. *Chem. Comm.* 2013;49(55):6170. doi:10.1039/c3cc43153c
39. Wang W, Dong ZZ, Yang G, Leung CH, Lin S, Ma DL. A long-lived iridium(iii) chemosensor for the real-time detection of GHB. *J Mater Chem B.* 2017;5(15):2739-2742. doi:10.1039/C6TB03396B
40. Baumes LA, Buaki Sogo M, Montes-Navajas P, Corma A, Garcia H. A Colorimetric Sensor Array for the Detection of the Date-Rape Drug  $\gamma$ -Hydroxybutyric Acid (GHB): A Supramolecular Approach. *Chem. Eur. J.* 2010;16(15):4489-4495. doi:10.1002/chem.200903127
41. Hu M, Han Q, Xing B. Metallic Nanoparticle-Enabled Sensing of a Drug-of-Abuse: An Attempt at Forensic Application. *ChemBioChem.* 2020;21(17):2512-2517. doi:10.1002/cbic.202000157
42. Son SU, Jang S, Kang B, et al. Colorimetric paper sensor for visual detection of date-rape drug  $\gamma$ -hydroxybutyric acid (GHB). *Sens Actuators B Chem.* 2021;347:130598-130605. doi:10.1016/j.snb.2021.130598
43. Ryu J, Kim Y. Overcoming interferences in the colorimetric and fluorimetric detection of  $\gamma$ -hydroxybutyrate in spiked beverages. *Sens Actuators B Chem.* 2022;364:131861-131866. doi:10.1016/j.snb.2022.131861
44. G. de Campos E, Krotulski AJ, S. De Martinis B, Costa JL. Identification of synthetic cathinones in seized materials: A review of analytical strategies applied in forensic chemistry. *WIREs Forensic Science.* Published online September 13, 2022. doi:10.1002/wfs2.1455
45. Cuypers E, Bonneure AJ, Tytgat J. The use of presumptive color tests for new psychoactive substances. *Drug Test Anal.* 2016;8(1):137-141. doi:10.1002/dta.1847
46. Toole KE, Fu S, Ronald G Shimmon RG, Kraymen N. Color Tests for the Preliminary Identification of Methcathinone and Analogues of Methcathinone. *Microgram Journal.* 2001;9(1):27-32. Accessed in

- July 2022. [https://www.dea.gov/sites/default/files/pr/microgram-journals/2012/mj9-1\\_27-32.pdf](https://www.dea.gov/sites/default/files/pr/microgram-journals/2012/mj9-1_27-32.pdf)
47. Cheng SY, Ng-A-Quei T, Eng B, Ho J. Detection of cathinone and mephedrone in plasma by LC-MS/MS using standard addition quantification technique. *J Anal Sci Technol*. 2017;8(1):19-24. doi:10.1186/s40543-017-0128-7
  48. Hagan KS, Reidy L. Detection of synthetic cathinones in victims of sexual assault. *Forensic Sci Int*. 2015;257:71-75. doi:10.1016/j.forsciint.2015.07.040
  49. Glicksberg L, Bryand K, Kerrigan S. Identification and quantification of synthetic cathinones in blood and urine using liquid chromatography-quadrupole/time of flight (LC-Q/TOF) mass spectrometry. *J Chromatogr B Analyt Technol Biomed Life Sci*. 2016;1035:91-103. doi:10.1016/j.jchromb.2016.09.027
  50. Al-Obaid AM, Al-Tamrah SA, Aly FA, Alwarthan AA. Determination of (S)(-)-Cathinone by Spectrophotometric Detection. *J. Pharm. Biomed. Anal*. 1998;17:321-326. doi:10.1016/S0731-7085(97)00203-3
  51. Philp M, Shimmon R, Tahtouh M, Fu S. Development and validation of a presumptive color spot test method for the detection of synthetic cathinones in seized illicit materials. *Forensic Chemistry*. 2016;1:39-50. doi:10.1016/j.forc.2016.06.001
  52. Yen Y te, Chen TY, Chen CY, Chang CL, Chyueh SC, Chang HT. A photoluminescent colorimetric probe of bovine serum albumin-stabilized gold nanoclusters for new psychoactive substances: Cathinone drugs in seized street samples. *Sensors*. 2019;19(16):3554-3564. doi:10.3390/s19163554
  53. Yen Y te, Lin YS, Chen TY, Chyueh SC, Chang HT. Carbon dots functionalized papers for high-throughput sensing of 4-chloroethcathinone and its analogues in crime sites. *R Soc Open Sci*. 2019;6(9):1-11. doi:10.1098/rsos.191017
  54. Yan Y, Jiang L, Zhang S, Shen X, Huang C. Specific "light-up" sensor made easy: An aggregation induced emission monomer for molecular

- imprinting. *Biosens Bioelectron.* 2022;205:114113-114123. doi:10.1016/j.bios.2022.114113
55. Kharisov BI, Martínez PE, Jiménez-Pérez VM, Kharissova O v., Martínez BN, Pérez N. Recent advances on ditopic ligands. *J Coord Chem.* 2010;63(1):1-25. doi:10.1080/00958970903325534
56. Krämer J, Kang R, Grimm LM, de Cola L, Picchetti P, Biedermann F. Molecular Probes, Chemosensors, and Nanosensors for Optical Detection of Biorelevant Molecules and Ions in Aqueous Media and Biofluids. *Chem Rev.* 2022;122(3):3459-3636. doi:10.1021/acs.chemrev.1c00746
57. Chowdhury AR, Ghosh P, Paul S, et al. A novel ditopic chemosensor for cadmium and fluoride and its possible application as a pH sensor. *Anal. Methods.* 2016;9(1):124-133. doi:10.1039/C6AY02656G
58. Kaewtong C, Pulpoka B, Tuntulani T. Reversible fluorescent and colorimetric rhodamine based-chemosensor of Cu<sup>2+</sup> contact ion-pairs using a ditopic receptors. *Dyes Pigm.* 2015;123:204-211. doi:10.1016/j.dyepig.2015.08.001
59. Hossain SM, Lakma A, Pradhan RN, Chakraborty A, Biswas A, Singh AK. Synthesis and characterization of a novel, ditopic, reversible and highly selective, "Turn-On" fluorescent chemosensor for Al<sup>3+</sup> ion. *RSC Adv.* 2015;5(78):63338-63344. doi:10.1039/C5RA12040C
60. Gotor R, Costero AM, Gil S, Parra M, Gaviña P, Rurack K. Boolean operations mediated by an ion-pair receptor of a multi-readout molecular logic gate. *Chem. Comm.* 2013;49(94):11056-11058. doi:10.1039/c3cc45377d
61. Gotor R, Costero AM, Gil S, Gaviña P, Rurack K. On the ion-pair recognition and indication features of a fluorescent heteroditopic host based on a BODIPY core. *Eur. J Org Chem.* 2014;2014(19):4005-4013. doi:10.1002/ejoc.201402214
62. Zhou X bo, Yip YW, Chan WH, Lee AWM. An easy assembled fluorescent sensor for dicarboxylates and acidic amino acids. *Beilstein Journal of Organic Chemistry.* 2011;7:75-81. doi:10.3762/bjoc.7.11

63. Costero AM, Colera M, Gaviña P, Gil S. Fluorescent sensing of maleate versus fumarate by a neutral cyclohexane based thiourea receptor. *Chemical Communications*. 2006;(7):761-763. doi:10.1039/b515320d
64. Martí A, Costero AM, Gaviña P, Parra M. Selective Recognition and Sensing of Succinate vs. Other Aliphatic Dicarboxylates by Thiourea-Functionalized Gold Nanoparticles. *ChemistrySelect*. 2016;1(5):1057-1060. doi:10.1002/slct.201600313
65. O'Neil LG, Bower JF. Electrophilic Aminating Agents in Total Synthesis. *Angew. Chem. Int.* 2021;60(49):25640-25666. doi:10.1002/anie.202102864
66. Juliá F, Shao Q, Duan M, et al. High Site Selectivity in Electrophilic Aromatic Substitutions: Mechanism of C–H Thianthrenation. *J Am Chem Soc*. 2021;143(39):16041-16054. doi:10.1021/jacs.1c06281
67. Smith DT, Vitaku E, Njardarson JT. Dearomatization Approach to 2-Trifluoromethylated Benzofuran and Dihydrobenzofuran Products. *Org Lett*. 2017;19(13):3508-3511. doi:10.1021/acs.orglett.7b01479
68. Zhou D, Yu X, Zhang J, Wang W, Xie H. Organocatalytic asymmetric addition of alcohols to cyclic trifluoromethyl ketimines: highly enantioselective synthesis of chiral N,O-ketals. *Org Biomol Chem*. 2016;14(26):6193-6196. doi:10.1039/C6OB00890A
69. Katritzky AR, Ramsden CA, Scriven EF, Taylor RJK. Comprehensive Heterocyclic Chemistry III. 1<sup>st</sup> Edition. Elsevier. 2008
70. Dnyanadeo Mahajan N, Jain N. Heterocyclic Compounds And Their Applications In The Field Of Biology: A Detailed Study. *Nat. Volatiles Essent. Oils*. 2021; 8(4): 13223-13229
71. Rynearson KD, Charrette B, Gabriel C, et al. 2-Aminobenzoxazole ligands of the hepatitis C virus internal ribosome entry site. *Bioorg Med Chem Lett*. 2014;24(15):3521-3525. doi:10.1016/j.bmcl.2014.05.088
72. Fan L, Luo Z, Yang C, et al. Design and synthesis of small molecular 2-aminobenzoxazoles as potential antifungal agents against

- phytopathogenic fungi. *Mol Divers.* 2022;26(2):981-992. doi:10.1007/s11030-021-10213-7
73. Kakkar S, Tahlan S, Lim SM, et al. Benzoxazole derivatives: design, synthesis and biological evaluation. *Chem Cent J.* 2018;12(1):92-107. doi:10.1186/s13065-018-0459-5
74. Erol M, Celik I, Uzunhisarcikli E, Kuyucuklu G. Synthesis, Molecular Docking, and DFT Studies of Some New 2,5-Disubstituted Benzoxazoles as Potential Antimicrobial and Cytotoxic Agents. *Polycycl Aromat Compd.* 2022;42(4):1679-1696. doi:10.1080/10406638.2020.1802305
75. Ghoshal T, Patel TM. One-pot synthesis of 2-aminobenzoxazole derivatives using acetic acid as an electrolyte under electrochemical conditions. *J. Iran. Chem. Soc.* 2021;18(9):2241-2248. doi:10.1007/s13738-021-02184-1
76. Šlachťová V, Chasák J, Brulíková L. Synthesis of Various 2-Aminobenzoxazoles: The Study of Cyclization and Smiles Rearrangement. *ACS Omega.* 2019;4(21):19314-19323. doi:10.1021/acsomega.9b02702
77. Jung SL, Kim SG, Lee GH, Gong YD. An efficient solid-phase parallel synthesis of 2-amino and 2-amidobenzo[d]oxazole derivatives via cyclization reactions of 2-hydroxyphenylthiourea resin. *Bull Korean Chem Soc.* 2012;33(12):4109-4116. doi:10.5012/bkcs.2012.33.12.4109
78. Tanaka K, Kumagai T, Aoki H, Deguchi M, Iwata S. Application of 2-(3,5,6-trifluoro-2-hydroxy-4-methoxyphenyl)benzoxazole and -benzothiazole to fluorescent probes sensing pH and metal cations. *J. Org. Chem.* 2001;66(22):7328-7333. doi:10.1021/jo010462a
79. Xu Y, Xiao L, Sun S, Pei Z, Pei Y, Yi P. Switchable and selective detection of Zn<sup>2+</sup> or Cd<sup>2+</sup> in living cells based on 3'-O-substituted arrangement of benzoxazole-derived fluorescent probes. *Chem. Comm.* 2014;50(56):7514-7516. doi:10.1039/c4cc02335h

80. Kim HJ. Fluorescent Nano-Assembly of Organic Conjugate Molecules with Benzoxazole Moiety and Its Application in Sensor. *J Nanosci Nanotechnol.* 2018;19(2):1052-1055. doi:10.1166/jnn.2019.15928
81. Rahmawati R, Purwono B, Hadisaputera S. A 4-(1H-Benzo[d]oxazole-2-yl)-2-methoxyphenol as dual selective sensor for cyanide ion detection. *Asian J. Chem.* 2019;31(3):555-558. doi:10.14233/ajchem.2019.21679
82. Abeywickrama CS, Pang Y. Fused bis[2-(2'-hydroxyphenyl)benzoxazole] derivatives for improved fluoride sensing: The impact of regiochemistry and competitive hydrogen bonding. *Tetrahedron Lett.* 2017;58(16):1627-1632. doi:10.1016/j.tetlet.2017.03.030
83. Tian Y, Chen CY, Yang CC, et al. 2-(2'-Hydroxyphenyl)benzoxazole-containing two-photon-absorbing chromophores as sensors for zinc and hydroxide ions. *Chem. Mater.* 2008;20(5):1977-1987. doi:10.1021/cm702527m
84. Asaithambi G, Periasamy V, Karuppannan N. Fluorescence sensing response of zinc(II) and pyrophosphate ions by benzoxazole appended dipodal Schiff base. *J Photochem Photobiol A Chem.* 2019;370:75-83. doi:10.1016/j.jphotochem.2018.10.036
85. Costa SPG, Oliveira E, Lodeiro C, Manuela M, Raposo M. Synthesis, Characterization and Metal Ion Detection of Novel Fluoroionophores Based on Heterocyclic Substituted Alanines. *Sensors.* 2007;7:2096-2114. doi:10.3390/s7102096
86. Li Y, Zhao JF, Chu TS. Glutathione sensing mechanism of a fluorescent probe: Excited state intramolecular proton transfer and photoinduced electron transfer. *J Lumin.* 2018;204:642-648. doi:10.1016/j.jlumin.2018.08.073
87. Barhoum A, García-Betancourt ML, Rahier H, van Assche G. *Physicochemical characterization of nanomaterials: Polymorph, composition, wettability, and thermal stability.* In: *Emerging Applications of Nanoparticles and Architectural Nanostructures:*



- Current Prospects and Future Trends*. 1<sup>st</sup> Edition. Elsevier Inc.; 2018. doi:10.1016/B978-0-323-51254-1.00009-9
88. Amin MT, Alazba AA, Manzoor U. A review of removal of pollutants from water/wastewater using different types of nanomaterials. *Advances in Materials Science and Engineering*. 2014;2014(1):1-24. doi:10.1155/2014/825910
89. Moores A, Goettmann F. The plasmon band in noble metal nanoparticles: An introduction to theory and applications. *New J. Chem*. 2006;30(8):1121-1132. doi:10.1039/b604038c
90. Saha K, Agasti SS, Kim C, Li X, Rotello VM. Gold nanoparticles in chemical and biological sensing. *Chem Rev*. 2012;112(5):2739-2779. doi:10.1021/cr2001178
91. Liz-Marzán LM. Nanometals. *Materials Today*. 2004;7(2):26-31. doi:10.1016/S1369-7021(04)00080-X
92. Herizchi R, Abbasi E, Milani M, Akbarzadeh A. Current methods for synthesis of gold nanoparticles. *Artif Cells Nanomed. Biotechnol*. 2016;44(2):596-602. doi:10.3109/21691401.2014.971807
93. Priyadarshini E, Pradhan N. Gold nanoparticles as efficient sensors in colorimetric detection of toxic metal ions: A review. *Sens Actuators B Chem*. 2017;238:888-902. doi:10.1016/j.snb.2016.06.081
94. Zhao P, Li N, Astruc D. State of the art in gold nanoparticle synthesis. *Coord Chem Rev*. 2013;257(3-4):638-665. doi:10.1016/j.ccr.2012.09.002
95. Maturi M, Locatelli E, Monaco I, Comes Franchini M. Current concepts in nanostructured contrast media development for: In vivo photoacoustic imaging. *Biomater Sci*. 2019;7(5):1746-1775. doi:10.1039/c8bm01444b
96. Ghoto SA, Khuhawar MY, Jahangir TM, Mangi J ul D. Applications of copper nanoparticles for colorimetric detection of dithiocarbamate pesticides. *J Nanostructure Chem*. 2019;9(2):77-93. doi:10.1007/s40097-019-0299-4

97. Tran H v., Nguyen T v., Nguyen LTN, Hoang HS, Huynh CD. Silver nanoparticles as a bifunctional probe for label-free and reagentless colorimetric hydrogen peroxide chemosensor and cholesterol biosensor. *J. Sci. Adv. Mater. Dev.* 2020;5(3):385-391. doi:10.1016/j.jsamd.2020.06.001
98. Azzazy HME, Mansour MMH, Samir TM, Franco R. Gold nanoparticles in the clinical laboratory: Principles of preparation and applications. *Clin Chem Lab Med.* 2012;50(2):193-209. doi:10.1515/cclm.2011.732
99. Liu G, Lu M, Huang X, Li T, Xu D. Application of gold-nanoparticle colorimetric sensing to rapid food safety screening. *Sensors.* 2018;18(12):4166-4181. doi:10.3390/s18124166
100. Bai X, Wang Y, Song Z, et al. The basic properties of gold nanoparticles and their applications in tumor diagnosis and treatment. *Int J Mol Sci.* 2020;21(7):2480-2496. doi:10.3390/ijms21072480
101. Martínez-Aquino C, Costero AM, Gil S, Gaviña P. Resorcinol functionalized gold nanoparticles for formaldehyde colorimetric detection. *Nanomaterials.* 2019;9(2):302-308. doi:10.3390/nano9020302
102. Rodríguez-Nuévalos S, Costero AM, Arroyo P, et al. Protection against chemical submission: Naked-eye detection of  $\gamma$ -hydroxybutyric acid (GHB) in soft drinks and alcoholic beverages. *Chem. Comm.* 2020;56(83):12600-12603. doi:10.1039/d0cc05387b
103. Mazik M, Hartmann A, Jones PG. Highly effective recognition of carbohydrates by phenanthroline-based receptors:  $\alpha$ - versus  $\beta$ -anomer binding preference. *Chem. Eur. J.* 2009;15(36):9147-9159. doi:10.1002/chem.200900664
104. Loudet A, Burgess K. BODIPY dyes and their derivatives: Syntheses and spectroscopic properties. *Chem Rev.* 2007;107(11):4891-4932. doi:10.1021/cr078381n

105. Boens N, Verbelen B, Dehaen W. Postfunctionalization of the BODIPY Core: Synthesis and Spectroscopy. *Eur. J Org. Chem.* 2015;2015(30):6577-6595. doi:10.1002/ejoc.201500682
106. Boens N, Leen V, Dehaen W. Fluorescent indicators based on BODIPY. *Chem Soc Rev.* 2012;41(3):1130-1172. doi:10.1039/c1cs15132k
107. Boens N, Verbelen B, Ortiz MJ, Jiao L, Dehaen W. Synthesis of BODIPY dyes through postfunctionalization of the boron dipyrromethene core. *Coord Chem Rev.* 2019;399:213024-213108. doi:10.1016/j.ccr.2019.213024
108. Gurubasavaraj PM, Sajjan VP, Muñoz-Flores BM, Jiménez Pérez VM, Hosmane NS. Recent Advances in BODIPY Compounds: Synthetic Methods, Optical and Nonlinear Optical Properties, and Their Medical Applications. *Molecules.* 2022;27(6):1877-1906. doi:10.3390/molecules27061877
109. de Bonfils P, Péault L, Nun P, Coeffard V. State of the Art of Bodipy-Based Photocatalysts in Organic Synthesis. *Eur. J Org Chem.* 2021;2021(12):1809-1824. doi:10.1002/ejoc.202001446
110. Gupta G, Sun Y, Das A, Stang PJ, Yeon Lee C. BODIPY based metal-organic macrocycles and frameworks: Recent therapeutic developments. *Coord Chem Rev.* 2022;452:214308-214336. doi:10.1016/j.ccr.2021.214308
111. Li FZ, Yin JF, Kuang GC. BODIPY-based supramolecules: Construction, properties and functions. *Coord Chem Rev.* 2021;448:214157-214185. doi:10.1016/j.ccr.2021.214157
112. Antina E, Bumagina N, Marfin Y, et al. BODIPY Conjugates as Functional Compounds for Medical Diagnostics and Treatment. *Molecules.* 2022;27(4):1396-1454. doi:10.3390/molecules27041396
113. Gopala L, Yan YJ, Chen ZL. Chemical Review and Letters Detail Synthetic Study of Infrared Fluorescent Dyes: Design, Synthesis and Chemical Properties of their Photodynamic Therapy Probes. *Chem Rev Lett.* 2022;5:12-67. doi:10.22034/CRL.2021.287098.1109

114. Li FZ, Wu Z, Lin C, Wang Q, Kuang GC. Photophysical properties regulation and applications of BODIPY-based derivatives with electron donor-acceptor system. *Results Chem.* 2022;4:100384-100398. doi:10.1016/j.rechem.2022.100384
115. Lakshmi V, Rajeswara Rao M, Ravikanth M. Halogenated boron-dipyrromethenes: Synthesis, properties and applications. *Org Biomol Chem.* 2015;13(9):2501-2517. doi:10.1039/c4ob02293a
116. Sheng W, Lv F, Tang B, Hao E, Jiao L. Toward the most versatile fluorophore: Direct functionalization of BODIPY dyes via regioselective C–H bond activation. *Chin. Chem. Lett.* 2019;30(10):1825-1833. doi:10.1016/j.ccllet.2019.08.004
117. Wang S, Liu H, Mack J, et al. A BODIPY-based ‘turn-on’ fluorescent probe for hypoxic cell imaging. *Chem. Comm.* 2015;51(69):13389-13392. doi:10.1039/C5CC05139H
118. Belmonte-Vázquez JL, Sola-Llano R, Bañuelos J, et al. A versatile synthetic approach to design tailor-made push-pull chromophores with intriguing and tunable photophysical signatures. *Dyes Pigm.* 2017;147:246-259. doi:10.1016/j.dyepig.2017.08.014
119. Roacho RI, Metta-Magaña A, Portillo MM, Peña-Cabrera E, Pannell KH. 8-amino-BODIPYs: Structural variation, solvent-dependent emission, and VT NMR spectroscopic properties of 8-R<sub>2</sub>N-BODIPY. *J. Org. Chem.* 2013;78(9):4245-4250. doi:10.1021/jo302758a
120. Bodio E, Goze C. Investigation of B-F substitution on BODIPY and aza-BODIPY dyes: Development of B-O and B-C BODIPYs. *Dyes Pigm.* 2019;160:700-710. doi:10.1016/j.dyepig.2018.08.062
121. Goud TV, Tutar A, Biellmann JF. Synthesis of 8-heteroatom-substituted 4,4-difluoro-4-bora-3a,4a-diaza-s-indacene dyes (BODIPY). *Tetrahedron.* 2006;62(21):5084-5091. doi:10.1016/j.tet.2006.03.036
122. Raveendran A, Sankeerthana PA, Jayaraj A, Chinna Ayya Swamy P. Recent developments on BODIPY based chemosensors for the

- detection of group IIB metal ions. *Results Chem.* 2022;4:100297-100350. doi:10.1016/j.rechem.2022.100297
123. Dzyuba S v. BODIPY Dyes as Probes and Sensors to Study Amyloid- $\beta$ -Related Processes. *Biosensors.* 2020;10(12):192-210. doi:10.3390/BIOS10120192
124. Gotor R, Gaviña P, Ochando LE, et al. BODIPY dyes functionalized with 2-(2-dimethylaminophenyl)ethanol moieties as selective OFF-ON fluorescent chemodosimeters for the nerve agent mimics DCNP and DFP. *RSC Adv.* 2014;4(31):15975-15982. doi:10.1039/c4ra00710g
125. Juárez LA, Costero AM, Parra M, Gaviña P, Gil S. 3-Formyl-BODIPY Phenylhydrazone as a Chromo-Fluorogenic Probe for Selective Detection of NO<sub>2</sub>(g). *Chem. Eur. J.* 2016;22(25):8448-8451. doi:10.1002/chem.201600929
126. Stevanović N, Zlatar M, Novaković I, et al. Cu(II), Mn(II) and Zn(II) complexes of hydrazones with a quaternary ammonium moiety: synthesis, experimental and theoretical characterization and cytotoxic activity. *Dalton Trans.* 2022;51(1):185-196. doi:10.1039/D1DT03169D
127. Patel AK, Jadeja RN, Patel N, et al. Copper(II) hydrazone complexes derived from (Z)-N'-{(2-hydroxynaphthalen-1-yl)methylene}acetohydrazide: Synthesis, spectral characterization, electrochemical behaviour, density functional study, in vitro catalytic activity and molecular docking. *Results Chem.* 2022;4:100244-100268. doi:10.1016/j.rechem.2021.100244
128. Zhou XP, Li D, Zheng SL, Zhang X, Wu T. Cu(I) or Cu(I)-Cu(II) mixed-valence complexes of 2,4,6-tri(2-pyridyl)-1,3, 5-triazine: Syntheses, structures, and theoretical study of the hydrolytic reaction mechanism. *Inorg Chem.* 2006;45(18):7119-7125. doi:10.1021/ic060564p
129. Giri C, Topić F, Cametti M, Rissanen K. Mixed valence mono- and hetero-metallic grid catenanes. *Chem Sci.* 2015;6(10):5712-5718. doi:10.1039/c5sc01851j



## **Annex I: NoSUM**





In this annex, chemical submission will be exposed from a local point of view, in other words, analysing the current situation in Spain. Before continuing, it must be mentioned that the Spanish criminal code, in terms of sexual crimes, has been recently updated. According to the new law (BOE-A-2022-14630 Ley Orgánica 10/2022), any attempt against the sexual liberty of a person will be considered as an aggression, understanding a person's consent as the free and clear manifestation of the willingness of having a sexual relationship. However, before September 2022, the law was different. There was a difference in the type of crime regarding the presence of violence or not. It used to be considered sexual abuse the violation of sexual freedom and integrity without violence, whereas the presence of violence implied a sexual aggression. [a,b] Since this change in law has taken place very recently, some statistical data will be provided as sexual abuse or sexual aggression.

According to INE (Instituto Nacional de Estadística, National Statistics Institute), the number of sexual abuses and aggressions in Spain have been increase since 2013, with a significant rise in the last years. These data are summarised in Figure A.1. [c]

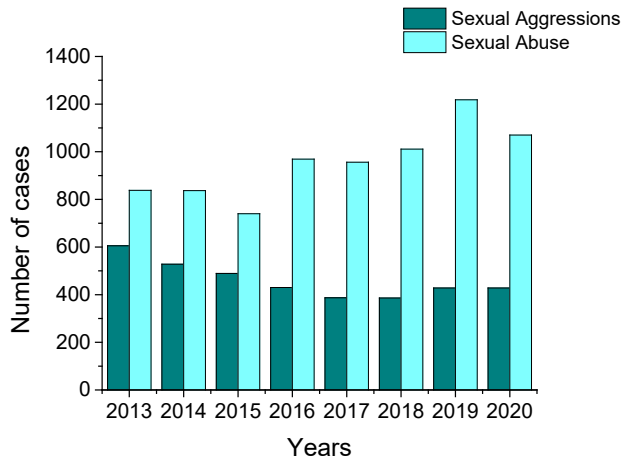


Figure A.1. Evolution of the number of sexual assault cases or abuse from 2013 to 2020 in Spain. [c]

By focusing our attention on the number of women who has suffered sexual violence in Spain, a macro-survey carried out by Government Delegation against Gender-Based Violence in 2019 found that they numbered 2.802.914, i.e. around 12% of women who were residing at that moment in Spain. Among them, 13,7%. were under the effects of alcohol or drugs. [d] On the other hand, a study carried out between 2009 and 2012 by the Forensic Medicine Institute of Alicante showed that 10,6% of the sexual aggressions perpetrated during those years were considered DFSA, being women in almost the totality of the cases and the aggressor a victim's acquaintance around 50%. [e]

Once we were fully aware of the dimensions of this social issue and knowing the satisfactory results showed by the two GHB sensors prepared (compounds **3.1** and **3.2**), we decided to create a kit to recognise the presence of this drug in drinks in real environment, to prevent people from being assaulted by someone else. With this idea in mind, our aim was to prepare a user-friendly kit, with an immediate response, sensitive and selective and useful in a wide range of drinks so this was the starting point to develop NoSUM.

NoSUM is a project sponsored by the AVI (Agencia Valenciana de Innovación, INNVA2/2021/2) and the Plan Nacional sobre Drogas - Ministerio de Sanidad y Conselleria d'Innovació, Universitats, Ciència i Societat Digital de la Generalitat Valenciana. (2020/040). The project was designed and developed by two research groups of the Universitat de València: MODeLiC and ScienceFlows (Figure A.2). The latter was in charge of the information dissemination and communication, whereas the first one was responsible for the synthesis of the sensors and the development of the kit.



Figure A.2. Some members of the project

This project was focused in two main goals: make society aware of DFSA and provide it with a useful tool to defend itself of them. To start with the project, the attention was focused on people aged between 18 and 28, specifically to those in the university community. To publicise the project a logo and some social networks profiles were created along with some advertising posters (see Figure A.3).



Figure A.3. Top) Logo created for the project NoSUM. Bottom) Example of one of the advertising posters done to publicise the workshops

Owing to the pandemic situation, some of these workshops were carried out in an online way, meanwhile others could be done face to face. Regardless the procedure, in both cases the content was the same: an explanation about what CS is, focusing especially on DFSA and its types, common drugs used on them and their symptoms, with special attention to GHB, and how to act in case they were a CS victim. The second part of the workshops was the demonstration of how the kit works. To do so, students were provided with drinks, some of them spiked with GHB and others not, and all the necessary material to carry out the analysis. Finally, a debate was created to share their own experiences related to this topic and how useful and convenient they found the kit. In Figure A.4, some of these moments during the workshops are shown.



Figure A.4. Examples of some of the workshops carried out

All the feedback provided by students was utterly meaningful not only to develop and improve the kit, specifically its appeal in order to use it, but also to make us aware of their perception of this problem and learn how to communicate with them.



Figure A.5. Top) Instructions to use NoSUM. Bottom) Current appearance of the kit

Moreover, all the interested attendees received 6 kits to be employed in real situations, a letter of appreciation and the appropriate phone number to be used in case they needed them (see Figure A.5). Most of the students were from the Universitat de València, but also from the Universidad Complutense de Madrid, the Universidad de Zaragoza and the Universidad de Salamanca. During the project lifespan, a total of 15 workshops were held and 274 people attended them. Recently, the Universitat de Salamanca

has contacted us to prepare 420 kits to give them to their students during the welcome day. Additionally, we have had a preliminary contact with the Mossos d'Esquadra (regional enforcement agents in Catalonia) to provide them with some kits.

On the other hand, some media echoed this project as a means of radio and TV programs, both at a regional and national level. In table A1 some of them are shown. Even, a website has been created to make people aware of this dramatic situation, to allow them to know more about DFSA, take part of this project and/or buy the kit: <https://nosum.net/>.

Table A1. Some examples of media appearances.

Media	Link
À Punt Ràdio	<a href="https://www.apuntmedia.es/programes/proxima-parada/complets/08-11-2021-proxima-parada-primera-hora_135_1465002.html">https://www.apuntmedia.es/programes/proxima-parada/complets/08-11-2021-proxima-parada-primera-hora_135_1465002.html</a>
RTVE	<a href="https://www.rtve.es/play/videos/programa/podemos-detectar-nos-han-introducido-droga-bebida/6194326/">https://www.rtve.es/play/videos/programa/podemos-detectar-nos-han-introducido-droga-bebida/6194326/</a>
Antena 3	<a href="https://www.antena3.com/programas/espejo-publico/noticias/kit-antidroga-comprobar-han-echado-extasis-copa-que-vendera-discotecas_20211110618bcad8d19d5b0001853f75.html">https://www.antena3.com/programas/espejo-publico/noticias/kit-antidroga-comprobar-han-echado-extasis-copa-que-vendera-discotecas_20211110618bcad8d19d5b0001853f75.html</a>
Cuatro	<a href="https://www.mitele.es/programas-tv/cuatro-al-dia/2021/diario/diario-08112021-40_1009228075059/player/">https://www.mitele.es/programas-tv/cuatro-al-dia/2021/diario/diario-08112021-40_1009228075059/player/</a>
El Mundo	<a href="https://www.elmundo.es/espana/2022/05/14/627f9f34fc6c83b31f8b4579.html#">https://www.elmundo.es/espana/2022/05/14/627f9f34fc6c83b31f8b4579.html#</a>

Lastly, a survey was carried out in order to obtain some information about if the students had used the kits, when and why they did it and how they found its use. The generated data showed us that most of them had not used the kit because they had not got involved in any troublesome situation and those who had used it was because of



they wanted to try it or they believed that their drinks or friends' drinks were contaminated. Regarding the usability of the kit, the majority of the opinions was it was comfortable, but they suggested that we could make it more discrete designing it, for example, as a mundane gadget such as a watch or a pack of chewing gum to hide it.

To conclude, NoSUM is currently active since the team is still working on improving the kit, generating material for the social networks and trying to disseminate this troublesome situation, beyond the university community, as much as possible. Besides, this project has received one prize (Programa UVEMPREN-STARTUP PREMIOS de la Universitat de València) and a honorific mention in the emergency field (Premio al Potencial Emprendedor de Proyectos de Investigación de Jóvenes Investigadores en los retos definidos por los Comités Estratégicos de Innovación Especializados de la Agencia Valenciana de la Innovación). Finally, some collaborations been established to create a corporate spin-off.



## References

- [a] Ley Orgánica 10/1995, de 23 de noviembre, del Código Penal. <https://www.boe.es/buscar/pdf/1995/BOE-A-1995-25444-consolidado.pdf> (Accessed in June 2022)
- [b] Ley Orgánica 10/2022, de 6 de septiembre, de garantía integral de la libertad sexual. [/https://www.boe.es/eli/es/lo/2022/09/06/10/dof/spa/pdf](https://www.boe.es/eli/es/lo/2022/09/06/10/dof/spa/pdf) (Accessed in September)
- [c] <https://www.ine.es/jaxiT3/Datos.htm?t=25997> (Accessed in June 2022)
- [d] Las cifras importan: datos para entender la violencia senxual. Recopilación de estadísticas sobre violencias sexuales, salud, consumo de drogas y ocio nocturno. Observatorio Noctámbul@s de la Fundación Salud y Comunidad.
- [e] Agresiones Sexuales Facilitadas por Sustancias Psicoactivas, detectadas en el Instituto de Medicina Legal de Alicante en el cuatrienio 2009-2012. Gac.int. cienc. Forense ISSN 2174-9019. Nº8. Julio-Septiembre, 2013.

